

### 6.3.8 Engineered Barrier System Transport

The EBS Transport Submodel calculates the time-dependent mass flux of radionuclides from failed WPs through the EBS to the UZ Transport Submodel. The EBS Transport Submodel implemented in the TSPA-LA Model is described in *EBS Radionuclide Transport Abstraction* (SNL 2007 [DIRS 177407]). The EBS Transport Submodel considers the transport of radionuclides through the EBS after the radionuclides are mobilized. The mass of radionuclides available for transport through the EBS is provided by the Waste Form Degradation Submodel for the various waste forms (Section 6.3.7.4). Additional inputs and boundary conditions for the EBS Transport Submodel are provided by the EBS Flow Submodel (Section 6.3.6), the EBS TH Environment Submodel (Section 6.3.2), the Dissolved Concentration Limits Submodel (Section 6.3.7.5), and the EBS Colloids Submodel (Section 6.3.7.6). Information flow between the EBS Transport Submodel and other TSPA-LA Model components and submodels is shown on Figure 6.3.8-1. Figure 6.3.8-2 presents an overview of the inputs, outputs, and foundation for confidence in the EBS Transport Submodel as implemented in the TSPA-LA Model. In summary, the inputs include:

- Water flow through failed WPs and the underlying invert provided by the EBS Flow Submodel (Section 6.3.6)
- Temperature, relative humidity, saturation in the invert, and imbibition flux from the host rock exiting the invert under gravity provided by the EBS TH Environment Submodel (Section 6.3.2)
- The waste form dissolution rates provided by the Waste Form Degradation Submodel for the various waste forms (Section 6.3.7.4)
- Solubility limits provided by the Dissolved Concentration Limits Submodel (Section 6.3.7.5)
- Colloidal concentrations and sorption coefficients required to define the mobilized concentration of colloid-associated radionuclides provided by the EBS Colloids Submodel (Section 6.3.7.6).

The EBS Transport Submodel and many of the above supporting submodels that provide feeds were abstracted to describe single representative CSNF and CDSP WPs for each percolation subregion. The determination of what comprises a representative WP is discussed in Section 6.3.2.2.2. The EBS Transport Submodel is implemented in the TSPA-LA Model in terms of a single WP. The pertinent EBS Transport Submodel properties (including the Waste Form Degradation and Mobilization Model Components) for a single representative WP are integrated over the total number of WPs that have failed in each percolation subregion. These properties include the mass of available inventory, pore water volumes, mass of solid materials, advective flow rates, and diffusion areas.

### 6.3.8.1 Conceptual Model

The EBS consists of the DS, the WP on an emplacement pallet, and an invert constructed with steel supports and filled with crushed tuff between the steel framework. The conceptual model of radionuclide transport through the EBS (Figure 6.3.8-3) discretizes the system into three primary domains: (1) the waste form domain, (2) the WP corrosion products domain, and (3) the invert domain composed of crushed tuff. An additional domain, the EBS-UZ Interface, is included beneath the invert domain to establish a boundary condition for calculating the diffusive flux from the invert to the UZ and to compute the mass flux fraction going into the UZ fracture and matrix continua. The waste form and corrosion products domains are more specifically described below by the WP type (CSNF or CDSP) (SNL 2007 [DIRS 177407], Section 6.5.2.5):

#### Commercial spent nuclear fuel (CSNF) WP

CSNF waste form domain	Waste form (CSNF rods), basket tubes (Stainless Steel Type 316), absorber plates (Stainless Steel Type 304B4)
Corrosion products domain	TAD canister (Stainless Steel Type 316), guide assembly (Stainless Steel Type 316), inner vessel (Stainless Steel Type 316)

#### Co-disposed (CDSP) WP

High-level (radioactive) waste (HLW) glass waste form subdomain	HLW glass, HLW glass canisters (Stainless Steel Type 316)
DOE spent nuclear fuel (DSNF) waste form subdomain	DSNF (SNF and Stainless Steel Type 304), DSNF canister (Carbon Steel Type A 516, Stainless Steel Type 304, and Stainless Steel Type 316)
Corrosion products domain	Divider plate (Carbon Steel Type A 516), inner brackets (Carbon Steel Type A 516), outer brackets (Carbon Steel Type A 516), support tube (Carbon Steel Type A 516), inner vessel (Stainless Steel Type 316)

In the EBS Transport Submodel, the transport along the surface of the emplacement pallet is conservatively ignored and the WPs are modeled as being in intimate contact with the invert, (SNL 2007 [DIRS 177407], Sections 5.6 and 6.3.1.1). Thus, the mass flux leaving the WPs flows directly into the invert, with no resistance offered by the pallets. A schematic representation and discretization of various domains for the CSNF WP is shown on Figure 6.3.8-4. The implementation details are described in Section 6.3.8.3.

Radionuclide transport through each domain occurs by advection and diffusion. After the WP fails (breached by either general or localized corrosion, seismic damage, igneous intrusion or early failure mechanisms), a portion of the water that may flow through the DS could enter the WP, mobilizing radionuclides from the degraded waste form, and transporting these radionuclides into the UZ. Diffusion is the primary transport mechanism when the water flux into the WP is negligibly small or zero. Advective transport becomes important when there is

appreciable flow through the WP. When stress corrosion cracks are the only penetrations through the DS and WP, no advective transport can occur through them (SNL 2007 [DIRS 177407], Section 6.3.3.1.2.1, Table 8.1-2). Advective transport can only occur when there are corrosion patch failures or when the DS and WP are damaged by igneous intrusion or ruptured by a seismic event. Species-dependent free-water diffusion coefficients are applied that are corrected for tortuosity and temperature. The diffusion coefficient for the colloids is separately computed based on the sampled size of the colloids (SNL 2007 [DIRS 177407], Section 6.3.4.4).

Conceptually, the waste form domain represents that portion of the fuel that has degraded to rind (alteration product), along with the associated corrosion products from degradation of the steel that are present in the domain. Within the waste form domain, a number of processes occur. The waste form degradation processes include dissolution of SNF and HLW glass (Section 6.3.7.4), rapid degradation of DSNF, and formation of waste form colloids from the alteration of HLW glass and SNF (Section 6.3.7.6). Radionuclides may be reversibly sorbed or embedded irreversibly in the waste form colloids. The amount of each radionuclide mobilized from a waste form is limited by the solubility of the radionuclide in water (Section 6.3.7.5) and the amount of the radionuclide associated with suspended colloids (Section 6.3.7.6). Colloids may be important to the total system performance because they can increase the mass release of radionuclides from the WP. Both dissolved and colloid-associated radionuclide mass are transported by advection and/or diffusion to the WP corrosion products domain.

The CDSP WP has two fuel types (HLW and DSNF) and thus the CDSP waste form domain is divided into two subdomains, one for the HLW and the other for DSNF. This is required because a CDSP WP consists of five cylindrical canisters containing HLW glass logs surrounding a central canister of DSNF. After the WP is breached, the HLW glass degrades at a specified rate to a clay-like alteration product. However, the DSNF degrades almost instantaneously to oxides and hydrated oxides of uranium. In addition to the ongoing fuel degradation, the steel support framework inside the inner vessel of the WP will corrode gradually, allowing the HLW glass logs to collapse slowly within the inner vessel, such that the general cylindrical shape of the glass logs is retained. On the other hand, because DSNF degrades almost instantaneously, and with no credit taken for the canister, it is expected that DSNF will not retain its cylindrical geometry, and may settle to the bottom of the interior of the inner vessel. With this assumption of the internal configuration of a degraded CDSP WP, two separate waste form subdomains are conceptualized, one for HLW and the other for DSNF. The transport characteristics are expected to be different in each waste form subdomain. Because the EBS Transport Submodel is a one-dimensional model, the two waste form subdomains are modeled sequentially, such that the HLW domain is upstream of the DSNF domain. The mass released from the degradation of HLW glass moves to the DSNF domain by advection and/or diffusion and then is transported to the corrosion products domain. Because of the one-dimensional assumption, each waste form subdomain and the corrosion products domain have the same seepage flux.

Conceptually, the corrosion products domain is composed of corroded internal components of the WP, predominantly from the inner vessel and TAD canister. The internal components of a breached WP will degrade slowly over tens of thousands of years, forming corrosion products (assumed to be iron oxyhydroxides) that can sorb and delay the release of radionuclides from the

WP (SNL 2007 [DIRS 177407], Sections 6.3.4.2 and 6.5.1.2). Degradation of the internal WP components results in two types of materials: (1) stationary iron oxyhydroxide corrosion products that are assumed to remain in the WP, and (2) iron oxyhydroxide colloids that are mobile and can move out of the WP. The primary interactions with the corrosion products are equilibrium and kinetic sorption of dissolved radionuclide species onto the stationary corrosion products and iron oxyhydroxide colloids. The sorption parameters are developed from a mechanistic surface-complexation-based competitive sorption model that is applicable over the range of pH and  $P_{CO_2}$  expected in the repository over the simulation timescales. Dissolved species also undergo reversible sorption onto groundwater (seepage-water) colloids and waste form colloids that are passing through the corrosion products domain. Radionuclides are transported by advection and diffusion from the corrosion products domain to the invert domain.

In the invert domain of the EBS Transport Submodel, radionuclide transport occurs by both advection and diffusion and the mass flux of radionuclides (in both the dissolved state and associated with colloids) is passed to the UZ. Reversible sorption of radionuclides on the crushed tuff is also considered. The EBS-UZ Interface domain is conceptualized to apply an effective semi-infinite zero-concentration boundary condition for computing the diffusive flux from the invert to the UZ. It is also used to calculate the mass fraction going into the UZ fracture and matrix continua.

In all of the EBS domains, there are additional parameters that influence the release of radionuclide mass from each domain. For example, the water volume, porosity, water saturation, cross-sectional area for diffusion, diffusive path length, temperature, relative humidity, and chemistry affect the rate of advective and diffusive transport of radionuclides through the EBS domains. The concentration of dissolved species may also be solubility limited, which could result in precipitation of radionuclide mass if the solubility limit is reached. Radionuclide transport is assumed not to occur when the temperatures are greater than 100°C (the boiling point of water) due to a lack of bulk water and a continuous film of water. However, below this temperature, a continuous thin film of adsorbed water is assumed to behave as bulk liquid in order to allow radionuclides to dissolve and diffuse through it (SNL 2007 [DIRS 177407], Section 5.5).

### **6.3.8.2 Abstraction**

The EBS Transport Submodel calculates the time-dependent rate of radionuclide releases from the EBS to the UZ. The mass of each radionuclide at any particular location is dependent on the transport characteristics of the radionuclide, the quantity of the radionuclide remaining at its source, the extent of radioactive decay or ingrowth associated with a particular radionuclide, and the diffusive area and diffusive length in a given domain. The continuum mass balance equations for the EBS Transport Submodel are described and developed in *EBS Radionuclide Transport Abstraction* (SNL 2007 [DIRS 177407], Section 6.5.1.2). These equations represent one-dimensional mass balance for:

- Transport of dissolved radionuclide species and radionuclide species that are reversibly sorbed onto three types of colloids: iron oxyhydroxide, waste form, and groundwater

- Transport of kinetically (and irreversibly) sorbed radionuclide species on iron oxyhydroxide colloids
- Kinetic sorption of radionuclide species onto stationary corrosion products in the WP
- Transport of embedded (irreversibly sorbed) radionuclide species in waste form colloids
- Decay and ingrowth for a given radionuclide.

Implementation of the three-domain EBS Abstraction requires that the following properties be specified for each domain: the domain water volume, volumetric flow rate, water saturation, porosity, diffusive area, diffusive path length, and diffusion coefficient. Note that species-dependent free water diffusion coefficients are used in each domain for dissolved radionuclides while a separate diffusion coefficient is computed for transport of radionuclides associated with colloids based on the sampled size of the colloids (SNL 2007 [DIRS 177407], Section 6.3.4.4). In addition, the diffusion coefficients are corrected for tortuosity and temperature. The preceding properties may vary among the dripping and non-dripping environments for each fuel type and WP (CSNF and CDSP WPs), the invert, and the EBS-UZ Interface. The advective or diffusive transport pathways and transport processes included in the EBS Transport Submodel of the TSPA-LA Model are summarized in Table 6.3.8-1. The parameters that define the transport of radionuclides through the waste form and the corrosion products domains, as discussed in the following sections, are summarized in Table 6.3.8-2. Table 6.3.8-3 and Table 6.3.8-4 summarize various sampled parameters used in the EBS Transport Submodel, with the ranges and distributions for each parameter provided. Table 6.3.8-5 provides the UZ fracture and matrix saturation and flux inputs for the four glacial transition climates (gt10, gt30, gt50, and gt90) and four post-10,000-year climates (pk10, pk30, pk50, and pk90) used in the EBS-UZ Interface model in each of the five percolation subregions (PS1, PS2, PS3, PS4, and PS5). Table 6.3.8-6 summarizes the parameters used in the rind volume calculation from the degradation of CSNF. The general modeling approach and properties used to calculate radionuclide transport in each of the domains are detailed in the following sections.

#### **6.3.8.2.1 Commercial Spent Nuclear Fuel Waste Form Domain**

The CSNF waste form domain represents material inside the TAD canister, which includes fuel rods, basket tubes, and absorbed plates, which may degrade once the WP is breached (Figure 6.3.8-5).

Transport out of the waste form domain can occur by advection, when there is liquid flow through the WPs, and by diffusion, through continuous thin water films assumed to be present in the WPs when temperatures are less than 100°C. Diffusion can occur in both dripping and non-dripping environments. In addition to being transported in the dissolved state, radionuclides in the CSNF waste form domain can be transported via waste form colloids and groundwater colloids. Two different waste form colloids are generated by the degradation and alteration of CSNF and have different stability fields and concentrations. One is modeled to only include embedded plutonium and americium, which are considered as intrinsic parts of the colloids and, thus, not in equilibrium with the aqueous system. These embedded radionuclides are modeled as

irreversibly attached to the host colloids. The second waste form colloid type is modeled to undergo only reversible sorption similar to groundwater colloids.

Solving the mass transport equations requires that the following properties be defined at the beginning of the timestep: (1) the volume of water in the domain, (2) the diffusive area of the domain, (3) the diffusive length of the domain, (4) diffusion coefficients, and (5) advective flow rates.

**CSNF Waste Form Water Volume**—The cladding degradation abstraction (SNL 2007 [DIRS 180616], Section 6.2.4) estimates the rind water volume for both dripping and non-dripping cases. The volume of water in the rind as a function of time is given by:

$$V_w(t) = \phi_{CSNF} S_{CSNF} V_{rr}(t) N_f(t) \quad (\text{Eq. 6.3.8-1})$$

where

- $V_w(t)$  = time-dependent volume of water in rind ( $\text{m}^3$ )
- $\phi_{CSNF}$  = porosity of the CSNF rind material (schoepite)
- $S_{CSNF}$  = saturation of the CSNF rind material (schoepite)
- $V_{rr}(t)$  = time-dependent volume of rind in a fuel rod ( $\text{m}^3$ )
- $N_f(t)$  = number of failed rods as a function of time.

The porosity of the waste form rind is an epistemic uncertain parameter, sampled from a uniform distribution between 0.05 and 0.3 (Table 6.3.8-6). The time-dependent number of failed fuel rods,  $N_f(t)$ , is not needed as all the rods are assumed to be failed, as there is no credit taken for the cladding in the base-case calculations (Section 6.3.7.3).

The volume of rind in a rod,  $V_{rr}(t)$ , is (SNL 2007 [DIRS 180616], Table 6-4, Equation 6-7):

$$V_{rr}(t) = \frac{V_{init} F_{cor}(t) V_{rm}}{N_f(t)} \quad (\text{Eq. 6.3.8-2})$$

where

- $V_{init}$  = initial volume of fuel in a WP ( $\text{m}^3$ )
- $F_{cor}(t)$  = time-dependent fraction of total corroded waste form inventory
- $V_{rm}$  = rind volume multiplier.

The initial volume of fuel in a CSNF WP is calculated as the product of the number of fuel rods in a CSNF WP and the volume of a single undegraded fuel rod (SNL 2007 [DIRS 180616], Table 6-4, Equation 6-4). The time-dependent fraction of total corroded (degraded) waste form inventory,  $F_{cor}$ , is calculated within the TSPA-LA Model using Equation 6.3.7-7 (Section 6.3.7.4.1.3).

For the purposes of modeling the rind formation, the CSNF matrix and schoepite inside a failed cladding rod are abstracted as concentric cylinders, with the fuel matrix modeled as a receding inner cylinder and with the schoepite modeled as an expanding outer cylinder, constrained by a split cladding rod (Figure 6.3.8-5). The rind volume multiplier,  $V_{rm}$ , accounts for the increase in volume associated with rind development due to density change between fuel matrix ( $\text{UO}_2$ ) and schoepite. This multiplier is proportional to the differences in density and molecular weight of the intact fuel and schoepite (SNL 2007 [DIRS 180616], Table 6-4, Equation 6-3):

$$V_{rm} = \left( \frac{MW_{sch}}{MW_{\text{UO}_2}} \right) \frac{\rho_{\text{UO}_2}}{(1 - \phi_{sch}) \rho_{sch}} \quad (\text{Eq. 6.3.8-3})$$

where

$MW_{sch}$  = molecular weight of schoepite (g/mol)

$MW_{\text{UO}_2}$  = molecular weight of  $\text{UO}_2$  (g/mol)

$\rho_{\text{UO}_2}$  = density of  $\text{UO}_2$  (g/cm<sup>3</sup>)

$\rho_{sch}$  = density of schoepite (g/cm<sup>3</sup>).

The parameters used in the TSPA-LA Model abstraction for CSNF rind volume are given in Table 6.3.8-6. The total bulk volume of the CSNF domain is the sum of the rind volume and the volume of basket tube and absorber plate steel corrosion products, which also increase over time:

$$V_{CSNF}(t) = V_{rind,CSNF}(t) + V_{CP,CSNF}(t). \quad (\text{Eq. 6.3.8-4})$$

The rind volume in a CSNF WP ( $V_{rind,CSNF}$ ) is calculated by multiplying the volume of rind in a rod ( $V_{rr}$ ) by the number of failed rods. The bulk volume of CSNF domain corrosion products is (SNL 2007 [DIRS 177407], Equation 6.5.2.2.2.1-4):

$$V_{CP,CSNF}(t) = \left( \frac{1}{1 - \phi_{CP}} \right) \sum_{CPm} \left[ \frac{m_{CPm,CS,CSNF}(t) + m_{CPm,SS,CSNF}(t)}{\rho_{CPm}} \right]. \quad (\text{Eq. 6.3.8-5})$$

where  $\phi_{CP}$  is the steel corrosion products porosity (a constant value of 0.4),  $m_{CPm,CS,CSNF}$  is the mass of corrosion products from degradation of carbon steel (zero for CSNF),  $m_{CPm,SS,CSNF}$  is the mass of corrosion products from degradation of stainless steel,  $\rho_{CPm}$  is the grain density of corrosion products, and subscript  $m$  refers to the metal type (iron or nickel or chromium) in the steel from which the type of corrosion products is formed (goethite, ferrihydrite, NiO,  $\text{Cr}_2\text{O}_3$ ).

The pore volume in the CSNF waste form domain is the sum of CSNF rind pore volume and steel corrosion products pore volume:

$$V_{\phi,CSNF}(t) = \phi_{CSNF} V_{rind,CSNF}(t) + \phi_{CP} V_{CP,CSNF}(t), \quad (\text{Eq. 6.3.8-6})$$

where the CSNF rind porosity,  $\phi_{CSNF}$ , is a sampled parameter.

The effective porosity of the CSNF waste form domain, which is needed for computing the diffusion coefficient using Archie's law, is time dependent because the pore volume and bulk volume of the domain are time dependent:

$$\phi_{CSNF}(t) = \frac{V_{\phi,CSNF}(t)}{V_{CSNF}(t)}. \quad (\text{Eq. 6.3.8-7})$$

The water volume in the CSNF waste form domain is the sum of CSNF rind water volume and steel corrosion products water volume:

$$V_{w,CSNF}(t) = \phi_{CSNF} S_{w,rind,CSNF} V_{rind,CSNF}(t) + \phi_{CP} S_{w,CP,CSNF} V_{CP,CSNF}(t). \quad (\text{Eq. 6.3.8-8})$$

The saturation of the rind and corrosion products is determined separately, when there is no flow through the WP, using separate water vapor adsorption isotherms that are functions of relative humidity and specific surface areas, among other parameters. The calculations are described in Section 6.5.2.2 of the *EBS Radionuclide Transport Abstraction* (SNL 2007 [DIRS 177407]). Since the adsorption isotherm functions are unbounded as relative humidity (*RH*) approaches 1.0, the saturation is limited to a value of 1.0. Under flowing conditions through the WP, complete saturation of the pore space is assumed. The effective water saturation for the CSNF waste form domain is given by:

$$S_{w,CSNF}(RH) = \min \left[ \frac{V_{w,CSNF}(RH, t)}{V_{\phi,CSNF}(t)}, 1.0 \right]. \quad (\text{Eq. 6.3.8-9})$$

**CSNF Waste Form Diffusive Area and Length**—The area through which radionuclides may diffuse after being released from fuel rods depends on the state of the waste form. No credit is taken for the fuel rod cladding, so once a WP is breached, all of the SNF is modeled as exposed to the environment inside the WP. As a result, the diffusive area for the waste form domain is based on the radial geometry inside the WP that is bounded by the TAD canister. Since the diffusive area increases with increasing distance from the origin point in the radial geometry, the area of the CSNF waste form domain is taken at half the radius of the TAD canister (Figure 6.3.8-5) and set at a constant value of 12.5 m<sup>2</sup> (Table 6.3.8-2). The diffusive path length is set to be the inside radius of the TAD canister (= 0.819 m) (Table 6.3.8-2). In calculating the diffusive conductance across the interface between the CSNF waste form domain and the downstream corrosion products domain the harmonic average of the diffusive areas and diffusive lengths of the two domains is considered. The radial transport is modeled in the Cartesian coordinates in a one-dimensional model by specifying the diffusive areas and lengths consistent with the radial geometry (SNL 2007 [DIRS 177407], Appendix L).

**Calculation of Diffusion Coefficients in the CSNF Waste Form Domain**—Diffusion coefficients for dissolved radionuclides in the CSNF waste form domain are calculated using Archie's law. This approach implicitly includes the effects of porosity, saturation, and tortuosity in calculating an effective diffusion coefficient for a porous medium. For the CSNF waste form domain, Archie's law is expressed as (SNL 2007 [DIRS 177407], Equation 6.3.4.3.5-2):

$$\phi_{CSNF} S_{w,CSNF} D_{WF} = D_{wi} \phi_{CSNF}^{1.3} S_{w,CSNF}^2 \quad (\text{Eq. 6.3.8-10a})$$

where

$D_{WF}$  = effective diffusion coefficient that includes the effect of tortuosity in a porous medium (cm<sup>2</sup>/s)

$D_{wi}$  = species dependent free water diffusion coefficient (cm<sup>2</sup>/s)

$\phi_{CSNF}$  = porosity of domain

$S_{w,CSNF}$  = liquid saturation of the domain (fraction).

After the effective diffusion coefficient has been calculated using Equation 6.3.8-10a, it is modified to account for temperature effects. The diffusion coefficient at a given temperature is given as (SNL 2007 [DIRS 177407], Equation 6.3.4.1.2-4):

$$D_T = D_{T_0} \frac{T}{T_0} 10^{\left[ \frac{1.3272(293.15-T_0) - 0.001053(T_0 - 293.15)^2}{T_0 - 168.15} \right] - \left[ \frac{1.3272(293.15-T) - 0.001053(T - 293.15)^2}{T - 168.15} \right]} \quad (\text{Eq. 6.3.8-10b})$$

where

$D_T$  = effective diffusion coefficient at temperature  $T$  (cm<sup>2</sup>/s)

$D_{T_0}$  = diffusion coefficient at temperature  $T_0$  (as calculated by Equation 6.3.8-10a) (cm<sup>2</sup>/s)

$T$  = invert temperature (K)

$T_0$  = reference temperature (298.15 K).

**Advective Transport in the CSNF Waste Form Domain**—Advective transport out of the waste form domain and into the corrosion products domain can only occur when there is liquid flow through the WPs. The EBS Flow Submodel determines the flux through the WP (flow pathway 4 on Figure 6.3.6-4) based on the flux through the DS, the damage fraction on a WP, and a WP flux-splitting logic (Section 6.3.6). Advective flux to the WPs is only possible when the DSs are breached. Details regarding the calculation of the flow through the WP are given in the EBS Flow Submodel (Section 6.3.6.2). If the only breaches in a WP are stress corrosion cracks, advective transport through the WP does not occur, but diffusion of radionuclides out of the WP could still take place.

### 6.3.8.2.2 Co-Disposed Waste Form Domain

As conceptualized in Section 6.3.8.1, the CDSP waste form domain is divided into two subdomains, one for the HLW glass and another for the DSNF. The two waste form subdomains are modeled sequentially, such that the HLW subdomain is upstream of the DSNF subdomain as described in Section 6.3.8.1. The mass released from the degradation of HLW glass moves to the DSNF domain by advection and/or diffusion and is then transported to the corrosion products domain. Radionuclide concentrations are subject to the solubility constraints defined by the Dissolved Concentration Limits Submodel (Section 6.3.7.5).

In addition to being transported in the dissolved state, radionuclides in the HLW subdomain can be transported via waste form colloids. These colloids are generated by the degradation and alteration of HLW glass and include embedded plutonium and americium, which are considered as intrinsic parts of the colloids and, thus, not in equilibrium with the aqueous system. These embedded radionuclides are modeled as irreversibly attached to the host colloids. Reversible sorption onto waste form colloids is also considered for various radionuclides. Details of the waste form colloid generation, stability, and sorption capability are given in Section 6.3.7.6.2.

Transport out of the CDSP waste form subdomains can occur by advection, when there is liquid flow through the WPs, and by diffusion, through continuous thin water films assumed to be present in the WPs. Diffusion can occur in both dripping and non-dripping environments. Solving the mass transport equation requires that the following properties be defined: (1) the volume of water in the degraded fuel, (2) the diffusive areas of the domains, (3) the diffusive length of the domains, (4) diffusion coefficients; (5) sorbent mass, and (6) advective flow rates. The diffusive areas through various subdomains are shown on Figure 6.3.8-6.

**HLW Waste Form Water Volume**—The HLW glass degradation abstraction (BSC 2004 [DIRS 169988]) estimates the rind water volume for both dripping and non-dripping cases. The rind volume in the altered rind is provided by the expression (BSC 2004 [DIRS 169988], Section D.1, Equation D-3b):

$$V_{rind,HLWG}(t) = \frac{1}{\rho_G} \sum M_t \quad (\text{Eq. 6.3.8-11})$$

where

$V_{rind,HLWG}$  = bulk rind volume (m<sup>3</sup>)

$\rho_G$  = the bulk HLW glass density (kg/m<sup>3</sup>)

$\sum M_t$  = total mass of degraded HLW glass up to time  $t$  (kg).

Because the properties of the HLW glass and the clay making up the rind layer are similar, Equation 6.3.8-11 assumes that a degraded volume of glass generates an equal volume of clay as the rind layer (BSC 2004 [DIRS 169988], Section D.2). Therefore, the glass density ( $2,700 \text{ kg/m}^3$ ) is the same for the unreacted glass and the clay alteration products (DTN: MO0502ANLGAMR1.016\_R0 [DIRS 172830], Table 8-1). The total mass of glass degraded over a timestep of size  $\Delta t$  is provided by the HLW Glass Waste Form Degradation Submodel (Section 6.3.7.4.3).

The total bulk volume of the HLW subdomain is the sum of the rind bulk volume and the bulk volume of corrosion products from degradation of steel canisters encasing the fuel, which also increase over time:

$$V_{HLWG}(t) = V_{rind,HLWG}(t) + V_{CP,HLWG}(t). \quad (\text{Eq. 6.3.8-12})$$

The bulk volume of HLW domain corrosion products is (SNL 2007 [DIRS 177407], Section 6.5.2.2):

$$V_{CP,HLWG}(t) = \left( \frac{1}{1 - \phi_{CP}} \right) \sum_{CPm} \left[ \frac{m_{CPm,CS,HLWG}(t) + m_{CPm,SS,HLWG}(t)}{\rho_{CPm}} \right]. \quad (\text{Eq. 6.3.8-13})$$

where  $\phi_{CP}$  is the steel corrosion products porosity (a constant value of 0.4),  $m_{CPm,CS,HLWG}$  is the mass of corrosion products from degradation of carbon steel,  $m_{CPm,SS,HLWG}$  is the mass of corrosion products from degradation of stainless steel,  $\rho_{CPm}$  is the grain density of corrosion products, and subscript  $m$  refers to the type of corrosion products formed (goethite, ferrihydrite, NiO, Cr<sub>2</sub>O<sub>3</sub>).

The pore volume in the HLW waste form domain is the sum of HLW rind pore volume and steel corrosion products pore volume:

$$V_{\phi,HLWG}(t) = \phi_{rind} V_{rind,HLWG}(t) + \phi_{CP} V_{CP,HLWG}(t), \quad (\text{Eq. 6.3.8-14})$$

where  $\phi_{rind}$  is the rind porosity given by a constant value of 0.17 (DTN: SN0703PAEBSRTA.001\_R3 [DIRS 183217], Table 8.2-6).

The effective porosity of the HLW waste form domain, which is needed for computing the diffusion coefficient using Archie's law, is time dependent because the pore volume and bulk volume of the domain are time dependent:

$$\phi_{HLWG}(t) = \frac{V_{\phi,HLWG}(t)}{V_{HLWG}(t)}. \quad (\text{Eq. 6.3.8-15})$$

The water volume in the HLW waste form domain is the sum of HLW rind water volume and steel corrosion products water volume:

$$V_{w,HLWG}(t) = \phi_{rind} S_{w,rind,HLWG} V_{rind,HLWG}(t) + \phi_{CP} S_{w,CP,HLWG} V_{CP,HLWG}(t) \quad (\text{Eq. 6.3.8-16})$$

The saturation of the rind and corrosion products is determined separately, when there is no flow through the WP, using separate water vapor adsorption isotherms that are functions of relative humidity and specific surface areas, among other parameters. The calculations are described in *EBS Radionuclide Transport Abstraction* (SNL 2007 [DIRS 177407], Section 6.5.2.2). Since the adsorption isotherm functions are unbounded as the relative humidity approaches one, the saturation is limited to a value of one. Under flowing conditions through the WP, complete saturation of the pore space is assumed.

The effective water saturation for the HLW waste form domain is given by:

$$S_{w,HLWG}(RH) = \min \left[ \frac{V_{w,HLWG}(RH,t)}{V_{\phi,HLWG}(t)}, 1.0 \right]. \quad (\text{Eq. 6.3.8-17})$$

**DSNF Waste Form Water Volume**—The water volume of the DSNF waste form is computed by multiplying the initial volume of DSNF in a CDSP WP, which is equal to 1 m<sup>3</sup> (BSC 2004 [DIRS 172453], Section 8.1), by its porosity and saturation. The porosity of DSNF rind is assumed to be 0.2, as degraded DSNF is conceptualized to be a porous medium (SNL 2007 [DIRS 177407], Section 6.5.2.1.2). The total bulk volume of the DSNF waste form subdomain is the sum of the rind volume and the volume of corrosion products from degradation of associated steel (Section 6.3.8.1), which also increases with time. The equations used for calculating the bulk volume, pore volume, effective porosity, water volume, and effective saturation are the same as those shown for CSNF.

**HLW Waste Form Diffusive Area and Length**—Consistent with the treatment for the CSNF waste form domain, radionuclides will tend to diffuse radially outward from the HLWG waste form subdomain. Since the diffusive area increases with increasing distance from the origin point in the radial geometry, the area of the HLW waste form domain is taken at half the radius of the inner vessel cavity (Figure 6.3.8-6) and set at a constant value of 13.7 m<sup>2</sup> (Table 6.3.8-2). The diffusive path length is set to be the inside radius of inner vessel of a CDSP WP (= 0.941 m) (Table 6.3.8-2). In calculating the diffusive conductance across the interface between the HLW waste form subdomain, and the downstream DSNF waste form subdomain the harmonic average of the diffusive areas and diffusive lengths of the two domains is used.

**DSNF Waste Form Diffusive Area and Length**—DSNF is modeled as degrading instantaneously upon WP breach. Since the carbon steel support tube, divider plates, and brackets that support the HLWG canisters surrounding the DSNF also degrade rapidly (compared to the degradation rates of HLWG and stainless steel inner vessel), the DSNF is not expected to retain its initial cylindrical shape, but rather will settle to the bottom of the interior of the inner vessel. In the 1-D EBS Transport Model, this implies that the DSNF diffusive area is the same as for the HLWG waste form subdomain (= 13.7 m<sup>2</sup>) (Table 6.3.8-2). The effective diffusive path length is calculated by dividing the initial volume of DSNF 1 m<sup>3</sup> by the diffusive area leading to a total diffusive length of 0.0730 m (Table 6.3.8-2).

**Calculation of Diffusion Coefficients in the CDSP Waste Form Domain**—The effective diffusion coefficient for dissolved radionuclides in the HLW and DSNF subdomain is computed using Archie's law (Equation 6.3.8-10a and b). Both subdomains are considered to be fully saturated when there is flow through the WP. The diffusion coefficient for the colloids is separately computed based on the sampled size of the colloids (SNL 2007 [DIRS 177407], Section 6.3.4.4).

**Advective Transport in the CDSP Waste Form Domain**—The HLW and DSNF waste form subdomains are modeled sequentially, such that the HLW subdomain is upstream of the DSNF subdomain. Because of the one-dimensional model geometry, the DSNF waste form subdomain sees the same water flux as the HLW waste form subdomain. The advective transport out of the HLW waste form subdomain and into the DSNF waste form subdomain can only occur when there is liquid flow through the WPs. The EBS Flow Submodel determines the flux through the WP (Section 6.3.6).

### 6.3.8.2.3 Corrosion Products Domain

The corrosion products domain represents that portion of the internal components of a WP that has degraded after the WP is breached (Section 6.3.8.1 for the steel components included in this domain). Degradation of the internal WP components results in two types of materials: (1) stationary iron oxyhydroxide corrosion products that are assumed to remain in the WP, and (2) iron oxyhydroxide colloids that are mobile and can move out of the WP. Although only iron oxyhydroxide colloids are generated in this domain, waste form colloids (generated from HLW degradation) and groundwater colloids (from seepage waters) can also be present.

A surface complexation-based competitive sorption model is developed for modeling sorption of dominant actinides in the inventory (uranium, neptunium, plutonium, americium, and thorium) to the iron oxyhydroxide surfaces. It is a mechanistic model based on a single-site diffuse-layer surface complexation model that couples the pH in the corrosion products domain with the type of surface complexes formed under varying chemical conditions and sorption site densities. The model is applicable to a wide range of concentrations and accounts for competition among various actinides for the finite number of sorption sites. The composition of the steel corrosion products is difficult to predict as it will vary over time but it is expected to be dominantly a mixture of iron oxyhydroxides (such as goethite, ferrihydrite, and hematite), chromium oxides, and nickel oxides. For the purposes of modeling radionuclide sorption on steel degradation products (stationary corrosion products and mobile colloids), only the iron oxyhydroxides are considered, which are assumed to be a mixture of goethite and ferrihydrite, the proportion of which is treated as uncertain. It should be noted that the pure iron oxide surface properties are used to model sorption onto what will in reality be a solid solution of Fe(III), Cr(III), and Ni(II). The details of the model development are described in *EBS Radionuclide Transport Abstraction* (SNL 2007 [DIRS 177407], Section 6.5.2.4).

The mass of corrosion products in a breached WP varies over time, from zero when the WP is first breached to a maximum amount (SNL 2007 [DIRS 177407], Table 6.3-8) when all of the steel in the domain is corroded. The mass, at any given time, is computed by linearly interpolating over the lifetime of each of the two major types of steel comprising the internal components of a WP—carbon steel and stainless steel. The equations used to calculate the

time-dependent mass of corrosion products, present in the corrosion products domain, are developed in *EBS Radionuclide Transport Abstraction* (SNL 2007 [DIRS 177407], Section 6.5.2.2.1). Note that only the mass of corrosion products contributed by goethite and ferrihydrite is used in competitive sorption calculations of radionuclides, while for water vapor adsorption calculations the entire mass of corrosion products is used, including nickel oxides and chromium oxides. The corrosion products mass from degradation of steel shield plug in the TAD canister is not considered in the TSPA as the mass is localized at one end of the WP and will not appreciably affect transport throughout the rest of the WP. A minimum initial mass of 10 kg of stationary corrosion products is assumed, as it is required to initiate the water volume and sorption calculations after the WP failure.

**Corrosion Products Domain within a CSNF WP**—Both advective and diffusive transport can occur from the corrosion products domain to the invert domain. Solving the mass transport equations requires that the following properties be defined: (1) mass of corrosion products, (2) volume of water in the corrosion products, (3) diffusive area of the domain, (4) diffusive length of the domain, and (5) advective flow rate.

**CSNF Corrosion Products Water Volume**—The volume of water in the CSNF corrosion products domain is calculated as the product of the pore volume and water saturation of the corrosion product mass. The pore volume of the corrosion products is calculated by the expression (SNL 2007 [DIRS 177407], Section 6.5.2.2.1)

$$V_{\phi,CP}(t) = \left( \frac{\phi_{CP}}{1 - \phi_{CP}} \right) \sum_{CPm} \left[ \frac{m_{CPm,CS}(t) + m_{CPm,SS}(t)}{\rho_{CPm}} \right] \quad (\text{Eq. 6.3.8-18})$$

where,  $\phi_{CP}$  is the steel corrosion products porosity (a constant value of 0.4),  $m_{CPm,CS}$  is the mass of corrosion products from degradation of carbon steel,  $m_{CPm,SS}$  is the mass of corrosion products from degradation of stainless steel,  $\rho_{CPm}$  is the grain density of corrosion products, and subscript 'm' refers to the type of corrosion products formed (goethite, ferrihydrite, NiO, and Cr<sub>2</sub>O<sub>3</sub>).

When there is flow through the WP, the water saturation is assigned a value of 1.0 (SNL 2007 [DIRS 177407], Section 6.5.2.2). In conditions when there is no flow through the WP, the only water present is adsorbed water and the water saturation in the domain for each type of corrosion product (goethite, ferrihydrite, NiO, and Cr<sub>2</sub>O<sub>3</sub>) is computed separately as given by (SNL 2007 [DIRS 177407], Section 6.5.2.2.1):

$$S_{w,CPm}(RH) = \min \left[ t_f \rho_{CPm} \bar{s}_{CPm} \left( \frac{1 - \phi_{CP}}{\phi_{CP}} \right) \theta_{CP}(RH), 1.0 \right] \quad (\text{Eq. 6.3.8-19})$$

where

$S_{w,CPm}$  = effective water saturation of corrosion products (fraction)

$\bar{s}_{CPm}$  = specific surface area of corrosion products (m<sup>2</sup>/kg)

- $\rho_{CPm}$  = corrosion products grain density (kg/m<sup>3</sup>)  
 $\theta_{CP}$  = number of monolayers of water adsorbed on the surface of corrosion products; a function of relative humidity  
 $t_f$  = thickness of a monolayer of water (m)  
 $RH$  = relative humidity (fraction).

A single adsorption isotherm is used for all corrosion products, so a single relative humidity-dependent value of  $\theta_{CP}(RH)$  is used for all corrosion products in this domain. The water volume for the entire domain is calculated as:

$$V_{w,CP}(RH, t) = \sum_m V_{\phi,CPm}(t) S_{w,CPm}(RH) \quad (\text{Eq. 6.3.8-20})$$

The water saturation for the entire domain is calculated as:

$$S_{we,CP}(RH) = \min \left[ \frac{V_{w,CP}(RH, t)}{V_{\phi,CP}(t)}, 1.0 \right] \quad (\text{Eq. 6.3.8-21})$$

**CSNF Corrosion Products Diffusive Area and Length**—Since the WP outer barrier undergoes variable damage specified by the scenario classes and modeling cases, the corrosion products domain is divided into two regions: (a) the region that only includes the outer barrier and (b) the region that includes the TAD canister and inner vessel but excludes the outer barrier. The diffusive area for the path excluding the outer barrier is given by the surface area of a cylinder halfway between the inside surface of the TAD canister and the outside surface of the inner vessel (= 29.9 m<sup>2</sup>) (Table 6.3.8-2), while the diffusive path length is given by the distance from the inside of the TAD canister to the outside of the inner vessel (= 0.0914 m) (Table 6.3.8-2). The diffusive area for the path through the outer barrier of the WP is taken to be the smaller of either: (a) the WP breached area (scenario class dependent) or (b) the surface area of a cylinder at the midpoint between the inner vessel outer surface and the outer surface of the CSNF WP outer barrier (= 33.1 m<sup>2</sup>) (Table 6.3.8-2). The diffusive path length through the outer barrier is the radial distance from the outside of the inner vessel to the outside of the outer barrier (= 0.0302 m) (Table 6.3.8-2).

**Calculation of Diffusion Coefficients in the CSNF Corrosion Products Domain**—The diffusion coefficient of the corrosion products is computed using Archie's law (Equation 6.3.8-10a, b) with the porosity of the corrosion products (0.4) and an assigned water saturation as discussed earlier.

**Advective Transport in the CSNF Corrosion Products Domain**—Advective transport through the CSNF corrosion products domain can only occur when there is liquid flow through the WPs. The EBS Flow Submodel determines the flux through the WP (Section 6.3.6).

**Corrosion Products Domain within a CDSP WP**—The CDSP corrosion products domain consists of corroded internal WP components (Section 6.3.8.1 for the steel components included

in this domain). Both advective and diffusive transport can occur in the corrosion products domain. Solving the mass transport equations requires that the following properties be defined for each domain: (1) mass of corrosion products, (2) volume of water in the corrosion products, (3) diffusive area of the corrosion products domain, (4) diffusive length, and (5) advective flow rates.

The discussion presented for the corrosion products domain within a CSNF WP is applicable to CDSP WP except for parameter values such as mass of steel, diffusive lengths, and diffusive areas. Since the WP outer barrier undergoes variable damage specified by the scenario classes and modeling cases, the corrosion products domain, just like for CSNF, is divided into the region that only includes the outer barrier and the one that is inside the WP but excludes the outer barrier. The diffusive area for the path excluding the outer barrier is given by the surface area of a cylinder halfway between the inside surface and the outside surface of the inner vessel (= 29.7 m<sup>2</sup>) and diffusive path length is given by the thickness of the inner vessel (= 0.0508 m). The diffusive area for the path through the outer barrier of the WP is taken to be the smaller of either (a) the WP breached area (scenario class dependent) or (b) the surface area of a cylinder at the midpoint between the inner vessel outer surface and the outer surface of the CDSP WP outer barrier (= 32.6 m<sup>2</sup>). The diffusive path length through the outer barrier is the radial distance from the outside of the inner vessel to the outside of the outer barrier (= 0.0301 m).

#### 6.3.8.2.4 Invert Domain

The invert domain is conceptualized as a single continuum rather than as a dual continuum for modeling radionuclide transport. Both advective and diffusive transport can occur from the invert domain to the UZ. Sorption of radionuclides may occur on the crushed tuff in the invert and is modeled by the linear sorption isotherm approach using the distribution coefficient ( $K_d$ ). The ranges and distributions of radionuclide sorption coefficients for sorption on crushed tuff in the invert are the same as those for devitrified tuff implemented in the UZ Transport Submodel (Table 6.3.9-2). [Note: Since  $K_d$  for Se is set to zero for the TSw unit in the UZ Transport Submodel, the  $K_d$  for Se in the invert is also set to zero as most of the repository host rock is composed of TSw unit.] Solving the mass transport equations requires that the following properties be defined: (1) the volume of water in the invert, (2) the diffusive area of the invert domain, (3) the diffusive length, and (4) advective flow rates.

**Invert Domain Water Volume**—The water volume of the invert domain is calculated as the product of the bulk volume and the water content of the invert (SNL 2007 [DIRS 177407], Section 6.5.2.3). The total bulk invert volume is equal to the cross-section area of the invert times the length of a WP (CDSP or CSNF). The water content of the invert cell is calculated according to the following relationship (SNL 2007 [DIRS 177407], Equation 6.5.2.3-11):

$$\theta_{inv} = \theta_{inter} + (1 - \phi_{inter})\theta_{intra} \quad (\text{Eq. 6.3.8-22})$$

where

- $\theta_{inv}$  = invert water content
- $\theta_{inter}$  = water content of the intergranular invert
- $\phi_{inter}$  = porosity of the intergranular invert
- $\theta_{intra}$  = water content of the intragranular invert.

Because the crushed tuff invert has both intergranular and intragranular porosity, the bulk water content of the invert is calculated by combining the water contents of both pore types as shown in Equation 6.3.8-22. The intragranular water content is calculated by multiplying the intragranular water saturation with the intragranular porosity. The intragranular water saturation is provided by the MSTHM Abstraction from the EBS TH Environment Submodel (Section 6.3.2). The intergranular water saturation is calculated based on the seepage flux per cross-sectional area of the drift over the length of a WP (BSC 2004 [DIRS 167652], Section 6.3.1) by using the van Genuchten moisture retention relationship for the crushed tuff, as described in *EBS Radionuclide Transport Abstraction* (SNL 2007 [DIRS 177407], Section 6.5.2.3). The porosity of the intragranular continuum is 0.111 and that of the intergranular continuum is 0.224 (DTN: SN0703PAEBSRTA.001\_R3 [DIRS 183217], Table 8.2-6) and the residual water content of the intergranular continuum is 0.00224 (DTN: MO0703PAHYTHRM.000\_R1 [DIRS 182093]). The bulk density of the invert material is estimated to be 1842 kg/m<sup>3</sup> (DTN: MO0703PAHYTHRM.000\_R1 [DIRS 182093]).

**Invert Diffusive Length**—The true geometry of the invert is that of a segment of a circle where the top of the invert is flat and the bottom is formed by the arc of the drift. However, for the purposes of modeling flow and diffusion through the invert, the invert is regarded as having a rectangular cross section with the top being the actual top surface of the invert (Figure 6.3.8-7). The bulk volume of the invert is conserved by calculating an average thickness of the invert using the following equation (SNL 2007 [DIRS 177407], Equation 6.5.2.3-5):

$$\bar{t}_I = \frac{A_I}{w_I} = 0.934 \text{ m} \quad (\text{Eq. 6.3.8-23})$$

where

- $\bar{t}_I$  = average invert thickness (m)
- $A_I$  = actual invert vertical cross-sectional area (4.39 m<sup>2</sup>) (SNL 2007 [DIRS 177407], Section 6.5.2.3)
- $w_I$  = actual width of invert top surface (4.70 m) (SNL 2007 [DIRS 177407], Section 6.5.2.3).

The diffusive path length from the WP outer barrier to the mid-point of the invert is a sampled value between 0.3 m and 1.24 m to represent uncertainty in the location of the breach on the WP and the average thickness from the invert (Table 6.3.8-4). The diffusive length from the mid-

point of the invert to the interface with the host rock (part of EBS-UZ Interface domain) is taken to be half of the average invert thickness.

**Invert Diffusive Area**—The diffusive area implemented for the invert cell is the plan area of the rectangular invert. It is equal to the width of the invert top surface times the length of a WP (CDSP or CSNF).

**Calculation of Diffusion Coefficients in the Invert Domain**—The diffusion coefficient for dissolved radionuclides in the invert is computed using the following formulation of Archie's law (SNL 2007 [DIRS 177407], Equation 6.3.4.1.1-22):

$$\phi_{inv} S_w D = D_{wi} \theta_{inv}^{1.863} 10^{ND(\mu=0.033, \sigma=0.218)} \quad (\text{Eq. 6.3.8-24})$$

where

- $D$  = invert diffusion coefficient (cm<sup>2</sup>/s)
- $D_{wi}$  = species dependent free water diffusion coefficient (cm<sup>2</sup>/s)
- $S_w$  = invert water saturation
- $\phi_{inv}$  = bulk invert porosity
- $ND$  = truncated normal distribution ( $\pm 3$  SDs from the mean)
- $\mu$  = mean
- $\sigma$  = SD.

After the invert diffusion coefficient has been calculated using Equation 6.3.8-24, it is modified to account for temperature effects. The diffusion coefficient at a given temperature is given by (SNL 2007 [DIRS 177407], Equation 6.3.4.1.2-4)

$$D_T = D_{T_0} \frac{T}{T_0} 10^{\left[ \frac{1.3272(293.15-T_0) - 0.001053(T_0-293.15)^2}{T_0-168.15} \right] \left[ \frac{1.3272(293.15-T) - 0.001053(T-293.15)^2}{T-168.15} \right]} \quad (\text{Eq. 6.3.8-25})$$

where

- $D_T$  = invert diffusion coefficient at temperature  $T$  (cm<sup>2</sup>/s)
- $D_{T_0}$  = invert diffusion coefficient at temperature  $T_0$  (as calculated by Equation 6.3.8-24) (cm<sup>2</sup>/s)
- $T$  = invert temperature (K)
- $T_0$  = reference temperature (298.15 K).

**Advective Transport in the Invert Domain**—There are two sources of advective water flux into the invert domain. The first is the advective flux that comes from the overlying corrosion

products domain. This flux is defined by Flow Pathway  $F_6$  (flux into the invert) of the EBS Flow Submodel (Section 6.3.6.2). The other advective flux source is due to possible imbibition from the host rock that enters the invert and flows out under gravity. This imbibition flux is defined by Flow Pathway  $F_7$  (Section 6.3.6.2 and Figure 6.3.6-4). The EBS TH Environment Submodel (Section 6.3.2) provides the rate of water imbibition from the host rock that enters the invert and flows out under gravity.

**EBS-UZ Interface Domain**—The EBS-UZ Interface domain is included beneath the invert domain to establish a boundary condition for calculating the diffusive flux from the invert to the UZ and to compute the radionuclide mass flux fraction going into each of the UZ fracture and matrix continua. The EBS Transport Abstraction applies a semi-infinite zero-concentration boundary condition near the base of the drift (SNL 2007 [DIRS 177407], Section 6.5.2.6). This boundary condition is approximated by applying an effective zero-concentration boundary in the UZ at approximately three drift diameters below the invert-UZ boundary. In the EBS-UZ Interface domain, the near-field UZ is modeled as a dual continuum consisting of overlapping UZ-matrix and UZ-fracture continua. This approach is consistent with the dual-permeability modeling approach used by the UZ Transport Submodel, as described in *Particle Tracking Model and Abstraction of Transport Processes* (SNL 2008 [DIRS 184748], Section 1). The ranges and distributions of radionuclide sorption coefficients for sorption on the UZ matrix are the same as those for devitrified tuff implemented in the UZ Transport Submodel (Table 6.3.9-2). [Note: Since  $K_d$  for Se is set to zero for the TSw unit in the UZ Transport Submodel, the  $K_d$  for Se in the UZ matrix of the EBS-UZ Interface domain is also set to zero as most rock near the drift is composed of TSw unit.] Advective fluid flux defined by Flow Pathway  $F_6$  (combined seepage and condensation) is passed to the UZ fracture from the invert, while the advective flux due to imbibition from the host rock, defined by Flow Pathway  $F_7$ , is passed from the invert to the UZ matrix. Details of the implementation of the EBS-UZ Interface boundary condition are given in Section 6.3.8.3.

The radionuclide mass flux fractions going into the near-field UZ-matrix and UZ-fracture continua is calculated from the EBS-UZ Interface domain for each radionuclide species and passed to the UZ model along with the mass flux from the invert. The mass flux fraction varies as a function of time and may differ for each radionuclide species based on its transport characteristics. A detailed description of how the mass fractions are calculated is given in the next section.

### 6.3.8.3 TSPA-LA Model Implementation

The transport of radionuclides through the EBS is modeled in the TSPA-LA Model by spatially discretizing the EBS components into transport domains, as described in Section 6.3.8.1. In each domain, the four EBS transport one-dimensional continuum-form mass balance equations described at the beginning of Section 6.3.8.2 are approximated and solved using a finite-difference approach. The implementation and numerical solution of the EBS Transport Submodel's equations are performed using the GoldSim software cell pathway capability, available in the *GoldSim Contaminant Transport Module* (GoldSim Technology Group 2007 [DIRS 183214]). The number of cell pathways in the finite-difference network and the discretization of the cells are chosen in such a way as to capture the physical and chemical properties of the EBS components with respect to radionuclide transport. The cell pathway acts

as a batch reactor, where radionuclide mass is modeled as instantaneously and completely mixed and partitioned among all media, fluid or solid, within the cell. Both advective and diffusive transport mechanisms can be explicitly represented using the cell pathways. When multiple cells are linked together via advective and diffusive connections, the performance of the cell network is mathematically described using a coupled system of differential equations, and is mathematically equivalent to a finite-difference network. The GoldSim software numerically solves the coupled system of equations to compute the radionuclide mass present in each cell and the mass fluxes between cells as a function of time. Both initial and boundary conditions for a cell can be defined explicitly, and systems of varying geometry can be modeled.

This finite-difference approach used to solve the mass balance equations requires the discretization of the time derivative (or mass accumulation term) and the advective and diffusive terms for both dissolved and colloidal transport. The spatially dependent derivative terms, which include advective and diffusive transport, are discretized using implicit difference approximations. Using an implicit difference approximation, if the solution is known at timestep,  $n$ , and is to be computed at the next timestep,  $n+1$ , the advective/diffusive flux difference approximations use the concentrations at timestep  $n+1$ . Further, the source terms, such as radionuclide decay/ingrowth and reactions due to reversible sorption, are also represented implicitly. Therefore, the difference equations are fully implicit in the unknown cell concentrations. The difference equations have variable coefficients (e.g., water content), which can be both time and space dependent. These coefficients are evaluated at the start of the timestep. The resulting system of difference equations is a linear algebraic system in the unknown cell concentrations. A complete description of the discretized transport equations is provided by *EBS Radionuclide Transport Abstraction* (SNL 2007 [DIRS 177407], Section 6.5.2.5). Another consideration is the computational time requirement. An implicit solution technique is used because it provides an unconditionally stable solution (i.e., a solution is obtainable for any size timestep). A study of sensitivity to timestep selection is provided in Section 7.3.3. In addition, the GoldSim equation-solver software tests solution accuracy by applying several mass balance and convergence tests based on a GoldSim model file precision setting of high, medium, or low. All simulations for the TSPA-LA are run using the high-precision setting. If a solution in a given cell pathway fails to meet the mass balance and convergence criteria in the user-specified timestep, the software will dynamically reduce the computational timestep until the required precision is obtained (for details see *GoldSim Contaminant Transport Module* (GoldSim Technology Group 2007 [DIRS 183214])).

Figure 6.3.8-4 shows a schematic representation of the GoldSim cell pathway network used to implement the EBS Transport Submodel for CSNF WPs. For the waste form domain, a single waste form cell (Cell 1) is used to represent the entire volume of the degraded waste form and the associated mass transport processes. Similarly, for CDSP WPs (figure not shown), two cell pathways representing each waste form subdomain are used: one for HLW fuel (Cell 1a) and another for DSNF fuel (Cell 1b). The mass transport processes in the corrosion products domain are modeled by the corrosion product cell (Cell 2), where sorption reactions are modeled. Similarly, the processes in the invert domain are modeled by the invert cell (Invert Cell). The EBS-UZ domain is modeled by an array of near-field UZ cells (UZ Fracture Cell and UZ Matrix Cell). The interface cell, namely, Invert-UZ Interface cell, shown on Figure 6.3.8-4, is used for computing the concentrations at the interface boundaries for maintaining diffusive flux

continuity between a single continuum domain and a dual continuum domain as described in (SNL 2007 [DIRS 177407], Section 6.5.2.5).

Within the GoldSim cell network, diffusive and advective flux connections are defined for each cell. The advective and diffusive flux connections between the various cells in the EBS Transport Submodel are indicated on Figure 6.3.8-4. The flow through various cells is based on the continuity equations and conservation of mass, as described in *EBS Radionuclide Transport Abstraction* (SNL 2007 [DIRS 177407], Section 6.3.1.1). Each computational cell is provided with parameters describing water volumes, diffusive properties, and advective and diffusive flux links to other cells. Between any two cells, the diffusive flux can be bidirectional, depending on the concentration gradient, while the advective flux is unidirectional. The output of a cell is given in terms of the advective and diffusive mass fluxes for each radionuclide species and its concentration at the cell center. Species-dependent free water diffusion coefficients are used in each domain for dissolved radionuclides while a separate diffusion coefficient is computed for transport of radionuclides associated with colloids based on the sampled size of the colloids (SNL 2007 [DIRS 177407], Section 6.3.4.4). In addition, the diffusion coefficients are corrected for tortuosity and temperature. The mass transport equations in a cell network are solved on a per package basis and then scaled by GoldSim to the number of failed WPs.

Implementation of the EBS Transport Submodel for the TSPA-LA Model uses the output of the Waste Form Degradation Submodel (Section 6.3.7.4), the EBS Flow Submodel (Section 6.3.6), the EBS TH Environment Submodel (Section 6.3.2), the Dissolved Concentration Limits Submodel (Section 6.3.7.5), and the EBS Colloids Submodel (Section 6.3.7.6). An overview of the computational model for the TSPA-LA Model, as implemented using the GoldSim software, is provided below.

**Waste Form Cells**—The waste form cell receives radionuclide mass from a specialized GoldSim Source element, which models the WP failure, degradation of the waste form, and release of the radionuclide inventory for possible transport through the EBS. The Source element provides the specified flux boundary condition for solving the mass transport equations. There is no advective or diffusive transport of dissolved radionuclides or radionuclides sorbed onto colloids when the temperature is greater than the boiling point of water in the TSPA-LA Model (Section 5.1.4). This is achieved by setting the radionuclide solubilities to zero at temperatures greater than 100°C (the boiling point of water).

**CSNF Waste Form**—The setup of a waste form cell for CSNF WPs and its relationship to other cells for modeling transport through the WP are illustrated on Figure 6.3.8-5. Both advective and diffusive transport can occur from the waste form cell (Cell 1) to the corrosion products cell (Cell 2). Radionuclides are transported from this cell to the downstream cell in the dissolved state and reversibly sorbed on waste form and groundwater colloids. Plutonium and americium can also be transported as irreversibly sorbed on the specified waste form colloids. Solving the mass transport equation requires that the following properties be defined: (1) the volume of water in the rind, (2) the diffusive area, (3) the diffusive length, and (4) advective flow rates.

**CDSP Waste Form**—The implementation of the waste form cells for CDSP WPs differs from the approach used for CSNF WPs, in that degraded fuel is represented by two cell pathways. The setup of the waste form cell pathways for both CDSP WP fuel types and their relationship to actual waste forms are illustrated on Figure 6.3.8-6. One cell pathway (Cell 1a) represents the degraded HLW glass logs, while the other cell pathway is for the degraded DSNF waste form (waste form Cell 1b). Solving the mass transport equations for these cells requires that the similar properties be defined as for the CSNF waste form.

Although presented in Section 6.3.8.2.2, Equation 6.3.8-11 is not directly implemented into the TSPA-LA Model. The TSPA-LA Model calculates the fraction of the HLW glass that is degraded at each timestep (Section 6.3.7.4.3.3) and the result is used to determine the rind volume at each timestep. For the CDSP WP rind volume, the TSPA-LA Model implements a modification to the relationship provided in Equation 6.3.8-11, which utilizes the fraction of mass degraded instead of the total mass degraded:

$$V_{rind,HLWG}(t) = \phi_{rind} V_{total} F_{cor} \quad (\text{Eq. 6.3.8-26})$$

where

$$\begin{aligned}
 V_{rind,HLWG}(t) &= \text{the time-dependent rind volume (m}^3\text{)} \\
 \phi_{rind} &= \text{rind porosity} \\
 V_{total} &= \text{the initial total volume of HLW glass in a CDSP WP (m}^3\text{)} \\
 F_{cor} &= \text{fraction of mass degraded into rind.}
 \end{aligned}$$

The rind porosity and initial total volume of HLW glass are based on values shown in Table 8-1 of DTN: MO0502ANLGAMR1.016\_R0 [DIRS 172830]. The fraction of mass degraded is calculated by Equation 6.3.7-8.

In addition to being transported in the dissolved state, radionuclides in the CDSP WP waste form cell can be transported via waste form colloids and groundwater colloids. The waste form colloids form from the degradation of HLW glass and can reversibly sorb radionuclide. They also include embedded plutonium and americium, which are considered as intrinsic parts of the colloids and, thus, not in equilibrium with the aqueous system. These embedded radionuclides are modeled as attached irreversibly to the host colloids. Details of the waste form colloid generation, stability, and sorption capability are given in Section 6.3.7.6.2. Waste form colloids are also produced in the DSNF waste form subdomain (Waste Form Cell 1b). The waste form colloids generated from the HLW waste form subdomain, as well as groundwater colloids from the seepage water, pass through the DSNF waste form cell.

**Corrosion Products Cell**—Conceptually, the corrosion products cell (Cell 2) is the part of the corrosion products domain (described in Section 6.3.8.1) that represents the degraded steel components of the WP, which is modeled as iron oxyhydroxides. However, it does not include the corrosion products from the degradation of the outer barrier, which is treated as a separate cell (see discussion below). The corrosion products cell includes both stationary corrosion

products and iron oxyhydroxide colloids, which both participate in equilibrium and kinetic sorption of radionuclide mass. A surface complexation-based competitive sorption model is used to calculate sorption of uranium, neptunium, plutonium, thorium, and americium onto stationary corrosion products and iron oxyhydroxide colloids as a function of available sorption sites,  $P_{CO_2}$ , and dissolved concentration of the radionuclides. For a detailed discussion of this mechanistic model, see *EBS Radionuclide Transport Abstraction* (SNL 2007 [DIRS 177407], Section 6.3.4.2.3 and Section 6.5.2.4). A multiple regression model for computing the sorbed mass is developed based on the dissolved concentration of the radionuclides computed at the end of the previous timestep. The effective  $K_d$  value, which is needed by the GoldSim solver, is calculated by dividing the sorbed mass by the dissolved concentration. The computed effective  $K_d$  value is directly used in the transport equation for uranium, neptunium, and thorium, which are modeled to undergo equilibrium sorption. Plutonium and americium are modeled to undergo kinetic sorption-desorption reactions where the desorption rate is calculated by dividing the forward reaction rate by the  $K_d$  for plutonium and americium (from the surface complexation based regression equation).

Table 6.3.8-3 summarizes the distributions used to determine the available sites for competitive sorption on the stationary corrosion products and iron oxyhydroxide colloids. The pH in the cell is also computed based on the results of surface complexation modeling by the following equation (SNL 2007 [DIRS 177407], Equation 6.5.2.4.6-2):

$$\text{pH} = 4.5342 + 0.6132(\text{pCO}_2) - 0.3805 \log_{10}[\text{U}] - 0.0254(\log_{10}[\text{U}])^2 + E \quad (\text{Eq. 6.3.8-27})$$

where,  $\text{pCO}_2$  is the negative log of the in-drift  $\text{CO}_2$  partial pressure (bars),  $[\text{U}]$  is the dissolved concentration of U in  $\text{mol L}^{-1}$ , and  $E$  is the error term ( $\text{pH\_Cell\_2\_Regression\_Error}$ ) defined by a normal distribution with mean of zero and SD of 0.32 truncated at  $\pm 2$  SDs.

As with the waste form cells there is no advective or diffusive transport of dissolved radionuclides or radionuclides sorbed onto colloids in the corrosion products cell when the WP temperature is greater than  $100^\circ\text{C}$  in the TSPA-LA Model. This is achieved by setting the radionuclide solubilities to zero at temperatures greater than  $100^\circ\text{C}$ .

**Outer Barrier Cell**—An additional cell pathway is added at the base of the corrosion products domain to represent transport through the outer barrier. The WP outer barrier is composed of Alloy 22 (UNS N06022) and undergoes general corrosion at a different rate than the stainless steel inside the WP and the corrosion products formed from the degradation of Alloy 22 are different from those formed from the degradation of stainless steel. The breach area of the outer barrier varies by the individual scenario class modeling cases and exerts strong control on the advective and diffusive releases out of the WP: (1) for the Nominal Scenario Class, the outer barrier degradation from general corrosion and stress corrosion is determined by WAPDEG code (Section 6.3.5.1.3); (2) for the Seismic Scenario Class, the outer barrier damage from the ground motion and fault displacement is variable and determined probabilistically by the seismic damage abstraction (Section 6.6); (3) for the Igneous Intrusion Modeling Case, the entire surface area of the outer barrier is assumed to be breached at the time of the igneous event (Section 6.5); (4) for the Waste Package EF and Drip Shield EF Modeling Cases, the entire surface of the outer barrier is assumed to be breached at the start of simulation (Section 6.4); and (5) for the Human

Intrusion Modeling Case, the breach area is considered to be the same as the cross-sectional area of the borehole (Section 6.7.3). No radionuclide sorption is modeled in the outer barrier cell even though the tortuosity computed for Cell 2 is applied to the outer barrier cell.

**Invert Cells**—In the TSPA-LA Model, the invert domain is represented by the invert cell pathway. For radionuclide transport, the invert is modeled as a single-continuum porous medium composed of crushed tuff (SNL 2007 [DIRS 177407], Section 6.5.2.3). The invert cell receives advective and diffusive mass flux from the outer barrier cell. The setup of the invert cell pathway is illustrated on Figure 6.3.8-7. Both advective and diffusive mass transport can occur from the invert cell to the near-field UZ cells.

**Invert-UZ Interface Cell**—This cell pathway is added between the invert cell and EBS-UZ Interface cells to model diffusive transport between a single-continuum invert (represented by one cell) and the dual-continuum UZ (represented by two cells). The diffusive flux needs to be bifurcated correctly between the two UZ continua while preserving the flux continuity condition at the interface. This is achieved by introducing the Invert-UZ Interface cell, which is conceptualized as a very thin slice of the invert cell (Figure 6.3.8-4). The purpose of this interface cell is to provide an approximate concentration boundary at the interface for diffusive flux calculation. All the properties of the interface cell are the same as the invert cell, except for the diffusive length, mass, and volume, which are computed by multiplying the equivalent invert cell properties by a scale factor of  $10^{-6}$ . The diffusive area is the same as that of the overlying invert cell. For more details, see *EBS Radionuclide Transport Abstraction* (SNL 2007 [DIRS 177407], Section 6.5.2.5).

**EBS-UZ Interface Cells**—The TSPA-LA Model uses an array of cells to model part of the near-field UZ below the invert. Modeling the near-field UZ serves to establish a far-field zero-concentration boundary for computing the flux from the invert to the UZ. The dual-continuum approach for modeling the near-field UZ is implemented by creating an overlapping continua of UZ matrix and fracture cells. Figure 6.3.8-8 illustrates how the conceptual model of the near-field UZ domain is implemented into the EBS Transport Submodel. The invert interface cell is connected with the UZ matrix and fracture cells directly below it in the UZ cell array.

The overlapping matrix and fracture continua are represented by a two-dimensional vertical array of cells oriented parallel to a cross section of a drift and located immediately beneath a drift. The entire cell array, consisting of three sets of two columns or vertical zones, with each zone containing both a fracture cell and a matrix cell, is shown on Figure 6.3.8-9. The invert is directly connected with the middle zone of UZ matrix/fracture cells. Each zone is four layers deep in the vertical direction. Thus, the array consists of 12 pairs of matrix and fracture cells within the UZ (Figure 6.3.8-9). Laterally, each zone is one drift diameter wide, with the middle zone centered beneath the drift, so that each layer of the array extends one drift diameter on either side of the drift. In the longitudinal direction of a drift, the length of the array is equal to the length of the WP being modeled.

As described in *EBS Radionuclide Transport Abstraction* (SNL 2007 [DIRS 177407], Section 6.5.2.6), the thickness of the first (top) layer of cells is 1.0274 m, or 10 percent greater than the 0.934 m average invert thickness beneath a WP. The thickness of the second layer is

double that of the first layer, or 2.05481 m. The third and fourth layers are given a thickness of 5 m and 10 m, respectively (Figure 6.3.8-9). Grid sizes are more refined near the base of the invert to accurately capture the higher concentration gradient in the region. A collector cell is placed beneath the fourth layer and is given a very large, numerically infinite water volume ( $10^{10} \text{ m}^3$ ) to simulate an effective zero-concentration boundary. This collector cell acts as a sink for all the mass flux from the UZ cells.

A description of the mass flux between the invert and UZ fracture and matrix cells is provided in *EBS Radionuclide Transport Abstraction* (SNL 2007 [DIRS 177407], Section 6.5.2.6). Each fracture cell interacts, via a diffusive connection only, with the matrix cell of the same zone (Figure 6.3.8-9). The fracture cell also interacts vertically via a diffusive connection with the fracture cell of overlying and underlying layers. The matrix cell interacts via a diffusive connection laterally with adjacent matrix cells in the same layer and vertically with the matrix cells of overlying and underlying layers. Radionuclides diffuse based on the concentration gradient between cells. Advection occurs vertically downward only, from the fracture cell of one layer to the fracture cell of the underlying layer and from the matrix cell of one layer to the matrix cell of the underlying layer in the same zone. Lateral advection is not considered. Figure 6.3.8-9 illustrates the diffusive and advective flux connections between the various cells in the network.

The pore volume of each continuum is computed by multiplying the bulk volume for each discretized zone (based on the geometry) by either the fracture continuum porosity or the matrix continuum porosity. Similarly, the water volume is calculated by multiplying the pore volume of each continuum by its respective saturation. Reversible sorption of radionuclides to the matrix is modeled by using the  $K_d$  values for the devitrified tuff sampled by the UZ Transport Submodel (Table 6.3.9-2). The mass of the UZ matrix is computed by multiplying the matrix volume (bulk volume  $\times$  (1- fracture porosity)) of the cell by the dry bulk density of the UZ matrix.

Advective fluid flux due to seepage flows from the invert into the top middle UZ fracture cell, while the advective flux due to imbibition from the host rock, which enters the invert and flows under gravity, goes from the invert into the top middle UZ matrix cell. This partitioning of fracture and matrix advective flux is based on the actual source of the two components. That is, seepage comes from the host-rock fractures and imbibition from the host-rock matrix. An additional component of flow from the invert to the UZ is flux due to condensation on the drift walls. The condensation flux is treated in the same manner as seepage flux and is combined with the seepage flux. In the dripping environment, the advective flux flowing through the UZ fracture cells in the middle zone is the larger of the advective flux out of the invert or the steady-state UZ fracture flux. The advective flux in the two outer zones is the steady-state UZ flux in each continuum at the repository horizon.

Diffusive mass flux from the invert can go into both fracture and matrix UZ continua based on the concentration gradient and effective diffusion coefficient. All three types of colloids in the TSPA-LA Model are transported from the invert to the UZ cells. Groundwater colloids are present in all four layers. Because the UZ Transport Submodel only models groundwater colloids (with reversibly sorbed radionuclide mass), in order to be consistent, the iron oxyhydroxide and waste form colloids with reversibly sorbed radionuclides are modeled as present in only the first two layers of the middle column, making the groundwater colloids the

only types of colloids available for far-field transport. As a result, the mass reversibly associated with the iron oxyhydroxide and waste form colloids is transferred into the solution where it is repartitioned onto the groundwater colloids based on the sorption coefficient. Americium and plutonium mass that is irreversibly sorbed on iron oxyhydroxide colloids or embedded in waste form colloids is transported from the invert to the UZ cells, as long as these colloids are stable in the invert. If the chemical conditions in the invert are such that the iron oxyhydroxide or waste form colloids become unstable, they are not transported from the invert to the UZ. However, if the colloids are stable in the invert, then they also remain stable in the UZ and SZ. Solubility constraints are not imposed on any species in the UZ cells. Additional details regarding the hydrologic parameters used in the EBS-UZ interface cells are provided in *EBS Radionuclide Transport Abstraction* (SNL 2007 [DIRS 177407], Section 6.5.2.6).

**EBS Transport Submodel Outputs**—The output from the EBS Transport Submodel consists of the total radionuclide mass flux out of the single-continuum invert. The mass flux from the single-continuum invert to the dual-continuum UZ, computed by the EBS-UZ Interface cells, is passed to the UZ Transport Submodel for TSPA-LA Model calculations. It is used as the mass flux boundary condition for the UZ Transport Submodel, as described in Section 6.3.9. Three different types of mass fluxes are passed to the UZ Transport Submodel. The first type of mass flux is applicable for all radionuclides transported in the TSPA-LA Model. This flux includes all of the radionuclide mass that exists in the dissolved state or is reversibly sorbed onto the three different colloid types: groundwater, waste form, and iron oxyhydroxide. After it is input into the UZ Transport Submodel, this mass is repartitioned onto the groundwater colloids in the UZ based on the sampled colloid concentration and sorption coefficients defined for the UZ Transport Submodel (Section 6.3.9.2). Radionuclides that are irreversibly sorbed onto waste form and iron oxyhydroxide colloids form the basis for the next two mass flux types. These masses are defined in the EBS Transport Submodel as distinct species (“Ic” species for mass irreversibly sorbed onto waste form colloids and “If” species for mass irreversibly sorbed onto iron oxyhydroxide species). After exiting the EBS, and before being passed to the UZ Transport Submodel, the “Ic” and “If” masses are added together for each irreversibly sorbed radionuclide. The total irreversibly sorbed mass, for a given radionuclide, is then repartitioned onto a fast and a slow colloid fraction through the UZ and SZ. The fraction of colloids that travel unretarded through the UZ and SZ are called the fast fraction, while the remaining colloids that undergo some degree of retardation are called the slow fraction. A value of 0.00168 is used in the TSPA to represent the fast fraction of colloids (GoldSim parameter: Fast\_Fraction) based on the cumulative probability distribution of unretarded fraction of colloids presented in the output DTN: LA0303HV831352.003\_R0 [DIRS 165624] and by choosing the value corresponding to the combined travel time of 100 years in the UZ and SZ (BSC 2004 [DIRS 170006], Section 6.6 and Table 6-4). The partitioning of irreversible mass associated with the fast fraction is calculated by multiplying the total irreversibly sorbed mass for a radionuclide by 0.00168, while that for the slow fraction is done by multiplying total irreversibly sorbed mass by (1–0.00168). The mass associated with the fast fraction is assigned to the “If” species, while the mass associated with the slow fraction is assigned to the “Ic” species in the UZ and SZ transport submodels. In effect, for the EBS Transport calculations, the terms “Ic” and “If” represent irreversibly sorbed mass on the waste form colloids and iron oxyhydroxide colloids, respectively, but for the UZ and SZ transport (and for the dose calculations) the “Ic” means irreversibly sorbed mass traveling on the slow colloid fraction while the “If” means irreversibly sorbed mass traveling on the fast colloid fraction.

In addition to the total mass flux, the relative fraction of the mass going into each of the fracture and matrix cells at the EBS-UZ boundary is required by the UZ Transport Submodel. This fracture-matrix partitioning of mass is calculated on the basis of the mass fraction going into the fracture continuum, as compared to the total going into the fracture and matrix continua, from the invert. This partitioning is time-dependent and captures the temporal processes active in the EBS, such as varying radionuclide concentrations in the WP and invert and changing water flow through various components of the EBS. Furthermore, this partitioning is computed by solving the mass transport equations for the EBS and part of the UZ as a coupled system with appropriate boundary conditions.

**Modification of Diffusive Lengths in GoldSim**—When two cells with different diffusive areas are connected, an adjustment is required in the GoldSim setup to properly compute the diffusive conductance. Figure 6.3.8-10 is a simplified depiction of a cell-to-cell connection in which two cells have different diffusive areas. Such differences in diffusive area between connected cells occur due to varying domain dimensions, for example, the diffusive area at the node of the waste form cell (Cell 1) is different from the diffusive area at the node of the corrosion products cell (Cell 2).

The diffusive conductance ( $C_{12}$ ) from the node in Cell 1 to the node in Cell 2 controls the diffusive mass flux to Cell 2. This conductance is properly calculated as the harmonic sum of two diffusive conductance links (SNL 2007 [DIRS 177407], Section 6.5.2.5, simplified from Equation 6.5.2.5-7):

$$C_{12} = \frac{1}{\frac{(L_1/2)}{D_1 A_1} + \frac{(L_2/2)}{D_2 A_2}} \quad (\text{Eq. 6.3.8-28})$$

where

$L_1$  = diffusive length of Cell 1 (m)

$D_1$  = effective diffusion coefficient of Cell 1 (includes effects of porosity, saturation, and tortuosity) ( $\text{m}^2/\text{s}$ )

$A_1$  = diffusive area of Cell 1 ( $\text{m}^2$ )

$L_2$  = diffusive length of Cell 2 (m)

$D_2$  = effective diffusion coefficient of Cell 2 (includes effects of porosity, saturation, and tortuosity) ( $\text{m}^2/\text{s}$ )

$A_2$  = diffusive area of Cell 2 ( $\text{m}^2$ ).

That is, each conductance link is properly defined using the effective diffusion coefficient, length, and area of that link. However, in the GoldSim cell pathway only a single diffusive area can be defined, which is the area of the upstream cell (in this case  $A_1$ ). In order to conform to the GoldSim formulation, the assigned diffusive area is set equal to a unit area of  $1.0 \text{ m}^2$  (the numerator in the following equation) and the cell areas are implicitly included in the

diffusive length terms by dividing the diffusive lengths by their respective areas, as shown below:

$$C_{12} = \frac{1}{\frac{(L_1/2)/A_1}{D_1} + \frac{(L_2/2)/A_2}{D_2}}. \quad (\text{Eq. 6.3.8-29})$$

In the TSPA-LA Model, the approach illustrated by Equation 6.3.8-29 is applied to all diffusive connections between cells in the EBS Transport Submodel. Within each GoldSim cell pathway the diffusive areas are set equal to 1.0 m<sup>2</sup> and the calculated diffusive half-length is divided by the appropriate diffusive area to compute an effective diffusive half-length. This modification results in the proper diffusive conductance being calculated in the solution of the EBS Transport mass balance equations.

#### **6.3.8.4 Model Component Consistency and Conservatism in Assumptions and Parameters**

To enhance understanding of the complex interactions within the TSPA-LA Model, a discussion of consistency among model components and submodels, and identification of conservative assumptions in abstractions, process models, and parameter sets supporting the EBS Transport Submodel are discussed below.

##### **6.3.8.4.1 Consistency of Assumptions**

**Water Balance in the TSPA-LA Model Within the EBS**—The conceptual, mathematical, and abstraction models for estimating how much water can enter, accumulate, and move through various EBS components are discussed in Sections 6.3.6 and 6.3.8.2. The water balance discussion can be divided into two categories, one related to water flow and the other to water volumes.

There are two potential inconsistencies with respect to water flow through various EBS components in the TSPA-LA Model: (1) the reduction in water flow due to evaporation and consumption by chemical reactions is conservatively ignored, and (2) the condensation flux calculations are performed separate from the MSTHM calculations that are used to define the temperature and relative humidity conditions in the EBS.

With respect to inconsistencies or differences related to water volume in the EBS, it should first be stated that these calculations in the TSPA-LA are primarily based on phenomenological laws for fluid retention in porous media. For example, the saturation and water volume in the invert are calculated based on the soil moisture retention relationships of crushed tuff, while the saturation of the corrosion products and waste form rind under no flow conditions are computed as a function of relative humidity based on measured adsorption isotherms. Although most calculations for the saturations (and water volumes) are based on phenomenological laws, some assumptions must be made under certain conditions. These include the assumption of 100 percent saturation of corrosion products and waste form rind under water flowing conditions. In addition, some inconsistencies in water volumes exist among process-level models mainly due to the limitation of the models used in the calculations. For example, a minimum water volume

is required for in-package chemistry calculations in order to keep the ionic strengths less than 4 molal, the effective limit of the B-dot activity coefficient equation used in the EQ3/6 computer code. This minimum water volume is independent of the relative humidity and temperature histories as predicted in the MSTHM abstraction and is likely larger than is realistic at low relative humidity conditions.

Chemical processes in the EBS will consume and, possibly, produce water. Conversion of CSNF to schoepite ( $\text{UO}_3 \cdot 2\text{H}_2\text{O}$ ) and steel to goethite ( $\text{FeOOH}$ ) and other hydrated corrosion products will likely remove large quantities of water from incoming fluids and the vapor phase. Over time, hydrated phases will alter to less hydrated phases and release water to the breached waste package in the process. While water uptake by waste form degradation should be relatively fast, the release of water from dehydration reactions should be slower. The overall uptake and release of water over time is certainly a complex function of water availability, temperature, and time and is difficult to predict accurately. The assumption of no water uptake or release is a simplification of a complex process that will tend to over-predict the water saturation in a breached WP.

For diffusion-dominated modeling cases after breach of the outer Alloy 22 WP barrier, the following assumptions are made in the TSPA-LA Model with respect to the water balance inside the WP: (1) sufficient condensate water is available for waste form degradation and metal alloy (e.g., steel) degradation, and (2) sufficient water vapor is present to establish a continuous film of liquid water on fuel and corroded-metal surfaces under no flow conditions when relative humidity is greater than 95 percent, which is thick enough to permit diffusive transport of radionuclides from the WP either as dissolved species or bound to colloids.

**Effect on the TSPA**—Within the EBS, water balance issues have more of an effect in diffusion-dominated modeling cases, where the limited water availability may control the degree of liquid saturation inside the WP and, therefore, the radionuclide transport rates through the WP. In the advection-dominated modeling cases, the water balance related issues are not as important because sufficient water flows through the WP to result in a rapid turnover rate with respect to pore volume in the WP and, thus, the assumption of complete saturation is a reasonable one. The overall effect of the previous assumptions regarding the complete saturation inside the WP under flowing conditions is a conservative over estimate of the release of radionuclides and timing of the release.

With respect to diffusion-dominated cases, the assumption that there is a high enough vapor flux to instantly saturate the WP internals to local equilibrium conditions (which is the assumption underlying the use of an adsorption isotherm) would tend to over estimate the timing and amount of EBS releases, by providing for no kinetic constraints on waste form degradation with respect to water availability for reactions and by assuming bulk chemical and bulk diffusion transport conditions (also a continuous liquid pathway to the outside of the WPs). All of these assumptions should be conservative with respect to release and dose.

#### **6.3.8.4.2 Identification of Conservatisms in Submodels and Abstractions**

**All Seepage Falls on DSs**—All seepage into the drifts is assumed to fall on the DSs, not just seepage above the DSs. This conservative approach is taken to simplify the modeling approach

and because the uncertainty in the seepage locations is difficult to quantify (SNL 2007 [DIRS 177407], Section 5.1). This approach will increase the seepage flux contacting the DS and thereby increase the radionuclide release in the scenarios where there is advective flux in the waste form cell.

**Seepage on the WP**—All the seepage penetrating a DS falls on the crown of the WP. This conservative approach is taken to simplify the modeling approach and because the uncertainty in the seepage locations is difficult to quantify (SNL 2007 [DIRS 177407], Section 5.1). This conservatism will increase the flux through the breached DSs and WPs and thereby increase the radionuclide release in the scenarios where there is advective flux in the waste form cell.

**No Evaporation of the Seepage Water from the Surfaces of the DSs**—A reduction in the quantity of water flux through the DS reduces the potential for advective transfer and subsequent release and transport of radionuclides from the WPs (SNL 2007 [DIRS 177407], Section 5.2). Ignoring evaporation from the DS surface tends to increase the seepage flux falling on the WPs.

**No Evaporation of the Seepage Water from the WPs**—Transport within the WP is not possible if evaporation eliminates liquid fluxes and effective water saturation (SNL 2007 [DIRS 177407], Section 5.3). Ignoring evaporation on the WP surface tends to increase the potential for advective and diffusive transport of radionuclides.

**Emplacement Pallets**—The presence of emplacement pallets for WPs is conservatively ignored to allow water and radionuclides to pass directly from the WP to the invert without increasing the transport distance (SNL 2007 [DIRS 177407], Section 6.3.1.1). This conservatism leads to a shortened advective flow path and increases the concentration gradient for diffusion.

**Consumption of Water**—There is no consumption of water by chemical reactions. The consumption of water by the corrosion of iron inside a WP and by hygroscopic salts deposited on the DS and WP surfaces would reduce the amount of water for dissolution and transport of radionuclides (SNL 2007 [DIRS 177407], Section 5.4). The assumption that there is no consumption of water is a bounding assumption, which increases the amount of water available for advective transport.

**Thin Water Films**—It is conservatively assumed that continuous thin water films exist on the internal components of the breached WPs and on the breached areas at temperatures less than the boiling point of water. Multiple water layers are needed in order for radionuclides to dissolve in and diffuse. Ignoring the thickness of the water film will overestimate the release of radionuclides. Assuming the presence of continuous water film allows radionuclides to diffuse from the degraded waste form to the outside of the breached WP (SNL 2007 [DIRS 177407], Section 5.5). Diffusive transport occurs continuously after the WP is breached and the waste form is degraded, irrespective of the path length.

**One-Dimensional Advective and Diffusive Transport through the EBS**—A one-dimensional vertical advective and diffusive transport from the WPs to the invert occurs irrespective of the breach location on the WP surface (SNL 2007 [DIRS 177407], Section 6.3.1.2) even though breaches in the WP are expected to occur randomly over the WP surface area. In other words,

assuming diffusion can occur through all breaches, regardless of location, maximizes the diffusive area thereby giving a conservative estimate of releases from the WP.

**Invert Corrosion Products**—No corrosion products exist in the invert. By assuming that there are no corrosion products in the invert, there will be no sorption or delay of radionuclides by corrosion products (SNL 2007 [DIRS 177407], Section 5.6). Not taking credit for the sorption of radionuclides onto the corrosion products will tend to increase the mass flux of radionuclides through the invert.

**No DS Shadow in the Invert**—Water will tend to divert around the DS and not flow through the region of the invert directly under the DS. However, because of the limited information regarding the flow paths and mixing of waters, this effect is not accounted for (SNL 2007 [DIRS 177407], Sections 6.3.3.4 and 6.5). The flux diverted by the DSs to the invert is assumed to mix with the water carrying the radionuclides from the WPs to the invert, which tends to increase the advective transport.

**No Physical Filtration or Gravitational Settling of Colloids**—Stable colloids once formed do not undergo physical filtration or gravitation settling in the CSNF and CDSP WPs and in the invert (SNL 2007 [DIRS 177407], Section 5.7). By assuming that there is no physical filtration or gravitational settling of colloids, the model will tend to overestimate the colloid mass flux and the colloid-facilitated radionuclide transport in the EBS.

**Colloid Retardation**—Colloid retardation due to sorption at the air-water interface and interaction with microbes and organic components is not modeled. Not including colloid retardation tends to increase the colloid mass flux and the colloid-facilitated radionuclide transport in the EBS (SNL 2007 [DIRS 177423], Section 5.9).

### **6.3.8.5 Alternative Conceptual Model(s) for Engineered Barrier System Transport**

Section 6.2 outlines the general consideration and treatment of ACMs used to support the TSPA-LA Model. A brief description of the EBS Transport Submodel ACMs summarized in Table 6.3.8-7 is presented below.

**Bathtub Flow Model ACM**—This ACM assumes that seepage collects within the WP before being released to the EBS (SNL 2007 [DIRS 177407], Section 6.6.1). The bathtub effect would be most important during the period when only a few patches or cracks have penetrated the DS and WP. In this situation, there may be penetrations through the top of the WP while the bottom surface remains intact, leading to retention of liquid. At later times, the presence of multiple penetrations makes a flow-through geometry the more likely configuration. The response of the bathtub geometry was evaluated for a primary case, with constant boundary conditions and material properties, and for three secondary cases. The three secondary cases considered a step change in inflow rate, such as would occur from a climatic change, a step change in water chemistry, or a step change in flow geometry, as would occur if a patch suddenly appeared beneath the waterline. All cases included consideration of two limiting conditions on radionuclide releases: dissolution rate limited and solubility limited.

This ACM was not used for the TSPA-LA EBS Transport Model because, for most of the pertinent cases, the basecase flow-through model is bounding with respect to the release of radionuclides.

**Constrained Water Vapor and Oxygen Diffusion through SCC ACM**—This ACM compares the rate of water vapor and oxygen diffusion through stress corrosion cracks with the rate of corrosion of steel components inside a WP (SNL 2007 [DIRS 177407], Section 6.6.2). If the consumption rate is greater than the diffusion rate then a film of adsorbed water cannot form, which could delay diffusive releases until all steel is fully corroded. The water vapor concentration inside a WP is assumed to be zero to maximize the concentration gradient. Alternative cases consider the effects of stress corrosion cracks that are assumed to be: (1) fully open, and (2) filled with corrosion products but still permeable. This ACM could potentially delay releases for hundreds to thousands of years. However, the assumption that no water is physically adsorbed until all steel is corroded is questionable, because adsorption is typically a fast process. On the other hand, if water consumption by corrosion keeps the relative humidity inside the WP low, the effective water saturation will be so low that the bulk liquid phase behavior allowing dissolution and diffusion of dissolved radionuclides will not exist until the corrosion is complete.

This ACM was not used for the TSPA-LA EBS Transport Submodel because it is potentially nonconservative and there are insufficient data to validate this ACM.

**Dual-Continuum Invert Model ACM**—The dual-continuum invert model is an alternative conceptual EBS Transport Model in which crushed tuff invert ballast is modeled as a dual-continuum material consisting of intergranular pore space and intragranular pore space (SNL 2007 [DIRS 177407], Section 6.6.3). All seepage into the drift flows through the intergranular pore space and into the UZ fractures. Imbibition from the UZ host rock into the invert flows through the intragranular pore space and into the UZ matrix under gravity. Diffusion of radionuclides also occurs in both the intergranular and intragranular pore spaces, from the WP corrosion products into UZ fractures and matrix, as well as between the two invert continua.

This ACM was not used for the TSPA-LA EBS Transport Model. It was screened out due to insufficient data to validate diffusion coefficients in individual continua and insufficient data to confirm whether this is a bounding approach with respect to chemical behavior in the invert.

**Alternative Invert Diffusion Coefficient ACM**—The invert diffusion coefficient model with a lower limit on water content is an alternative conceptual EBS Transport Model in which, as the water content of the crushed tuff decreases, the water films that connect pore spaces become disconnected, and the effective diffusion coefficient drops more rapidly than predicted by Archie's law (SNL 2007 [DIRS 177407], Section 6.6.4). Below some critical water content, the diffusion coefficient becomes zero, based on models of diffusion in soils.

This ACM was not used for the TSPA-LA EBS Transport Model because there is insufficient data to validate diffusive behavior at very low water contents.

**Reversible Sorption of Radionuclides onto WP Corrosion Products ACM**—In this ACM, an empirical approach based on sampling a partition coefficient ( $K_d$  value) for reversible sorption of radionuclides onto stationary corrosion products is considered (SNL 2007 [DIRS 177407], Section 6.6.5). Iron oxyhydroxides are generated through corrosion of mild steel and stainless steels within the WP. The iron oxyhydroxides are known to be excellent sorbers (as indicated by their high  $K_d$  values) of many radionuclide species. In this ACM, sorption is modeled as being completely reversible for all radionuclides and represented by linear adsorption isotherms in the form of  $K_d$  values. The  $K_d$  values allow retardation factors to be computed for transport through the EBS.

This ACM was not used for the TSPA-LA EBS Transport Submodel because it does not account for limitations on the total number of sorption sites. Also, this ACM does not account for competition with other radionuclides.

**Plutonium Sorption from Stationary Corrosion Products and Colloids ACM**—This ACM accounts for the slow desorption of plutonium observed in experiments investigating sorption and desorption of plutonium from iron oxyhydroxide (SNL 2007 [DIRS 177407], Section 6.6.6). Postulated mechanisms of plutonium sorption are described and the experimentally observed desorption is interpreted in the context of these mechanisms.  $K_d$  values are calculated for application to plutonium transport in the EBS.

This ACM is not incorporated into the basecase EBS Transport Submodel because the fitting parameters are specific to the experiment design and cannot be extrapolated to other transport conditions as would be expected in the TSPA-LA Model. Furthermore, the developed parameters do not take into account the competition with other radionuclides.

INTENTIONALLY LEFT BLANK

Table 6.3.8-1. Summary of EBS Transport Abstraction

Transport Pathway	Transport Modes	Transport Parameters and Data Sources
1. Waste form and corrosion products domains	Waste form domain: Diffusion and advection (when possible) through the waste form rind.  Corrosion products domain: Diffusion through SCC (no advective transport through stress corrosion cracks). Diffusion and advection through corrosion patches.	No lateral or longitudinal dispersion. Colloidal particles will transport radionuclides. Diffusive area for stress corrosion cracks is obtained. Diffusion coefficient (all radionuclides): <ul style="list-style-type: none"> <li>• Species-dependent free-water diffusion coefficients given in DTN: LB0702PAUZMTDF.001_R1 [DIRS 180776], file <i>Readme.doc</i>, Table 8</li> <li>• Modified for temperature, porosity, and saturation</li> <li>• Colloid diffusion coefficient computed as a function of waste form and corrosion product temperatures and sampled colloid particle diameter (SNL 2007 [DIRS 177407], Section 6.3.4.4).</li> </ul> Competitive sorption of radionuclides onto corrosion products; time-dependent mass of corrosion products available for sorption is calculated based on corrosion rates of carbon and stainless steels.  The breach area of the WP outer barrier for radionuclide transport is dependent on the scenario class modeled.
2. Invert domain	Diffusion and advection from corrosion products domain into the invert domain.	Liquid flux for advection (sum of drift seepage flux, drift condensation flux, and invert imbibition flux). Diffusion coefficient (all radionuclides): <ul style="list-style-type: none"> <li>• Species-dependent free-water diffusion coefficients given in DTN: LB0702PAUZMTDF.001_R1 [DIRS 180776], file <i>Readme.doc</i>, Table 8.</li> <li>• Modified for temperature, porosity, and saturation</li> <li>• Colloid diffusion coefficient computed as a function of invert temperature and sampled colloid particle diameter.</li> </ul> The diffusive area for radionuclide transport is the width of the invert times the waste package length. Transport of radionuclides is retarded by sorption onto crushed tuff in invert.
3. Invert-UZ interface domain	Advection from the invert to UZ fractures and matrix. Diffusion from the invert to UZ fractures and matrix.	The invert diffusion calculation uses radionuclide concentrations in the WP corrosion products domain as the boundary condition at the top of the invert and a series of UZ computational cells below the invert that provide a gradient to a zero radionuclide concentration at some distance from the bottom of the invert. For additional details, see SNL 2007 [DIRS 177407], Section 6.5.2.6.

Sources: Modified from DTN: SN0703PAEBSRTA.001\_R3 [DIRS 183217] from *EBS Radionuclide Transport Abstraction* (SNL 2007 [DIRS 177407], Table 8.1-2).

Table 6.3.8-2. Parameters for EBS Transport Abstraction

Waste Type	Transport Properties	Seeping Case	Non-Seeping Case
<b>Waste Form Domains</b>			
CSNF	Domain bulk volume, pore volume, and water volume	<p>Waste Form Domain consists of degradation products in fuel rods (SNF rind), fuel basket tubes (steel corrosion products), absorber plates (steel corrosion products):</p> <ul style="list-style-type: none"> <li>SNF rind volume (<math>V_{rind}</math>, function of time) and porosity (<math>\phi_{rind}</math>) provided by <i>Cladding Degradation Summary for LA</i> (SNL 2007 [DIRS 180616], Tables 6-3 and 6-4)</li> <li>Steel corrosion products (CP) mass from Equation 8-4, pore volume (<math>V_{\phi,CP}</math>) from Equation 8-7, bulk volume from Equation 8-8 of <i>EBS Radionuclide Transport Abstraction</i> (SNL 2007 [DIRS 177407])</li> <li>Total pore volume of CSNF Waste Form Domain, <math>V_{\phi,CSNF}</math>, given by Equation 8-13 of <i>EBS Radionuclide Transport Abstraction</i> (SNL 2007 [DIRS 177407])</li> <li><math>S_w</math> = water saturation in domain = 1.0</li> <li>Domain water volume = total pore volume.</li> </ul>	<ul style="list-style-type: none"> <li>Domain characteristics (rind volume, corrosion products mass and volume, total pore volume) same as for Seeping Case</li> <li><math>S_{w,rind}</math> function of relative humidity and sampled density and specific surface area of rind (SNL 2007 [DIRS 177407], Equation 8-12)</li> <li>Rind water volume: <math>V_{w,rind} = S_{w,rind} \phi_{rind} V_{rind}</math></li> <li><math>S_{w,CP}</math> function of relative humidity, density, and sampled specific surface area of corrosion products (SNL 2007 [DIRS 177407], Equation 8-5)</li> <li>Corrosion products water volume: <math>V_{w,CP} = S_{w,CP} V_{\phi,CP}</math></li> <li>Domain water volume = <math>V_{w,CSNF} = V_{w,rind} + V_{w,CP}</math>.</li> </ul>
	Advection and Diffusion	<p>Advective flow = volumetric flow rate through the waste package</p> <p>Diffusive area of Waste Form Domain:</p> <ul style="list-style-type: none"> <li>Set equal to surface area of a cylinder at half the radius of the TAD canister excluding ends (= 12.5 m<sup>2</sup>).</li> </ul> <p>Diffusive path length:</p> <ul style="list-style-type: none"> <li>Set equal to TAD inside radius (= 0.819 m).</li> </ul> <p>Diffusion coefficient in Waste Form Domain, <math>D_{WF}</math>:</p> <ul style="list-style-type: none"> <li><math>\phi S_w D_{WF} = \phi^{1.3} S_w^2 D_{wi}</math></li> <li><math>\phi</math> = effective porosity of CSNF Waste Form Domain given by Equation 8-14 of <i>EBS Radionuclide Transport Abstraction</i> (SNL 2007 [DIRS 177407])</li> <li><math>S_w</math> = water saturation in domain = 1.0</li> <li><math>D_{wi}</math> = species dependent free water diffusion coefficient.</li> </ul> <p>(<math>D_{WF}</math> is an effective value that implicitly includes the effect of tortuosity in a porous medium).</p>	<ul style="list-style-type: none"> <li>No advective flux</li> <li>Diffusive area same as for Seeping Case</li> <li>Diffusive path length same as for Seeping Case</li> </ul> <p>Diffusion coefficient in Waste Form Domain, <math>D_{WF}</math>:</p> <ul style="list-style-type: none"> <li><math>\phi S_w D_{WF} = \phi^{1.3} S_w^2 D_{wi}</math></li> <li>Effective porosity <math>\phi</math> of CSNF Waste Form Domain given by Equation 8-14 of <i>EBS Radionuclide Transport Abstraction</i> (SNL 2007 [DIRS 177407]), same as for Seeping Case</li> <li>Water saturation in Waste Form Domain is based on water vapor adsorption isotherms: <math>S_w = \min[(V_{w,CSNF} / V_{\phi,CSNF}), 1.0]</math></li> <li><math>D_{wi}</math> = species dependent free water diffusion coefficient</li> <li>Modified for temperature.</li> </ul> <p>(<math>D_{WF}</math> is an effective value that implicitly includes the effect of tortuosity in a porous medium).</p>

Table 6.3.8-2. Parameters for EBS Transport Abstraction (Continued)

Waste Type	Transport Properties	Seeping Case	Non-Seeping Case
<b>Waste Form Domains</b>			
CDSP	Domain bulk volume, pore volume, and water volume	<p>Waste Form Domain is divided into two subdomains: HLWG and DSNF Subdomains</p> <p><u>HLWG Subdomain:</u></p> <ul style="list-style-type: none"> <li>• Consists of degradation products of five stainless steel canisters and HLW glass contained therein</li> <li>• Volume of HLWG degradation rind provided as function of time by <i>Defense HLW Glass Degradation Model</i> (BSC 2004 [DIRS 169988], Section 8.1, Eq. 54)</li> <li>• Porosity of HLWG rind provided by <i>Defense HLW Glass Degradation Model</i> (BSC 2004 [DIRS 169988], Table 8-1)</li> <li>• Steel corrosion products (CP) mass from Equation 8-4, pore volume (<math>V_{\phi,CP}</math>) from Equation 8-7, bulk volume from Equation 8-8 of <i>EBS Radionuclide Transport Abstraction</i> (SNL 2007 [DIRS 177407])</li> <li>• Total pore volume of HLWG Waste Form Subdomain, <math>V_{\phi,HLWG}</math>, given by Equation 8-13 of <i>EBS Radionuclide Transport Abstraction</i> (SNL 2007 [DIRS 177407])</li> <li>• <math>S_w</math> = water saturation in HLWG Waste Form Subdomain = 1.0.</li> </ul> <p><u>DSNF Subdomain:</u></p> <ul style="list-style-type: none"> <li>• Consists of degradation products of standard stainless steel DSNF canister containing degraded DSNF (rind)</li> <li>• Volume of DSNF rind, <math>V_{DSNF} = 1.0 \text{ m}^3</math> (BSC 2004 [DIRS 172453], Section 8.1)</li> <li>• Porosity of DSNF rind, <math>\phi_{DSNF} = 0.2</math></li> <li>• Steel corrosion products (CP) mass from Equation 8-4, pore volume (<math>V_{\phi,CP}</math>) from Equation 8-7, bulk volume from Equation 8-8 of <i>EBS Radionuclide Transport Abstraction</i> (SNL 2007 [DIRS 177407])</li> <li>• Total pore volume of DSNF Waste Form Subdomain, <math>V_{\phi,DSNF}</math>, given by Equation 8-13 of <i>EBS Radionuclide Transport Abstraction</i> (SNL 2007 [DIRS 177407])</li> <li>• <math>S_w</math> = water saturation in DSNF = 1.0.</li> </ul>	<p><u>HLWG Subdomain:</u></p> <p>Diffusion coefficient in HLWG Waste Form Subdomain, <math>D_{WF}</math>:</p> <ul style="list-style-type: none"> <li>• <math>\phi S_w D_{WF} = \phi^{1.3} S_w^2 D_{wi}</math></li> <li>• Effective porosity <math>\phi</math> of HLWG Waste Form Subdomain given by Equation 8-14 of <i>EBS Radionuclide Transport Abstraction</i> (SNL 2007 [DIRS 177407]), same as for Seeping Case</li> <li>• Water saturation in HLWG Waste Form Subdomain is based on water vapor adsorption isotherm: <math>S_w = \min[(V_{w,HLWG}/V_{\phi,HLWG}), 1.0]</math></li> <li>• Modified for temperature</li> <li>• <math>D_{wi}</math> = species dependent free water diffusion coefficient.</li> </ul> <p><u>DSNF Subdomain:</u></p> <p>Diffusion coefficient in DSNF Waste Form Subdomain, <math>D_{WF}</math>:</p> <ul style="list-style-type: none"> <li>• <math>\phi S_w D_{WF} = \phi^{1.3} S_w^2 D_{wi}</math></li> <li>• Effective porosity <math>\phi</math> of DSNF Waste Form Subdomain given by Equation 8-14 of <i>EBS Radionuclide Transport Abstraction</i> (SNL 2007 [DIRS 177407]), same as for Seeping Case</li> <li>• Water saturation in DSNF Waste Form Subdomain is based on water vapor adsorption isotherm: <math>S_w = \min[(V_{w,DSNF}/V_{\phi,DSNF}), 1.0]</math></li> <li>• Modified for temperature</li> <li>• <math>D_{wi}</math> = species dependent free water diffusion coefficient.</li> </ul> <p>(<math>D_{WF}</math> is an effective value that implicitly includes the effect of tortuosity in a porous medium).</p>

Table 6.3.8-2. Parameters for EBS Transport Abstraction (Continued)

Waste Type	Transport Properties	Seeping Case	Non-Seeping Case
<b>Waste Form Domains</b>			
CDSP (continued)	Advection and Diffusion	<p>Advective flow = volumetric flow rate through the waste package.</p> <p><u>HLWG Subdomain:</u></p> <p>Diffusive area:</p> <ul style="list-style-type: none"> <li>Diffusive area equal to surface area of cylinder with radius equal to half the radius of inner vessel cavity of five DHLW/DOE SNF Long waste package, excluding ends (= 13.7 m<sup>2</sup>).</li> </ul> <p>Diffusive path length:</p> <ul style="list-style-type: none"> <li>Set equal to the radius of inner vessel of 5 DHLW/DOE SNF Long waste package (= 0.941 m).</li> </ul> <p>Diffusion coefficient in HLWG Waste Form Subdomain, <math>D_{WF}</math>:</p> <ul style="list-style-type: none"> <li><math>\phi S_w D_{WF} = \phi^{1.3} S_w^2 D_{wi}</math></li> <li><math>\phi</math> = effective porosity of HLWG Waste Form Subdomain given by Equation 8-14 of <i>EBS Radionuclide Transport Abstraction</i> (SNL 2007 [DIRS 177407])</li> <li><math>S_w</math> = water saturation = 1.0</li> <li><math>D_{wi}</math> = species dependent free water diffusion coefficient.</li> </ul> <p>(<math>D_{WF}</math> is an effective value that implicitly includes the effect of tortuosity in a porous medium).</p>	<ul style="list-style-type: none"> <li>No advective flux</li> <li>Diffusive area same as for Seeping Case</li> <li>Diffusive path length same as for Seeping Case</li> </ul>
		<p><u>DSNF Subdomain:</u></p> <p>Diffusive area:</p> <ul style="list-style-type: none"> <li>Diffusive area set equal to the geometric surface area of HLWG subdomain (= 13.7 m<sup>2</sup>).</li> </ul> <p>Diffusive path length:</p> <ul style="list-style-type: none"> <li>The effective diffusive path length is calculated by dividing the initial volume of DSNF (1 m<sup>3</sup>) by the diffusive area leading to total diffusive length of 0.0730 m.</li> </ul> <p>Diffusion coefficient in Waste Form Subdomain, <math>D_{WF}</math>:</p> <ul style="list-style-type: none"> <li><math>\phi S_w D_{WF} = \phi^{1.3} S_w^2 D_{wi}</math></li> <li><math>\phi</math> = effective porosity of DSNF Waste Form Subdomain given by Equation 8-14 of <i>EBS Radionuclide Transport Abstraction</i> (SNL 2007 [DIRS 177407])</li> <li><math>S_w</math> = water saturation = 1.0</li> <li><math>D_{wi}</math> = species dependent free water diffusion coefficient.</li> </ul>	<ul style="list-style-type: none"> <li>No advective flux</li> <li>Diffusive area same as for Seeping Case</li> <li>Diffusive path length same as for Seeping Case</li> </ul>

Table 6.3.8-2. Parameters for EBS Transport Abstraction (Continued)

Waste Type	Transport Properties	Seeping Case	Non-Seeping Case
<b>Corrosion Products Domain</b>			
CSNF	Bulk volume and water volume	Pore volume of Corrosion Products Domain, $V_{\phi_{CP}}$ : <ul style="list-style-type: none"> <li>• Mass of corrosion products, <math>m_{CP}</math>, is function of time, Equation 8-4 of <i>EBS Radionuclide Transport Abstraction</i> (SNL 2007 [DIRS 177407])</li> <li>• Porosity <math>\phi_{CP} = 0.4</math></li> <li>• <math>V_{\phi_{CP}}</math> from Equation 8-7 of <i>EBS Radionuclide Transport Abstraction</i> (SNL 2007 [DIRS 177407]).</li> </ul>	<ul style="list-style-type: none"> <li>• Same as Seeping Case.</li> </ul>
		Volume of water: <ul style="list-style-type: none"> <li>• <math>S_w</math> = water saturation in corrosion products = 1.0</li> <li>• Water volume: <math>V_{w,CP} = S_w V_{\phi_{CP}}</math>.</li> </ul>	Volume of water: <ul style="list-style-type: none"> <li>• <math>S_{we,CP}</math> = effective water saturation in Corrosion Products Domain from Equation 8-11 of <i>EBS Radionuclide Transport Abstraction</i> (SNL 2007 [DIRS 177407])</li> <li>• Water volume = <math>S_{we,CP} V_{\phi_{CP}}</math>.</li> </ul>
	Advection and Diffusion	Advective flow = volumetric flow rate through the waste package	<ul style="list-style-type: none"> <li>• No advective flux.</li> </ul>
		Diffusive area: <ul style="list-style-type: none"> <li>• Diffusive area, for the path excluding the outer barrier, is the surface area of a cylinder halfway between the inside surface of the TAD canister and the outside surface of the inner vessel (= 29.9 m<sup>2</sup>)</li> <li>• Diffusive area for the path through the outer barrier of the waste package is taken to be the minimum of total area of all waste package breaches (scenario class dependent) and surface area of CSNF waste package (= 33.1 m<sup>2</sup>).</li> </ul>	<ul style="list-style-type: none"> <li>• Same as Seeping Case.</li> </ul>
		Diffusive path length: <ul style="list-style-type: none"> <li>• Diffusive path excluding the outer barrier is given by the combined thickness of TAD canister and inner vessel, constant parameter (= 0.0914 m)</li> <li>• Diffusive path through the outer barrier is the radial distance from the outside of the inner vessel to the outside of the outer barrier (= 0.0302 m).</li> </ul>	<ul style="list-style-type: none"> <li>• Same as Seeping Case.</li> </ul>

Table 6.3.8-2. Parameters for EBS Transport Abstraction (Continued)

Waste Type	Transport Properties	Seeping Case	Non-Seeping Case
		<p>Diffusion coefficient in Corrosion Products Domain, <math>D_{CP}</math>:</p> <ul style="list-style-type: none"> <li><math>\phi_{CP} S_w D_{CP} = \phi_{CP}^{1.3} S_w^2 D_{wi}</math></li> <li><math>\phi_{CP}</math> = porosity of corrosion products = 0.4</li> <li><math>S_w</math> = water saturation in corrosion products = 1.0</li> <li><math>D_{wi}</math> = species dependent free water diffusion coefficient.</li> </ul> <p>(<math>D_{CP}</math> is an effective value that implicitly includes the effect of tortuosity in a porous medium).</p>	<p>Diffusion coefficient in Corrosion Products Domain, <math>D_{CP}</math>:</p> <ul style="list-style-type: none"> <li><math>\phi_{CP} S_{we,CP} D_{CP} = \phi_{CP}^{1.3} S_{we,CP}^2 D_{wi}</math></li> <li><math>S_{we,CP}</math> = effective water saturation in corrosion products, Equation 8-11 of <i>EBS Radionuclide Transport Abstraction</i> (SNL 2007 [DIRS 177407])</li> <li><math>\phi_{CP}</math> = porosity of corrosion products = 0.4</li> <li>Modified for temperature</li> <li><math>D_{wi}</math> = species dependent free water diffusion coefficient.</li> </ul> <p>(<math>D_{CP}</math> is an effective value that implicitly includes the effect of tortuosity in a porous medium).</p>
<b>Corrosion Products Domain</b>			
CDSP	Bulk volume and water volume	<p>Pore volume of Corrosion Products Domain, <math>V_{\phi,CP}</math>:</p> <ul style="list-style-type: none"> <li>Same as for CSNF Seeping Case</li> <li><math>\phi_{CP}</math> = porosity of corrosion products = 0.4.</li> </ul>	<ul style="list-style-type: none"> <li>Same as Seeping Case</li> </ul>
		<p>Volume of water:</p> <ul style="list-style-type: none"> <li><math>S_w</math> = water saturation in corrosion products = 1.0</li> <li>Water volume = <math>S_w V_{\phi,CP}</math>.</li> </ul>	<ul style="list-style-type: none"> <li><math>S_{we,CP}</math> = effective water saturation in corrosion products, Equation 8-11 of <i>EBS Radionuclide Transport Abstraction</i> (SNL 2007 [DIRS 177407])</li> <li>Water volume = <math>S_{we,CP} V_{\phi,CP}</math>.</li> </ul>

Table 6.3.8-2. Parameters for EBS Transport Abstraction (Continued)

Waste Type	Transport Properties	Seeping Case	Non-Seeping Case
	Advection and Diffusion	<p>Advective flow = volumetric flow rate through the waste package</p> <p>Diffusive area:</p> <ul style="list-style-type: none"> <li>Diffusive area, for the path excluding the outer barrier, is given by the surface area of a cylinder halfway between the inside surface and the outside surface of the inner vessel (= 29.7 m<sup>2</sup>)</li> <li>Diffusive area for the path through the outer barrier of the waste package is taken to be the minimum of total area of all waste package breaches (scenario class dependent) and surface area of CDSP waste package given by the constant parameter (= 32.6 m<sup>2</sup>).</li> </ul> <p>Diffusive path length:</p> <ul style="list-style-type: none"> <li>Diffusive path excluding the outer barrier is given by the thickness of the inner vessel, constant parameter (= 0.0508 m)</li> <li>Diffusive path through the outer barrier is the radial distance from the outside of the inner vessel to the outside of the outer barrier (= 0.0301 m).</li> </ul> <p>Diffusion coefficient in Corrosion Products Domain, <math>D_{CP}</math>:</p> <ul style="list-style-type: none"> <li><math>\phi_{CP} S_w D_{CP} = \phi_{CP}^{1.3} S_w^2 D_{wi}</math></li> <li><math>\phi_{CP}</math> = porosity of corrosion products = 0.4</li> <li><math>S_w</math> = water saturation = 1.0</li> <li><math>D_{wi}</math> = species dependent free water diffusion coefficient.</li> </ul> <p>(<math>D_{CP}</math> is an effective value that implicitly includes the effect of tortuosity in a porous medium).</p>	<ul style="list-style-type: none"> <li>No advective flux</li> <li>Diffusive area same as for Seeping Case</li> <li>Diffusive path length same as for Seeping Case.</li> </ul> <p>Diffusion coefficient in Corrosion Products Domain, <math>D_{CP}</math>:</p> <ul style="list-style-type: none"> <li><math>\phi_{CP} S_{we,CP} D_{CP} = \phi_{CP}^{1.3} S_{we,CP}^2 D_{wi}</math></li> <li><math>S_{we,CP}</math> = effective water saturation in corrosion products, Equation 8-11 of <i>EBS Radionuclide Transport Abstraction</i> (SNL 2007 [DIRS 177407])</li> <li><math>\phi_{CP}</math> = porosity of corrosion products = 0.4</li> <li><math>D_{wi}</math> = species dependent free water diffusion coefficient.</li> </ul> <p>(<math>D_{CP}</math> is an effective value that implicitly includes the effect of tortuosity in a porous medium).</p>

Sources: Modified from DTN: SN0703PAEBSRTA.001\_R3 [DIRS 183217] from *EBS Radionuclide Transport Abstraction* (SNL 2007 [DIRS 177407], Table 8.2-1).

Table 6.3.8-3. Sampled Parameter Ranges and Distributions Used for Kinetic Sorption on Stationary Corrosion Products

Input Name	Input Description	Range	Distribution
Goethite_Site_Density_a	Goethite site density; discrete distribution	Density (sites nm <sup>-2</sup> )	Probability Level
		1.02	0.01786
		1.21	0.01786
		1.32	0.03571
		1.46	0.01786
		1.50	0.01786
		1.66	0.01786
		1.68	0.03571
		1.70	0.01786
		1.80	0.01786
		1.87	0.01786
		1.93	0.01786
		1.95	0.01786
		1.97	0.01786
		2.20	0.01786
		2.30	0.07143
		2.31	0.01786
		2.32	0.01786
		2.55	0.01786
		2.60	0.03571
		2.70	0.01786
		2.89	0.01786
		2.90	0.03571
		3.00	0.01786
3.12	0.01786		
3.13	0.01786		
3.30	0.03571		
3.40	0.01786		
4.00	0.01786		
4.20	0.01786		
4.60	0.01786		
4.84	0.01786		
4.90	0.01786		

Table 6.3.8-3. Sampled Parameter Ranges and Distributions Used for Kinetic Sorption on Stationary Corrosion Products (Continued)

Input Name	Input Description	Range	Distribution
Goethite_Site_Density_a (continued)	Goethite site density; discrete distribution (continued)	5.00	0.01786
		5.53	0.01786
		6.15	0.01786
		6.30	0.01786
		6.31	0.03571
		6.60	0.01786
		7.00	0.05357
		7.20	0.01786
		7.40	0.01786
		8.00	0.01786
		8.16	0.01786
		8.38	0.01786
		8.59	0.01778
HFO_Site_Density_a	HFO site density; discrete distribution	Density (sites nm <sup>-2</sup> )	Probability Level
		0.56	0.05263
		1.13	0.10526
		1.47	0.05263
		1.58	0.05263
		1.69	0.10526
		1.81	0.05263
		2.03	0.10526
		2.26	0.26316
		2.60	0.05263
		2.71	0.05263
		4.00	0.05263
		5.65	0.05265

Sources: Modified from DTN: SN0703PAEBSRTA.001\_R3 [DIRS 183217] from *EBS Radionuclide Transport Abstraction* (SNL 2007 [DIRS 177407], Table 8.2-2).

Table 6.3.8-4. Sampled Model Inputs Used in the EBS Radionuclide Transport Abstraction

Input Name	Input Description	Range	Distribution
Invert_Diff_Coeff_Uncert_a	Invert diffusion coefficient uncertainty	Range: $10^{\mu \pm 3\sigma}$ (dimensionless) Mean: $\mu = 0.033$ ; Std. Dev. $\sigma = 0.218$	$10^{ND}$
SS_Corrosion_Rate_a	Stainless steel corrosion rate	0.01 – 0.51 $\mu\text{m yr}^{-1}$ Mean = 0.267 $\mu\text{m yr}^{-1}$ Std. Dev. = 0.209 $\mu\text{m yr}^{-1}$	Truncated Lognormal
CS_Corrosion_Rate_a	Carbon steel corrosion rate	25 – 135 $\mu\text{m yr}^{-1}$ Mean = 78.5 $\mu\text{m yr}^{-1}$ Std. Dev. = 25.0 $\mu\text{m yr}^{-1}$	Truncated Lognormal
DS_Flux_Uncertainty_a	Drip shield flux-splitting uncertainty factor	0 – 0.85 (dimensionless)	Uniform
WP_Flux_Uncertainty_a	Waste package flux-splitting uncertainty factor	0 – 2.41 (dimensionless)	Uniform
Diameter_Colloid_a	Diameter of colloid particle	50 – 300 nm	Uniform
Goethite_SA_a	Specific surface area of goethite (FeOOH)	14.7 – 110 $\text{m}^2 \text{g}^{-1}$ Mean = 51.42 $\text{m}^2 \text{g}^{-1}$ Std. Dev. = 30.09 $\text{m}^2 \text{g}^{-1}$	Log-Normal (Truncated)
HFO_SA_a	Specific surface area of HFO	68 – 600 $\text{m}^2 \text{g}^{-1}$ Mean = 275.6 $\text{m}^2 \text{g}^{-1}$ Std. Dev. = 113.4 $\text{m}^2 \text{g}^{-1}$	Log-Normal (Truncated)
NiO_SA_a	Specific surface area of NiO	1 – 30 $\text{m}^2 \text{g}^{-1}$	Uniform
Cr2O3_SA_a	Specific surface area of Cr <sub>2</sub> O <sub>3</sub>	1 – 20 $\text{m}^2 \text{g}^{-1}$	Uniform
Relative_Abundance_Goethite_a	Mass fraction of iron oxides (goethite and HFO) that is goethite	0.45 – 0.80 (fraction)	Uniform
FHH_Isotherm_k_CP_a	FHH adsorption isotherm parameter <i>k</i> for corrosion products	1.048 – 1.370 (dimensionless)	Uniform
FHH_Isotherm_s_CP_a	FHH adsorption isotherm parameter <i>s</i> for corrosion products	1.525 – 1.852 (dimensionless)	Uniform
CSNF_Rind_SA_a	Specific surface area of CSNF rind	0.5 – 60 $\text{m}^2 \text{g}^{-1}$	Uniform
Density_CSNF_Rind_a	Density of CSNF rind	5,600 – 11,500 $\text{kg m}^{-3}$	Uniform
Porosity_Rind_CSNF_a	Porosity of CSNF rind	0.05 – 0.3 (fraction)	Uniform
FHH_Isotherm_k_CSNF_Rind_a	FHH adsorption isotherm parameter <i>k</i> for CSNF rind	1.606 – 8.215 (dimensionless)	Uniform
FHH_Isotherm_s_CSNF_Rind_a	FHH adsorption isotherm parameter <i>s</i> for CSNF rind	1.656 – 3.038 (dimensionless)	Uniform
HLWG_Rind_SA_a	Specific surface area of HLWG rind	10 – 38 $\text{m}^2 \text{g}^{-1}$	Uniform
Diameter_Colloid_a	Colloid particle diameter	50 – 300 nm	Uniform
Gamma_AFM_a	Active fracture model gamma parameter DTN: LA0701PANS02BR.003_R2 [DIRS 180497]	0.2 – 0.6	Uniform

Table 6.3.8-4. Sampled Model Inputs Used in the EBS Radionuclide Transport Abstraction (Continued)

Input Name	Input Description	Range	Distribution
EBS_UZ_Flux_Sat_PS1 EBS_UZ_Flux_Sat_PS2 EBS_UZ_Flux_Sat_PS3 EBS_UZ_Flux_Sat_PS4 EBS_UZ_Flux_Sat_PS5	Unsaturated zone fracture saturation DTN: LA0701PANS02BR.003_R2 [DIRS 180497] This includes the average fracture and matrix percolation fluxes and saturations for both glacial transition and post-10,000-year periods. There are a total of five percolation subregions.	Average values for the five percolation subregions based on the average of repository nodes in each percolation subregion.	2-D Table; see Table 6.3.8-5
pH_Cell_2_Regression_Error	Error term added to the surface complexation based pH calculation in the corrosion products domain.	Mean: $\mu = 0$ ; Std. Dev. $\sigma = 0.32$ Truncated at $\pm 2$ Std. Dev.	Truncated Normal
Diff_Path_Length_Invert_Top_a	Diffusive path length from waste package outer corrosion barrier to mid-point of invert.	0.30 – 1.24 m	Uniform

Sources: Modified from DTN: SN0703PAEBSRTA.001\_R3 [DIRS 183217] from *EBS Radionuclide Transport Abstraction* (SNL 2007 [DIRS 177407], Table 8.2-4).

NOTES: ND = Truncated normal distribution

Table 6.3.8-5. Unsaturated Zone Saturation and Flux Inputs Used in the EBS Radionuclide Transport Abstraction

<b>Parameter: EBS_UZ_Flux_Sat_PS1</b>				
	<b>Fracture Saturation</b>	<b>Matrix Saturation</b>	<b>Fracture Flux</b>	<b>Matrix Flux</b>
gt10	1.29E-02	9.14E-01	3.44E-01	3.32E-01
gt30	1.65E-02	9.34E-01	1.82E+00	4.81E-01
gt50	1.41E-02	9.00E-01	1.94E+00	4.25E-01
gt90	1.43E-02	8.85E-01	4.77E+00	5.86E-01
pk10	1.57E-02	9.66E-01	1.55E+00	7.14E-01
pk30	1.65E-02	9.32E-01	1.99E+00	4.66E-01
pk50	1.52E-02	9.23E-01	3.55E+00	5.39E-01
pk90	1.52E-02	9.02E-01	7.10E+00	7.01E-01
<b>Parameter: EBS_UZ_Flux_Sat_PS2</b>				
	<b>Fracture Saturation</b>	<b>Matrix Saturation</b>	<b>Fracture Flux</b>	<b>Matrix Flux</b>
gt10	1.69E-02	9.75E-01	2.81E+00	5.12E-01
gt30	2.17E-02	9.83E-01	1.11E+01	6.21E-01
gt50	1.61E-02	9.68E-01	1.21E+01	6.45E-01
gt90	1.82E-02	9.39E-01	3.29E+01	7.77E-01
pk10	2.23E-02	9.87E-01	1.27E+01	7.23E-01
pk30	2.25E-02	9.84E-01	1.35E+01	6.55E-01
pk50	1.79E-02	9.73E-01	2.41E+01	7.37E-01
pk90	1.87E-02	9.41E-01	3.81E+01	8.16E-01
<b>Parameter: EBS_UZ_Flux_Sat_PS3</b>				
	<b>Fracture Saturation</b>	<b>Matrix Saturation</b>	<b>Fracture Flux</b>	<b>Matrix Flux</b>
gt10	2.06E-02	9.86E-01	9.10E+00	6.69E-01
gt30	2.50E-02	9.88E-01	2.43E+01	7.64E-01
gt50	1.86E-02	9.75E-01	3.28E+01	7.92E-01
gt90	2.09E-02	9.31E-01	6.96E+01	9.21E-01
pk10	2.51E-02	9.88E-01	2.18E+01	7.28E-01
pk30	2.76E-02	9.89E-01	3.67E+01	7.89E-01
pk50	2.03E-02	9.76E-01	5.15E+01	8.11E-01
pk90	2.06E-02	9.30E-01	6.34E+01	8.99E-01
<b>Parameter: EBS_UZ_Flux_Sat_PS4</b>				
	<b>Fracture Saturation</b>	<b>Matrix Saturation</b>	<b>Fracture Flux</b>	<b>Matrix Flux</b>
gt10	2.36E-02	9.87E-01	1.92E+01	7.25E-01
gt30	2.72E-02	9.88E-01	3.72E+01	7.99E-01
gt50	1.95E-02	9.70E-01	5.36E+01	8.14E-01
gt90	2.14E-02	9.14E-01	9.32E+01	9.77E-01
pk10	2.53E-02	9.87E-01	2.62E+01	7.34E-01
pk30	3.07E-02	9.88E-01	6.00E+01	8.12E-01
pk50	2.04E-02	9.70E-01	6.93E+01	8.24E-01
pk90	2.06E-02	9.11E-01	7.62E+01	9.20E-01

Table 6.3.8-5. Unsaturated Zone Saturation and Flux Inputs Used in the EBS Radionuclide Transport Abstraction (Continued)

Parameter: EBS_UZ_Flux_Sat_PS5				
	Fracture Saturation	Matrix Saturation	Fracture Flux	Matrix Flux
gt10	2.52E-02	9.88E-01	2.81E+01	7.34E-01
gt30	2.82E-02	9.89E-01	4.51E+01	8.04E-01
gt50	1.95E-02	9.73E-01	6.68E+01	8.15E-01
gt90	2.16E-02	9.30E-01	1.09E+02	1.02E+00
pk10	2.55E-02	9.88E-01	2.95E+01	7.36E-01
pk30	3.21E-02	9.90E-01	7.48E+01	8.20E-01
pk50	2.03E-02	9.74E-01	8.11E+01	8.18E-01
pk90	2.05E-02	9.26E-01	8.49E+01	9.42E-01

Sources: Modified from DTN: SN0703PAEBSRTA.001\_R3 [DIRS 183217] from *EBS Radionuclide Transport Abstraction* (SNL 2007 [DIRS 177407], Table 8.2-5).

NOTE: Flux values are given in mm/yr but are entered as dimensionless in database. The units are added later in the model.

Table 6.3.8-6. Summary of CSNF Rind Volume Calculation Parameters for TSPA-LA

TSPA-LA Parameter Name	Model Abstraction Symbol	Description	Units	Distribution Type	Distribution Specification
Initial_Rod_Failures_a	None	Initial fraction of failed cladding, as received	None	Constant	100%
Fuel_Split_Fraction	None	Fraction of fuel available for corrosion at any timestep	None	Deterministic	1.0
Density_UO2	$\rho_{UO_2}$	Density of UO <sub>2</sub>	g/cm <sup>3</sup>	Deterministic	10.97
Density_Schoepite	$\rho_{sch}$	Density of schoepite	g/cm <sup>3</sup>	Deterministic	4.83
MW_UO2	$MW_{UO_2}$	Molecular weight of UO <sub>2</sub>	g/mole	Deterministic	270
MW_Schoepite	$MW_{sch}$	Molecular weight of schoepite	g/mole	Deterministic	322.1
Rind_Porosity_CS NF_a	$\phi_{sch}$	Porosity in rind	None	Uniform	Min = 0.05 Max = 0.3
Rod_Length_CS NF	$L_r$	Active fuel rod length	cm	Deterministic	366
Num_Rods_WP_CS NF	$N_r$	Number of rods per WP	None	Deterministic	5,544
Pellet_Diameter_CS NF	$D_{init}$	Initial pellet diameter	cm	Deterministic	0.819

Source: SNL 2007 [DIRS 180616], Tables 7-1[a] and 7-2[a]

Table 6.3.8-7. Alternative Conceptual Models Considered for EBS Transport

Alternative Conceptual Models	Key Assumptions	Assessment and Basis
Bathtub flow model	Seepage water flowing into breached waste package accumulates until void volume is filled before water containing dissolved radionuclides flows out. Various cases, such as changing inflow rates and effect of solubility and dissolution rate limits, are evaluated (SNL 2007 [DIRS 177407], Section 6.6.1).	For several of the most pertinent cases, the flow-through model is bounding with respect to releases of radionuclides.
Constrained water vapor and oxygen diffusion model	The rate of steel component corrosion inside a WP is compared with the rate of diffusion of water vapor and oxygen through stress corrosion cracks into a WP. A continuous film of adsorbed water cannot form if the consumption rate is higher, which could delay the diffusive releases until all steel is fully corroded (SNL 2007 [DIRS 177407], Section 6.6.2).	Insufficient data to validate.
Dual-continuum invert model	Crushed tuff invert ballast is modeled as a dual-continuum material consisting of intergranular pore space and intragranular pore space. All seepage flow into the drift flows through the intergranular pore space and into the UZ fractures. Imbibition from UZ host rock into the invert flows through the intragranular pore space. Diffusion of radionuclides also occurs in both the intergranular and intragranular pore spaces, from the WP corrosion products into UZ fractures and matrix, as well as between the two invert continua (SNL 2007 [DIRS 177407], Section 6.6.3).	Insufficient data to validate diffusion coefficients in individual continua. Insufficient data to confirm whether this is a bounding approach with respect to chemical conditions in the invert for calculating solubility and colloid stability.
Invert diffusion coefficient model with lower limit on water content	As the water content of the crushed tuff ballast decreases, the water films that connect pore spaces become disconnected, and the effective diffusion coefficient drops more rapidly than predicted by Archie's law. Below some critical water content, the diffusion coefficient becomes zero, based on models of diffusion in soils (SNL 2007 [DIRS 177407], Section 6.6.4).	Insufficient data to validate diffusive behavior at very low water contents.
Reversible sorption of radionuclides onto WP corrosion products (empirical $K_d$ sorption model)	Iron oxyhydroxide corrosion products sorb many radionuclide species. Sorption is assumed to be reversible and will not compete with other radionuclides nor compete for irreversible sorption sites (SNL 2007 [DIRS 177407], Section 6.6.5).	Does not account for limitations on total number of sorption sites. Does not account for competition with other radionuclides for sorption sites.
Plutonium sorption from stationary corrosion products and colloids	Plutonium sorbs strongly to iron oxyhydroxide corrosion product colloids and stationary corrosion products. Sorption may be considered slowly reversible (and modeled by computing the forward and reverse rate constants for the two-site model) (SNL 2007 [DIRS 177407], Section 6.6.6).	Experiment durations are short (hours to weeks) compared to the repository time scale. The mechanisms of plutonium sorption are not understood well enough to extrapolate the results outside the experiment design. Plutonium sorption and desorption data are not available for the highest pH ranges expected in the repository environment.

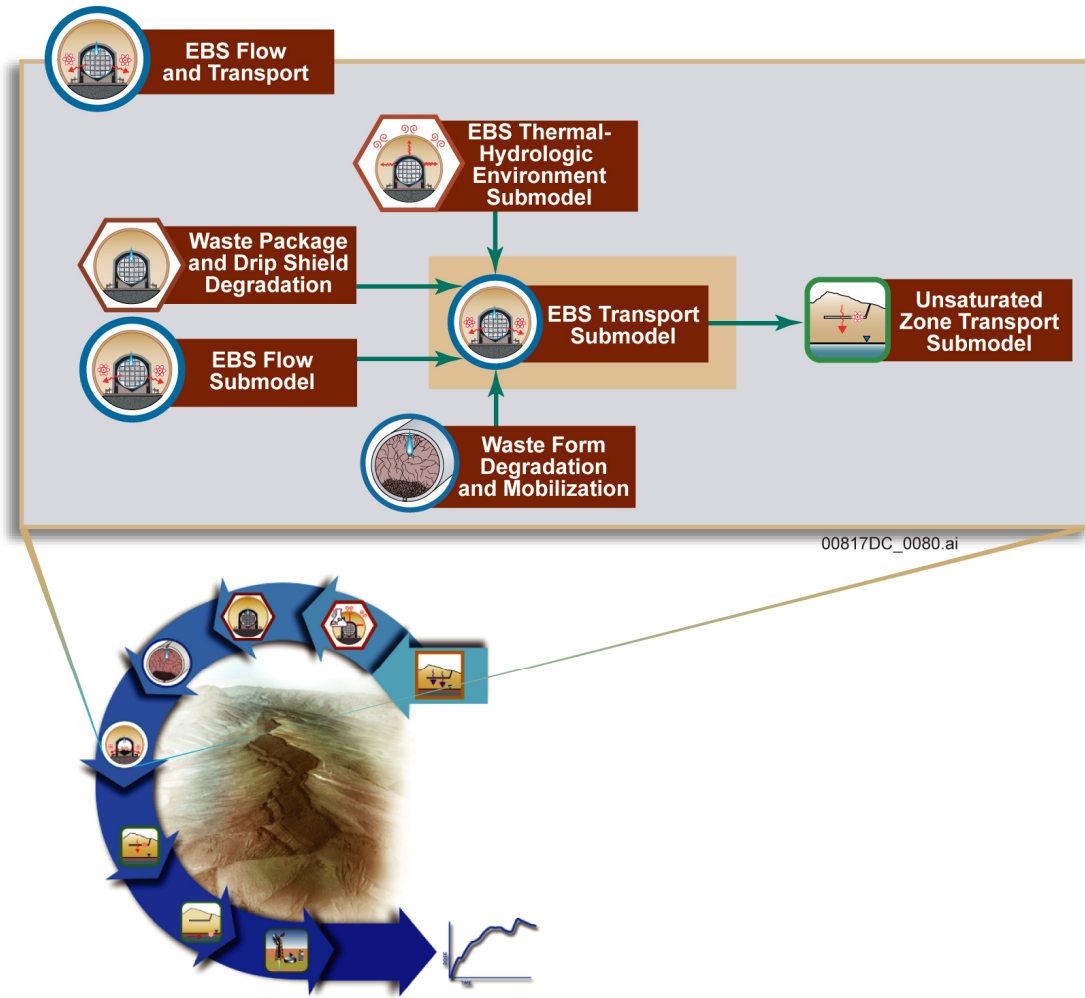


Figure 6.3.8-1. Information Flow Diagram for the EBS Transport Submodel

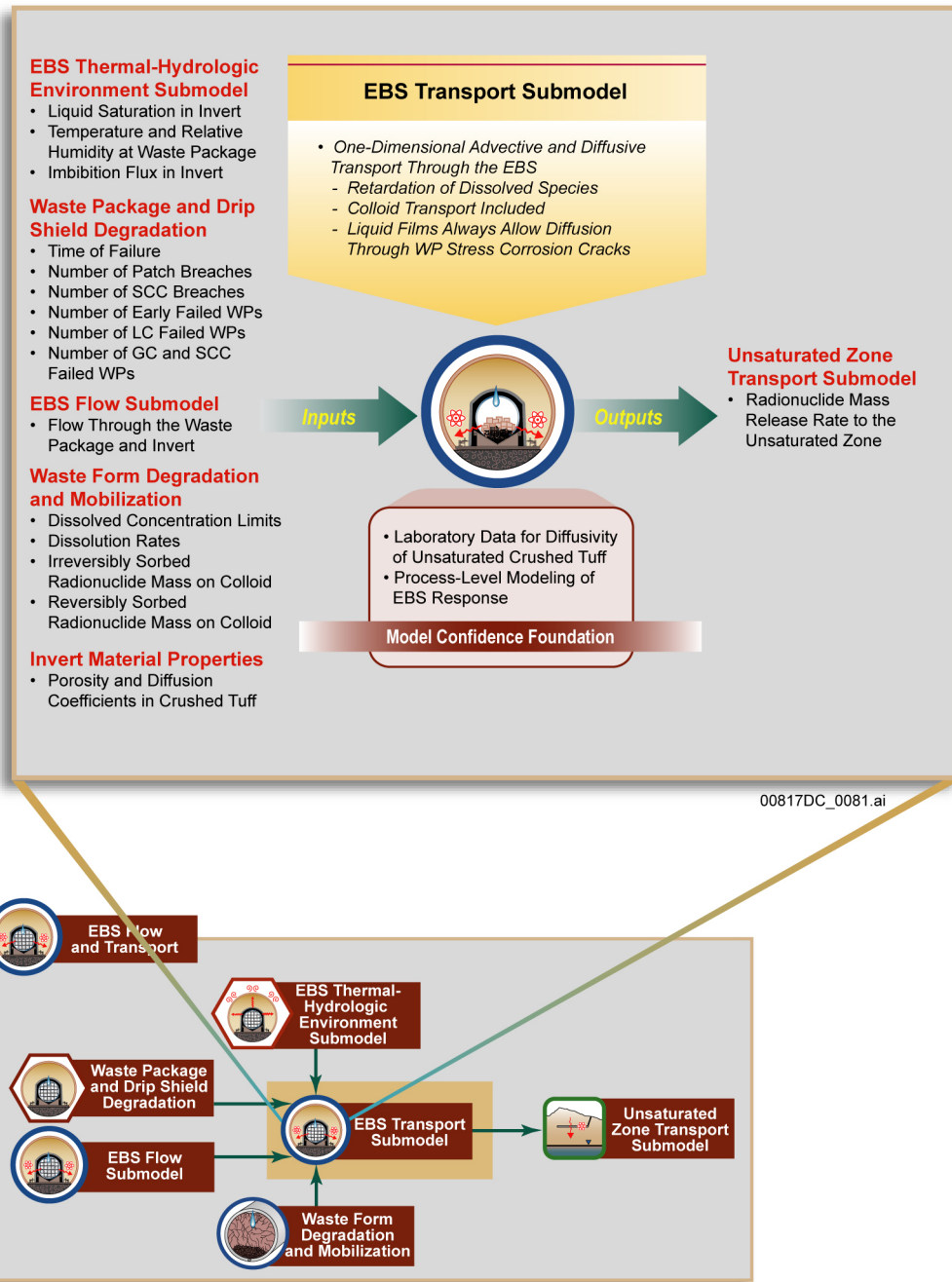


Figure 6.3.8-2. Inputs, Outputs, and Basis for Model Confidence for the EBS Transport Submodel

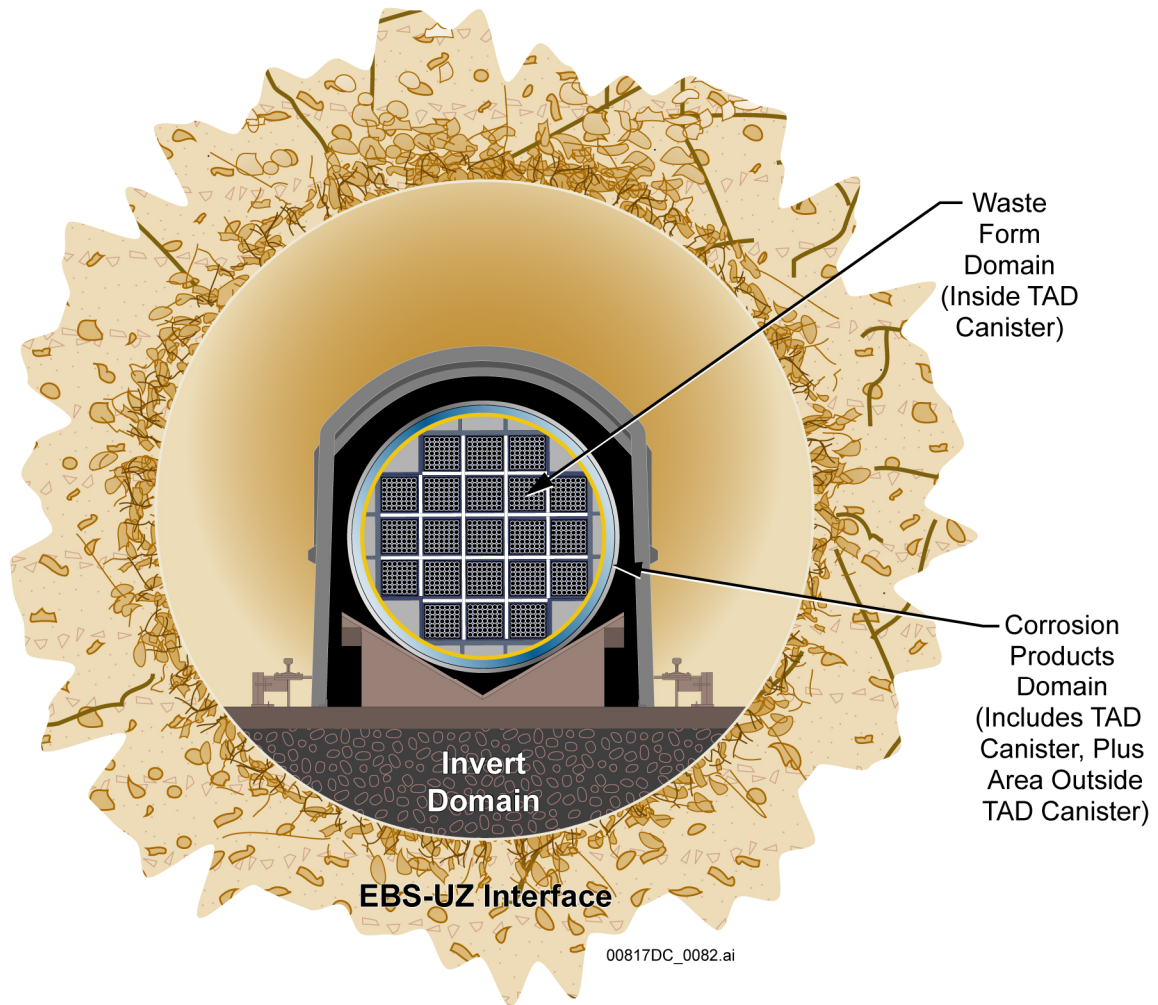


Figure 6.3.8-3. Cross Section of Idealized Drift Showing EBS Transport Submodel Domains for a CSNF Waste Package



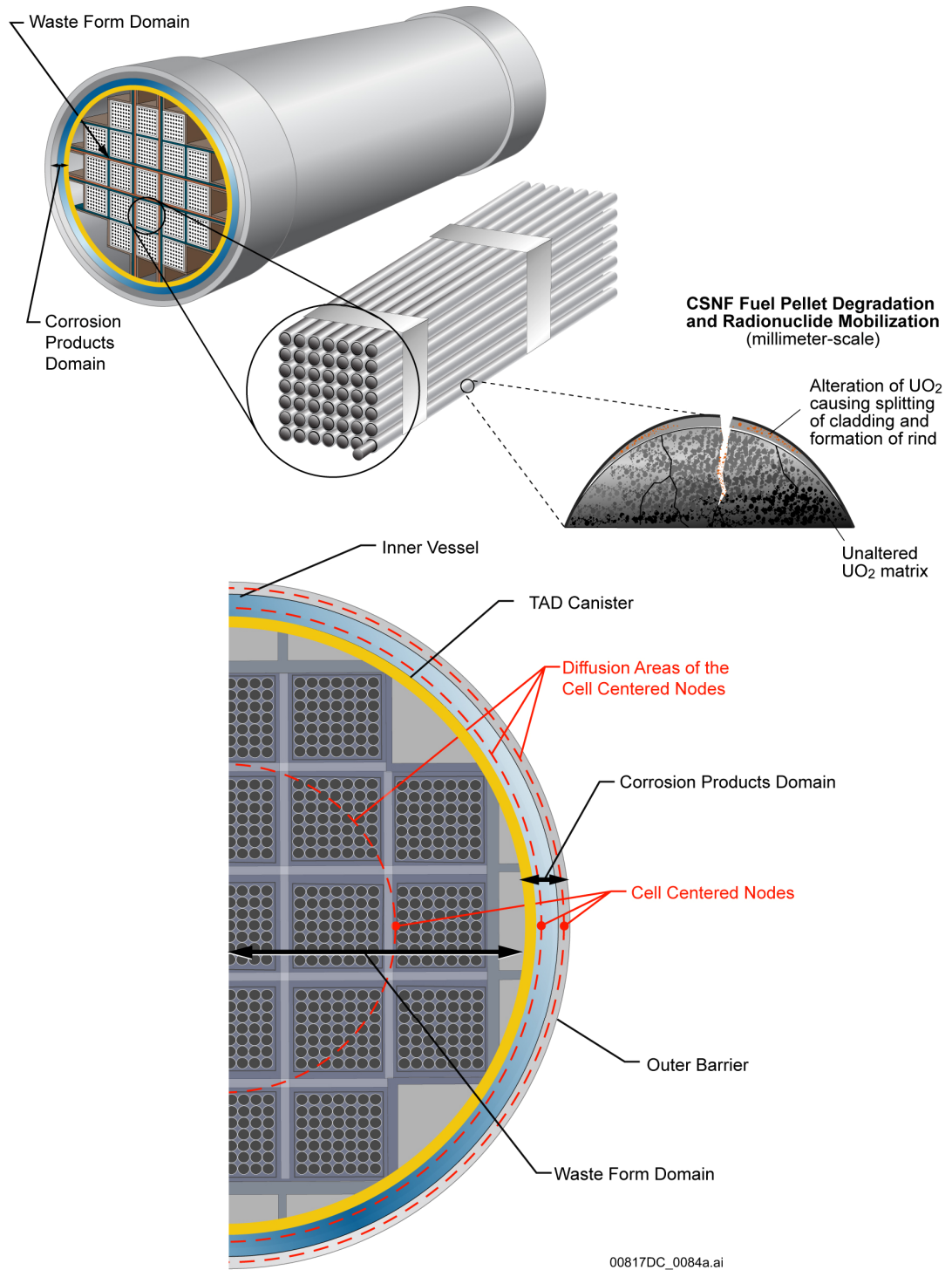


Figure 6.3.8-5. Setup of Cell Pathways for a CSNF Waste Package Used in the EBS Transport Submodel

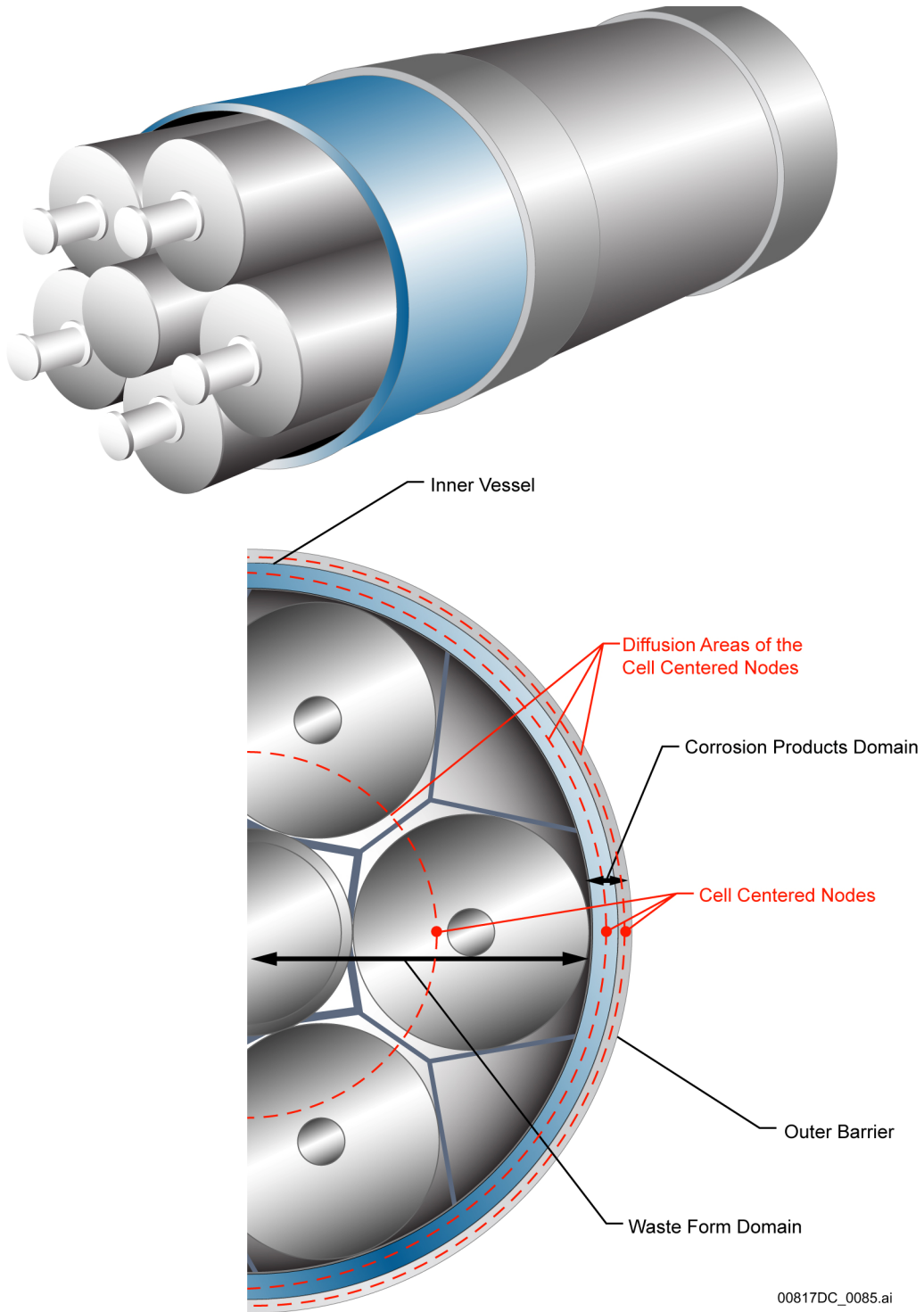
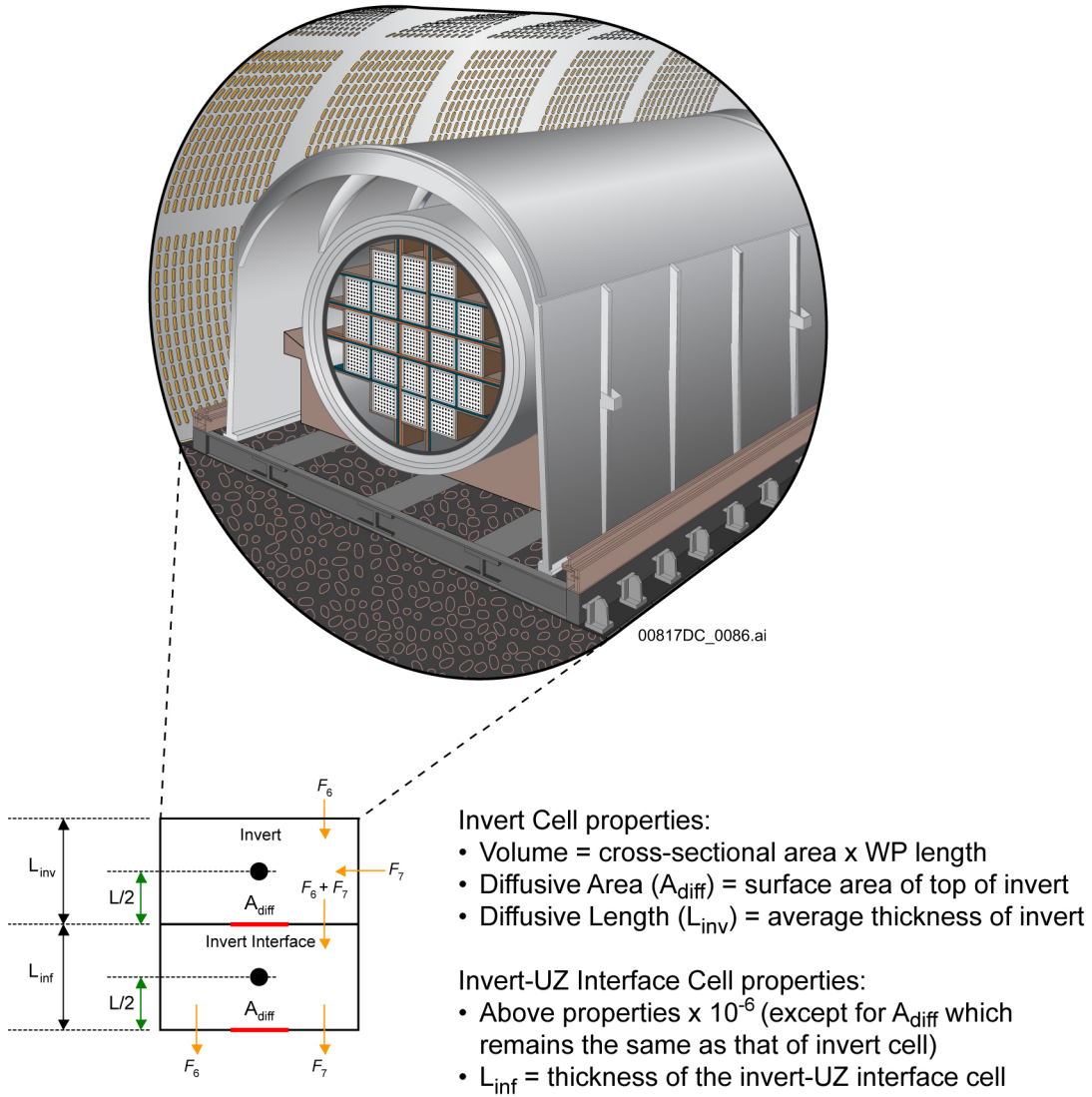
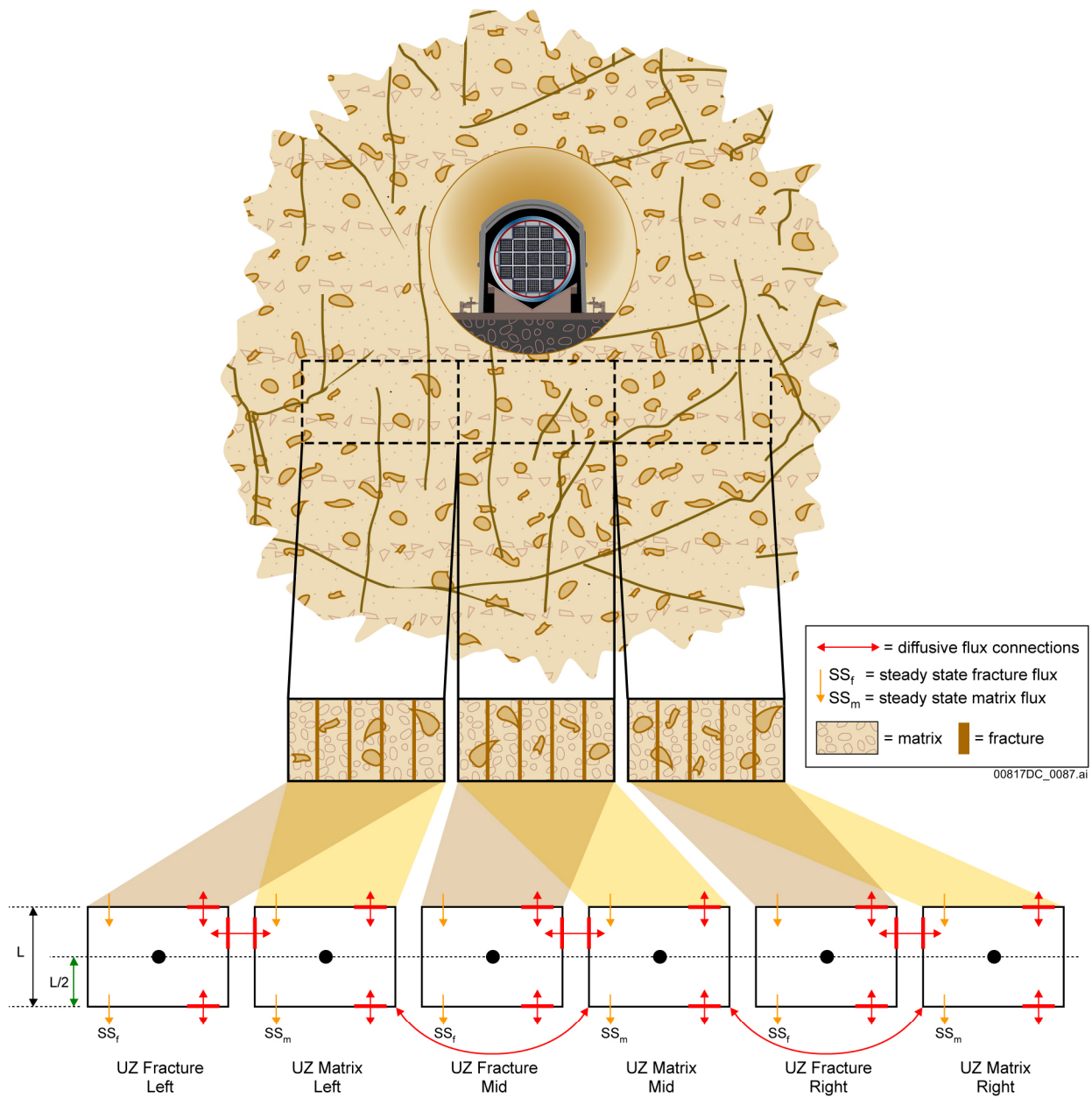


Figure 6.3.8-6. Setup of Cell Pathways for a CDSP Waste Package Used in the EBS Transport Submodel



NOTE: The flow pathways ( $F_6$  and  $F_7$ ) are discussed in Section 6.3.6.1 and on Figure 6.3.6-4.

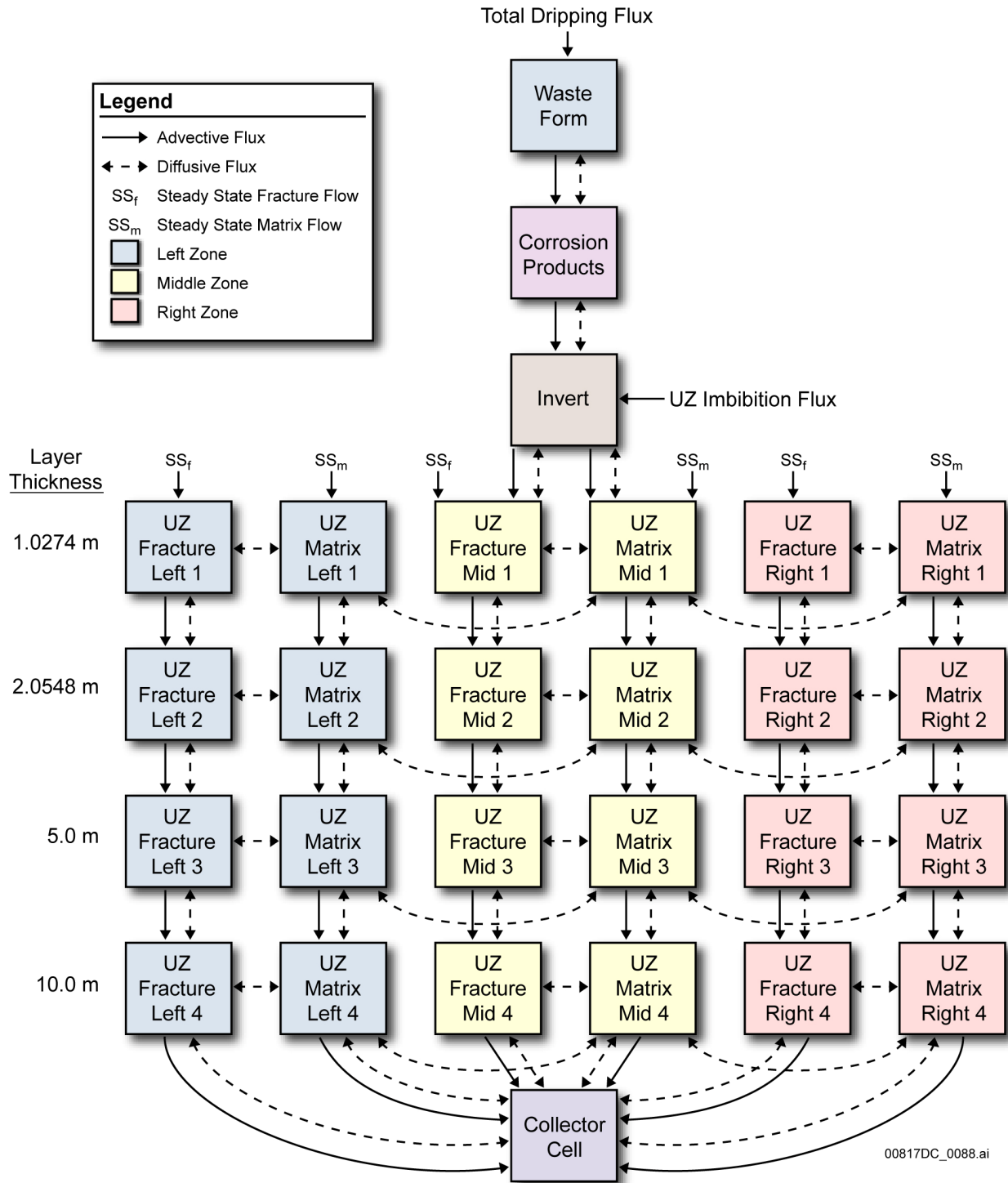
Figure 6.3.8-7. Setup of Invert Cell Pathways Used in the EBS Transport Submodel and their Relationship to the Actual Invert Geometry



**EBS-UZ Cell Properties:**

- Bulk Volume = Drift Diameter × Cell Height × Waste Package Length
- Pore Volume (Matrix) = Bulk Volume × Matrix Porosity × (1-Fracture Fraction)
- Pore Volume (Fracture) = Bulk Volume × Fracture Fraction
- Diffusive length and area are based on geometry

Figure 6.3.8-8. Setup of Dual-Continuum EBS-UZ Interface Cell Pathway Network and its Relationship to the Near-Field Unsaturated Zone



Source: SNL 2007 [DIRS 177407], Figure 6.5-4.

Figure 6.3.8-9. Schematic Representation of the Computational Grid for the EBS-UZ Interface Model

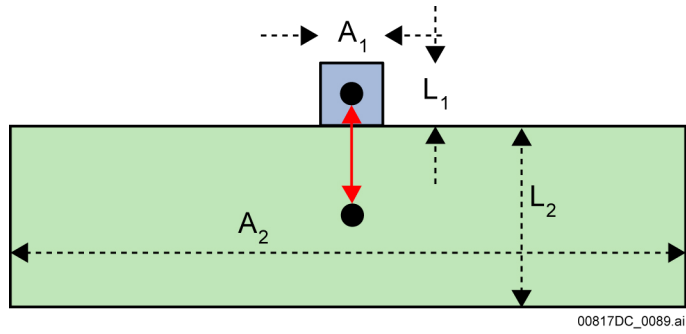


Figure 6.3.8-10. Simple Model Setup Using Cell Pathways with Different Diffusive Areas

### 6.3.9 Unsaturated Zone Transport

The UZ Radionuclide Transport Submodel of the TSPA-LA Model calculates the transport of radionuclides from the EBS of the Yucca Mountain repository, through the UZ to the SZ. UZ transport will depend on the flow fields from the *UZ Flow Models and Submodels* (SNL 2007 [DIRS 184614]) and on the rates of radionuclide mass releases from the waste emplacement drifts, as well as uncertainties associated with transport parameters. The UZ Transport Submodel provides, as output, the rate and spatial distribution of radionuclide releases to the SZ Flow and Transport Model Component. Information flow between the UZ Transport Submodel and other TSPA-LA Model components and submodels is shown on Figure 6.3.9-1. Figure 6.3.9-2 shows the connections between the UZ Transport Submodels and indicates elements of the foundation for confidence in the UZ Transport Submodel, the characteristics of radionuclide transport in the UZ, and the inputs and outputs associated with the UZ Transport Submodel. Note to differentiate between the first Addendum or the revision to that Addendum, and the base version, all references to the Addendums for *Particle Tracking Model and Abstraction of Transport Processes* (SNL 2008 [DIRS 184748], will be denoted by “[a]” or “[b]” after Section, Table and Figure numbers. References to the base version will have no bracketed index.

Note that for the UZ Transport Submodel, the basic parameters used in the model are input from the external input files from the FEHM DLL (FEHM V2.24-01, STN: 10086-2.24-01-00 [DIRS 179419]). These basic FEHM DLL input parameters and their sources are described in this section. Input variable names presented in the tables of this section are of two origins. For deterministic values of parameters, the names provided in the tables are consistent with the input variable names defined in the FEHM user guide (LANL 2003 [DIRS 167579]; DOE 2007 [DIRS 181096]). For stochastic input parameters, found in FEHM external files, the variable names reference the GoldSim elements that are used to generate the sampled values. These sampled values are downloaded from a supplemental GoldSim TSPA-LA Model simulation, performed at any stage in the model development or utilization, when any parameter stochastic distribution changes. The sampled values are downloaded from GoldSim into the FEHM stochastic parameter external files (Appendix F2.1.13). Using the updated FEHM stochastic parameter external files, simulations are then performed using these files until there is any change in any stochastic parameter. The names of the external input files, used by the FEHM DLL in the TSPA-LA Model, are listed in Table F-2 of Appendix F. A description of the contents of these external files can be found in Appendix F2.1.

Also, note that all references to FEHM in this section (Section 6.3.9) refer to FEHM Version 2.24-01 [DIRS 179419], which is the version used in the TSPA-LA Compliance Model and it will not be repeated every time FEHM is mentioned.

#### 6.3.9.1 Conceptual Model

Transport of dissolved and colloid-bound radionuclides through the UZ below the repository will occur in both the fractures and the rock matrix, as shown on the conceptual drawing of UZ transport processes on Figure 6.3.9-3. Flow pathways will be determined by the hydrogeologic characteristics of the rock units, the presence or absence of faults, and whether or not there is perched water present along individual flow pathways. These characteristics will control the

extent of downward versus lateral flow, advective transport between the fractures and matrix, matrix diffusion, and the partitioning of flow between the fractures and rock matrix. Fractures and faults can provide fast flow paths. Additionally, diffusion into the rock matrix and/or sorption onto the rock/mineral surfaces are important retardation processes for radionuclide transport (BSC 2004 [DIRS 170035], Sections 6.2.2 and 6.2.3).

Five basic processes will affect the transport of radionuclides:

- **Advection**—Advection is the movement of dissolved in conjunction with the bulk flow of water containing radionuclides. Advection tends to enhance radionuclide transport.
- **Matrix Diffusion**—Diffusion of radionuclides from fluid flowing in fractures into rock-matrix pores will be a potential retardation mechanism because matrix transport is typically slower than fracture transport. Conversely, diffusion from the matrix to the fractures would tend to decrease transport times. Figure 6.3.9-4 is a conceptual drawing of diffusion into and out of matrix pores. Diffusion within the matrix is also considered in the fracture matrix interaction model (SNL 2008 [DIRS 184748], Section C1).
- **Sorption**—Sorption onto the rock/mineral surfaces will slow or retard the transport of certain dissolved radionuclides through the UZ. Sorption also results in radionuclide attachment to colloids, which can enhance radionuclide transport.
- **Hydrodynamic Dispersion**—Hydrodynamic dispersion, which is the spreading of a plume of dissolved constituents, such as radionuclides released from the repository as they are transported, is caused by localized variations in the flow field. Hydrodynamic dispersion tends to smear sharp concentration gradients and reduce the concentration at the leading edge of a breakthrough curve of radionuclides at the water table. Hydrodynamic dispersion is an approximate way of accounting for flow system heterogeneities of various scales that are not captured in the simulated flow fields. The UZ Transport Submodel only considers longitudinal hydrodynamic dispersion and does not consider transverse dispersion (SNL 2008 [DIRS 184748], Section 5.0, Assumption 3).
- **Radioactive Decay and Ingrowth**—Radioactive decay reduces the concentration of radionuclides in a predictable way, but it also produces decay products that typically have sorption characteristics different from those of the source radionuclides.
- **Colloid Transport**—In addition to being transported in a dissolved state, radionuclides can be transported while attached to colloids which are subject to advective-dispersive transport in the fractures and rock matrix. The colloid attachment can be effectively irreversible or reversible as described by an equilibrium sorption constant between the colloid and groundwater (SNL 2008 [DIRS 184748], Section 6.4.5). Colloids in turn may be subject to retardation within the fractures and other processes including size exclusion between the fractures and rock matrix and permanent filtration in the rock matrix, especially when entering units of differing pore size. A more complete discussion of colloid transport and the processes that control it follows below.

Colloid transport in the UZ is primarily in the fractures because colloids are limited in their capacity to diffuse into rock matrix as reflected in the low estimated values for diffusion coefficients (SNL 2007 [DIRS 177396], Section 6.18.2). Colloid transport into the rock matrix is also limited by size exclusion. Colloids can also be transported between the fractures and rock matrix and through the rock matrix by advection as long as the colloids are smaller than the matrix pores. In the UZ Transport Submodel, diffusion of colloids between the fractures and rock matrix is assumed to be negligible, while advective transport between the fractures and rock matrix is modeled explicitly. Figure 6.3.9-5 is a conceptual drawing showing some of the elements related to colloid-facilitated transport. Two principal types of colloid attachment can exist: reversible attachment where the radionuclides are temporarily attached to the surface of colloids and irreversible attachment where the radionuclides are permanently imbedded in the colloid structure. Advection of colloids through fractures is expected to dominate colloid transport in welded and zeolitic tuffs because permeability in the welded and zeolitic tuff matrix is much lower than that in the fractures. The rock matrix pores are typically smaller than the fracture apertures and the colloids themselves in many instances. Colloid filtration can occur in the matrix during transport from one hydrogeologic unit to another. That is, when the size of the colloids is larger than the matrix pores in the downgradient unit, the colloids are stopped at the unit interface. This filtration effect results in permanent immobilization of radionuclides irreversibly attached to the colloids but not of radionuclides reversibly attached to colloids. In the latter instance, the radionuclides could desorb from the colloids and continue to migrate. For this reason only irreversible colloids are filtered at unit interfaces in the TSPA-LA Model. In addition, colloid exclusion from the matrix can occur when there is a component of flow from the fractures into the matrix, and some colloids that would otherwise migrate from the fracture continuum to the matrix continuum are excluded due to their size relative to the matrix pore size. Filtration of colloids during transport within fractures is implicitly considered in the colloidal retardation factor.

A change to wetter climates may also impact the transport of radionuclides through the UZ by increasing net infiltration at the ground surface and, subsequently, the percolation flux through the UZ. Along with increased transport rates through the UZ, wetter climates would also lead to an increase in water table elevation. A higher water table shortens transport distances from the EBS to the water table. In the TSPA-LA Model, a rise in the water table is accompanied by an instantaneous release, to the SZ, of the radionuclides that are presently in the geologic units impacted by the water table rise.

### **6.3.9.2 TSPA-LA Model Abstraction**

Consistent with the Mountain-Scale UZ Flow Submodel, the UZ Transport Submodel is a dual-continuum model. In the UZ Transport Submodel, fracture and matrix transport are coupled and calculated using the FEHM [DIRS 179419] residence-time transfer-function particle-tracking technique, as described in *Particle Tracking Model and Abstraction of Transport Processes* (SNL 2008 [DIRS 184748], Section 6.4). This technique is a cell-based approach in which particles move from cell to cell in the FEHM numerical grid. Particle movement from cell to cell is computed probabilistically based on flow balance, dispersivity, and matrix diffusion. The fracture matrix interactions are evaluated using transfer functions when diffusive transport between fracture and matrix (i.e., dual-permeability or discrete fracture models) is simulated. The transfer functions used in the TSPA-LA Model are a set of

breakthrough curves defined using dual-permeability numerical solutions of the transport equations for parallel flow in a fracture and adjacent rock matrix and diffusion normal to the flow direction (SNL 2008 [DIRS 184748], Appendix C). After a particle enters a cell, the adjacent cell it will travel to next (or whether it will switch media in the same cell) is probabilistically determined using random sampling based on the water flow balance. Note that only outflows from cells are included in the calculations; particles are not moved to a cell if water flows from that cell to the current cell. For the dissolved species and reversible colloids simulated in the TSPA-LA Model, the transfer functions are used to randomly decide if a particle will change medium (go from fracture to matrix or from matrix to fracture) and to determine the cell residence times for each particle. For the irreversible colloids, which are not subject to matrix diffusion, the residence times for each particle are a function of the cell pore volumes, the flux out of the cells, and the colloid retardations (for the retarded or  $I_c$  species only). To simulate the effects of longitudinal dispersivity in dissolved species, reversible colloids, and irreversible colloids, the residence times are updated with a random factor based on the Peclet number between cells, where the Peclet number is a function of the dispersivity and the distance between cells.

The dual-continuum UZ Transport Submodel includes a numerical grid of fracture cells representing the fracture continuum and a grid of matrix cells representing the matrix continuum, with each fracture cell connected to a corresponding matrix cell. Twenty-seven radionuclides are transported through the UZ. The radionuclide half-lives and decay products used in the TSPA-LA Model are listed in Table 6.3.9-1. The following processes are simulated in the TSPA-LA Model:

- Advective-dispersive transport of dissolved radionuclides in the fracture and matrix continua and between continua
- Fracture-matrix interaction and matrix diffusion
- Sorption of dissolved radionuclides in the matrix continuum
- Advective-dispersive transport of colloids with radionuclides attached (transport of colloids is explicitly simulated when radionuclides are considered to be irreversibly attached and implicitly simulated in conjunction with the transport storage term when radionuclides are considered to be reversibly sorbed)
- Retardation in the fracture continuum of colloids, on which radionuclides are reversibly and irreversibly sorbed
- Colloid filtration at interfaces between rock-matrix units
- Colloid size exclusion at fracture-matrix continua interfaces
- Radioactive decay and ingrowth

- Climate change and its effect on fluid flow rates in the UZ
- Rise in water-table elevation and its effect on radionuclide release to the SZ.

Uncertainty is included in the UZ Transport Submodel by defining statistical distributions for a number of input parameters. Thus, each realization of the total system has a unique set of input parameters. In addition, each realization is considered to be equally likely. Some of the uncertainty in UZ transport results from uncertainties passed to the UZ Transport Submodel from other submodels. For example, there may be uncertainty in infiltration and UZ flow from the Site-Scale UZ Flow Process Model; uncertainty in the number of failed WPs from the WP and DS Degradation Model Component; and uncertainty in numerous EBS parameters and processes used to define the radionuclide source term received from the EBS Transport Submodel. These uncertainties from upstream submodels are passed to the UZ Transport Submodel either implicitly through the passing of the radionuclide fluxes and ratios of fluxes applied to the fractures versus total fluxes (fluxes applied to fractures and rock matrix) from GoldSim to FEHM, or explicitly through the passing of data, such as the number of WPs failed in each percolation subregion (source bin) or indices denoting which infiltration rate scenario should be applied (10th percentile, 30th percentile, 50th percentile, or 90th percentile rate scenario). For the sampled infiltration rate scenario, a set (10th percentile, 30th percentile, 50th percentile, or 90th percentile) of four flow fields representing the three climates of present day, monsoon, and, glacial-transition, is read in by the FEHM DLL for that realization. Note that the classification of 10<sup>th</sup>, 30<sup>th</sup>, 50<sup>th</sup>, and 90<sup>th</sup> percentile infiltration scenarios is based on the infiltration maps used to develop the flow fields for the first three climates. For the post-10,000-year climate, the four equivalent flow fields are generated using the scaled 90th percentile present-day, 50th percentile Glacial Transition, 90th percentile glacial transition, and the 90th percentile monsoon infiltration maps, respectively (see Section 6.3.1). The uncertainty distributions sampled to derive parameters for the FEHM DLL are summarized in Tables 6.3.9-2 through 6.3.9-12. The uncertainty distribution for the infiltration scenarios is presented in Table 6.3.1-2. Note that some of the parameters derived for the UZ Transport Submodel, such as matrix sorption and matrix diffusion coefficients, are also used in the EBS Submodel for sections of cell networks representing the UZ directly below the repository.

The UZ Transport Model Abstraction is based on FEHM's multi-species particle tracking option that uses the 16 flow fields from the UZ Flow Model Abstraction to evaluate the movement of radionuclides from the repository to the water table. The UZ Flow Model Abstraction is comprised of 16 steady-state flow fields generated by the three-dimensional Site-Scale UZ Flow Model (Section 6.3.1.2). The 16 flow fields consist of four flow fields representing uncertainty for each of four climate states, including present-day, monsoon, glacial transition, and post-10,000-year (Section 6.3.1.2). The flow fields provide spatial distributions of fracture-fracture, matrix-matrix, and fracture-matrix water flow rates and moisture contents in the UZ. During TSPA-LA Model simulations, temporal changes in climate are approximated by changes from one steady-state flow field to another. For example, at the onset of the monsoon climate stage, a present-day climate stage flow field is replaced with a monsoon climate stage flow field. Uncertainty in the UZ Flow Model Abstraction is implemented through probabilistic sampling of the four flow fields that correspond to the infiltration uncertainty maps generated for each climate state (Section 6.3.1.2). The sampling of four infiltration cases is based on a set of weighting factors (Table 6.3.1-2) developed using a generalized likelihood uncertainty estimate

methodology to determine meaningful weighting factors for the selected infiltration maps (Section 6.3.1.2). To approximate the effects of a rising water table on a radionuclide transport simulated by the FEHM multi-species particle tracking option, the monsoon climate, glacial-transition, and post-10,000-year climate flow-field files used in the transport model have been post-processed (see Section 6.3.1.1). In the updated files, the water table elevations for the monsoon, glacial-transition, and post-10,000-year climate flow fields have been constrained to a minimum level of 850 m above mean sea level. For the future climates, any locations where the present-day water table is below 850 m, it is set to 850 m and any locations where the present-day water table is above 850 m, the water table is not adjusted from the present day level (see BSC 2004 [DIRS 169855]). Note that the bottom boundary for the flow models of all climate states is the present day water table. Within the repository footprint, the present-day water table varies from around 730 m to 850 m above mean sea level (BSC 2004 [DIRS 169855] Figure 6.2). The changes to the monsoon, glacial-transition, and post-10,000-year climate flow fields, represent a water table rise of up to 120 m within the repository fingerprint (Section 6.3.1.1), effectively shortening the transport path through the UZ. After the instantaneous change in water table levels following the onset of the monsoon climate, all radionuclide mass associated with particles residing between the original and updated water tables are instantaneously added to the SZ source term.

In the TSPA-LA Model, radionuclide sorption on the rock matrix is approximated using a linear, equilibrium sorption model characterized by a single parameter, the sorption coefficient  $K_d$ . A set of three probability distributions for the  $K_d$ s used in the model have been developed for each radioelement. Each set of  $K_d$ s describes the radioelement's sorptive behavior in each of three major rock types (vitric, devitrified, and zeolitic tuffs) in the UZ (SNL 2007 [DIRS 177396], Appendices A[a] and B[a] for selenium and tin, and Appendices A and B for all other species). These effective sorption coefficients are a function of many factors, including mineralogy, groundwater aqueous chemistry, and heterogeneity, at scales smaller than those considered in the numerical model. Furthermore, in developing the sorption coefficients, the kinetics of sorption reactions and nonlinear sorption effects that would lead to lower  $K_d$ s were considered. The above factors were considered when establishing the parameter uncertainty distributions for the  $K_d$  values. In addition, sorption coefficients may be affected by temperature. With elevated temperatures, the sorption coefficient generally increases for cationic species, thereby causing longer transport times (SNL 2007 [DIRS 177396], Section 6.1.2.9). The linear equilibrium sorption coefficients used in the TSPA-LA Model do not account for elevated temperatures and, therefore, are conservative with respect to transport times for cationic species through the UZ (SNL 2007 [DIRS 177396], Section 6.1.5.2). Note that shorter travel times are considered to be conservative. The parameter distributions used in the UZ Transport Submodel for matrix sorption coefficients are provided in Table 6.3.9-2.

For the TSPA-LA Model, unsaturated matrix diffusion coefficients are generated as the product of the matrix tortuosities for specified rock groups and the free-water diffusion coefficients for the elements considered. The tortuosities are based on a correlation between matrix diffusion, matrix porosity, and matrix saturated permeability developed from diffusion data in saturated samples by Reimus et al. (2007 [DIRS 179246]). To adapt the relationship for the UZ, porosity is replaced by water content, and saturated permeability is replaced by effective permeability. The methodology used in the derivation of the distributions for tortuosities is described in *Particle Tracking Model and Abstraction of Transport Processes* (SNL 2008 [DIRS 184748],

Section 6.5.5[a] and Appendix A[a]). The resultant tortuosity distributions are found in DTN: LB0702PAUZMTDF.001\_R1 [DIRS 180776]. The derivation of the constant values for element specific free-water matrix diffusion coefficients is also described in *Particle Tracking Model and Abstraction of Transport Processes* (SNL 2008 [DIRS 184748], Section 6.5.5[a] and Appendix A[a]). The free-water matrix diffusion coefficients used in the UZ Transport Submodel of the TSPA-LA Model are found in DTN: LB0702PAUZMTDF.001\_R1 [DIRS 180776].

The equation describing the correlation between matrix diffusion (or matrix tortuosity), porosity (or water content for the UZ), and saturated permeability (or effective permeability for the UZ) used for calculating the matrix diffusion coefficient, is (SNL 2008 [DIRS 184748], Eq. A-1[a]):

$$\log_{10}(D_m / D^*) = 1.42 + 1.91\theta_m + 0.19\log_{10}(k_m) \quad (\text{Eq. 6.3.9-1})$$

where

- $D_m/D^*$  = the matrix tortuosity
- $D_m$  = the matrix diffusion coefficient in  $\text{m}^2/\text{s}$
- $D^*$  = the free water diffusion coefficient in  $\text{m}^2/\text{s}$
- $\theta_m$  = the matrix water content
- $k_m$  = the effective permeability to water in  $\text{m}^2$ .

Note that Equation 6.3.9-1 is an adaptation of the original equation for the UZ with water content replacing matrix porosity and effective permeability replacing permeability. The element-specific values for free-water diffusion coefficients are presented in Table 6.3.9-3. The  $\log_{10}$  values of the mean tortuosities for the three rock groups that are assembled based on similar attributes are presented in Table 6.3.9-4. The SDs of the  $\log_{10}$  tortuosities, based on the standard error of the regression curves defined by Equation 6.3.9-1, are also presented in Table 6.3.9-4 (also SNL 2008 [DIRS 184748], Table 6.5.5-1[a] and Section 6.5.5.4 [a]). The uncertainty is implemented in the TSPA-LA Model for each rock group by selecting a standard normal random number and adding the product of the standard normal random number and SD (in  $\log_{10}$  space) to the  $\log_{10}$  value of the mean tortuosity, taking the antilog of the value to derive the tortuosity for the present realization and multiplying each element-specific free-water diffusion coefficient by the tortuosity to derive 15 element-specific effective diffusion coefficients (SNL 2008 [DIRS 184748], A-3 [a]).

As previously noted for TSPA-LA simulations, the diffusion of colloids from the fracture to the matrix is not simulated. This treatment is considered conservative with respect to reducing colloid transport times to the SZ (SNL 2008 [DIRS 184748], Section 6.5.5).

In the UZ Transport Submodel, the fracture dispersivity is set to 10 m. According to *Particle Tracking Model and Abstraction of Transport Processes* (SNL 2008 [DIRS 184748], Section 4.1.6[a] and Section 6.5.2), the value of 10 m represents a conservative value chosen from the lower end of the field studies. A higher dispersivity tends to spread the plume and reduce the peak concentrations. In addition, in comparison with the effects of matrix diffusion

and the large-scale heterogeneities in the UZ, dispersivity effects are expected to have a small influence on the breakthrough curves (SNL 2008 [DIRS 184748], Section 6.5.2). Note that FEHM's multi-species particle tracking model limits the Peclet number between adjacent nodes to  $\geq 1$ , where the Peclet number is the ratio of path length to dispersivity (SNL 2008 [DIRS 184748], Section 6.4.2). This means that for nodal distances  $\leq 10.0$  m, the dispersivity will be set equal to the path length. For most of the TSPA-LA Model, the dispersivity will be 10 m; just below the repository, for some of the links between cells, the dispersivities may be as low as 5 m.

Part of the conceptual model upon which the UZ Transport Submodel is based, is the Active Fracture Model (AFM) of Liu et al. (1998 [DIRS 105729]). The AFM takes into consideration the fact that due to the nonlinearities associated with unsaturated flow, only a portion of fractures in the UZ fracture network are subject to water flow and the others are bypassed. The AFM assumes that since only a portion of the fractures in a network have water flowing through them, there is an effect on the spacing of flow and transport pathways in the fracture network, the fracture/matrix interface area, and the number of active fractures in a grid block. In the TSPA-LA Model, the spacing between flowing fractures is calculated as a function of the geometric fracture spacing, fracture saturation, fracture residual saturation, and the active AFM parameter ( $\gamma$ ) (Liu et al. 1998 [DIRS 105729]). In the TSPA-LA Model, a constant fracture residual saturation of 0.01 is used for all layers (SNL 2008 [DIRS 184748], Section 6.5.6).

In addition to adjusting the spacing between flowing fractures, the active fracture conceptualization calls for an adjustment to the interface area across which matrix diffusion occurs. The effective area reduction factor ( $R$ ) described by Liu et al. (1998 [DIRS 105729]) can be written in the form:

$$R = S_e^{1+\gamma} \quad (\text{Eq. 6.3.9-2})$$

where  $S_e$  is the effective water saturation. As implemented in FEHM, the effective area reduction factor can be broken down into the product of the  $S_e$  and  $S_e^\gamma$ , where the first term represents the area adjustment factor and the second term represents the fracture spacing adjustment factor (SNL 2008 [DIRS 184748], Section C5). The interface adjustment accounts for the reduction of the wetted area within an individual fracture and for the reduction in area caused by the smaller number of active fractures. This adjustment to the interface area is a reduction by a factor of the effective saturation (SNL 2008 [DIRS 184748], Appendix C, Section C-5). Note that the effective interface area (Equation 6.3.9.2) between the fracture and matrix is reduced by a factor of the effective saturation even when all fractures are considered active ( $\gamma = 0$ ). The area reduction associated with the active fracture model is a conservative representation for situations in which radionuclide mass is introduced into the fracture continuum. An underestimation of the diffusive area would slow the movement of mass applied to the rock matrix and increase the rate of movement of mass through the fractures. For mass applied to the rock matrix, there would be a decrease in mass diffusing out of the matrix slowing its movement through the system. As implemented, the active fracture conceptualization is consistent with the assumptions of the fracture-matrix interaction, as validated in *Particle Tracking Model and Abstraction of Transport Processes* (SNL 2008 [DIRS 184748], Section 7.2.3.3). Note that the UZ Transport Submodel uses different active fracture model parameter values than the UZ Flow Field Abstraction. In the

UZ Flow Model, the active fracture model parameter values are calibrated. To be rigorous, the AFM parameters should be consistent between the flow and transport model because the AFM parameters affect both flow and transport processes (SNL 2008 [DIRS 184748], Section 6.6.4). However, since process flow model studies (SNL 2007 [DIRS 184614]) have shown that the AFM parameter values have little influence on the fluid saturations and steady-state fracture to fracture and matrix to matrix flow, the use of the base case flow fields is justified (SNL 2008 [DIRS 184748], Section 6.6.4). Sensitivity studies presented in *Particle Tracking Model and Abstraction of Transport Processes* (SNL 2008 [DIRS 184748], Section 6.6.4, Figures 33 and 35) show the sensitivity of transport to the variance in the AFM  $\gamma$ , indicating that consideration of uncertainty is important for the transport process. Uncertainty in the active fracture parameter  $\gamma$  is applied to the TSPA-LA Model by sampling the parameter uniformly over a range between 0.2 and 0.6 as noted in Table 6.3.9-5 (SNL 2008 [DIRS 184748], Section 6.5.6[a]). This range of  $\gamma$  values spans the values considered appropriate for tsw32-tsw38, based on  $^{14}\text{C}$  data (SNL 2008 [DIRS 184748], Section 6.5.6[a]) and the values based on the flow model calibration.

Fracture spacing and aperture values are used to estimate the effect of matrix diffusion on radionuclide transport. In the TSPA-LA Model, the fracture spacing is the inverse of fracture frequency. Fracture apertures are calculated from randomly sampled fracture porosity and frequency values using the following relationship (SNL 2008 [DIRS 184748], Section 6.5.7, Equation 6-26):

$$2b = \phi_f / f \quad (\text{Eq. 6.3.9-3})$$

where

- $2b$  = the fracture aperture (m)
- $\phi_f$  = the fracture porosity (dimensionless)
- $f$  = the fracture frequency ( $\text{m}^{-1}$ ).

The distributions used by the TSPA-LA Model for fracture porosity values ( $\phi_f$ ) and fracture frequency values ( $f$ , unit 1/m) are presented in Tables 6.3.9-6 and 6.3.9-7, respectively. The fracture porosity estimates determined from air permeability testing in TSw34 are considered fairly reliable (BSC 2004 [DIRS 170038], Section 6.1.3.3), even though several factors are not explicitly accounted for, including gas compressibility, heterogeneity, anisotropy, cavity occurrence, and dispersion (note that adjustments are made to account for matrix diffusion effects). The fracture porosities for other units are derived from 1-D borehole and 2-D mapping data which are used in conjunction with the average aperture widths to provide relative ratios of fracture porosity for different stratigraphic units. These relative ratios are used in conjunction with the TSw34 air permeability testing estimates to provide unit-specific estimates. Note that there is a large amount of uncertainty in the estimates of fracture porosity for the other units (BSC 2004 [DIRS 170038], Section 6.1.3). This uncertainty stems from two areas: (1) the estimated apertures are hydraulic apertures that may be quite different from average geometric apertures, and (2) the estimates for other units are based on 1-D borehole data and 2-D mapping data used to approximate 3-D fracture networks (BSC 2004 [DIRS 170038], Section 6.1.3.1).

The uncertainty in the fracture porosities is addressed by the sampling of the parameter to derive the apertures.

Retardation of dissolved radionuclides associated with sorption onto fracture surfaces is not simulated in the TSPA-LA Model. Therefore, fracture retardation factors are set to 1.0 to conservatively minimize travel times to the SZ (SNL 2008 [DIRS 184748], Section 6.5.8).

For irreversible colloids, colloid sizes and matrix pore sizes are used in FEHM to determine filtration of irreversible colloids at interfaces between rock matrix units. At the start of each FEHM simulation, each potential particle is assigned a size based on sampling from a colloid size distribution. The uncertainty in colloid size is represented by a CDF, shown in Table 6.3.9-8 (SNL 2008 [DIRS 184748], Section 6.5.11). During particle tracking, when a particle in the rock matrix moves to the matrix of another unit, the size of each particle is compared to a randomly sampled value from a CDF for colloid transport at a matrix interface, which reflects the distribution of pore sizes of the matrix rock unit(s) (SNL 2008 [DIRS 184748], Section 6.5.9). If the particle size is larger than the sampled pore size, then the colloid does not enter the underlying rock matrix unit and is removed from the simulation or permanently filtered out. Table 6.3.9-9 lists the cumulative probability distributions for colloid transport at matrix interfaces for UZ transport in the various UZ rock units.

For the case in which colloids travel from fractures to the matrix via advection, an exclusion process may occur based on the matrix pore size. This colloid-exclusion process is implemented for irreversible colloids in the TSPA-LA Model through the use of an exclusion factor,  $f_c$ , based on the percentage of pores that are greater than the expected colloid size of 100 nm (SNL 2008 [DIRS 184748], Section 6.5.10). Each colloid particle has a chance of being excluded from entering the matrix based on a probability, equal to the fraction of matrix pores that are smaller than the expected colloid size. The colloid exclusion factors used in the TSPA-LA Model are presented in Table 6.3.9-10.

The sorption of radionuclides onto colloids may be either a reversible or an irreversible process. When the sorption process is irreversible, a very large number ( $10^{20}$ ) is assigned to the colloid equilibrium sorption coefficient,  $K_c$  (SNL 2008 [DIRS 184748], Section 6.5.12). For reversible radionuclide sorption on the colloids, the  $K_c$  values are calculated by multiplying a radionuclide's sorption coefficient for a species onto a colloid,  $K_d$ , by the colloid concentrations in the water. Table 6.3.9-8 provides the CDF for colloid concentration (SNL 2008 [DIRS 184748], Section 6.5.12[a]).

Uncertainties associated with colloid sorption coefficients for various radionuclides are represented by a set of CDFs, as shown in Table 6.3.9-11. These colloid sorption coefficient distributions are consistent with those used in the EBS Transport Submodel and SZ Flow and Transport Submodel although sampled independently for each submodel (SNL 2008 [DIRS 184748], Section 6.5.12[a]). The colloid sorption coefficient distributions for americium, protactinium, and thorium are the same and are considered to be 100 percent correlated (sampled as one) in the UZ. Note that only the CDFs for smectite colloids are presented in Table 6.3.9-11. The use of smectite colloids in the UZ is consistent with the guidance presented in *Waste Form and In-Drift Colloids-Associated Radionuclide Concentrations: Abstraction and Summary* (SNL 2007 [DIRS 177423], Section 6.5.3).

A colloid retardation factor,  $R_{coll}$ , is used in the TSPA-LA Model to simulate the impact of reversible filtration of both the reversible and irreversible colloids in fractures. Because there is no information regarding colloid retardation factors in the UZ, the TSPA-LA Model uses the SZ output, which is deemed appropriate for use in the UZ (SNL 2008 [DIRS 184748], Section 6.5.13). Table 6.3.9-12 shows the CDF for colloid retardation factors used in the UZ Submodel. The CDF for colloid retardation factors, presented in Table 6.3.9-12, is consistent with the CDF for the colloidal retardation factor in volcanic units for the SZ, as presented in Table 6.3.10-2. There is also a fraction of colloids escaping retardation due to physical and chemical processes. In the TSPA-LA Model, this fraction is defined as a function of the residence time of the colloid. In this relationship, progressively fewer colloids migrate unretarded with time. Based on a combined UZ/SZ travel time of 100 years, the model uses a value of 0.00168 for the fraction of colloids migrating unretarded, as recommended in *Particle Tracking Model and Abstraction of Transport Processes* (SNL 2008 [DIRS 184748], Section 6.5.13). Colloids traveling unretarded are given a retardation factor of 1.0.

### 6.3.9.3 TSPA-LA Model Implementation

The TSPA-LA Model implementation of UZ transport calculations is primarily achieved through the use of the FEHM DLL. The UZ Transport Submodel is directly coupled (i.e., dynamically linked) with the TSPA-LA Model using an external pathway element within the GoldSim software (STN: 10344-9.60.100.00 [DIRS 181903]) to link with the UZ transport code, FEHM. The FEHM external pathway element is used to call the FEHM DLL, pass it a set of inputs, define the set of inflows from the EBS that the DLL will receive, and define the outflow cells to which the FEHM results will be sent.

The FEHM DLL receives inputs at run time both directly from GoldSim and from a set of external files. At run time, GoldSim passes direct inputs to FEHM, such as the flow field index (used to select the desired UZ flow field abstraction based on climate state and infiltration scenario), the number of radionuclides, and the number of source zones (i.e., percolation subregions). In addition, for each realization, a randomly selected initial random seed is passed from GoldSim to FEHM for use in FEHM's particle migration logic. Similarly, a second random seed is passed to FEHM for use in the logic that locates the release points associated with each failed WP. GoldSim also passes inputs from the EBS, such as the combined EBS releases for both WP types (from each of the five percolation subregions), the ratio of the EBS release applied to fractures to the total EBS release (which is used to apportion the released radionuclides between fracture and matrix nodes), and the total number of failed CSNF WPs and CDSP WPs in each repository subregion. The FEHM DLL receives new sets of inputs from GoldSim every realization and for time-dependent inputs every timestep in each realization.

FEHM must also read in a set of external files that provides many inputs including the control parameters, deterministic transport parameters, and values for all the stochastic transport parameters (see Appendix F for a detailed accounting of the files and their contents). Data provided from the external input files include: (1) the numerical grid structure; (2) rock properties, such as porosity and bulk density; (3) solute transport parameters, such as fracture apertures, matrix diffusion coefficients, matrix  $K_d$  values, colloid distribution parameters, colloid retardation factors, and AFM  $\gamma$ s; and (4) the UZ flow fields. A complete list of these files can be found in Table F-2 of Appendix F of this report. One line of input comprised of fracture

apertures, AFM  $\gamma$ , matrix diffusion coefficients, matrix  $K_d$  values, colloid distribution parameters, and colloid retardation factors is read from an external file for each realization. Each TSPA-LA realization also uses one of four sets of UZ flow fields based on four infiltration scenarios (Sections 6.1.4.1 and 6.3.1). Each set has four flow fields: one each for present-day, monsoon, glacial-transition, and post-10,000-year climates (Section 6.3.1). The input flow fields for the present-day climate can be found in DTN: LB0612PDFEHMFF.001\_R0 [DIRS 179296]. The input flow fields with raised water tables for the monsoon, glacial-transition, and post-10,000-year climates can be found in DTNs: LB0701MOFEHMFF.001\_R0 [DIRS 179297]; LB0701GTFEHMFF.001 [DIRS 179160]; and LB0702PAFEM10K.002\_R0 [DIRS 179507], respectively. When a climate change occurs, a new flow field is read in and the particles instantly travel with the updated water fluxes. In addition, when transition occurs from present-day to monsoon climate with a raised water table, mass associated with all particles located between the previous water table, and the new water table is released to the SZ Submodel during the timestep when the flow field change takes place.

The set of uncertain transport properties, consisting of matrix sorption coefficients, matrix diffusion coefficients, fracture apertures, AFM  $\gamma$ s, colloid sorption coefficients, and colloid retardation factors (SNL 2008 [DIRS 184748], Sections 6.5.4, 6.5.5[a], 6.5.6[a], 6.5.7, 6.5.9, 6.5.10, 6.5.11, and 6.5.12[a]), is statistically sampled or generated from a set of statistically sampled parameters using GoldSim. During a supplemental simulation, the TSPA-LA Model is used to generate a set of external files containing these sampled parameters for FEHM. The set contains files sampled for 300 and 1,000 realizations. The TSPA-LA Model can then be run for simulations of 300 or 1,000 realizations. These files are used until there is a change in a parameter distribution or sampling seed, in which case a new set of files is generated. To use these files, the multiple species particle-tracking files contain placeholder indices identifying which of the variables in the external FEHM stochastic sample file belongs at the locations of the placeholder indices (Appendix F and Sections F.2.1.11 and F.2.1.13). Additionally, to ensure compatibility between the UZ and EBS Transport Submodels, matrix  $K_d$  values generated by the sampling elements in the TSPA-LA GoldSim Model are fed from these elements to the EBS for use in cell-networks representing the UZ immediately beneath the repository.

The matrix  $K_d$  values as generated in the process described above take their distributions from *Radionuclide Transport Models Under Ambient Conditions* (SNL 2007 [DIRS 177396], Table 6-1[a]). The  $K_d$  values are also correlated based on the similarities in the chemical dependencies of the sorption coefficients for the various radionuclides as discussed in *Radionuclide Transport Models Under Ambient Conditions* (SNL 2007 [DIRS 177396], Appendix B[a]). Starting with the correlation matrix defined by the similarities in the chemical dependencies of the sorption coefficients for the various radionuclide (DTN: LB0701PAKDSESN.001\_R0 [DIRS 179299], *Sorption Correlation Table.xls*), a subset containing only a single representative (basis) species for each subset of 100 percent correlated species is developed. Such a subset or non-singular correlation matrix is presented in *Radionuclide Transport Models Under Ambient Conditions* (SNL 2007 [DIRS 177396], Appendix B[a], Table B-2[a]). Note that in the TSPA-LA analysis, the correlation matrix presented in *Radionuclide Transport Models Under Ambient Conditions* (SNL 2007 [DIRS 177396], Appendix B[a], Table B-2[a]) is redefined as two separate non-singular correlation matrices. The use of two matrices is based on the non-correlation of uranium and selenium to any of the other species. Therefore, the TSPA-LA model utilizes a 10 by 10

non-singular correlation matrix for all species except uranium and selenium, and a 2 by 2 non-singular correlation matrix for uranium and selenium. The method used in the TSPA-LA Model to induce correlations is the Cholesky factorization method (SNL 2007 [DIRS 177396], Appendix B[a]).

The basic correlation procedure used is as follows. The  $m$  (rows) by  $m$  (columns) matrix,  $\mathbf{C}$ , is the target rank correlation to be imposed. Note that in the TSPA-LA model, two  $\mathbf{C}$  matrices, one 10 by 10 and one 2 by 2, are evaluated. For each non-singular correlation matrix and associated species, which is 100 percent correlated with any of the basis species, the procedure used in the TSPA-LA model is as follows:

1. Compute by Cholesky factorization (Press et al. 1992 [DIRS 103316], Section 2.9), the  $m$  by  $m$  lower triangular matrix,  $\mathbf{P}$ , such that  $\mathbf{P}\mathbf{P}^T = \mathbf{C}$  (Tables 6.3.9-13 and 6.3.9-14, respectively)
2. Create  $\mathbf{z}$ , a vector of length,  $m$ , consisting of independent standard normal values
3. Compute the vector,  $\mathbf{x}$ , of length,  $m$ , such that  $\mathbf{x} = \mathbf{P}\mathbf{z}$ . Note  $\mathbf{x} \sim N(0, \mathbf{C})$
4. Compute the result sample vector,  $\mathbf{u}$ , such that  $\mathbf{u}_i = \mathbf{F}_i^{-1}(\Phi(x_i))$ , for the  $m$  different variables,  $i = 1, \dots, m$ , where  $\mathbf{F}_i(x)$  are the marginal CDFs for each of the  $m$  variables and  $\Phi(x)$  is the standard normal CDF.

The resultant vector,  $\mathbf{u}$ , has a rank correlation structure that approximates  $\mathbf{C}$ . The sample vector  $\mathbf{w}$  for the species not chosen as basis species can then be generated as  $\mathbf{w}_{ij} = \mathbf{F}_i^{-1}(\Phi(x_j))$ , where  $j$  is the index denoting the basis species with which the species  $i$  is 100 percent correlated. The two lower triangular matrices used in the TSPA-LA Model can be found in (Output DTN: MO0707UZKDCORR.000 [DIRS 183003], radio\_020807a.xmcd, and radio\_020807a\_SE\_U.xmcd).

Within FEHM, the matrix  $K_d$  values are used in conjunction with bulk density, matrix porosity, and matrix saturation values to derive the retardation factor used to determine the effective transport rate for sorbing species. The retardation factor,  $R$ , can be defined as

$$R = 1 + \frac{\rho_{bulk} K_d}{\phi_{matrix} S_{matrix}} \quad (\text{Eq. 6.3.9-4})$$

where

- $\rho_{bulk}$  = the bulk density (g/mL)
- $K_d$  = the rock matrix sorption coefficient (mL/g)
- $\phi_{matrix}$  = the rock matrix porosity (-)
- $S_{matrix}$  = the rock matrix saturation (-).

The values of bulk density and matrix porosity used in the TSPA-LA Model are presented in *Particle Tracking Model and Abstraction of Transport Processes* (SNL 2008 [DIRS 184748],

Section 6.5.3[a]). The rock matrix saturations, used by FEHM to derive the matrix retardation factors, are read from the appropriate input flow-field files (based on the sampled infiltration scenario) and are updated during the simulation to account for present-day, monsoon, glacial-transition, and post-10,000-year climates (DTNs: LB0612PDFEHMFF.001\_R0 [DIRS 179296]; LB0701MOFEHMFF.001\_R0 [DIRS 179297]; LB0701GTFEHMFF.001\_R0 [DIRS 179160]; and LB0702PAFEM10K.002\_R0 [DIRS 179507]).

Radionuclide mobilization and transport through the EBS are calculated during each TSPA-LA Model simulation, and the radionuclide mass flux at the EBS boundary at each timestep is provided as the boundary condition for UZ transport (Section 6.3.8). The UZ Transport Submodel then provides radionuclide mass fluxes at the water table, for each timestep, as the boundary condition for SZ transport (Section 6.3.10). The elevation of the water table changes instantaneously when a climate change occurs. Any change in the water table level redefines the release points for mass leaving the UZ. In addition, as previously noted, any radionuclides between the old water table and the updated water table at the time the water table elevation changes are immediately removed from the UZ Transport Submodel and are provided as input to the SZ Flow and Transport Model Component (SNL 2008 [DIRS 184748], Section 6.4.8).

Releases from the EBS are computed for each environmental group: dripping and non-dripping CSNF WPs, dripping and non-dripping CDSP WPs, and each selected early-failed WP group, including CSNF-Zircaloy, CSNF-stainless steel, and CDSP WPs, in each repository percolation subregion. As described in Section 6.3.8 of the EBS Transport Submodel, radionuclide releases from the EBS enter both the fracture and matrix continua of the UZ Transport Submodel. Radionuclide releases from each of the five repository percolation subregions are modeled using a random release model that accounts for early failed WPs and temporally and spatially variable radionuclide releases (SNL 2008 [DIRS 184748], Section 6.4.7). This random release model avoids spreading out radionuclide releases artificially by taking into account the number of WPs that have failed within each of the five subregions. If only one WP has failed in a subregion, the releases for that subregion are put into a single numerical grid node that is randomly sampled from the nodes in that subregion. If two WPs have failed, releases are put into two randomly selected nodes. This process continues for additional WPs until the number of failed WPs is equal to the number of nodes in the subregion. The nodes are randomly selected without replacement. After the number of failed WPs exceeds the number of nodes in a subregion, later releases are evenly spread over all nodes in the subregion, and additional WP failures cause no change to the release locations (SNL 2008 [DIRS 184748], Section 6.4.7).

The process used to assign repository radionuclide release nodes to each of the five repository percolation subregions accounted for in the FEHM zone2 file is described in DTN: LA0702PANS02BR.001\_R1 [DIRS 180322] and *Particle Tracking Model and Abstraction of Transport Processes* (SNL 2008 [DIRS 184748], Section 6.5.15[a]). Note that only the first three climate states were considered in the analysis used to find a single zone file with five sets of source nodes that best represent all the infiltration/climate combinations. The repository-release nodes comprising each of the five repository percolation subregions were chosen based on the cumulative probability of percolation for the 12 flow fields (three different climate periods: present-day, monsoon, and glacial-transition; each climate period is categorized with 4 infiltration scenarios: 10 percent, 30 percent, 50 percent, and 90 percent). A 4-step binning process was applied to each of the twelve flow fields, resulting in a list of repository

release nodes divided into 5 percolation subregions (bins) that share common infiltration ranges, based on the cumulative probability intervals for these bins (SNL 2008 [DIRS 184748], Section 6.5.15[a]). The cumulative probability intervals for these five bins of percolation rates sorted in ascending order are 0.0-0.05, 0.05-0.30, 0.30-0.70, 0.70-0.95, and 0.95-1.00 (SNL 2008 [DIRS 184748], Section 6.5.15a). An analysis of the degree of similarity or difference of the results of the binning process, depending on which flow field is considered, was performed. The results indicated that the bins for the 12 flow fields are quite similar to one another. As noted in *Particle Tracking Model and Abstraction of Transport Processes* (SNL 2008 [DIRS 184748], Section 6.5.15[a]), if a bin is identified for a particular node in the glacial-transition, 10th percentile flow field, it is very often identified as the same bin for the other flow fields. When they are different, they almost always differ by only one bin; that is, a 3 in one flow field becomes a 4 in another flow field or a 2 becomes a 1. Based upon this result, it was considered acceptable to use bins from one flow field to approximate all infiltration scenarios and climate states. Therefore, for the compliance model, the file `fehmn.zone2_GT10%` (based on the 10th percentile infiltration scenario for the glacial transition climate) from the DTN is used to define the bins for all simulations, including the post-10,000-year climate. Figure 6.3.9-6 shows the locations of the FEHM repository release nodes, colored by percolation bin for the glacial-transition, 10th-percentile flow field.

The fraction of irreversible colloids traveling through the UZ unretarded is determined before releasing colloids from the EBS (Section 6.3.8). After they are released into the UZ, the fraction of unretarded colloids remains unchanged. Based on a conservative estimate for transport time in the natural system (UZ and SZ) of 100 years (SNL 2008 [DIRS 184748], Section 6.5.13 and Table 6-23), the fraction of unretarded colloids leaving the EBS is estimated to be 0.00168. This value is used in all TSPA-LA Model realizations and is referred to as the fast fraction in the implementation of the EBS Colloids Transport Submodel. Since the transport time through the UZ and SZ of the fast fraction of colloids is uncertain, and the fast fraction model is also uncertain, a conservative approach is taken for implementing the fast fraction of colloids (BSC 2004 [DIRS 170006], Section 6.6). The approach is conservative because it is highly unlikely that any TSPA-LA Model realization will have a combined UZ-SZ transport time of less than 100 years (BSC 2004 [DIRS 170006], Section 6.6).

To account for arrival locations and reduce artificial spreading in releases to the SZ, all nodes at or below the water table of the UZ Transport Submodel are grouped into four collecting bins (equivalent to SZ source regions), as shown on Figure 6.3.10-6. Radionuclide mass reaching the water table in one location may have a different SZ travel path and transport time than mass arriving at some other location. To reduce the effects of artificial dilution at the interfaces between TSPA-LA Model submodels, the total radionuclide mass flow rate in each of these four source regions is focused at a random point within each of the four source regions in the SZ Flow and Transport Model Component.

The random release point in each of the four UZ Transport Submodel (Figure 6.3.10-6) collecting bins is a function of sampling during each realization. The four UZ collecting bins are named 701, 702, 703, and 704 in FEHM, corresponding to the SZ source inflow regions 1, 2, 3, and 4, respectively (SNL 2008 [DIRS 184748], Section 6.5.16).

The four FEHM UZ collecting bins (Figure 6.3.10-6) are as follows (SNL 2008 [DIRS 184748], Section 6.5.16):

- Collecting bin 701 contains all nodes with a Universal Transverse Mercator (UTM) grid easting coordinate less than 548500 m (Nevada State Plane [NSP]: 171189.79 m) and a UTM northing coordinate greater than 4078630 m (NSP: 233459.87 m).
- Collecting bin 702 contains all nodes with a UTM easting coordinate greater than 548500 m (NSP: 171189.79 m) and a UTM northing coordinate greater than 4078630 m (NSP: 233459.87 m).
- Collecting bin 703 contains all nodes with a UTM easting coordinate less than 548500 m (NSP: 171189.79 m) and a UTM northing coordinate less than 4078630 m (NSP: 233459.87 m).
- Collecting bin 704 contains all nodes with a UTM easting coordinate greater than 548500 m (NSP: 171189.79 m) and a UTM northing coordinate less than 4078630 m (NSP: 233459.87 m).

The radionuclide mass release from FEHM is applied to four UZ collecting bins modeled using four GoldSim mixing cells. The mass outflows of the four cells are then fed to the SZ convolution integral model, SZ\_Convolute (SZ\_Convolute V3.10, STN: 10207-3.10-10 [DIRS 181060]), at each TSPA-LA Model timestep. The release rates are also integrated over time using GoldSim integrator elements for use as input to the alternative SZ one-dimensional pipe element model (SNL 2008 [DIRS 183750], Section 6.5.1.2).

#### **6.3.9.4 Model Component Consistency and Conservatism in Assumptions and Parameters**

To enhance understanding of the complex interactions within the TSPA-LA Model, a discussion of consistency among model components and submodels and the identification of conservative assumptions in abstractions, process models, and parameter sets supporting the UZ Transport Submodel is presented below.

##### **6.3.9.4.1 Consistency of Assumptions**

**UZ Transport Properties**—The UZ Transport Submodel uses different material properties than those used to develop the UZ flow fields. In the UZ Transport Submodel, fracture frequency and fracture porosity, which are used to derive fracture apertures, are sampled for every realization for nine different rock groups (SNL 2008 [DIRS 184748], Table 6-13). However, in developing the 16 different UZ flow fields that are used in the UZ transport calculations, fracture frequency and fracture porosity were held constant. The AFM  $\gamma$  values are calibrated values in the UZ Flow Submodel calculations. Although calibrated, the flow model is relatively insensitive to this parameter. To the contrary, during transport modeling when subject to matrix diffusion  $\gamma$  represents a parameter to which the system is sensitive. For this reason,  $\gamma$  is sampled from a distribution that is based both on the flow model calibrated values and field test-based values. Thus, fracture frequency, fracture porosity, and AFM  $\gamma$  values used to derive UZ transport

processes may differ between the UZ Transport Submodel and the UZ Flow Fields Abstraction (Section 6.3.1).

**Effect on TSPA-LA Results**—Pairs of randomly sampled fracture porosity and fracture frequency values are used to generate fracture apertures for the fracture-matrix interface submodel of the UZ Transport Submodel. By using the sampled values, uncertainty in the fracture-matrix diffusion process in the model is considered. Note that the fracture porosity values used to define the advective transport process in the particle tracking are the same values used in the flow model. Random sampling of the AFM  $\gamma$  in the UZ Transport Submodel also allows for consideration of uncertainty in the fracture-matrix diffusion process. This is important because the fracture-matrix diffusion process is sensitive to AFM  $\gamma$ . Since the sampled values range between 0.2 and 0.6 (SNL 2008 [DIRS 184748], Section 6.5.6[a]) and the calibrated flow values are 0.4 or less (SNL 2007 [DIRS 184614], Appendix B), the TSPA-LA Model will allow for faster transport in some realizations while better representing the uncertainty in the parameter. These and other transport parameters, along with their uncertainties as used in the UZ Transport Submodel, are discussed and justified in *Particle Tracking Model and Abstraction of Transport Processes* (SNL 2008 [DIRS 184748], Sections 6.5 and 6.5[a]). Therefore, even though the material properties may be different among respective submodels, separate sampling is necessary to adequately propagate uncertainty in mass transport under steady-state flow conditions.

**UZ Mass Release to the SZ**—The particles leaving the UZ at the water table are assigned to one of four collecting bins that are defined by four quadrants (NE, NW, SE, SW) (see Sections 6.3.9.3 and Figure 6.3.10-6). For a specific zone and water-table configuration, when a particle reaches a node that is considered an exit node, it becomes inactive in the UZ model, and its assigned mass is added to the spatially appropriate collecting bin. The four source terms defined by the collecting bins are then used as source terms for the four SZ source regions (NE, NW, SE, SW). The breakthrough curves used in the SZ-Convolute algorithm are based on a randomly sampled release location within each source region. The release zone assignment process is described in *Particle Tracking Model and Abstraction of Transport Processes* (SNL 2008 [DIRS 184748], Section 6.5.16).

**Effect on TSPA-LA Results**—Release of the mass for each SZ source region to a randomly selected location within the region during a single realization will focus the mass release. A point source of radionuclides is appropriate for release from a single WP or for considering the influence of groundwater flow focusing along a fault or single fracture. A more diffuse release of radionuclides at the water table may be more physically appropriate for later times when more numerous WPs are leaking and flow focusing does not occur. The use of a point source will overestimate the concentration of the radionuclides near the source (SNL 2008 [DIRS 183750], Section 6.5.2.13).

#### **6.3.9.4.2 Identification of Conservatism in Submodels and Abstractions**

**Climate Change**—Climate changes can be considered in an approximate way by imparting an instantaneous jump from one steady-state flow field to another with a corresponding instantaneous rise in the water table (SNL 2008 [DIRS 184748], Section 6.4.8). This approximation is considered conservative because it instantaneously shortens the time it takes for

mass to reach the SZ. The method instantaneously increases the flow velocities due to the change in climate and shortens the pathway to the SZ due to the rising of the water table. In addition, all mass between the original water table and the updated water table is immediately applied to the SZ (SNL 2008 [DIRS 184748], Section 5, Assumption 6). This conservatism is a logical approach, given the uncertainties associated with temporal delays in reaching the more rapid transport conditions and the inability to observe the process directly (SNL 2008 [DIRS 184748], Section 5, Assumption 6).

This conservatism tends to shorten radionuclide transport times (SNL 2008 [DIRS 184748], Section 6.4.8).

**Fixed Water Table Rise**—To approximate the effects of a rising water table on a radionuclide transport simulated by the finite element heat and mass (FEHM) transfer code (FEHM V2.24-01, STN: 10086-2.24-01-00 [DIRS 179419]), the external monsoon climate, glacial-transition, and post-10,000-year climate flow field files used in the transport model are post-processed. In the UZ flow model area, the present-day water table varies from less than 730 m to greater than 980 m above mean sea level (BSC 2004 [DIRS 169855] Figure 6.2). Within the repository footprint, the present-day water table varies from around 730 m to 850 m above mean sea level (BSC 2004 [DIRS 169855] Figure 6.2). Note that the bottom boundary for the flow models of all climate states is the present day water table. For use in conjunction with FEHM's multi-species particle tracking model the flow-field files for the monsoon, glacial-transition, and post-10,000-year climate flow fields from the UZ Flow Model Abstraction are post-processed to approximate the affects of a rising water table. The rising water table is approximated by constraining the water table to a minimum elevation of 850 m above mean sea level (SNL 2008 [DIRS 184748] Section 6.4.8). That is for future climates, at any locations where the present-day water table is below 850 m the water table is set to 850 m and at any locations where the present-day water table is above 850 m, the water table is not adjusted from the present day level (see BSC 2004 [DIRS 169855]). The rise in the water table of up to 120 m is assumed to occur immediately following the change from present-day to monsoon climate, instantly reducing the flow path of radionuclides in the UZ by up to 120 m. However, there could be a significant period of water table adjustment associated with transition to a wetter climate. After the water table is raised to a minimum of 850 m above sea level, it is assumed to remain at that level for the duration of the simulation period; there is no change to the water table elevation assumed between the monsoon and glacial-transition climates. This conservatism is evaluated as part of the PMA documented in Appendix C.

**Sorption on Fractures**—Sorption of radionuclides on fracture surfaces is neglected in the UZ Transport Submodel because sufficient data are not available to consider the process (SNL 2008 [DIRS 184748], Section 6.5.8). This assumption eliminates retardation of radionuclides within the fractures and results in shorter radionuclide transport times (SNL 2008 [DIRS 184748], Section 6.5.8).

**Unretarded Colloid Fraction**—Unretarded fraction of irreversible colloids used in the UZ model is based on a 100-year transport time. Travel time is uncertain through both the UZ and SZ, but it is unlikely that any TSPA realization will have a combined UZ-SZ travel time of less than 100 years (BSC 2004 [DIRS 170006], Section 6.6).

This assumption results in an increase in the unretarded colloidal fraction, rapidly increasing the mass that reaches the SZ (BSC 2004 [DIRS 170006], Section 6.6; and SNL 2008 [DIRS 184748], Section 6.5.13).

**Isothermal Transport Conditions in the UZ**—UZ transport occurs at isothermal 25°C conditions. Increased temperature would result in increased diffusion from the fractures into the matrix (SNL 2007 [DIRS 177396], Section 6.1.2.9). However, to simplify the modeling approach, higher temperatures from decay heat and the geothermal gradient are conservatively ignored. Additionally, increased temperature leads to increased sorption of cationic species and decreased sorption of anionic species (SNL 2007 [DIRS 177396], Section 6.1.2.9). Conclusions of the  $K_d$  temperature dependence study presented in *Radionuclide Transport Models under Ambient Conditions* (SNL 2007 [DIRS 177396], Section I) indicate that for various radionuclides a small positive increase in  $K_d$  with temperature is seen. Therefore, neglecting temperature dependence as suggested in *Radionuclide Transport Models under Ambient Conditions* (SNL 2007 [DIRS 177396]) would conservatively decrease travel time to the SZ.

This assumption results in a reduction of matrix diffusion at early times and a shortening of radionuclide transport times (SNL 2007 [DIRS 177396], Section 6.1.2.9).

**No Drift Shadow Effects**—No drift shadow effects from flow diversion around the waste emplacement drift are included in the UZ Transport Model Component. Capillary diversion, even under ambient conditions, may result in low fracture saturation below the drift. Reductions in fracture saturations below the drift would delay diffusive radionuclide transport from the EBS.

Ignoring drift shadow effects is a conservative assumption that will result in faster mass release to the UZ (SNL 2008 [DIRS 184748], Section 6.7).

**Effects of Perched Water Zones**—Effects of perched water low permeability zones are implicit to the UZ flow fields used in the UZ Transport Submodel. Although perched water indicates areas of lower permeability, which can delay and dilute radionuclide concentration and result in a reduced advective transport of radionuclides from the UZ (DTN: MO0706SPAFAEPLA.001 [DIRS 181613]), another impact of the perched (and zeolitic) zone in the TSPA-LA Model is to create a lateral diversion of water into the faults and downward to the water table (SNL 2007 [DIRS 184614], Section 8.6).

The lateral diversion of water around perched zones and into faults may result in shorter transport times to the UZ.

### 6.3.9.5 Alternative Conceptual Model(s) for Unsaturated Zone Transport

Section 6.2 outlines the general consideration and treatment of ACMs used to support the TSPA-LA Model. A brief description of the UZ Transport Submodel ACMs is summarized in Table 6.3.9-15. A detailed discussion of these ACMs can be found in *Particle Tracking Model and Abstraction of Transport Processes* (SNL 2008 [DIRS 184748], Section 6.7).

**Discretization of the UZ Matrix (DFM and MINC Models)**—Discrete Fracture Models and Multiple Interacting Continua (MINC) models of UZ fracture/matrix interaction represent ACMs. A set of transfer functions obtained using a Discrete Fracture Model with fine

discretization in the matrix has been developed to allow FEHM's multi-species particle-tracking model to capture sharp concentration gradients. In this Discrete Fracture Model abstraction of the fracture/matrix interaction, the more accurate depiction of the concentration gradients between the fracture and the matrix represents an ACM, which is also more consistent with a MINC formulation (SNL 2008 [DIRS 184748], Section 7.2.2 and Section 7.2.2[a]). Note that the FEHM multi-species particle-tracking model using the Discrete Fracture Model transfer functions still uses the dual-permeability (dual-k) flow fields, while the MINC formulation, as described in *Particle Tracking Model and Abstraction of Transport Processes* (SNL 2008 [DIRS 184748]), differs in the flow regimes. Simulations performed using Discrete Fracture Model and MINC models are shown to result in later breakthrough times than the Dual-k Model (SNL 2008 [DIRS 184748], Section 7.2.2 and Section 7.2.2[a]). A comparison of Discrete Fracture Model and MINC model results showed that the MINC model predicts even later breakthrough times than the Discrete Fracture Model (SNL 2008 [DIRS 184748], Section 7.2.2 and Section 7.2.2[a]). Presently, a Multiple Interacting Continua formulation is not directly used in the TSPA because of its large computational burden.

To evaluate the impact on the dose calculations associated with the use of the Discrete Fracture Model ACM, the sensitivity of the model simulations to the choice of matrix diffusion models was examined in a simulation using the Discrete Fracture Model transfer functions described in *Particle Tracking Model and Abstraction of Transport Processes* (SNL 2008 [DIRS 184748], Section 6.8.2[a]). The ACM impact evaluation is described in *Particle Tracking Model and Abstraction of Transport Processes* (SNL 2008 [DIRS 184748], Section 7.2.3.2[a]).

**Alternate Finite Difference Numerical Models**—The UZ Transport Submodel used FEHM particle tracking. Alternate finite difference numerical models include EOS9nT, T2R3D, and DCPT particle tracking. Two of these models provide a basis for modeling coupled flow and transport of single (T2R3D) or multiple radionuclides (EOS9nT). They were used primarily to provide validated models of UZ transport processes that form the basis for the abstraction models used in the TSPA-LA Model. The computationally intensive nature of these models limits the finite difference ACMs use for multiple realizations that can provide uncertainty estimates. The FEHM Particle Tracking Transport Abstraction Model can reproduce the results predicted by dual-k models by using transfer functions developed using a dual-k formulation (SNL 2008 [DIRS 184748], Sections 7.2.2[a] and 7.2.3.1[a]).

**Lateral Flow Diversion in UZ above the Repository**—Lateral flow in the PTn will divert percolating water to the faults and reduce the percolation flux at the repository. The original base case model, which shows more lateral flow occurring within the PTn than the ACM, was chosen due to better predictions of chloride and moisture data (SNL 2007 [DIRS 184614], Section 6.9.2). It was also generally more conservative with respect to reducing radionuclide transport times to the SZ (SNL 2007 [DIRS 184614], Section 6.9.2). The updated base case model predicts significant diversion and redistribution into faults for the PTn (SNL 2007 [DIRS 184614], Section 8.6).

**No Radionuclide Release into Faults**—The fault zones are defined as high permeability zones subject to fast advective transport to the top of the TSw and to the water table. The effects of not allowing direct release of radionuclides into the fault zones on the overall transport to the water

table are not significant because lateral diversion directs the radionuclides into the fault zones (SNL 2007 [DIRS 177396], Section 6.20.2).

**Inclusion of Drift Shadow Effects**—Inclusion of drift shadow effects would approximate the influence of capillary diversion that may cause low fracture saturation below the drift. It is considered conservative to ignore drift shadow effects and associated faster mass release to the UZ (SNL 2008 [DIRS 184748], Section 6.7). Additionally, the increase of infiltration associated with later climate states may decrease the effects (SNL 2008 [DIRS 184748], Section 6.7).

**Inclusion of TH, THC, and Thermal-Hydrologic-Mechanical Effects on UZ Flow and Transport**—Vaporization due to repository heat will keep the drift dry for several hundred to a few thousand years. TH, THC, and thermal-hydrologic-mechanical effects may alter flow and transport properties of the UZ rocks. TH, THC, and thermal-hydrologic-mechanical effects are insignificant after the change to glacial-transition climate, the period when most radionuclide transport would take place (SNL 2008 [DIRS 184748], Section 6.7). Additional conclusions with respect to TH, THC, and thermal-hydrologic-mechanical effects on UZ Flow and Transport presented in *Mountain-Scale Coupled Processes (TH/THC/THM)* include: (1) mountain-scale TH will have a large impact on fluid flow near the repository at early times but insignificant impact on UZ flow fields (BSC 2005 [DIRS 174101], Section 8.1); (2) changes in water chemistry, mineralogy, and hydrologic properties in the ambient temperature regions are minimal over the 7,000 years the THC model was simulated (BSC 2005 [DIRS 174101], Section 8.2); and (3) thermal-hydrologic-mechanical induced changes in mountain-scale hydrologic properties have no significant impact on vertical percolation through the repository horizon (BSC 2005 [DIRS 174101], Section 8.3).

**Alternative Fracture Model**—The TSPA-LA Model utilizes the active fracture model (Liu et al. 1998 [DIRS 105729]), which takes into consideration flow focusing and the associated reduction in fracture/matrix interaction. The active fracture model, with its reduced effective area of diffusion between fracture and matrix, is used in the TSPA-LA Model because of its more conservative nature in reducing fracture to matrix diffusion, which retards radionuclide transport and its ability to explain travel times associated with <sup>14</sup>C test data (SNL 2008 [DIRS 184748], Section 5, Assumption 1, and BSC 2004 [DIRS 170035], Section 7.4.1). An alternative fracture model would use the standard methodology, which does not consider a reduced fracture-matrix interface area. Using the standard methodology would enhance diffusion between the fracture and matrix. Because the active fracture model is more conservative and has better reflected field test results, the standard methodology was not recommended for inclusion in the TSPA-LA Model.

No ACMs were recommended for inclusion in the TSPA-LA Model.

INTENTIONALLY LEFT BLANK

Table 6.3.9-1. Radionuclide Half-Life and Daughter Products Used in the TSPA-LA Model

No.	Species	Half Life (years)	Daughter Index
1	$^{14}\text{C}$	$5.715 \times 10^3$	NA
2	$^{135}\text{Cs}$ (rev)	$2.3 \times 10^6$	NA
3	$^{137}\text{Cs}$ (rev)	$3.007 \times 10^1$	NA
4	$^{129}\text{I}$	$1.57 \times 10^7$	NA
5	$^{90}\text{Sr}$	$2.878 \times 10^1$	NA
6	$^{99}\text{Tc}$	$2.13 \times 10^5$	NA
7	$^{243}\text{Am}$ (rev)	$7.37 \times 10^3$	10
8	$^{243}\text{Am}$ (lc)	$7.37 \times 10^3$	11
9	$^{243}\text{Am}$ (lf)	$7.37 \times 10^3$	12
10	$^{239}\text{Pu}$ (rev)	$2.410 \times 10^4$	13
11	$^{239}\text{Pu}$ (lc)	$2.410 \times 10^4$	13
12	$^{239}\text{Pu}$ (lf)	$2.410 \times 10^4$	13
13	$^{235}\text{U}$	$7.04 \times 10^8$	14
14	$^{231}\text{Pa}$ (rev)	$3.28 \times 10^4$	NA
15	$^{241}\text{Am}$ (rev)	$4.327 \times 10^2$	18
16	$^{241}\text{Am}$ (lc)	$4.327 \times 10^2$	18
17	$^{241}\text{Am}$ (lf)	$4.327 \times 10^2$	18
18	$^{237}\text{Np}$	$2.14 \times 10^6$	19
19	$^{233}\text{U}$	$1.592 \times 10^5$	20
20	$^{229}\text{Th}$ (rev)	$7.3 \times 10^3$	NA
21	$^{240}\text{Pu}$ (rev)	$6.56 \times 10^3$	24
22	$^{240}\text{Pu}$ (lc)	$6.56 \times 10^3$	24
23	$^{240}\text{Pu}$ (lf)	$6.56 \times 10^3$	24
24	$^{236}\text{U}$	$2.342 \times 10^7$	25
25	$^{232}\text{Th}$ (rev)	$1.40 \times 10^{10}$	NA
26	$^{232}\text{U}$	$6.98 \times 10^1$	NA
27	$^{242}\text{Pu}$ (rev)	$3.75 \times 10^5$	33
28	$^{242}\text{Pu}$ (lc)	$3.75 \times 10^5$	33
29	$^{242}\text{Pu}$ (lf)	$3.75 \times 10^5$	33
30	$^{238}\text{Pu}$ (rev)	$8.77 \times 10^1$	34
31	$^{238}\text{Pu}$ (lc)	$8.77 \times 10^1$	34
32	$^{238}\text{Pu}$ (lf)	$8.77 \times 10^1$	34
33	$^{238}\text{U}$	$4.47 \times 10^9$	34
34	$^{234}\text{U}$	$2.46 \times 10^5$	35
35	$^{230}\text{Th}$ (rev)	$7.54 \times 10^4$	36

Table 6.3.9-1. Radionuclide Half-Life and Daughter Products Used in the TSPA-LA Model  
(Continued)

No.	Species	Half Life (years)	Daughter Index
36	<sup>226</sup> Ra	1.599x10 <sup>3</sup>	NA
37	<sup>36</sup> Cl	3.01x10 <sup>5</sup>	NA
38	<sup>79</sup> Se	2.95x10 <sup>5</sup>	NA
39	<sup>126</sup> Sn (rev)	2.50x10 <sup>5</sup>	NA

Sources: SNL 2008 [DIRS 184748], Table 6-25 [a].

Reference for Half-Lives: Parrington et al. 1996 [DIRS 103896] for all radionuclides except <sup>79</sup>Se, which comes from Singh 2002 [DIRS 164741].

Table 6.3.9-2. Matrix Sorption Coefficient Distributions for Unsaturated Zone Units in the Unsaturated Zone Transport Submodel

Parameter Name in TSPA-LA Model	Description	Distribution Type	Coefficients Describing Distribution ( $K_d$ : mL/g)
KdU_Zeo_a	$K_d$ of Uranium in Zeolitic Tuff	Cumulative	( $K_d$ value, probability) (0, 0) (0.5, 0.5) (30, 1.0)
KdU_Devit_a	$K_d$ of Uranium in Devitrified Tuff	Cumulative	( $K_d$ value, probability) (0, 0) (0.2, 0.5) (4, 1.0)
KdU_Vit_a	$K_d$ of Uranium in Vitric Tuff	Cumulative	( $K_d$ value, probability) (0, 0) (0.2, 0.5) (3, 1.0)
KdNp_Zeo_a	$K_d$ of Neptunium in Zeolitic Tuff	Cumulative	( $K_d$ value, probability) (0, 0) (0.5, 0.5) (6, 1.0)
KdNp_Devit_a	$K_d$ of Neptunium in Devitrified Tuff	Cumulative	( $K_d$ value, probability) (0, 0) (0.5, 0.5) (6, 1.0)
KdNp_Vit_a	$K_d$ of Neptunium in Vitric Tuff	Cumulative	( $K_d$ value, probability) (0, 0) (1.0, 0.5) (3, 1.0)
KdPu_Zeo_a	$K_d$ of Plutonium in Zeolitic Tuff	Cumulative	( $K_d$ value, probability) (10, 0) (100, 0.5) (200, 1.0)
KdPu_Devit_a	$K_d$ of Plutonium in Devitrified Tuff	Cumulative	( $K_d$ value, probability) (10, 0) (70, 0.5) (200, 1.0)
KdPu_Vit_a	$K_d$ of Plutonium in Vitric Tuff	Cumulative	( $K_d$ value, probability) (10, 0) (100, 0.5) (200, 1.0)
KdAm_Zeo_a	$K_d$ of Americium in Zeolitic Tuff	Truncated Normal	Range = 1,000 – 10,000; $\mu$ = 5,500, $\sigma$ = 1,500
KdAm_Devit_a	$K_d$ of Americium in Devitrified Tuff	Truncated Normal	Range = 1,000 – 10,000; $\mu$ = 5,500, $\sigma$ = 1,500
KdAm_Vit_a	$K_d$ of Americium in Vitric Tuff	Cumulative	( $K_d$ value, probability) (100, 0) (400, 0.5) (1,000, 1.0)
KdPa_Zeo_a	$K_d$ of Protactinium in Zeolitic Tuff	Truncated Normal	Range = 1,000 – 10,000; $\mu$ = 5,500, $\sigma$ = 1,500
KdPa_Devit_a	$K_d$ of Protactinium in Devitrified Tuff	Truncated Normal	Range = 1,000 – 10,000; $\mu$ = 5,500, $\sigma$ = 1,500
KdPa_Vit_a	$K_d$ of Protactinium in Vitric Tuff	Truncated Normal	Range = 1,000 – 10,000; $\mu$ = 5,500, $\sigma$ = 1,500
KdCs_Zeo_a	$K_d$ of Cesium in Zeolitic Tuff	Cumulative	( $K_d$ value, probability) (425, 0) (5,000, 0.5) (20,000, 1.0)
KdCs_Devit_a	$K_d$ of Cesium in Devitrified Tuff	Uniform	Minimum = 1 Maximum = 15
KdCs_Vit_a	$K_d$ of Cesium in Vitric Tuff	Cumulative	( $K_d$ value, probability) (0, 0) (2, 0.5) (100, 1.0)
KdSr_Zeo_a	$K_d$ of Strontium in Zeolitic Tuff	Uniform	Minimum = 50 Maximum = 2,000
KdSr_Devit_a	$K_d$ of Strontium in Devitrified Tuff	Uniform	Minimum = 10 Maximum = 70
KdSr_Vit_a	$K_d$ of Strontium in Vitric Tuff	Uniform	Minimum = 0 Maximum = 50
KdRa_Zeo_a	$K_d$ of Radium in Zeolitic Tuff	Uniform	Minimum = 1,000 Maximum = 5,000
KdRa_Devit_a	$K_d$ of Radium in Devitrified Tuff	Uniform	Minimum = 100 Maximum = 1,000
KdRa_Vit_a	$K_d$ of Radium in Vitric Tuff	Uniform	Minimum = 50 Maximum = 600
KdTh_Zeo_a	$K_d$ of Thorium in Zeolitic Tuff	Uniform	Minimum = 1,000 Maximum = 30,000
KdTh_Devit_a	$K_d$ of Thorium in Devitrified Tuff	Uniform	Minimum = 1,000 Maximum = 10,000

Table 6.3.9-2. Matrix Sorption Coefficient Distributions for Unsaturated Zone Units in the Unsaturated Zone Transport Submodel (Continued)

Parameter Name in TSPA-LA Model	Description	Distribution Type	Coefficients Describing Distribution ( $K_d$ : mL/g)
KdTh_Vit_a	$K_d$ of Thorium in Vitric Tuff	Uniform	Minimum = 1,000 Maximum = 10,000
KdSe_Zeo_a	$K_d$ of Selenium in Zeolitic Tuff	Truncated Log-Normal	Mean = 14.3 Standard deviation = 7.9 Minimum = 1.0 Maximum = 35.0
KdSe_Devit_a	$K_d$ of Selenium in Devitrified Tuff	Truncated Log-Normal	Mean = 14.0 Standard deviation = 11.2 Minimum = 1.0 Maximum = 50.0
KdSe_Vit_a	$K_d$ of Selenium in Vitric Tuff	Truncated Log-Normal	Mean = 8.6 Standard deviation = 7.9 Minimum = 0.0 Maximum = 25.0
KdSn_Zeo_a	$K_d$ of Tin in Zeolitic Tuff	Log-Uniform	Minimum = 100.0 Maximum = 5,000.0
KdSn_Devit_a	$K_d$ of Tin in Devitrified Tuff	Log-Uniform	Minimum = 100.0 Maximum = 100,000.0
KdSn_Vit_a	$K_d$ of Tin in Vitric Tuff	Log-Uniform	Minimum = 100.0 Maximum = 5,000.0

Sources: DTN: LA0408AM831341.001\_R0 [DIRS 171584]

DTN: LB0701PAKDSESN.001\_R0 [DIRS 179299], *Readme.pdf*, Table 3-1.

NOTES: Se is set to zero for rock in the TSw.

All non-sorbing species utilize a  $K_d$  of 0.0 mL/g in the TSPA-LA Model (SNL 2007 [DIRS 184748], Table 8.2).

The parameter names given here are those from the TSPA-LA Model and more detail on these source inputs can be found in Table K3-3.

Table 6.3.9-3. Species Dependent Free Water Diffusivities Used to Calculate the Effective Matrix Diffusion Coefficients for Unsaturated Zone Transport

Parameter Name in TSPA-LA Model	Description	Distribution Type	Coefficients Describing Distribution
Am_Dfw	Americium free water diffusivity (m <sup>2</sup> /s)	Constant	9.49E-10
C_Dfw	Carbon free water diffusivity (m <sup>2</sup> /s)	Constant	1.18E-09
Cl_Dfw	Chlorine free water diffusivity (m <sup>2</sup> /s)	Constant	2.03E-09
Cs_Dfw	Cesium free water diffusivity (m <sup>2</sup> /s)	Constant	2.06E-09
I_Dfw	Iodine free water diffusivity (m <sup>2</sup> /s)	Constant	2.05E-09
Np_Dfw	Neptunium free water diffusivity (m <sup>2</sup> /s)	Constant	6.18E-10
Pa_Dfw	Protactinium free water diffusivity (m <sup>2</sup> /s)	Constant	6.04E-10
Pu_Dfw	Plutonium free water diffusivity (m <sup>2</sup> /s)	Constant	1.30E-09
Ra_Dfw	Radium free water diffusivity (m <sup>2</sup> /s)	Constant	8.89E-10
Se_Dfw	Selenium free water diffusivity (m <sup>2</sup> /s)	Constant	1.04E-09
Sn_Dfw	Tin free water diffusivity (m <sup>2</sup> /s)	Constant	1.55E-09
Sr_Dfw	Strontium free water diffusivity (m <sup>2</sup> /s)	Constant	7.91E-10
Tc_Dfw	Technicium free water diffusivity (m <sup>2</sup> /s)	Constant	1.95E-09
Th_Dfw	Thorium free water diffusivity (m <sup>2</sup> /s)	Constant	5.97E-10
U_Dfw	Uranium free water diffusivity (m <sup>2</sup> /s)	Constant	6.64E-10

Source: DTN: LB0702PAUZMTDF.001\_R1 [DIRS 180776], *Free-Water Diffusion Coefficients.xls*

Table 6.3.9-4. Parameter Distributions for Tortuosities Used to Calculate the Effective Matrix Diffusion Coefficients for Unsaturated Zone Transport

Parameter Name in TSPA-LA Model	Description	Parameters (in Log10) Describing Distribution
UZDC_Mean_RG1	Log mean tortuosity for rock units: ch1z, ch6v, pp3, pp2, bf2/tr2	-1.15
UZDC_SD_RG1	Log standard deviation of tortuosity for rock units: ch1z, ch6v, pp3, pp2, bf2/tr2	0.29
UZDC_Mean_RG2	Log mean tortuosity for rock units: tsw33, tsw39z, tsw39v, ch1v, ch[2-5]z, ch[2-5]v, ch6z, pp4, bf3/tr3, pcM1z, pcM[2,5]z, pcM6z, M	-1.57
UZDC_SD_RG2	Log standard deviation of tortuosity for rock units: tsw33, tsw39z, tsw39v, ch1v, ch[2-5]z, ch[2-5]v, ch6z, pp4, bf3/tr3, pcM1z, pcM2,5]z, pcM6z, pcM4p	0.29
UZDC_Mean_RG3	Log mean tortuosity for rock units: tsw34, tsw35, tsw3[6,7], tsw38, pp1, pcM38, pcM39	-1.84
UZDC_SD_RG3	Log standard deviation of tortuosity for rock units: : tsw34, tsw35, tsw3[6,7], tsw38, pp1, pcM38, pcM39	0.29

Source: DTN: LB0702PAUZMTDF.001\_R1 [DIRS 180776], *Readme.pdf*, Table 2-5.  
See also SNL 2008 [DIRS 184748], Tables 6.5.5-1 and Section 6.5.5.4.

NOTE: The Log10 values are rounded off to two decimal places that could give slightly different mean values than the antilogs.

Table 6.3.9-5. Fracture  $\gamma$  Parameter Distribution for all Rock in the Unsaturated Zone Transport

Parameter Name in TSPA-LA Model	Description	Distribution Type	Lower-Bound Infiltration	Upper-Bound Infiltration
GAMMA_AFM_a	Fracture $\gamma$ for all rock units	Uniform	0.2	0.6

Source: DTN: LA0701PANS02BR.003\_R2 [DIRS 180497], *Readme.doc*.

NOTE : A detailed description for this input can be found in Table K3-3.

Table 6.3.9-6. Parameter Distributions for Fracture Porosity for Unsaturated Zone Transport

Parameter Name in TSPA-LA Model	Description	Distribution Type	Coefficients Describing Distribution
Por_group1_a	Porosity for chnFf rock unit	Beta	Mean = 1.0E-03 Standard deviation = 3.09E-04 Minimum = 0 Maximum = 1
Por_group2_a	Porosity for tswFf rock unit	Beta	Mean = 2.5E-02 Standard deviation = 7.25E-03 Minimum = 0 Maximum = 1
Por_group3_a	Porosity for rock units: ch[2, 5]Fz/ pcF[2,5]z, ch[3,4]Fz, pp4Fz/pcf4p, pp1Fz, bf2Fz, tr2Fz	Beta	Mean = 3.7E-04 Standard deviation = 1.09E-04 Minimum = 0 Maximum = 1
Por_group4_a	Porosity for rock units: pp3Fd, pp2Fd, bf3Fd, tr3Fd	Beta	Mean = 9.7E-04 Standard deviation = 2.85E-04 Minimum = 0 Maximum = 1
Por_group5_a	Porosity for rock units: ch1Fz/pcF1z, ch6Fz/pcF6z	Beta	Mean = 1.6E-04 Standard deviation = 4.71E-05 Minimum = 0 Maximum = 1
Por_group6_a	Porosity for rock units: ch[1,2,3,4,5,6]Fv	Beta	Mean = 6.9E-04 Standard deviation = 2.03E-04 Minimum = 0 Maximum = 1
Por_group7_a	Porosity for rock units: tswFv, tswFz/pcF39 (tswF9)	Beta	Mean = 4.3E-03 Standard deviation = 1.26E-03 Minimum = 0 Maximum = 1
Por_group8_a	Porosity for rock units: tswF[4,5], tswF[6,7], tswF8/pcF38	Beta	Mean = 1.05E-02 Standard deviation = 3.10E-03 Minimum = 0 Maximum = 1
Por_group9_a	Porosity for tswF3 rock unit	Beta	Mean = 5.8E-03 Standard deviation = 1.71E-03 Minimum = 0 Maximum = 1

Source: DTN: LA0701PANS02BR.003\_R2 [DIRS 180497], Table 1.doc.

Table 6.3.9-7. Parameter Distributions for Fracture Frequency for Unsaturated Zone Transport

Parameter Name in TSPA-LA Model	Description	Distribution Type	Coefficients Describing Distribution
ff_group1_a	Fracture frequency [1/m] for chnFf rock unit	Log normal	Mean $\ln f = -2.33E00$ Standard deviation $\ln f = 7.24E-01$
ff_group2_a	Fracture frequency [1/m] for tswFf rock unit	Log normal	Mean $\ln f = 2.96E-01$ Standard deviation $\ln f = 7.24E-01$
ff_group3_a	Fracture frequency [1/m] for rock units: ch[2, 5]Fz/pcF[2,5]z, ch[3,4]Fz, pp4Fz/pcf4p, pp1Fz, bf2Fz, tr2Fz	Log normal	Mean $\ln f = -2.23E00$ Standard deviation $\ln f = 7.24E-01$
ff_group4_a	Fracture frequency [1/m] for rock units: pp3Fd, pp2Fd, bf3Fd, tr3Fd	Log normal	Mean $\ln f = -1.87E00$ Standard deviation $\ln f = 7.24E-01$
ff_group5_a	Fracture frequency [1/m] for rock units: ch1Fz/pcF1z, ch6Fz/pcF6z	Log normal	Mean $\ln f = -3.48E00$ Standard deviation $\ln f = 7.24E-01$
ff_group6_a	Fracture frequency [1/m] for rock units: ch[1,2,3,4,5,6]Fv	Log normal	Mean $\ln f = -2.38E00$ Standard deviation $\ln f = 7.24E-01$
ff_group7_a	Fracture frequency [1/m] for rock units:tswFv, tswFz/pcF39 (tswF9)	Log normal	Mean $\ln f = -3.03E-01$ Standard deviation $\log f = 7.24E-01$
ff_group8_a	Fracture frequency [1/m] for rock units: tswF[4,5], tswF[6,7], tswF8/pcF38	Log normal	Mean $\ln f = 1.12E00$ Standard deviation $\ln f = 7.24E-01$
ff_group9_a	Fracture frequency [1/m] for tswF3 rock unit	Log normal	Mean $\ln f = -6.92E-01$ Standard deviation $\ln f = 9.81E-01$

Source: DTN: LA0701PANS02BR.003\_R2 [DIRS 180497], Table 1.doc.

Table 6.3.9-8. Colloid Size and Concentration Distributions for Unsaturated Zone Transport

Parameter Name in TSPA-LA Model	Description	Distribution Type	Coefficients Describing Distribution
PART_SIZE <sup>a, b</sup>	Colloid size [nm] distribution data for use in simulating colloid filtration effect at matrix interface	Cumulative	(Colloid size, probability): (450, 1.0) (200, 0.8) (100, 0.6) (50, 0.4) (6, 0.2) (1, 0)
Colloidal_Concentration_uz_a <sup>c</sup>	Colloid concentration [mg/L] when ionic strength is less than 0.05	Cumulative	(Colloid concentration, probability): (200, 1.0) (50, 0.98) (10, 0.9) (1.0, 0.75) (0.1, 0.5), (0.001, 0.0)

<sup>a</sup> This parameter has no formal name in the TSPA-LA Model because it is implemented directly in the FEHM UZ Particle Tracking Submodel.

<sup>b</sup> DTN: LA0701PANS02BR.003\_R2 [DIRS 180497], Table 4.doc .

<sup>c</sup> DTN: LA0701PANS02BR.003\_R2 [DIRS 180497], Table 7.doc .

Table 6.3.9-9. Cumulative Probability Distributions for Colloid Transport at Matrix Interfaces for Unsaturated Zone Transport

Parameter Name in TSPA-LA Model <sup>a</sup>	Description	Distribution Type	Coefficients Describing Distribution
ITFCPORSIZE	Effective pore size [nm] for rock units: TMN/TSW4	Cumulative	(Effective pore size, probability): (2,000, 1.0) (1,000, 0.92) (450, 0.87) (200, 0.81) (100, 0.71) (50, 0.55) (6, 0.31)
ITFCPORSIZE	Effective pore size [nm] for rock units: TLL/TSW5	Cumulative	(Effective pore size, probability): (2,000, 1.0) (1,000, 0.8) (450, 0.79) (200, 0.70) (100, 0.61) (50, 0.51) (6, 0.19)
ITFCPORSIZE	Effective pore size [nm] for rock units: TM2/TSW6	Cumulative	(Effective pore size, probability): (2,000, 1.0) (1,000, 0.94) (450, 0.9) (200, 0.82) (100, 0.65) (50, 0.51) (6, 0.21)
ITFCPORSIZE	Effective pore size [nm] for rock units: TM1/TSW7	Cumulative	(Effective pore size, probability): (2,000, 1.0) (1,000, 0.99) (450, 0.99) (200, 0.99) (100, 0.93) (50, 0.68) (6, 0.36)
ITFCPORSIZE	Effective pore size [nm] for rock units: PV3/TSW8	Cumulative	(Effective pore size, probability): (2,000, 1.0) (1,000, 0.98) (450, 0.96) (200, 0.94) (100, 0.90) (50, 0.89) (6, 0.68)
ITFCPORSIZE	Effective pore size [nm] for rock units: PV2/TSW9	Cumulative	(Effective pore size, probability): (2,000, 1.0) (1,000, 0.72) (450, 0.57) (200, 0.47) (100, 0.39) (50, 0.35) (6, 0.22)
ITFCPORSIZE	Effective pore size [nm] for rock units: BT1a/CH1	Cumulative	(Effective pore size, probability): (2,000, 1.0) (1,000, 0.91) (450, 0.89) (200, 0.87) (100, 0.85) (50, 0.83) (6, 0.53)
ITFCPORSIZE	Effective pore size [nm] for rock units: CHV	Cumulative	(Effective pore size, probability): (2,000, 1.0) (1,000, 0.58) (450, 0.49) (200, 0.43) (100, 0.39) (50, 0.36) (6, 0.07)
ITFCPORSIZE	Effective pore size [nm] for rock units: CHZ	Cumulative	(Effective pore size, probability): (2,000, 1.0) (1,000, 0.79) (450, 0.76) (200, 0.73) (100, 0.68) (50, 0.56) (6, 0.3)
ITFCPORSIZE	Effective pore size [nm] for rock units: BT/CH6	Cumulative	(Effective pore size, probability): (2,000, 1.0) (1,000, 0.95) (450, 0.94) (200, 0.92) (100, 0.92) (50, 0.85) (6, 0.40)
ITFCPORSIZE	Effective pore size [nm] for rock units: PP1	Cumulative	(Effective pore size, probability): (2,000, 1.0) (1,000, 0.79) (450, 0.68) (200, 0.63) (100, 0.57) (50, 0.48) (6, 0.21)
ITFCPORSIZE	Effective pore size [nm] for rock units: PP2	Cumulative	(Effective pore size, probability): (2,000, 1.0) (1,000, 0.91) (450, 0.86) (200, 0.81) (100, 0.65) (50, 0.53) (6, 0.22)
ITFCPORSIZE	Effective pore size [nm] for rock units: PP3	Cumulative	(Effective pore size, probability): (2,000, 1.0) (1,000, 0.49) (450, 0.34) (200, 0.26) (100, 0.21) (50, 0.16) (6, 0.07)
ITFCPORSIZE	Effective pore size [nm] for rock units: PP4	Cumulative	(Effective pore size, probability): (2,000, 1.0) (1,000, 0.99) (450, 0.99) (200, 0.98) (100, 0.98) (50, 0.96) (6, 0.32)
ITFCPORSIZE	Effective pore size [nm] for rock units: BF2	Cumulative	(Effective pore size, probability): (2,000, 1.0) (1,000, 0.98) (450, 0.97) (200, 0.96) (100, 0.96) (50, 0.83) (6, 0.25)
ITFCPORSIZE	Effective pore size [nm] for rock units: BF3	Cumulative	(Effective pore size, probability): (2,000, 1.0) (1,000, 0.97) (450, 0.94) (200, 0.83) (100, 0.74) (50, 0.66) (6, 0.14)

Source: DTN: LA0701PANS02BR.003\_R2 [DIRS 180497], Table 2.doc.

<sup>a</sup> These parameters are listed with one name in the TSPA-LA Model because they are implemented directly in the FEHM UZ Particle Tracking Submodel.

Table 6.3.9-10. Colloid Size Exclusion Factor Used in the Compliance Model

HGU (Group Numbers)	UZ Model Units (Entry Layer)	Size Exclusion Factor
TMN / TSW4	tswF4	0.29
TLL / TSW5	tswF5	0.39
TM2 / TSW6	tswF6	0.35
TM1 / TSW7	tswF7	0.07
PV3 / TSW8	tswF8/pcF38	0.10
PV2 / TSW9	tswFz, tswFv (tswF9) / pcF39	0.61
BT1a / CH1	ch1Fv, ch1Fz/pcF1z	0.15
CHV	ch[2,3,4,5]Fv	0.61
CHZ	ch[3,4]Fz, ch[2,5,6]Fz/pcF[2,5,6]z	0.27
BT / CH6	ch6Fv	0.08
PP4	pp4Fz/pcF4p	0.02
PP3	pp3Fd	0.79
PP2	pp2Fd	0.35
PP1	pp1Fz	0.43
BF3	bf3Fd, tr3Fd	0.26
BF2	bf2Fz, tr2Fz	0.04
	tswFf	0.29
	chnFf	0.27

Source: DTN: LA0701PANS02BR.003\_R2 [DIRS 180497], *Table 3.doc*.

FEHM = finite element heat and mass (model)

HGU = Hydrogeologic Units or layers (SNL 2007 [DIRS 184614], Section 6.1); Correlation of HGU units and list of all UZ Model layers (FEHM zones) (SNL 2008 [DIRS 184748], Table 6-3).

Table 6.3.9-11. Radionuclide Sorption Coefficients onto Colloids for Unsaturated Zone Transport (revised groundwater colloid mass concentration parameters for TSPA-LA Model)

Parameter Name in TSPA-LA Model	Description	Distribution Type	$K_d$ Value Intervals	$K_d$ Value Interval Probability of Occurrence
Colloidal_Kd_Pu_uz_a	$K_d$ [mL/g] of Plutonium on Smectite Colloid	Cumulative	$1 \times 10^3$ to $5 \times 10^3$	0.45
			$5 \times 10^3$ to $1 \times 10^4$	0.8
			$1 \times 10^4$ to $5 \times 10^4$	0.95
			$5 \times 10^4$ to $1 \times 10^5$	1.00
Colloidal_Kd_Am_uz_a	$K_d$ [mL/g] of Americium on Smectite Colloid	Cumulative	$1 \times 10^4$ to $5 \times 10^4$	0.07
			$5 \times 10^4$ to $1 \times 10^5$	0.17
Colloidal_Kd_Th_uz_a	$K_d$ [mL/g] of Thorium on Smectite Colloid	Cumulative	$1 \times 10^5$ to $5 \times 10^5$	0.40
			$5 \times 10^5$ to $1 \times 10^6$	0.60
Colloidal_Kd_Pa_uz_a	$K_d$ [mL/g] of Protactinium on Smectite Colloid	Cumulative	$1 \times 10^6$ to $5 \times 10^6$	0.92
			$5 \times 10^6$ to $1 \times 10^7$	1.00
Colloidal_Kd_Cs_uz_a	$K_d$ [mL/g] of Cesium on Smectite Colloid	Cumulative	$5 \times 10^1$ to $1 \times 10^2$	0.05
			$1 \times 10^2$ to $5 \times 10^2$	0.40
			$5 \times 10^2$ to $1 \times 10^3$	0.70
			$1 \times 10^3$ to $5 \times 10^3$	1.00
Colloidal_Kd_Sn_uz_a	$K_d$ [mL/g] of Tin on Smectite Colloid	Log Uniform	$1 \times 10^5$ to $1 \times 10^6$	NA

Source: SNL 2008 [DIRS 184748], Table 6-22[a].

Table 6.3.9-12. Colloid Retardation Factors (Colloidal\_Retard\_Factor\_dist) for Unsaturated Zone Transport

Colloid Retardation Factor	Cumulative Probability	Input Description
6.00	0	The colloid retardation factor is used by FEHM in simulating the effects of colloid retardation in fractured rock on colloid-facilitated radionuclide transport.
6.00 <sup>a</sup>	0.15	
10.23	0.25	
26.00	0.5	
59.98	0.8	
799.83 <sup>b</sup>	1	

Source: DTN: LA0701PANS02BR.003\_R2 [DIRS 180497], Table 5.doc.

<sup>a</sup> The value used in the TSPA-LA Model is 6.00000001. This change was implemented to coincide with the GoldSim requirement that cumulative probability functions are defined by monotonically increasing values.

<sup>b</sup> The source DTN: LA0303HV831352.002\_R0 (for the TSPA-LA feed DTN [DIRS 180497]) presents the colloid retardation factor as 799.83 for a cumulative probability of 1.00 rather than rounded to 800 as presented in Table 5 [DIRS 180497].

Table 6.3.9-13. Lower Triangular Matrix for all Species Except Uranium and Selenium as Generated from the Correlation (Covariance) Matrix by Cholesky Factorization Using MathCad

Basic Species	Am_devit	Cs_devit	Cs_zeo	Np_devit	Pa_devit	Pu_devit	Ra_zeo	Sn_devit	Sr_devit	Th_devit
Am_devit	1	0	0	0	0	0	0	0	0	0
Cs_devit	0	1	0	0	0	0	0	0	0	0
Cs_zeo	0	0.1	0.995	0	0	0	0	0	0	0
Np_devit	0.25	0	0	0.968	0	0	0	0	0	0
Pa_devit	0.75	0	0	-0.194	0.632	0	0	0	0	0
Pu_devit	0.1	0	0.754	0.077	-0.095	0.638	0	0	0	0
Ra_zeo	0	0.1	0.492	0	0	0.202	0.841	0	0	0
Sn_devit	0.75	0	0	-0.09	0.269	0.09	-0.022	0.59	0	0
Sr_devit	0	0.25	0.075	0.516	0.158	-0.128	0.076	0.029	0.786	0
Th_devit	0	0	0	0.516	0.158	-0.039	0.0094 14	0.013	0.576	0.612

Source: Output DTN: MO0707UZKDCORR.000 [DIRS 183003], radio\_020807a.xmcd.

Table 6.3.9-14. Lower Triangular Matrix for Uranium and Selenium as Generated from the Correlation (Covariance) Matrix by Cholesky Factorization Using MathCad

Basic Species	Se_devit	U_devit
Se_devit	1	0
U_devit	0.75	0.661

Source: Output DTN: MO0707UZKDCORR.000 [DIRS 183003], radio\_020807a\_SE\_U.xmcd.

Table 6.3.9-15. Alternative Conceptual Models Considered for the Unsaturated Zone Transport Model

Alternative Conceptual Model	Key Assumptions	Screening Assessment and Basis
Discretization of the UZ Matrix (MINC Model)	The matrix is discretized to allow for a more accurate approximation of the concentration gradient at the matrix-fracture interface and within the matrix. Use of the Discrete Fracture Model or Multiple Interacting Continua (MINC) Model results in later breakthrough times than generated using the dual-k model. The breakthrough times of the Multiple Interacting Continua Model are later than those generated using the Discrete Fracture Model.	The dual-k model is conservative. The Multiple Interacting Continua Model is not used because of its large computational burden.
Alternative Finite Difference Numerical Models	An alternate method of approximating radionuclide transport in groundwater based upon approximating the governing equations using finite difference equations.	Although used for validation of the UZ Abstraction, large computational burden limits the utility of models such as T2R3D and EOS9nT.
Lateral Flow Diversion In UZ Above The Repository	Lateral flow in the PTn will divert percolating water to the faults and reduce the percolation flux at the repository.	The original base case model, which shows more lateral flow occurring within the PTn than the ACM, was chosen due to better predictions of chloride and moisture data (SNL 2007 [DIRS 184614], Section 6.9.2). It was also generally more conservative with respect to radionuclide transport. The updated base case model predicts significant diversion and redistribution into faults for the PTn (SNL 2007 [DIRS 177396], Section 6.20.2).
No Radionuclide Release Into Faults	The fault zones are defined as high permeability zones subject to fast advective transport to the top of the TSw and to the water table.	The effects of not allowing direct release of radionuclides into the fault zones, on the overall transport to the water table, are not significant because lateral diversion directs the radionuclides into the fault zones (SNL 2007 [DIRS 177396], Section 6.20.2).

Table 6.3.9-15. Alternative Conceptual Models Considered for the Unsaturated Zone Transport Model  
(Continued)

Alternative Conceptual Model	Key Assumptions	Screening Assessment and Basis
Inclusion of Drift Shadow Effects	Inclusion of drift shadow effects would approximate the influence of capillary diversion which may cause low fracture saturation below the drift.	It is considered conservative to ignore drift shadow effects. Additionally, the increased infiltration associated with later climate states may decrease the effects.
Perched Water Permeability Zones	Perched water may delay and dilute radionuclide concentration and reduce advective transport. Large scale lateral flow of water can also occur in perched water zones which can divert and redistribute flow into faults. Continuous well-connected fractures are used to model transport processes in the particle tracking method and the flow fields from the UZ Flow Submodel account for perched water effects.	Perched water may only be present in the northern part of the repository. Treating perched water in a manner such that well connected pathways exist is a conservative treatment.
Inclusion of TH, THC, and THM Effects on UZ Flow and Transport	Vaporization due to repository heat will keep the drift dry for several hundred to a few thousand years. THC and THM effects may alter flow and transport properties of the UZ rocks.	TH, THC, and THM effects are insignificant after the change to glacial-transition climate.
Alternative Fracture-Matrix Interaction Model	The TSPA-LA Model utilizes the Active Fracture Model (AFM) (Liu et al. 1998 [DIRS 105729]), which assumes that only a fraction of connected fractures are active in conducting water. The AFM is implemented by applying a fracture-matrix effective interface area reduction term or a fracture-matrix interface area adjustment factor and a fracture spacing adjustment factor. The ACM assumes that all connected fractures are active in conducting water and represents a standard methodology with no fracture-matrix effective interface area reduction term applied. The active fracture model, with its reduced effective area of diffusion between fracture and matrix, is used in the TSPA-LA Model because of its more conservative nature and its ability to explain travel times associated with <sup>14</sup> C data (SNL 2008 [DIRS 184748], Section 5, Assumption 1) and (BSC 2004 [DIRS 170035], Section 7.4.1).	Using the standard methodology would enhance diffusion between the fracture and matrix. Because the active fracture model is more conservative and has better reflected field test results, the standard methodology was not recommended for inclusion in the TSPA-LA Model.

Source: SNL 2008 [DIRS 184748], Table 6-30. Additional sources are noted within the text.

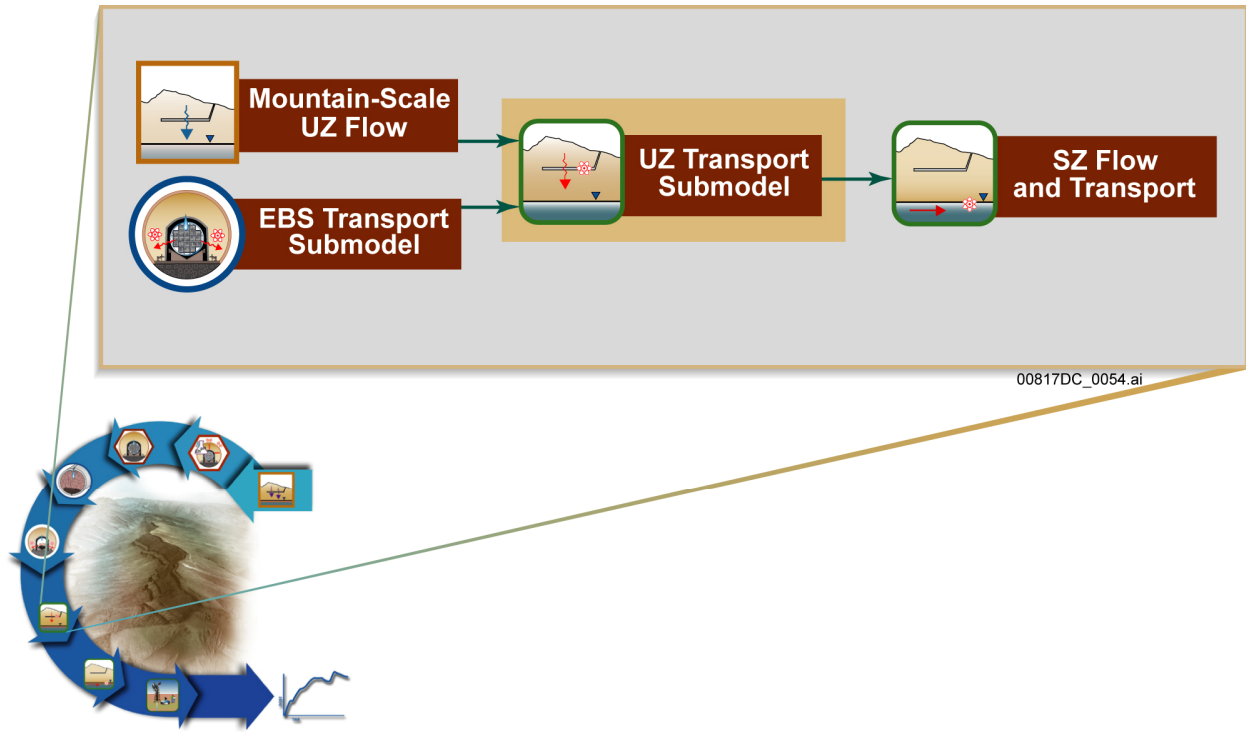


Figure 6.3.9-1. Information Flow Diagram for Unsaturated Zone Transport

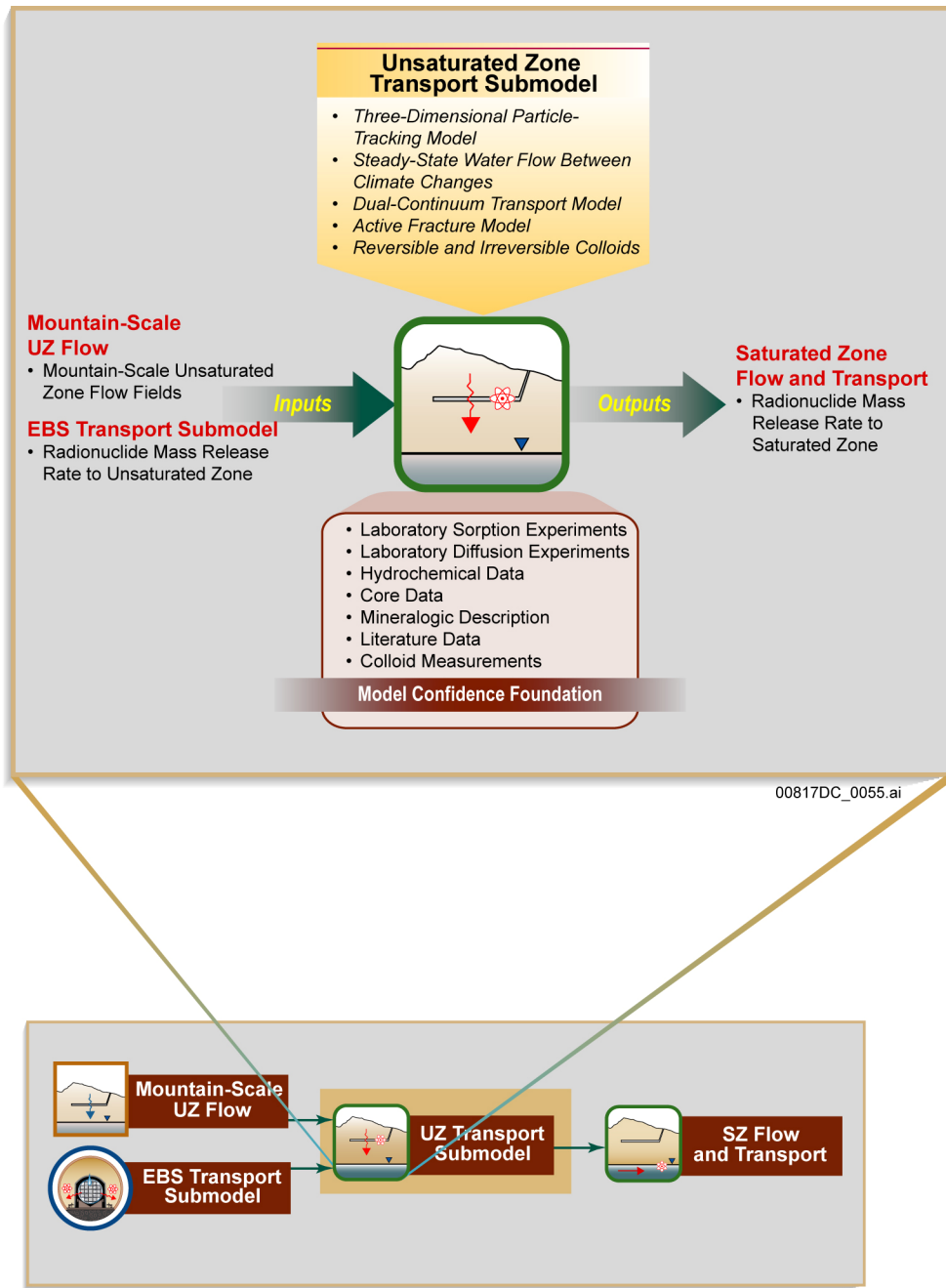


Figure 6.3.9-2. Inputs, Outputs, and Basis for Model Confidence for the Unsaturated Zone Transport Submodel

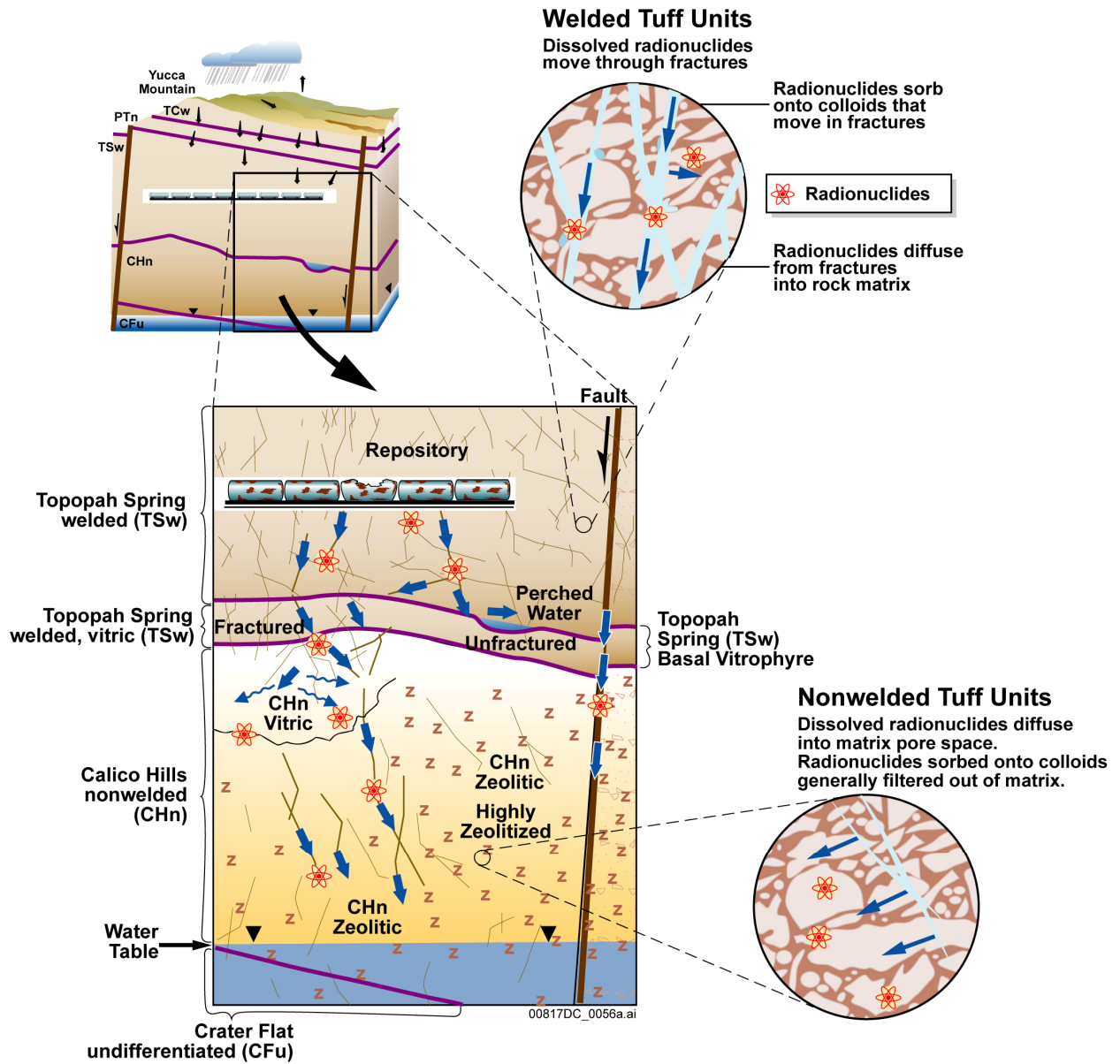


Figure 6.3.9-3. Conceptualization of Unsaturated Zone Transport Processes

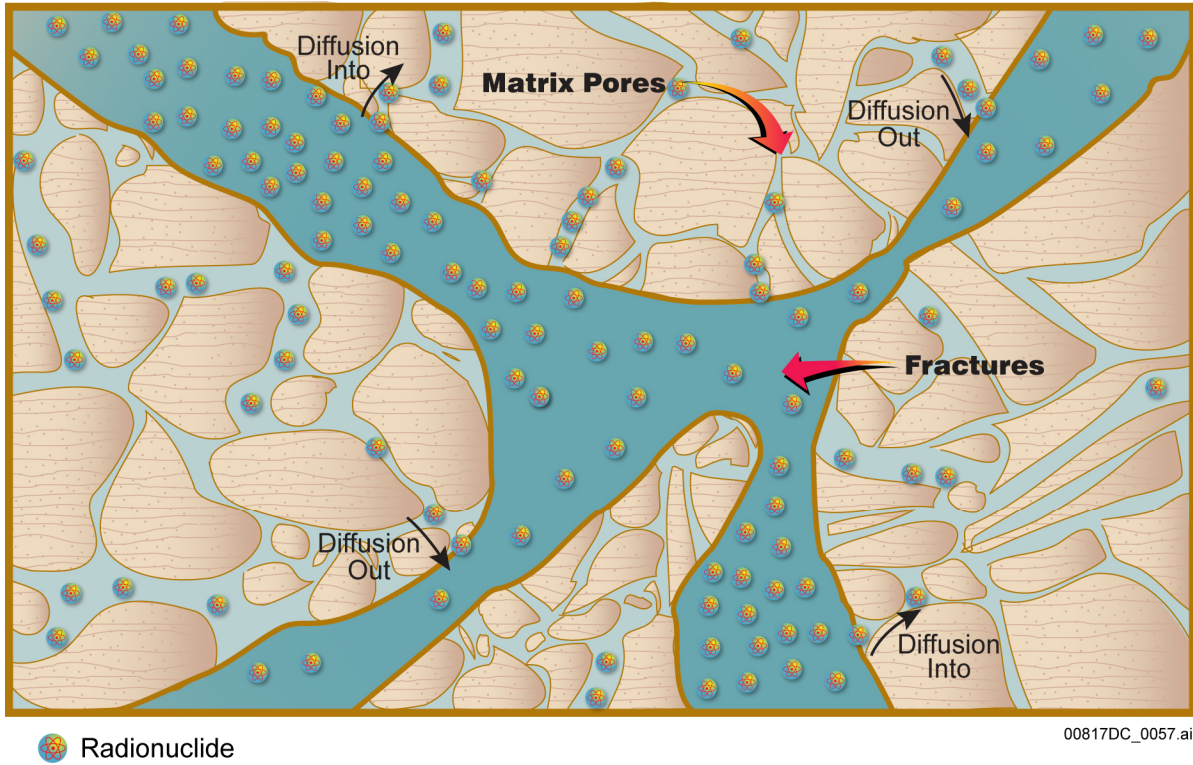
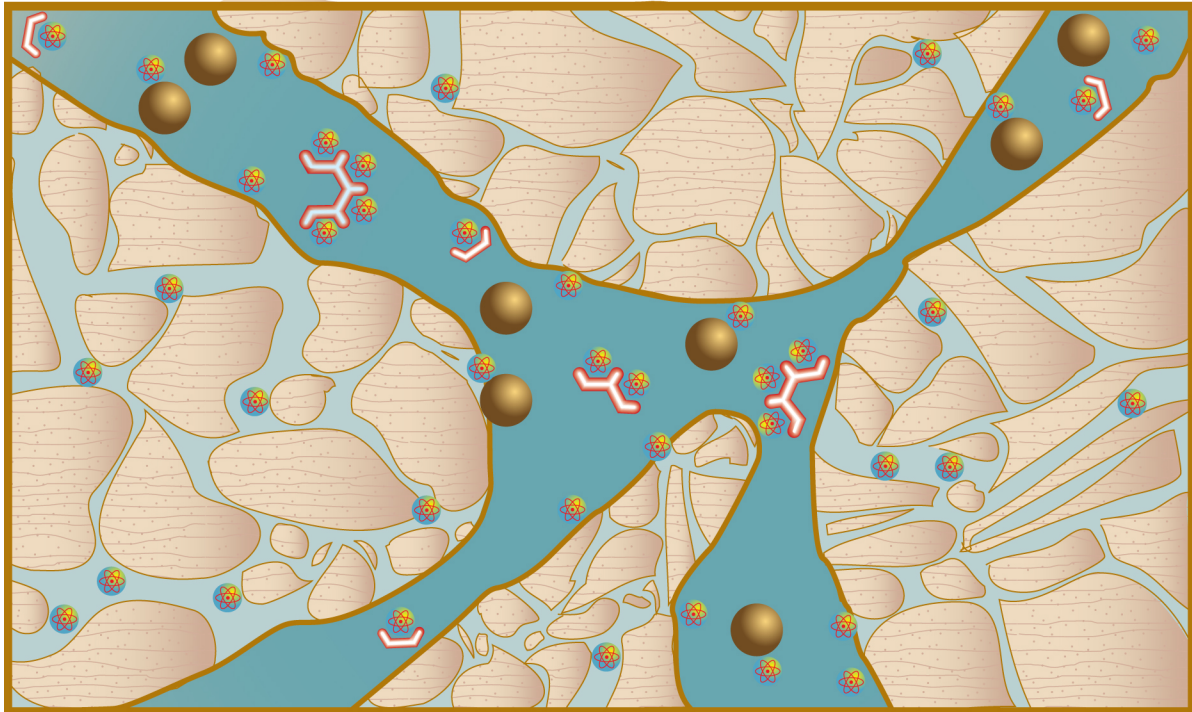


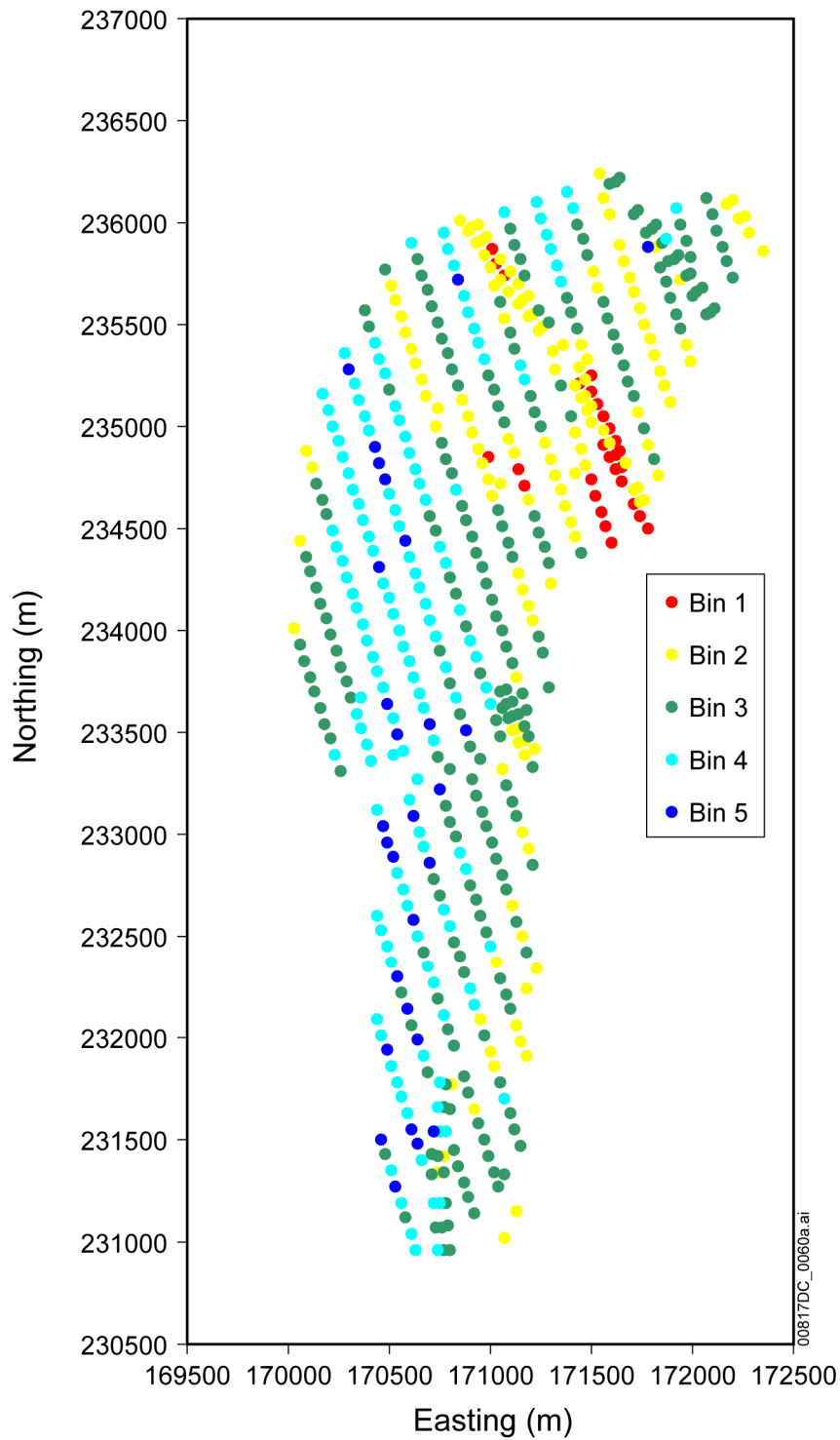
Figure 6.3.9-4. Illustration of Radionuclide Diffusion Into and Out of Matrix Pores



00817DC\_0059.ai

-  Radionuclide
-  Reversible Sorption Colloid (shown with radionuclide temporarily attached)
-  Reversible Sorption Colloid (shown without radionuclide attached)
-  Irreversible Sorption Colloid (shown with radionuclide permanently attached)

Figure 6.3.9-5. Illustration of Colloid-Facilitated Transport Processes



Source: DTN: LA0702PANS02BR.001\_R1 [DIRS 180322], *feh\_m\_repo\_nodes\_PD10%.xls*.

Figure 6.3.9-6. Location of Repository Release Nodes for Five Percolation Subregions

### 6.3.10 Saturated Zone Flow and Transport Model Component

The SZ Flow and Transport Model Component of the TSPA-LA Model (Table 6-1 and Figure 6-1) is used to evaluate the transport of radionuclides from their introduction at the water table to the accessible environment that is approximately 18 km downgradient from the repository. Figure 6.3.10-1 shows the relationship between the SZ Flow and Transport Model Component and other model components and submodels of the TSPA-LA Model. The UZ Transport Submodel provides the magnitude and distribution of radionuclide mass release rates to the SZ. Figure 6.3.10-2 summarizes the principal inputs and outputs, model features, and the foundations for confidence in the SZ Flow and Transport Model Component. The SZ Flow and Transport Model Component is linked to the Biosphere Model Component through the simulated time histories of radionuclide concentrations in groundwater at the boundary to the accessible environment. In the TSPA-LA Model analyses for different scenario classes and groundwater protection per 10 CFR 63.331 [DIRS 180319], radionuclide concentrations are calculated by including the mass of all radionuclides that reaches the accessible environment in any given annual period into 3,000 acre-feet of water, as specified in 10 CFR 63.312(c) [DIRS 180319].

#### 6.3.10.1 Conceptual Model

Figure 6.3.10-3 provides a conceptual illustration of SZ flow and transport between Yucca Mountain and the biosphere, showing the relevant processes and geologic media in the SZ. The conceptual model of SZ flow includes southerly groundwater flow from recharge areas at higher elevations north of Yucca Mountain, through the Tertiary age volcanic rocks, and into the alluvium and other valley-fill deposits. For the SZ flow and transport abstraction used in the TSPA-LA Model (SNL 2008 [DIRS 183750]), groundwater flow between the repository and the biosphere is modeled using three-dimensional steady-state flow conditions. A continuum representation is used for the fracture network in the volcanic rocks beneath the repository, and the alluvium and valley-fill deposits are modeled as porous media. The model of the SZ flow system includes higher groundwater flux during potential wetter and cooler monsoon and glacial-transition climate states that are likely to occur within the 20,000-year and one-million-year modeling time periods.

Several processes are involved in the transport of radionuclides through the SZ. Advection in groundwater, dispersion, matrix diffusion in fractured media, sorption of radionuclides, colloid-facilitated transport, radioactive decay, and radioactive ingrowth are explicitly included in the TSPA-LA Model simulations. The processes are represented in the TSPA-LA Model as follows:

- **Advective transport**—This process occurs only within the fracture network of the volcanic hydrogeologic units due to the very high contrast in permeability between the fractures and the rock matrix but is widely distributed within the alluvium, except in low-permeability materials. This mode of transport is the primary mechanism for the transport of radionuclides from the SZ to the accessible environment. Climate change affects radionuclide transport by changing the rates of groundwater advection, which results from increased hydraulic gradient associated with the rise in the water table.

- **Dispersion of radionuclide mass**—This process, which includes hydrodynamic dispersion and molecular diffusion, occurs in both the fractured volcanic units and in the alluvium, with longitudinal dispersion typically much greater than transverse dispersion.
- **Matrix diffusion in fractured volcanic units**—This process determines the transfer of dissolved radionuclide mass from the flowing groundwater within fractures to the relatively stagnant groundwater contained in the pores of the rock matrix. The mass transfer, which could be in either direction, is a function of the concentration of the radionuclide in the fractures and matrix. The process of matrix diffusion of colloids is considered to be small and thus is not accounted for. The diffusion of colloids from fractures into the rock matrix is not included in the TSPA-LA Model.
- **Radionuclide sorption**—Sorption in fractured media occurs in the rock matrix only. In the alluvium, sorption occurs only in the effective porosity of the alluvium.
- **Colloid-facilitated transport**—This process can occur by two modes: (1) when radionuclides are reversibly sorbed onto colloids and (2) when radionuclides are irreversibly sorbed onto colloids. A large fraction of the colloids with irreversibly sorbed radionuclides undergoes reversible filtration during transport. Figure 6.3.10-4 illustrates the mechanisms involved in colloid-facilitated transport. Reversible filtration of irreversible colloids is represented by a retardation factor in the SZ Flow and Transport Model Component.
- **Radioactive decay and ingrowth**—Radioactive decay occurs for all radionuclides. Radionuclide ingrowth is represented for the daughter radionuclides in four principal decay chains.

Section 6.3.9.2 describes transport processes in the UZ. Two ACMs regarding groundwater flow and radionuclide transport in the SZ were considered in the development of the SZ Flow and Transport Model Component. These ACMs are discussed in Section 6.3.10.5.

### 6.3.10.2 TSPA-LA Model Abstraction

Two abstractions of the SZ Flow and Transport Model Component were implemented for the TSPA-LA Model:

- The 3-D SZ Flow and Transport Abstraction Model was developed outside of the TSPA-LA Model to calculate the flow and transport through the SZ to the accessible environment for individual radionuclides important to dose. The output from the 3-D SZ Flow and Transport Abstraction Model is developed in the form of unit-source radionuclide breakthrough curves (DTN: SN0702PASZFTMA.001\_R0 [DIRS 179504]). Within the TSPA-LA Model, a convolution integral technique combines these radionuclide breakthrough curves with the time-varying radionuclide sources from the UZ to quantify radionuclide transport to the accessible environment. The convolution technique inherently assumes the system being simulated exhibits a linear response to the input function and a steady-state flow condition in the SZ. This approach was validated for the 3-D SZ Flow and Transport Abstraction, as documented

in *Saturated Zone Flow and Transport Model Abstraction* (SNL 2008 [DIRS 183750], Section 7.1.1[a]).

- The 1-D SZ Flow and Transport Abstraction is implemented directly in the TSPA-LA Model to calculate the radioactive decay, ingrowth, and transport for four decay chains. Although the decay products from these chains are not significant contributors to total dose, regulations for groundwater protection (contained in 10 CFR 63.331 [DIRS 180319]) require explicit analysis of their concentrations in the water supply of the critical group.

A brief summary of these two submodels is presented below.

**3-D SZ Flow and Transport Abstraction**—The three-dimensional SZ flow and transport process modeling, described in *Saturated Zone Site-Scale Flow Model* (SNL 2007 [DIRS 177391]) and *Site-Scale Saturated Zone Transport* (SNL 2007 [DIRS 177392]) forms the technical bases for the 3-D SZ Flow and Transport Abstraction, as implemented in the TSPA-LA Model. Figure 6.3.10-5 is a regional map showing the area of the SZ flow system, the direction of SZ flow, and an outline of the 3-D SZ Flow and Transport Process Model domain. The 3-D SZ Flow and Transport Abstraction is based on the 3-D SZ Flow and Transport Abstraction Model that uses a control-volume, finite-element method to model groundwater flow and a particle-tracking method to model SZ radionuclide transport. These methods, as implemented in FEHM V2.24-01 (FEHM V2.24-01, STN: 10086-2.24-01-00 [DIRS 179419]), simulate groundwater flow in fractured and porous media, as well as advection along groundwater streamlines, dispersion, retardation due to sorption, matrix diffusion, and colloid-facilitated transport. The groundwater flow boundary conditions for the 3-D SZ Flow and Transport Abstraction Model are specified heads at the lateral boundaries, a no-flow condition on the lower model boundary, and specified groundwater flux for recharge at the upper model boundary. These boundary conditions are described in detail in *Saturated Zone Site-Scale Flow Model* (SNL 2007 [DIRS 177391], Sections 6.3.1.6 and 6.3.1.7). The new percolation fluxes used in the UZ Flow Model were derived from the updated infiltration flux estimates documented in *Simulation of Net Infiltration for Present-Day and Potential Future Climates* (SNL 2007 [DIRS 182145]). However, the fluxes derived from the UZ Flow Model that are used in SZ Flow and Transport Model Abstraction (SNL 2008 [DIRS 183750]) are those of the previous UZ Flow Model. As discussed in *Saturated Zone Site-Scale Flow Model* (SNL 2007 [DIRS 177391], Section 6.4.3.9), the change in net infiltration through the UZ footprint is very small compared to the entire flow budget through the lateral boundaries.

The specified flux for recharge at the upper model boundary is scaled in proportion to an uncertainty in groundwater specific discharge that is represented by an uncertainty distribution (SNL 2008 [DIRS 183750], Table 6.7[a]). This parameter (groundwater specific discharge scaling factor) is a multiplier that is applied to all values of permeability, and values of specified recharge fluxes, in the 3-D SZ Flow and Transport Abstraction Model to effectively scale the simulated specific discharge in the model. Scaling the recharge flux and the values of permeability in proportion to the uncertainty in groundwater specific discharge maintains the calibration of the 3-D SZ Flow and Transport Abstraction Model with regard to water-level measurements (SNL 2008 [DIRS 183750], Section 6.5[a]). The uncertainty in groundwater specific discharge is applied to all of the climate states.

The sources of radionuclides entering the SZ are specified as point sources within each of the four source regions beneath the repository, as described in Section 6.3.9 (UZ Radionuclide Transport). Figure 6.3.10-6 shows the repository outline and the four SZ source regions used in the TSPA-LA Model. The horizontal location of the point source in each of the four source regions varies randomly from simulation to simulation. Source Regions 1 and 3 and part of Source Region 2 are primarily located directly below the repository to capture radionuclides transported vertically downward in the UZ Transport Submodel. Portions of Source Regions 2 and 4 are located to the east of the repository to capture radionuclides transported by the lateral diversion of groundwater to the east along dipping volcanic strata in the UZ. In addition, the northern part of Source Region 2 underlies a northeasterly extension of the repository. The random locations of the radionuclide source terms for each realization are defined by eight stochastic parameters (input names listed in the first column, last row of Table 6.3.10-2) that determine the areal model coordinates for the source locations within Source Regions 1 to 4, respectively. These parameter values are drawn from independent, uniform distributions from 0.0 to 1.0 and result in randomly located point sources within each of the four source regions for each realization of the SZ Flow and Transport Submodel.

In addition to the transport of radionuclides as solutes in groundwater, radionuclides may also be sorbed onto colloids and travel through the SZ to the accessible environment (BSC 2004 [DIRS 170006], Section 6.3). The radionuclides may be reversibly or irreversibly sorbed onto colloids. A retardation factor is established for radionuclides that are irreversibly sorbed onto colloids. Implied in the use of a retardation factor to describe colloid transport is that colloid filtration and detachment rates are fast relative to groundwater transport times through the system (BSC 2004 [DIRS 170006], Section 7.1). In addition, a small fraction of colloids, also called the fast fraction, is transported unretarded through the SZ, based on groundwater transport times (BSC 2004 [DIRS 170006], Section 6.6). As discussed in *Saturated Zone Colloid Transport* (BSC 2004 [DIRS 170006], Section 6.6), field experimental work has shown that a small percentage of colloids transport in groundwater with no retardation. Experimental results show that the attachment rate constant can be used to determine the fraction of colloids that are transported with no retardation. Specifically, colloids for which the reciprocal of the attachment rate constant is smaller than the transport time through the system will transport with no retardation. Radionuclides that are reversibly sorbed onto colloids are in equilibrium with the aqueous phase and the geologic medium. In this mode of transport, the effective retardation of these radionuclides during transport in the SZ depends on the sorption of radionuclides to colloids, the concentration of colloids in the groundwater, and the sorption coefficient of the radionuclide onto the geologic medium. Because the effective sorptive capacity of the porous medium is reduced when groundwater colloids carry a significant fraction of radionuclide mass in the system, an adjusted sorption coefficient is calculated for the alluvium and undifferentiated valley fill hydrologic units (SNL 2008 [DIRS 183750], Section 6.5.1.1, Equation 6-5). For transport in fractured media, the effective diffusion coefficient into the rock matrix is reduced due to the affinity of radionuclides for sorption onto colloids in the fractures (SNL 2008 [DIRS 183750], Section 6.5.1.1, Equation 6-9).

As discussed in Section 6.3.7.1.2, 27 of the 31 important radionuclides are tracked and transported by the SZ Transport Submodel. The 4 radionuclides that are not tracked and transported are  $^{245}\text{Cm}$ ,  $^{241}\text{Pu}$ ,  $^{227}\text{Ac}$ , and  $^{228}\text{Ra}$ . Details on the 4 radionuclides can be found in Section 6.3.7.1.2. The radionuclides tracked by the SZ Flow and Transport Model Component

are divided into 12 groups, based on their transport characteristics. These 12 groups and their modes of transport are summarized in Table 6.3.10-1. The first group contains the nonsorbing radionuclides technetium, iodine, carbon, and chlorine; they are grouped together in the TSPA-LA Model because their solute migration is identical. Carbon is considered nonsorbing and is transported without chemical reactions or ionic exchange with the host rocks, thus providing a conservative bound on transport in the absence of a detailed model for reactive transport. The second group contains americium, thorium, and protactinium, representing colloid-facilitated transport of the radionuclides reversibly sorbed onto colloids. The third group contains cesium, representing colloid-facilitated transport of the radionuclide reversibly sorbed onto colloids. The fourth group contains plutonium, representing colloid-facilitated transport of the radionuclide reversibly sorbed onto colloids. The fifth group contains neptunium, being transported as a solute. The sixth group contains plutonium and americium, representing colloid-facilitated transport of the radionuclides irreversibly sorbed onto colloids. The seventh, eighth, and ninth groups contain radium, strontium, and uranium, respectively, all transported as a solute. The tenth group contains plutonium and americium, representing the fast fraction of colloid-facilitated transport of the radionuclides irreversibly sorbed onto colloids. The eleventh group contains selenium, transported as a solute. Lastly, the twelfth group contains tin, representing colloid-facilitated transport of the radionuclide reversibly attached to colloids.

The 3-D SZ Flow and Transport Abstraction breakthrough curves are calculated outside of the TSPA-LA Model, as shown on Figure 6.1.4-1. The epistemic uncertain parameters shown in Table 6.3.10-2 are sampled 200 times to produce 200 sets of input parameters to the 3-D SZ Flow and Transport Abstraction Model (DTN: SN0702PASZFTMA.001\_R0 [DIRS 179504]). The 3-D SZ Flow and Transport Abstraction Model then uses these 200 input parameter sets to perform a series of probabilistic transport simulations for a unit mass flux source. The simulated transport particle paths from the Site-Scale Saturated Zone Transport Model (SNL 2007 [DIRS 177392]) are illustrated on Figure 6.3.10-7. The output of these simulations is a set of 200 breakthrough curves for each of the four source regions and 12 radionuclide groups (DTN: SN0702PASZFTMA.001\_R0 [DIRS 179504]). The resulting 9,600 breakthrough curves describe the (unit-source) mass of radionuclides that cross the 18-km boundary as a function of time. These breakthrough curves, the SZ\_Convolute DLL (SZ\_Convolute V3.10.01, STN: 10207-3.10.01-00 [DIRS 181060]) and control files for SZ\_Convolute (described in DTN: SN0702PASZFTMA.001\_R0 [DIRS 179504]), are the principal parts of the 3-D SZ Flow and Transport Abstraction. The convolution integral method employed in SZ\_Convolute exhibits a linear response to the input function. In the case of solute transport in the SZ, this approach implies, for example, that a doubling of the input mass flux results in a doubling of the output mass flux. This approach is valid for the SZ Flow and Transport Submodel because the underlying transport processes (e.g., advection and sorption) are described by linear partial differential equations with respect to solute mass (SNL 2007 [DIRS 177392], Section 6.4.2.1, Equation 1 and Section 6.4.2.5, Equation 42).

The processes of colloid filtration and sorption are both represented as equilibrium retardation processes. Simple retardation affects the timing of the release of radionuclides from the SZ but still constitutes a linear relationship between mass input and mass output for the SZ. Future monsoonal and glacial-transition climate states with potentially wetter and cooler climate conditions would increase groundwater recharge, which in turn would increase the specific discharge. When climate change occurs, the convolution technique accounts for the change in

specific discharge explicitly (*Design Document for: SZ\_Convolute Version 3.0* (DOE 2003 [DIRS 167588], Section 3.1). The climate state groundwater flow scaling factors presented in Table 6.3.10-3 (i.e., parameters Flow\_Rate\_Fact\_Vclim\_CS1, Flow\_Rate\_Fact\_Vclim\_CS2, and Flow\_Rate\_Fact\_Vclim\_CS3) are based on mean case conditions and do not include uncertainty in groundwater flux estimates within a given climate state. The uncertainty is captured by the stochastic parameter groundwater specific discharge multiplier (Table 6.3.10-2). The uncertainty in groundwater specific discharge multiplier is applied to all of the climate states. It is assumed that the instantaneous change from one climate steady-state flow condition to another steady-state condition in the SZ can be described as a linear function (SNL 2008 [DIRS 183750], Section 6.5, p. 6-18). For post-10,000-year (climate state 4) calculations, the scaling factor Flow\_Rate\_Fact\_Vclim\_CS3, which represents the glacial transition climate conditions, is applicable.

As discussed in *Saturated Zone Flow and Transport Model Abstraction* (SNL 2008 [DIRS 183750], Section 6.5.3[a]), the glacial-transition climate state is appropriate for use in the post-10,000-year simulations of SZ flow and transport because hydrologic conditions for this state are consistent with proposed regulations (10 CFR 63.342 [DIRS 178394]). The proposed regulation (10 CFR 63.342 [DIRS 178394]) specifies that the constant value for climate change in the post-10,000-year period be based on a distribution of deep percolation ranging from 13 to 64 mm/yr. As shown in *Saturated Zone Flow and Transport Model Abstraction* (SNL 2008 [DIRS 183750], Table 6-1[a]), the range of simulated average glacial-transition infiltration from the MASSIF model (SNL 2007 [DIRS 182145]) (16.0 mm/yr at the 10th percentile to 46.2 mm/yr at the 90th percentile) approximately covers the range of deep percolation specified in 10 CFR 63.342 [DIRS 178394]. Therefore, the glacial-transition climate, as defined in the MASSIF infiltration model (SNL 2007 [DIRS 182145]) and in the SZ Flow and Transport Abstraction Model, is the appropriate constant representation of climate change for use in the post-10,000-year simulations of radionuclide transport.

**1-D SZ Flow and Transport Abstraction**—Because the ingrowth of radionuclides is not explicitly included in the 3-D SZ Flow and Transport Abstraction, a 1-D SZ Flow and Transport Abstraction is used to account for the decay and ingrowth of radionuclide daughter products for the four decay chains shown on Figure 6.3.10-8. The representation of the radionuclide decay chains is simplified in a manner that overestimates the concentration of daughter radionuclides by calculating the secular equilibrium between the final daughter products and their parents in two decay chains (SNL 2008 [DIRS 183750], Section 6.5.1.2).  $^{227}\text{Ac}$  is in secular equilibrium with  $^{231}\text{Pa}$  in the actinium chain at the downstream end of the one-dimensional SZ flow pathway, and  $^{228}\text{Ra}$  is in secular equilibrium with  $^{232}\text{Th}$  in the thorium series.

A conceptualization of the 1-D SZ Flow and Transport Abstraction is shown on Figure 6.3.10-9. The 1-D SZ Flow and Transport Abstraction is implemented directly in the TSPA-LA Model as a series of one-dimensional GoldSim model elements (called pipes). The one-dimensional pipes are able to simulate advection, longitudinal dispersion, retardation, decay and ingrowth, and matrix diffusion. Thus, the same radionuclide transport processes that are simulated in the 3-D SZ Flow and Transport Abstraction are included in the one-dimensional pipes, with the exception of transverse dispersion, which cannot be included in a one-dimensional model. Groundwater specific discharge in each pipe segment and pipe segment lengths in the 1-D SZ transport model are based on estimates derived from the 3-D SZ Flow and Transport Abstraction

Model (SNL 2008 [DIRS 183750], Section 6.5.1.2[a]). The 1-D SZ Flow and Transport Abstraction includes the same uncertain input parameters as the 3-D SZ Flow and Transport Abstraction (DTN: SN0702PASZFTMA.001\_R0 [DIRS 179504]), shown in Table 6.3.10-2. The two abstractions are coupled so that, for a given realization, the same set of sampled input parameters is used. In addition, the 1-D SZ abstraction uses the constant parameters given in Table 6.3.10-3. Flow rates in the one-dimensional pipe segments are modified for the transitions in climate state, using the same climate state scaling factors listed in Table 6.3.10-3 that are used to modify the flow rates in the 3-D SZ Flow and Transport Abstraction. However, note that limitations in the Laplace transform solution implemented in the pipe module of GoldSim (GoldSim V9.60.100, STN: 10344-9.60-01 [DIRS 181903]; *User's Guide, GoldSim Probabilistic Simulation Environment* (GoldSim Technology Group 2007 [DIRS 181727])) preclude a change to the migration velocity of radionuclides that have entered the pipe segments. The values of longitudinal dispersivity in the SZ one-dimensional transport model have also been increased by one order of magnitude from the sampled values. This adjustment results in a better agreement between the SZ one-dimensional transport model and the SZ Site-Scale Transport Model as documented in *Saturated Zone Flow and Transport Model Abstraction* (SNL 2008 [DIRS 183750], Section 7.3.2[a]). This adjustment to the values of dispersivity are made because of the higher contrasts in permeability among the hydrogeologic units in the three-dimensional SZ site-scale transport model and the resulting enhancement to the dispersion in the random walk particle tracking algorithm (SNL 2008 [DIRS 183750], Section 6.5.1.2[a]). However, the adjustment and the use of unbounded log-normal distribution for longitudinal dispersivity resulted in large values for some sampled points. The impact of these large longitudinal dispersivity values is addressed in Appendix P, Section P15.2.

Radionuclide mass already within a given pipe segment of the 1-D SZ Flow and Transport Abstraction does not increase in velocity in response to increased specific discharge resulting from climate change. Radionuclide mass introduced after the change in specific discharge is transported at the proper, correspondingly faster rate. Therefore, a potential discrepancy exists between the rate at which the radionuclides are transported using the 3-D SZ Flow and Transport Abstraction Model and the 1-D SZ Flow and Transport Abstraction. The impacts of this limitation to calculations in the TSPA-LA Model are not large due to the following considerations. First, the 1-D SZ Flow and Transport Abstraction results are used only for the daughter products of the decay chains in the TSPA-LA Model calculations. Second, this limitation applies only to radionuclide mass that enters a given pipe segment prior to 2,000 years, after which glacial-transition climatic conditions continue unchanged. The radionuclide mass that enters the 1-D SZ Flow and Transport Abstraction prior to 600 years, at the time of change from present to monsoon conditions, would experience this limitation to the largest extent because it would be subject to two climate changes. Section 6.3.10.3 describes the implementation of this process in greater detail.

In the 1-D SZ Flow and Transport Abstraction, the flow path from the repository to the accessible environment is subdivided into three concentric zones centered on the repository that are nominally: (1) 0 km to 5 km from the repository, (2) 5 km to 13 km from the repository, and (3) 13 km to 18 km from the repository. The actual flow path length (Table 6.3.10-4) of each pipe segment in zones 2 and 3 varies as a function of: (1) the northwestern boundary of the alluvial uncertainty zone (FPLANW in Table 6.3.10-2), (2) the value of horizontal anisotropy (HAVO in Table 6.3.10-2), and (3) the source region from which the radionuclide source

originates beneath the repository. The value of the parameter defining the location of the northwestern boundary of the alluvial uncertainty zone varies from zero to one and is used to establish the location of the contact between tuff and alluvium below the water table. The length of the first pipe segment is fixed at 5 km for all realizations. The second pipe segment represents that portion of the flow path from a 5-km distance to contact between the volcanic aquifer and the alluvial aquifer in the SZ. The third pipe segment represents the portion of the flow path from the contact between the volcanic units and the alluvium out to the accessible environment. The lengths of the second and third pipe segments are estimated from the particle-tracking results of the 3-D SZ Flow and Transport Abstraction Model, as summarized in Table 6.3.10-4. It is important to note that the total length of the three pipe segments for a given source region can be greater than 18 km due to the effects of the horizontal anisotropy on the simulated flow paths (Figure 6.3.10-10). Estimated pipe segment lengths are shown for differing values of the horizontal anisotropy and for the four source regions. Each entry in the table contains a range of values in pipe length, where the minimum value shown for the second pipe (5- to 13-km zone) is used when the parameter defining the location of the northwestern boundary of the alluvial uncertainty zone is equal to 1.0, and the maximum value is used when the northwestern boundary parameter is equal to 0.0. By contrast, the minimum value of length for the third (13-to 18-km zone) pipe segment is used when the parameter defining the location of the northwestern boundary of the alluvial uncertainty zone is equal to 0.0, and the maximum value corresponds to a northwestern boundary parameter equal to 1.0. In other words, the maximum length of the flow path in the alluvial aquifer corresponds to the maximum northwesterly extent of the alluvial uncertainty zone, and the minimum length of the flow path in the alluvial aquifer corresponds to the minimum northwesterly extent of the alluvial uncertainty zone. The values in Table 6.3.10-4 are input into the SZ One-Dimensional Transport Model as a look-up table.

The average specific discharge along each pipe segment of the 1-D SZ Flow and Transport Abstraction varies as a function of the horizontal anisotropy. The resulting values of average specific discharge, as used in the 1-D SZ Flow and Transport Abstraction, are shown in Table 6.3.10-5. Figure 6.3.10-10 shows the simulated flow paths from Source Region 1 for the different values of horizontal anisotropy listed in Table 6.3.10-5.

The values of specific discharge are also scaled linearly using the groundwater specific discharge multiplier (Table 6.3.10-2) to represent the uncertainty in specific discharge. The values of specific discharge within the three pipe segments are calculated within the 1-D SZ Flow and Transport Abstraction by interpolating between the values of horizontal anisotropy, shown in Table 6.3.10-5, and through scaling by the value of the groundwater specific discharge multiplier (Table 6.3.10-2). The volumetric flow rate is the same for all segments in the 1-D SZ Flow and Transport Abstraction, and variations in specific discharge along the flow path are incorporated into the model by varying the cross-sectional areas of the pipe segments.

A summary of alpha concentration results in Amargosa Valley groundwater is given in Table 6.3.10-6 (DTN: SN0702PASZFTMA.002\_R1 [DIRS 183471]). The best estimate for the mean gross alpha concentration in groundwater is 0.50 pCi/L with a 95 percent confidence that the concentration will not exceed 0.71 pCi/L. In the absence of data on the combined concentrations of  $^{226}\text{Ra}$  and  $^{228}\text{Ra}$ , it should be conservatively assumed for these radionuclides that they are responsible for all gross alpha activity. For  $^{226}\text{Ra}$  and  $^{228}\text{Ra}$ , the mean concentration is 0.50 pCi/L with a 95 percent confidence that the concentration will not exceed 0.71 pCi/L. To

allow for sampling, the values found in output DTN: MO0708TSPAGENT.000 ([DIRS 183000], file BL-TSPA-DTN-5, PEF #89) are those of mean, standard deviation, and upper limit, where the standard deviation is derived from the mean and 95th percentile values and the upper limit represents three standard deviations above the mean. The standard deviation can be derived using the fact that, by definition in a normal distribution, the 95th percentile is 1.645 standard deviations above the mean. For both mean gross alpha concentration and background  $^{226}\text{Ra}$  and  $^{228}\text{Ra}$ , the 95th percentile is 0.21 pCi/L above the mean of 0.50 pCi/L. The standard deviation is therefore  $(0.21 \text{ pCi/L})/1.645$  or 0.128 pCi/L. Details can be found in *Saturated Zone Flow and Transport Model Abstraction* (SNL 2008 [DIRS 183750], Section 6.8.6). These parameters are used in the biosphere model component of the TSPA-LA Model (Section 6.3.11).

### 6.3.10.3 TSPA-LA Model Implementation

Figure 6.3.10-11 presents a flow chart that shows the implementation of the SZ Flow and Transport Submodel.

The 3-D SZ Flow and Transport Submodel calculations are performed by an external DLL, SZ\_Convolute V3.10.01, which is directly coupled to the TSPA-LA Model. The input files for SZ\_Convolute are described in Appendix F, Section F2.5. At the beginning of each realization, an integer variable (SZ index) with a range of 1 to 200 is randomly sampled in the TSPA-LA Model and is used to select the radionuclide breakthrough curve to be used for that realization. The same breakthrough curve is selected for each radionuclide group based on the sampled SZ index value. This maintains consistency among the different radionuclide groups because the breakthrough curves for each value of the SZ index were produced using the same set of input parameters. For each timestep, the SZ\_Convolute DLL takes the radionuclide source mass from the nodes at the water table of the UZ Transport Submodel (Section 6.3.9.1) and combines it with the selected breakthrough curve for that radionuclide and source region.

Because the 3-D SZ Flow and Transport Abstraction does not account for ingrowth of daughter products in the chain decay, adjustments are necessary to properly account for these radionuclides (Figure 6.3.10-8). The TSPA-LA Model adjustments increase the inventory of the first-generation daughters (namely:  $^{239}\text{Pu}$ ,  $^{237}\text{Np}$ ,  $^{236}\text{U}$ ,  $^{238}\text{U}$ , and  $^{234}\text{U}$ ) before they are released into the 3-D SZ Flow and Transport Abstraction. This adjustment is performed using a method termed inventory boosting in the TSPA-LA Model's GoldSim model file. For each timestep, the inventory of each of these first-generation daughters is increased or boosted by the amount that their respective parent radionuclides would decay during the remaining simulation time.

The 1-D SZ Flow and Transport Abstraction is used to account for the ingrowth of the second-generation daughters:  $^{235}\text{U}$ ,  $^{231}\text{Pa}$ ,  $^{227}\text{Ac}$ ,  $^{233}\text{U}$ ,  $^{229}\text{Th}$ ,  $^{232}\text{Th}$ ,  $^{228}\text{Ra}$ ,  $^{230}\text{Th}$ , and  $^{226}\text{Ra}$ . The 1-D SZ Flow and Transport Abstraction is incorporated directly into the TSPA-LA Model as four sets of three pipe elements (one set for each SZ source region). The radionuclide mass input to the 1-D SZ Flow and Transport Abstraction also comes from the UZ Transport Submodel. The same integer value used by the 3-D SZ Flow and Transport Abstraction to select a set of breakthrough curves is used in the 1-D SZ Flow and Transport Abstraction to choose additional input parameter values from look-up tables in the TSPA-LA Model. This method ensures

consistency between the 1-D and 3-D SZ Flow and Transport Abstractions on a realization-by-realization basis.

Even though they are accounted for in the 3-D SZ Flow and Transport Abstraction, the parents of the second-generation daughters are also transported in the 1-D SZ Flow and Transport Abstraction. The parents are included in the 1-D SZ Flow and Transport Abstraction to account for the ingrowth of the second-generation daughters. The first-generation daughter products are not boosted for the 1-D SZ Flow and Transport Abstraction because the GoldSim software correctly calculates the decay and ingrowth of radionuclides.

The radionuclide mass for all species is tracked in both the 1-D and 3-D SZ Flow and Transport Abstractions. However, the radionuclide mass exiting each submodel is then screened, such that only the mass for second-generation daughter species is taken from the 1-D SZ Flow and Transport Abstraction. All the other radionuclide results are taken from the 3-D SZ Flow and Transport Abstraction.

Radionuclides are released from the SZ to the accessible environment approximately 18 km from the repository (66 FR 55732 [DIRS 156671], III Public Comments and Responses, 3.5, p. 55753). The 18-km regulatory boundary represents the location where a RMEI resides (66 FR 55732 [DIRS 156671], III Public Comments and Responses, 3.2, p. 55750). All of the radionuclide mass that crosses this regulatory boundary in the SZ is assumed to be homogeneously distributed in a 3,000 acre-ft volume per annum (10 CFR 63.332(3) [DIRS 180319]). The resulting release of radionuclide mass to the biosphere is then used to calculate dose to the RMEI (Section 6.3.11).

#### **6.3.10.4 Model Component Consistency and Conservatism in Assumptions and Parameters**

To enhance understanding of the complex interactions within the TSPA-LA Model, a discussion of consistency among model components and submodels and identification of conservative assumptions in abstractions, process models, and parameter sets supporting SZ flow and transport are discussed below.

##### **6.3.10.4.1 Consistency of Assumptions**

**SZ Release Location**—The 3-D SZ Flow and Transport Abstraction, which is used to transport all parent radionuclides and first-generation daughters, is based on three-dimensional simulations that use a random release location beneath the repository for each of the four SZ source regions (Section 6.3.10.2). However, the 1-D SZ Flow and Transport Abstraction, used for most granddaughters, is based on a central release location for each of the four source regions. This can result in different transport behavior for isotopes of the same chemical element in a given realization. For example,  $^{234}\text{U}$  (a daughter of  $^{238}\text{Pu}$ , but a granddaughter of  $^{242}\text{Pu}$ ) is transported with the three-dimensional model, whereas  $^{233}\text{U}$  is transported with the one-dimensional model. Thus, for certain realizations, where the three-dimensional random-release model produces a significantly different transport pathway than the one-dimensional central-location model, the transport times through the SZ for the two radionuclides can be different by thousands of years,

even though they would be expected to behave similarly because they have similar transport properties.

**Effect on TSPA**—The effect of this difference is minimal because the central release location used in the 1-D SZ Flow and Transport Abstraction is representative of the average behavior taken over multiple realizations.

#### **6.3.10.4.2 Identification of Conservatisms in Submodels and Abstractions**

**Radionuclide Mass Release from the UZ Matrix to the SZ**—The transfer of radionuclide mass reaching the water table from the matrix of the UZ directly to the fractures of the SZ tends to maximize the simulated concentrations of radionuclides at the outlet to the accessible environment. This approximation results in less dispersion of the radionuclide transport times through the SZ and, thus, to less attenuation of peaks in radionuclide discharge. This conservatism is used because it simplifies the modeling approach (SNL 2008 [DIRS 183750], Sections 6.3.3 and 6.5.2.13). Appendix C contains an analysis in which the mass from the UZ matrix is transferred to new cells that model matrix diffusion before reaching the SZ.

**Instantaneous Change in SZ Groundwater Flow at Climate State Changes**—The increase in groundwater flux will be gradual during the transition period going from drier conditions to wetter conditions. However, in the TSPA-LA Model, groundwater flux is assumed to increase instantaneously at climate state changes. This conservatism is applied because it simplifies the modeling approach (SNL 2008 [DIRS 183750], Section 6.5, p. 6-18). This approach tends to overestimate the rate of radionuclide transport in the SZ. Appendix C contains an analysis on the effect of climate changes in UZ transport, which directly affects the SZ.

**Colloids are Retarded by Filtration**—The conceptual model of filtration for colloids with irreversibly sorbed radionuclides assumes that colloids are retarded by filtration. Permanent removal of colloids by mechanical filtration in the SZ is not considered in the TSPA-LA Model, although it is likely to occur (SNL 2008 [DIRS 183750], Sections 6.3.1, 6.3.2, 6.5.1[a], and 6.5.2.11). The exclusion of permanent colloid filtration tends to overestimate the quantity of colloids that are transported through the SZ. In the compliance model (SNL 2008 [DIRS 183750], Section 6.5.2.11), transport of retarded irreversible colloids in both the volcanic units and the alluvium is calculated using single retardation factors (one for the volcanic units and another for the alluvium). Analysis of experimental data shows that use of a single retardation factor does not fit experimental observations (output DTN: LA0705PR150304.001 [DIRS: 181744]). Appendix C contains an analysis of the colloid diversity model, in which colloids are assigned a wide range of retardation factors that are based on experimental data.

**No Solubility Limits or Enhanced Sorption Applied to Radionuclide Concentrations in the SZ**—No solubility limits are applied to radionuclide concentrations in the SZ. Dissolved radionuclide concentrations in the far field are assumed to be the same as in the near field regardless of the chemical conditions. The application of solubility limits in the SZ is screened out as part of FEP 2.2.08.07.0A (DTN: MO0706SPAFEPLA.001\_R0 [DIRS 181613]). In addition, significantly greater sorption could occur for some redox-sensitive radionuclides if chemically reducing conditions occur locally in the SZ. Changes due to redox conditions in the SZ could have a potential impact on solubility, sorption, and radionuclide transport through the

SZ. Enhanced sorption due to the presence of reducing zones in the SZ could increase retardation, resulting in longer travel times in the SZ. The potential impact of redox conditions in the SZ is discussed in Appendix C.

**Implementation of Ingrowth of radionuclides in the SZ Model**—Ingrowth of radionuclides is not explicitly included in the SZ transport model component of the TSPA-LA model for some radionuclides. A simplified approach, inventory boosting, accounts for this process for some of the radionuclides that have parent radionuclides as described in *Saturated Zone Flow and Transport Model Abstraction* (SNL 2008 [DIRS 183750], Sections 6.3.1). The TSPA-LA 1-D SZ Transport Model adds the pre-decayed daughter products to transported inventory in the SZ and also transports the full inventory of the parents by applying inventory boosting. The parent radionuclides of these boosted decay products are not diminished, resulting in an overestimation of the mass of radionuclides transported in the SZ.

#### **6.3.10.5 Alternative Conceptual Model(s) for Saturated Zone Flow and Transport**

Section 6.2 outlines the general consideration and treatment of ACMs used to support the TSPA-LA Model. A brief description of the SZ flow and transport ACMs summarized in Table 6.3.10-7 is presented below.

**Minimal Matrix Diffusion ACM**—Diffusion of radionuclides into the pore space of the rock matrix in the fractured volcanic units is potentially extremely limited due to highly channelized groundwater flow, fracture coatings, or other factors. The uncertain input parameters influencing matrix diffusion in the SZ Flow and Transport Submodel include effective diffusion coefficient, flowing interval spacing, and flowing interval porosity. Minimal matrix diffusion in the SZ Flow and Transport Submodel would tend to increase the rate of radionuclide transport. However, this ACM is implicitly included in the 3-D SZ Flow and Transport Abstraction and in the 1-D SZ Flow and Transport Abstraction through the range of uncertainty in the key input parameters mentioned above (SNL 2008 [DIRS 183750], Section 6.4).

This ACM was shown to be captured within the range of uncertainty already in the SZ Flow and Transport Submodel and, therefore, is not recommended for inclusion in the TSPA-LA Model.

**Horizontal Anisotropy in Permeability ACM**—Alternative interpretations of pump test results in the fractured volcanic units indicate preferential permeability along structural features oriented in the NNE-SSW direction or in the WNW-ESE direction. This ACM is implicitly included in the 3-D SZ Flow and Transport Abstraction and in the 1-D SZ Flow and Transport Abstraction through the range of uncertainty in the input parameter HAVO. The uncertain input parameter influencing horizontal anisotropy in permeability in the volcanic units near Yucca Mountain is the ratio of N-S to E-W permeability (SNL 2008 [DIRS 183750], Section 6.5.2.10). This continuously distributed parameter varies from less than one to greater than one with most of the realizations greater than one.

This ACM was also shown to be captured within the range of uncertainty already in the SZ Flow and Transport Submodel and, therefore, is not recommended for inclusion in the TSPA-LA Model.

Table 6.3.10-1. Radionuclides Transported in the Saturated Zone Flow and Transport Submodel

<b>Radionuclide Group Number</b>	<b>Transport Mode</b>	<b>Radionuclides</b>
1	Solute	Carbon, Technetium, Iodine, Chlorine
2	Colloid-facilitated (Reversible)	Americium, Thorium, Protactinium
3	Colloid-facilitated (Reversible)	Cesium
4	Colloid-facilitated (Reversible)	Plutonium
5	Solute	Neptunium
6	Colloid-facilitated (Irreversible)	Plutonium, Americium
7	Solute	Radium
8	Solute	Strontium
9	Solute	Uranium
10	Colloid-facilitated (Fast fraction of Irreversible)	Plutonium, Americium
11	Solute	Selenium
12	Colloid-facilitated (Reversible)	Tin

Source: *Saturated Zone Flow and Transport Model Abstraction* (SNL 2008 [DIRS 183750], Table 6-9[a]).

Table 6.3.10-2. Uncertain Model Inputs Used in the 3-D Saturated Zone Flow and Transport Process Model and 1-D Saturated Zone Flow and Transport Abstraction

Input Name	Input Description	Value or Distribution	Units	Type of Uncertainty
Kd_Np_Vo	Neptunium sorption coefficient in volcanic units	CDF: <u>Probability</u> <u>Value</u> 0.0                  0.0 0.05                0.99 0.90                1.83 1.0                  6.0	mL/g	Epistemic
Kd_Np_AI	Neptunium sorption coefficient in alluvium	CDF: <u>Probability</u> <u>Value</u> 0.0                  1.8 0.05                4.0 0.95                8.7 1.0                  13.0	mL/g	Epistemic
Kd_Sr_Vo	Strontium sorption coefficient in volcanic units	Uniform: Minimum          20.0 Maximum         400.0	mL/g	Epistemic
Kd_Sr_AI	Strontium sorption coefficient in alluvium	Uniform: Minimum          20.0 Maximum         400.0	mL/g	Epistemic
Kd_U_Vo	Uranium sorption coefficient in volcanic units	CDF: <u>Probability</u> <u>Value</u> 0.0                  0.0 0.05                5.39 0.95                8.16 1.0                  20.0	mL/g	Epistemic
Kd_U_AI	Uranium sorption coefficient in alluvium	CDF: <u>Probability</u> <u>Value</u> 0.0                  1.7 0.05                2.9 0.95                6.3 1.0                  8.9	mL/g	Epistemic
Kd_Ra_Vo	Radium sorption coefficient in volcanic units	Uniform: Minimum          100.0 Maximum         1,000.0	mL/g	Epistemic
Kd_Ra_AI	Radium sorption coefficient in alluvium	Uniform: Minimum          100.0 Maximum         1,000.0	mL/g	Epistemic
Kd_Pu_Vo	Plutonium sorption coefficient in volcanic units	CDF: <u>Probability</u> <u>Value</u> 0.0                  10.0 0.25                89.9 0.95                129.87 1.0                  300.0	mL/g	Epistemic
Kd_Pu_AI	Plutonium sorption coefficient in alluvium	Beta: Mean                100 Standard Deviation   15 Minimum            50 Maximum            300	mL/g	Epistemic

Table 6.3.10-2. Uncertain Model Inputs Used in the 3-D Saturated Zone Flow and Transport Process Model and 1-D Saturated Zone Flow and Transport Abstraction (Continued)

Input Name	Input Description	Value or Distribution	Units	Type of Uncertainty
Kd_Am_Vo	Americium sorption coefficient in volcanic units	Truncated Normal: Mean 5,500 Standard Deviation 1,500 Minimum 1,000 Maximum 10,000	mL/g	Epistemic
Kd_Am_Al	Americium sorption coefficient in alluvium	Truncated Normal: Mean 5,500 Standard Deviation 1,500 Minimum 1,000 Maximum 10,000	mL/g	Epistemic
Kd_Cs_Vo	Cesium sorption coefficient in volcanic units	CDF: <u>Probability</u> <u>Value</u> 0.0                  100.0 0.05                3,000.59 1.0                  6,782.92	mL/g	Epistemic
Kd_Cs_Al	Cesium sorption coefficient in alluvium	Truncated Normal: Mean 728 Standard Deviation 464 Minimum 100 Maximum 1,000	mL/g	Epistemic
Kd_Se_Vo	Selenium sorption coefficient in volcanic units	Truncated Log_Normal: Mean 14.0 Standard Deviation 11.2 Minimum 1.0 Maximum 50.0	mL/g	Epistemic
Kd_Se_Al	Selenium sorption coefficient in alluvium	Truncated Log_Normal: Mean 14.0 Standard Deviation 11.2 Minimum 1.0 Maximum 50.0	mL/g	Epistemic
Kd_Sn_Vo	Tin sorption coefficient in volcanic units	Log-Uniform: Minimum 1.e2 Maximum 1.e5	mL/g	Epistemic
Kd_Sn_Al	Tin sorption coefficient in alluvium	Log-Uniform: Minimum 1.e2 Maximum 1.e5	mL/g	Epistemic
Correlation matrix for $K_d$ sampling in the SZ	Correlation coefficient values among radionuclides and between volcanic units and alluvium	DTN: LA0702AM150304.001 [DIRS 184763]	None	Matrix of Single Values

Table 6.3.10-2. Uncertain Model Inputs Used in the 3-D Saturated Zone Flow and Transport Process Model and 1-D Saturated Zone Flow and Transport Abstraction (Continued)

Input Name	Input Description	Value or Distribution	Units	Type of Uncertainty																										
FISVO	Flowing interval spacing in volcanic units	CDF: <table border="1"> <thead> <tr> <th>Probability</th> <th>Value</th> </tr> </thead> <tbody> <tr><td>0.0</td><td>1.860</td></tr> <tr><td>0.01</td><td>2.925</td></tr> <tr><td>0.20</td><td>12.036</td></tr> <tr><td>0.50</td><td>25.773</td></tr> <tr><td>0.80</td><td>39.965</td></tr> <tr><td>0.90</td><td>45.797</td></tr> <tr><td>0.92</td><td>47.207</td></tr> <tr><td>0.94</td><td>49.115</td></tr> <tr><td>0.96</td><td>51.710</td></tr> <tr><td>0.98</td><td>55.249</td></tr> <tr><td>0.99</td><td>58.439</td></tr> <tr><td>1.0</td><td>80.0</td></tr> </tbody> </table>	Probability	Value	0.0	1.860	0.01	2.925	0.20	12.036	0.50	25.773	0.80	39.965	0.90	45.797	0.92	47.207	0.94	49.115	0.96	51.710	0.98	55.249	0.99	58.439	1.0	80.0	M	Epistemic
Probability	Value																													
0.0	1.860																													
0.01	2.925																													
0.20	12.036																													
0.50	25.773																													
0.80	39.965																													
0.90	45.797																													
0.92	47.207																													
0.94	49.115																													
0.96	51.710																													
0.98	55.249																													
0.99	58.439																													
1.0	80.0																													
CORAL	Colloid retardation factor in alluvium	CDF: (Log <sub>10</sub> -transformed) <table border="1"> <thead> <tr> <th>Probability</th> <th>Value</th> </tr> </thead> <tbody> <tr><td>0.0</td><td>0.903</td></tr> <tr><td>0.331</td><td>0.904</td></tr> <tr><td>0.50</td><td>1.531</td></tr> <tr><td>1.0</td><td>3.715</td></tr> </tbody> </table>	Probability	Value	0.0	0.903	0.331	0.904	0.50	1.531	1.0	3.715	None	Epistemic																
Probability	Value																													
0.0	0.903																													
0.331	0.904																													
0.50	1.531																													
1.0	3.715																													
CORVO	Colloid retardation factor in volcanic units	CDF: (Log <sub>10</sub> -transformed) <table border="1"> <thead> <tr> <th>Probability</th> <th>Value</th> </tr> </thead> <tbody> <tr><td>0.0</td><td>0.778</td></tr> <tr><td>0.15</td><td>0.779</td></tr> <tr><td>0.25</td><td>1.010</td></tr> <tr><td>0.50</td><td>1.415</td></tr> <tr><td>0.80</td><td>1.778</td></tr> <tr><td>1.0</td><td>2.903</td></tr> </tbody> </table>	Probability	Value	0.0	0.778	0.15	0.779	0.25	1.010	0.50	1.415	0.80	1.778	1.0	2.903	None	Epistemic												
Probability	Value																													
0.0	0.778																													
0.15	0.779																													
0.25	1.010																													
0.50	1.415																													
0.80	1.778																													
1.0	2.903																													
HAVO	Ratio of horizontal anisotropy (north-south over east-west) in permeability	CDF: <table border="1"> <thead> <tr> <th>Probability</th> <th>Value</th> </tr> </thead> <tbody> <tr><td>0.0</td><td>0.05</td></tr> <tr><td>0.0042</td><td>0.2</td></tr> <tr><td>0.0168</td><td>0.4</td></tr> <tr><td>0.0379</td><td>0.6</td></tr> <tr><td>0.0674</td><td>0.8</td></tr> <tr><td>0.10</td><td>1.0</td></tr> <tr><td>0.60</td><td>5.0</td></tr> <tr><td>0.744</td><td>8.0</td></tr> <tr><td>0.856</td><td>11.0</td></tr> <tr><td>0.936</td><td>14.0</td></tr> <tr><td>0.984</td><td>17.0</td></tr> <tr><td>1.0</td><td>20.0</td></tr> </tbody> </table>	Probability	Value	0.0	0.05	0.0042	0.2	0.0168	0.4	0.0379	0.6	0.0674	0.8	0.10	1.0	0.60	5.0	0.744	8.0	0.856	11.0	0.936	14.0	0.984	17.0	1.0	20.0	None	Epistemic
Probability	Value																													
0.0	0.05																													
0.0042	0.2																													
0.0168	0.4																													
0.0379	0.6																													
0.0674	0.8																													
0.10	1.0																													
0.60	5.0																													
0.744	8.0																													
0.856	11.0																													
0.936	14.0																													
0.984	17.0																													
1.0	20.0																													
LDISP	Longitudinal dispersivity	Normal: (Log <sub>10</sub> -transformed) Mean 2.0 Standard Deviation 0.75	m	Epistemic																										

Table 6.3.10-2. Uncertain Model Inputs Used in the 3-D Saturated Zone Flow and Transport Process Model and 1-D Saturated Zone Flow and Transport Abstraction (Continued)

Input Name	Input Description	Value or Distribution	Units	Type of Uncertainty
Kd_Pu_Col	Plutonium sorption coefficient onto colloids	CDF: <u>Probability</u> <u>Value</u> 0.0                  1.e3 0.45                5.e3 0.80                1.e4 0.95                5.e4 1.0                  1.e5	mL/g	Epistemic
Kd_Am_Col	Americium sorption coefficient onto colloids	CDF: <u>Probability</u> <u>Value</u> 0.0 $1 \times 10^4$ 0.07 $5 \times 10^4$ 0.17 $1 \times 10^5$ 0.40 $5 \times 10^5$ 0.60 $1 \times 10^6$ 0.92 $5 \times 10^6$ 1.0 $1 \times 10^7$	mL/g	Epistemic
Kd_Cs_Col	Cesium sorption coefficient onto colloids	CDF: <u>Probability</u> <u>Value</u> 0.0                  5.e1 0.05                1.e2 0.40                5.e2 0.70                1.e3 1.0                  5.e3	mL/g	Epistemic
Kd_Sn_Col	Tin sorption coefficient onto colloids	Log-Uniform: Minimum 1.e5 Maximum 1.e6	mL/g	Epistemic
Conc_Col*	Groundwater concentration of colloids	CDF: (Log <sub>10</sub> -transformed) <u>Probability</u> <u>Value</u> 0.0                  -9.0 0.50                -7.0 0.75                -6.0 0.90                -5.0 0.98                -4.3 1.0                  -3.6	g/mL	Epistemic
FPLANW	Northwestern boundary of alluvial uncertainty zone	Uniform: Minimum          0.0 Maximum          1.0	None	Epistemic
NVF26	Effective porosity in shallow alluvium	Truncated Normal: Mean                0.18 Standard Deviation 0.051 Minimum            0.00 Maximum            0.30	None	Epistemic
NVF11	Effective porosity in undifferentiated valley fill	Truncated Normal: Mean                0.18 Standard Deviation 0.051 Minimum            0.00 Maximum            0.30	None	Epistemic

Table 6.3.10-2. Uncertain Model Inputs Used in the 3-D Saturated Zone Flow and Transport Process Model and 1-D Saturated Zone Flow and Transport Abstraction (Continued)

Input Name	Input Description	Value or Distribution	Units	Type of Uncertainty
FPVO	Fracture porosity in volcanic units	CDF: (Log <sub>10</sub> -transformed) Probability      Value 0.0                -5.0 0.05              -4.0 0.50              -3.0 0.80              -2.0 1.0                -1.0	None	Epistemic
DCVO	Effective diffusion coefficient in volcanic units	CDF: (Log <sub>10</sub> -transformed) Probability      Value 0.0                -11.3 0.08              -10.7 0.50              -10.3 0.83              -9.9 1.0                -9.3	m <sup>2</sup> /s	Epistemic
GWSPD	Groundwater specific discharge multiplier	CDF: (Log <sub>10</sub> -transformed) Probability      Value 0.0                -0.951 0.05              -0.506 0.10              -0.394 0.25              -0.208 0.5                0.000 0.75              0.208 0.90              0.394 0.95              0.506 1.0                0.951	None	Epistemic
Alluvium_Density	Bulk density of alluvium	Normal: Mean              1,910 Standard Deviation      78	kg/m <sup>3</sup>	Epistemic
SRC1X SRC1Y SRC2X SRC2Y SRC3X SRC3Y SRC4X SRC4Y	Source regions beneath the repository	Uniform: Minimum              0.0 Maximum              1.0	None	Epistemic and Aleatory

Sources: Modified from Saturated Zone Flow and Transport Model Abstraction (SNL 2008 [DIRS 183750], Tables 6-7[a] and 6-8). The following updated or new parameters are from Table 6-7[a]: GWSPD, FISVO, FPLANW, Kd\_Pu\_Col, Kd\_Cs\_Col, Kd\_Sn\_Col, Kd\_Sn\_Vo, Kd\_Sn\_Al, Kd\_Se\_Vo, Kd\_Sn\_Al, and Correlation matrix for Kd sampling in the SZ. Parameters NVF26 and NVF11 are new names for Parameters NVF19 and NVF7 in Table 6-8. Only the names are changed. The rest of the parameters are from Table 6-8.

NOTES: Only those parameters in the source that are uncertain were included in this table; Log<sub>10</sub>-transformed values are given in Log<sub>10</sub>. They are transformed to actual values when used.

\* Please refer Saturated Zone Flow and Transport Model Abstraction (SNL 2008 [DIRS 183750], Section 6.5.3[b]) for a discussion on the distribution of parameter Conc\_Col.

Table 6.3.10-3. Constant TSPA Parameters for Saturated Zone Flow One-Dimensional Transport Model

Parameter Name	Input Description	Input Value	Units
Coating Porosity	Porosity of the fracture coating	0.01	None
Coating Thickness	Fracture coating thickness	0.00001	m
Flow_Rate_fact_Vclim_CS1	SZ_1D, Discharge flowrate multiplier for climate state 1 (present day)	1	None
Flow_Rate_fact_Vclim_CS2	SZ_1D, Discharge flowrate multiplier for climate state 2 (monsoonal)	1.9	None
Flow_Rate_fact_Vclim_CS3	SZ_1D, Discharge flowrate multiplier for climate state 3 (glacial)	3.9	None
Pipe_Length_Pipe_a	Pipe length for pipe segment a	5,000	m
Volcanic_Fracture_Perimeter	Volcanic fracture perimeter for the determination of fracture surface area	2	m
Alluvium_Porosity	Effective porosity of the alluvium	0.30	None
Volcanic_Matrix_Porosity	Porosity of the volcanic matrix	0.22	None
Volcanic_Density	Bulk density of the volcanic matrix material	1,880	kg/m <sup>3</sup>
Fracture_Porosity	Average fracture porosity of the volcanic units	0.001	None

Source: DTN: SN0702PASZFTMA.002 R1 [DIRS 183471].

Table 6.3.10-4. Flow Path Lengths of Pipe Segments

Horizontal Anisotropy	Minimum and Maximum Flow Path Lengths of Pipe Segments (km)							
	Source Region 1		Source Region 2		Source Region 3		Source Region 4	
	5 - 13 km	13 - 18 km	5 - 13 km	13 - 18 km	5 - 13 km	13 - 18 km	5 - 13 km	13 - 18 km
0.05	15.9 - 16.4	7.7 - 8.2	15.2 - 15.5	7.7 - 8.0	13.6 - 14.4	6.9 - 7.7	14.1 - 15.0	6.7 - 7.6
1.00	11.3 - 12.3	6.7 - 7.7	10.3 - 11.0	7.2 - 7.9	7.7 - 8.6	6.5 - 7.4	7.3 - 8.3	6.8 - 7.8
5.00	11.3 - 12.3	6.7 - 7.7	10.0 - 10.6	7.3 - 7.9	7.7 - 8.6	6.5 - 7.4	7.3 - 8.3	6.8 - 7.8
20.00	11.3 - 12.3	6.7 - 7.7	10.0 - 10.7	7.2 - 7.9	7.7 - 8.6	6.5 - 7.4	7.3 - 8.3	6.8 - 7.8

Source: DTN: SN0702PASZFTMA.002 R1 [DIRS 183471]. (Located in file DTN\_TDIP\_SZFT-2.doc).

Table 6.3.10-5. Average Specific Discharge in Flow Path Segments

Horizontal Anisotropy	Average Specific Discharge (m/yr)		
	0 - 5 km	5 - 13 km	13 - 18 km
0.05	0.354	0.408	2.56
1.00	0.459	0.486	0.769
5.00	0.409	0.544	5.98
20.00	0.555	0.500	5.93

Source: DTN: SN0702PASZFTMA.002 [DIRS 183471].  
(Located in file DTN\_TDIP\_SZFT-2.doc).

Table 6.3.10-6. Summary of Alpha Concentration Results in Amargosa Valley Groundwater

<b>Input</b>	<b>Expected Value (mean) pCi/L</b>	<b>Upper (95%) Limit pCi/L</b>
Gross Alpha Concentration	0.50	0.71
Combined Concentration of 226Ra and 228Ra	0.50	0.71

Source: DTN: SN0702PASZFTMA.002 R1 [DIRS 183471]. (Located in file DTN\_TDIP\_SZFT-2.doc).

Table 6.3.10-7. Alternative Conceptual Models Considered for Saturated Zone Flow and Radionuclide Transport

<b>Alternative Conceptual Model</b>	<b>Key Assumptions</b>	<b>Screening Assessment and Basis</b>
Minimal Matrix Diffusion	Diffusion of radionuclides into the pore space of the rock matrix in the fractured volcanic units is extremely limited due to highly channelized groundwater flow, fracture coatings, or other factors.	This ACM is implicitly included in the 3-D SZ Flow and Transport Abstraction and in the 1-D SZ Flow and Transport Abstraction through the range of uncertainty in key input parameters. The uncertain input parameters influencing matrix diffusion include DCVO, FISVO, and FPVO (Table 6.3.10-2).
Horizontal Anisotropy in Permeability	Alternative interpretations of pump test results in the fractured volcanic units indicate preferential permeability along structural features oriented in the NNE-SSW direction or in the WNW-ESE direction.	This ACM is implicitly included in the 3-D SZ Flow and Transport Model Abstraction and in the 1-D SZ Flow and Transport Abstraction through the range of uncertainty in an input parameter. The uncertain input parameter influencing horizontal anisotropy in permeability in the volcanic units near Yucca Mountain is the ratio of N-S to E-W permeability (HAVO; Table 6.3.10-2). This continuously distributed parameter varies from less than one to greater than one, with most of the realizations greater than one.

Source: *Saturated Zone Flow and Transport Model Abstraction* (SNL 2008 [DIRS 183750], Section 6.4).

NOTES: 1-D = one-dimensional; DCVO = effective diffusion coefficient in volcanic units; FISVO = flowing interval spacing in volcanic units; FPVC = flowing interval porosity; HAVO = ratio of horizontal anisotropy (north-south over east-west) in permeability.

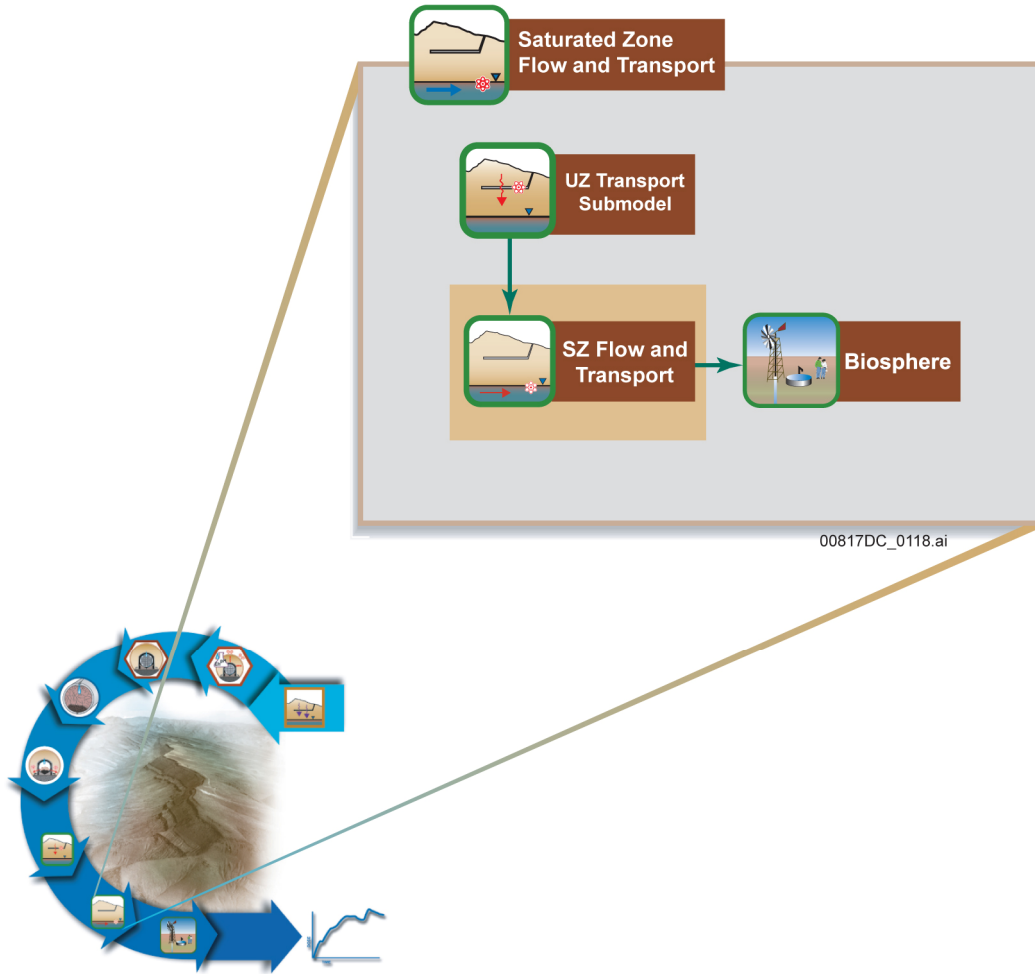


Figure 6.3.10-1. Information Flow Diagram for Saturated Zone Flow and Transport

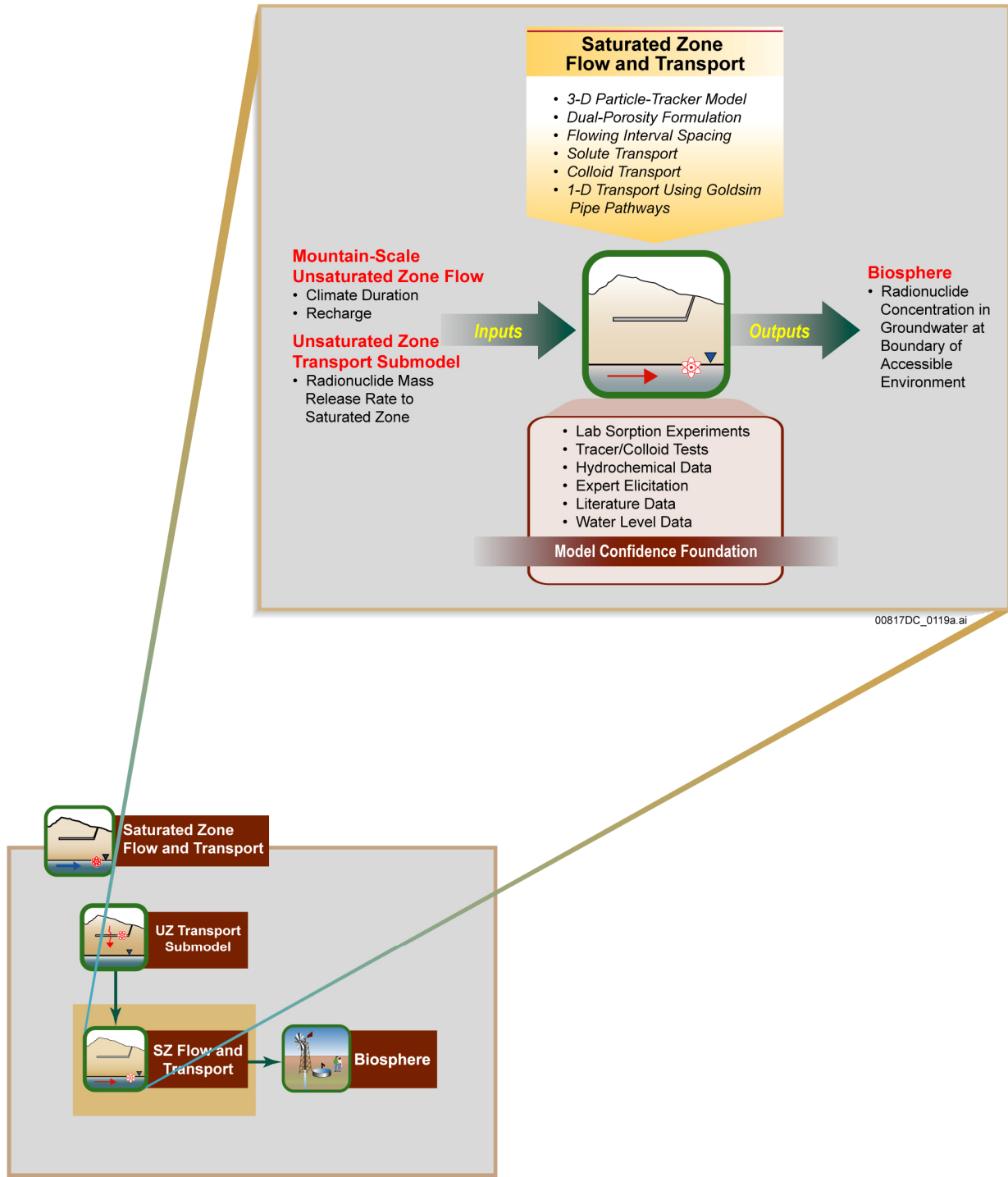


Figure 6.3.10-2. Inputs, Outputs, and Basis for Model Confidence for the Saturated Zone Flow and Transport Model Component

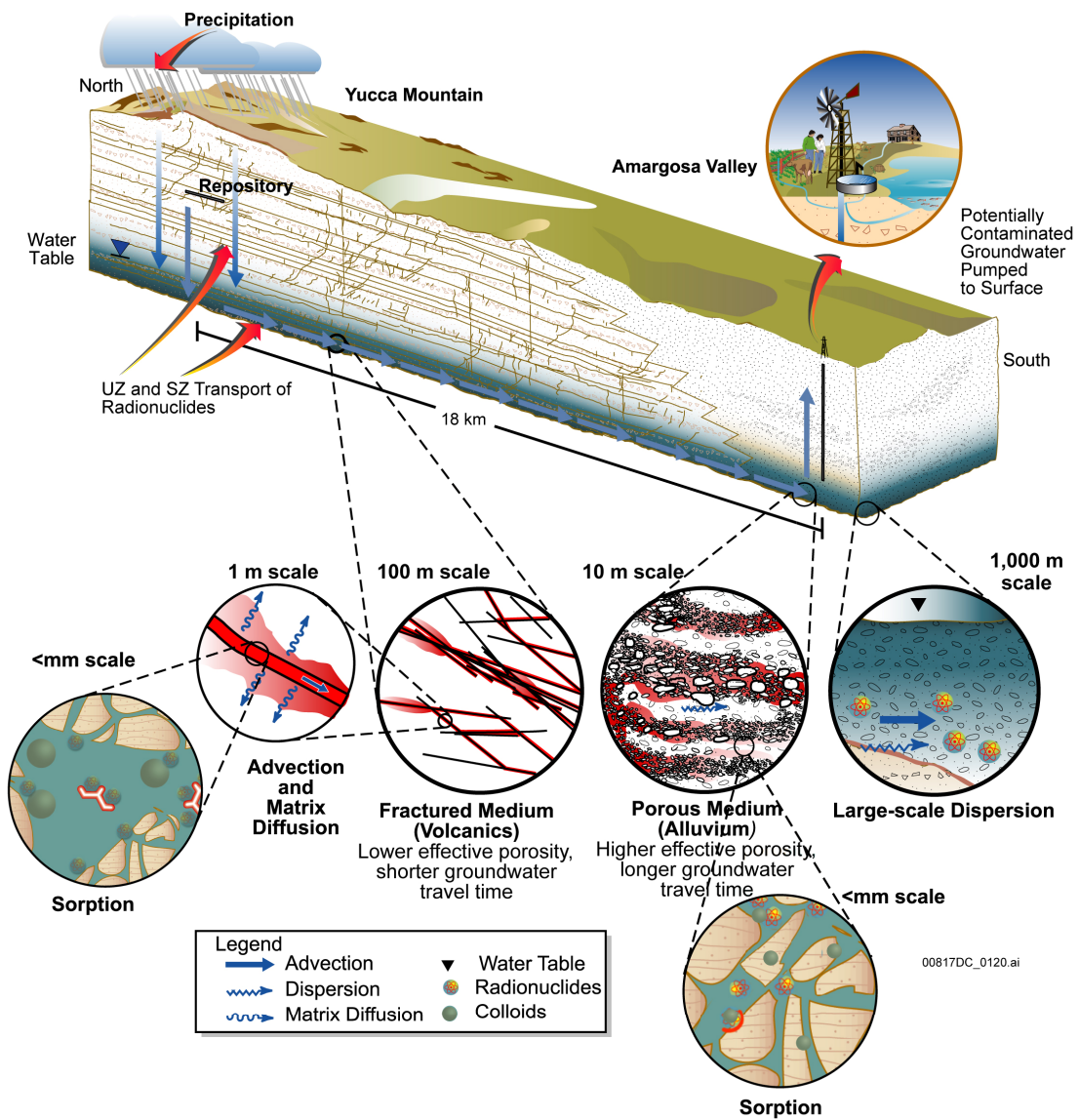
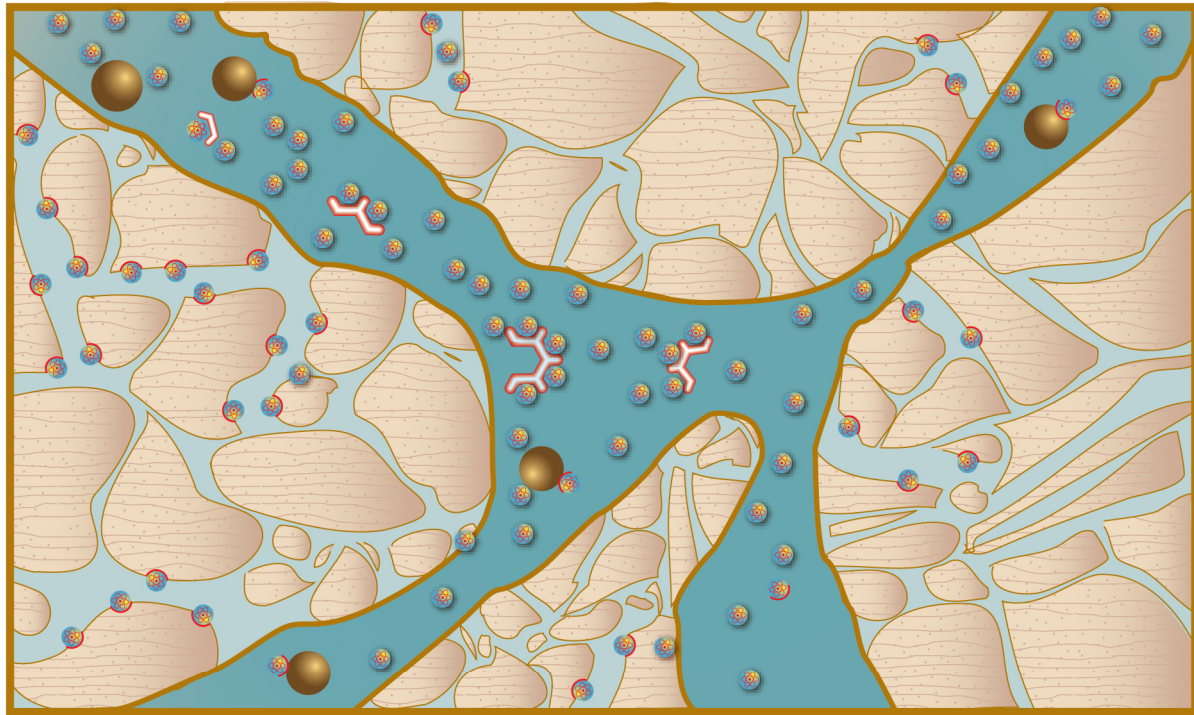


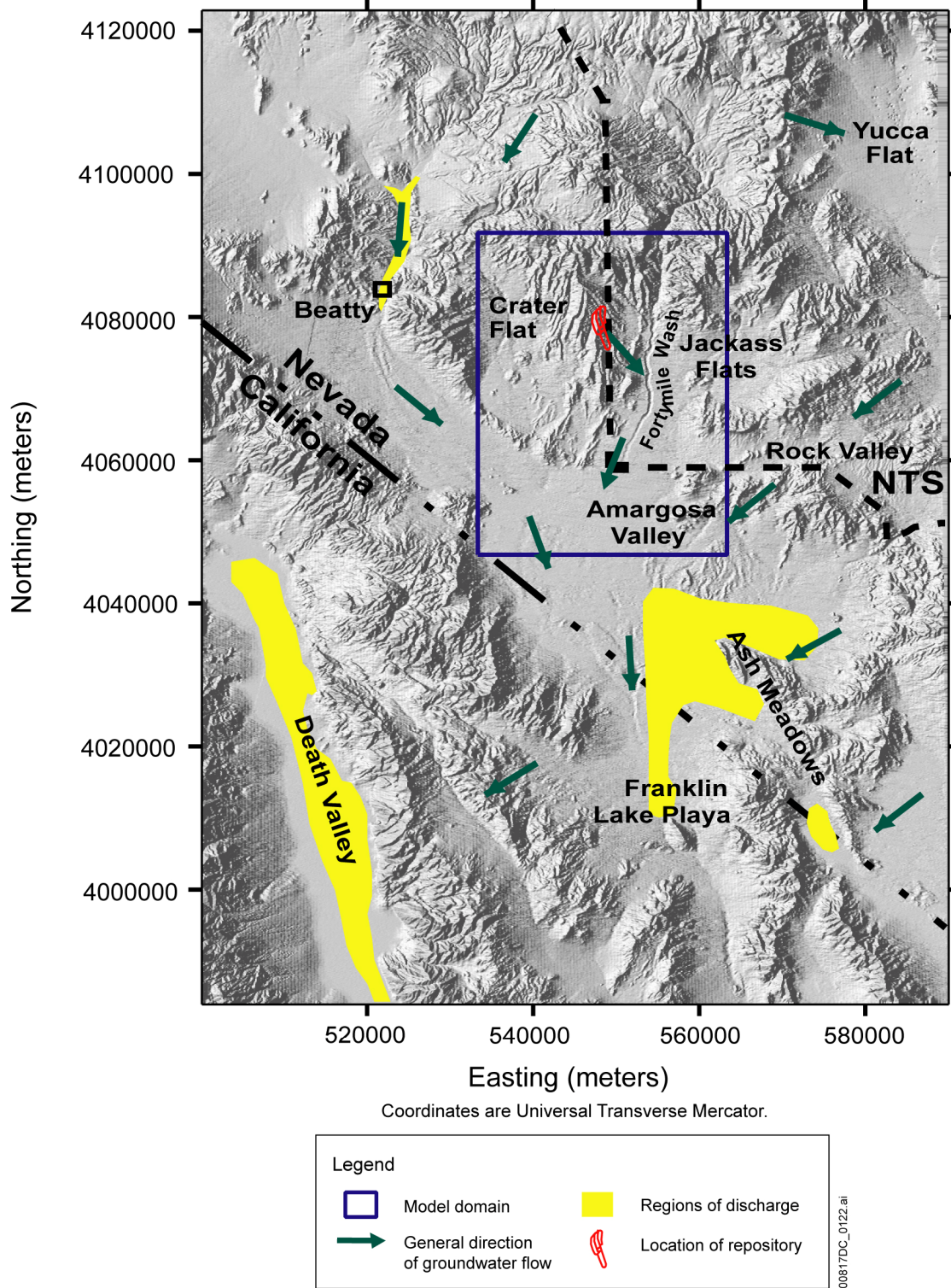
Figure 6.3.10-3. Conceptualization of Features and Processes Important to Saturated Zone Transport



00817DC\_0121.ai

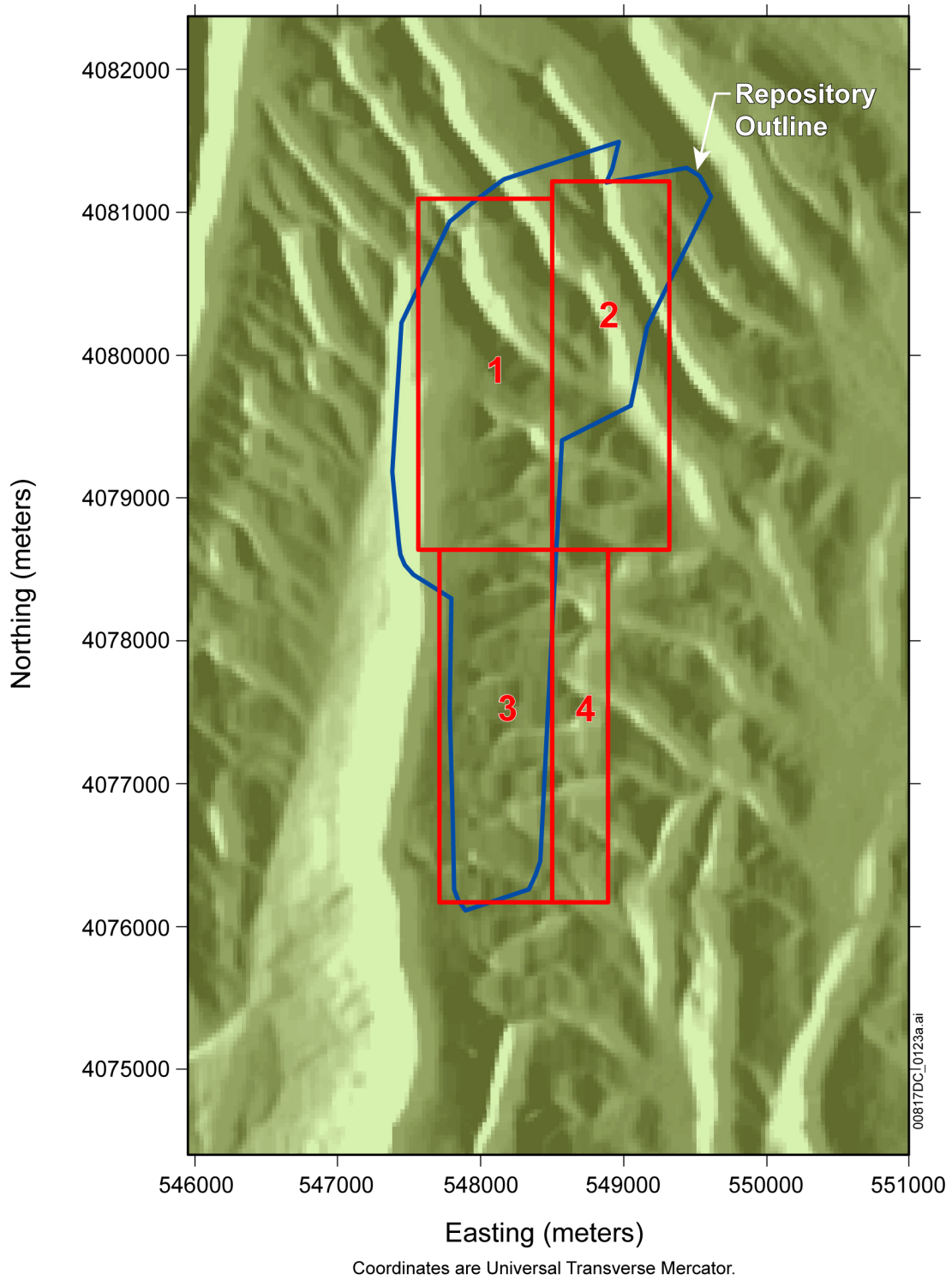
- |  |  |   |
|--|--|---|
|  Fracture |  Radionuclide   |  Reversible Sorption Colloid (shown without radionuclide attached)             |
|  Matrix |  Sorbed Radionuclide  |  Irreversible Sorption Colloid (shown with radionuclide permanently attached) |
|  |  Reversible Sorption Colloid (shown with radionuclide temporarily attached) |   |

Figure 6.3.10-4. Illustration of Colloid-Facilitated Transport Processes



Source: Compiled from BSC 2004 [DIRS 169734], Figures 8-2, 8-5, and 8-6.

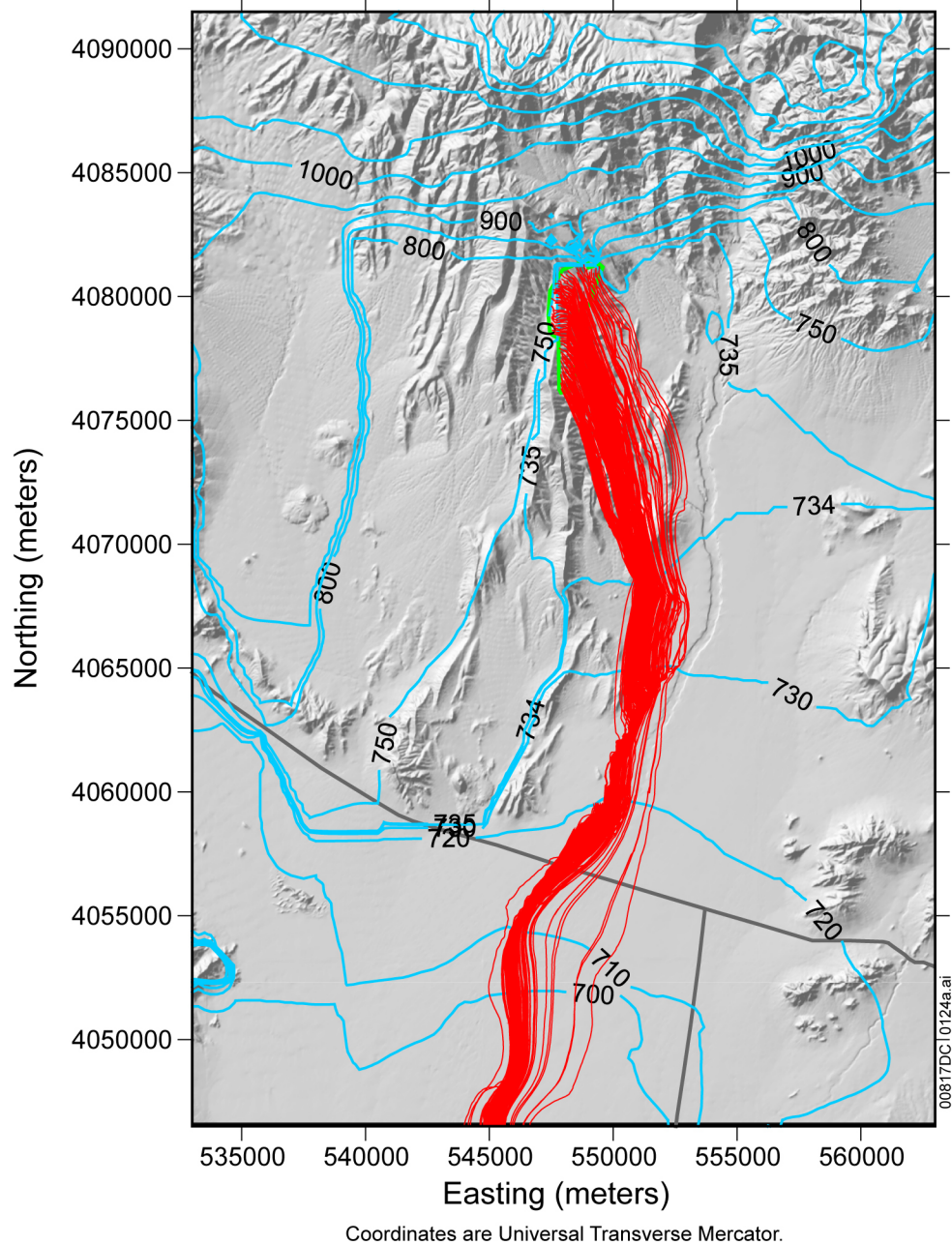
Figure 6.3.10-5. Regional Map of the Saturated Zone Flow System Showing Direction of Flow and Outline of the 3-D Saturated Zone Site-Scale Flow Model Domain



Source: Modified from SNL 2008 [DIRS 183750], Figure 6-27.

NOTE: The solid blue line shows repository outline and the solid red lines show the four source regions.

Figure 6.3.10-6. Source Regions for Radionuclide Release in the Saturated Zone Flow and Transport Abstraction Model

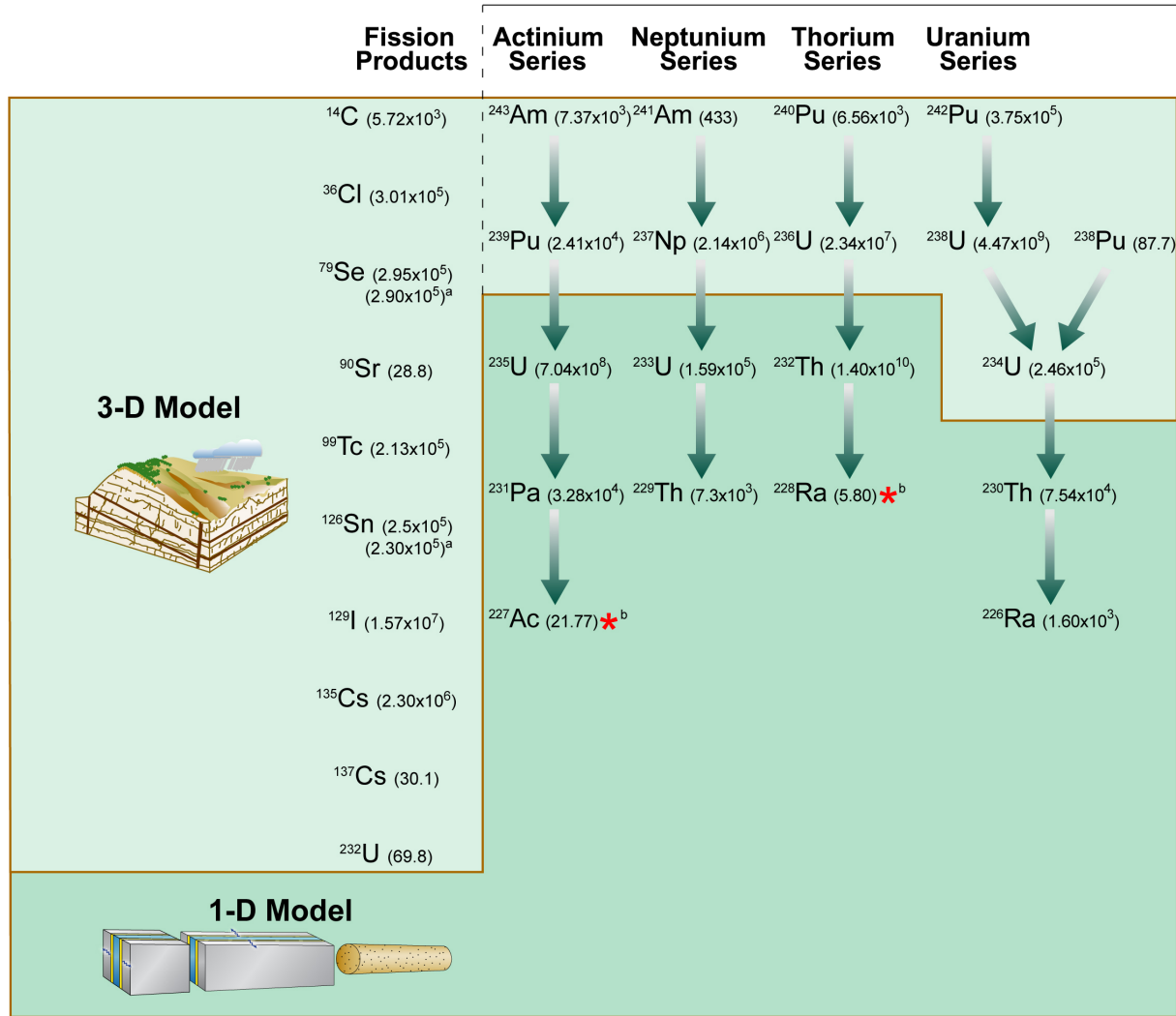


Source: Modified from SNL 2007 [DIRS 177391], Figure 6-43.

NOTE: Blue lines refer to simulated head contours at the water table in meters; red lines refer to simulated particle paths; direction of flow is from the repository to the accessible environment (bottom of figure).

Figure 6.3.10-7. Map of the 3-D Saturated Zone Model Domain Showing Simulated Particle Paths

### Actinide Decay Chains



00817DC\_0125d.ai

\* Mass of RN calculated by assuming secular equilibrium with parent RN  
 (2.3x10<sup>6</sup>) Half-life of RN indicated in parentheses (years)

Sources: DTNs: SN0702PASZFTMA.002\_R1 [DIRS 183471]; MO0702PASTREAM.001\_R0 [DIRS 179925].

NOTE: (a) Half-life values used in the 1-D Transport Model and (b) Half-life values used in secular equilibrium calculations.

Figure 6.3.10-8. Radionuclide Decay Chains Considered in Saturated Zone Transport Calculations

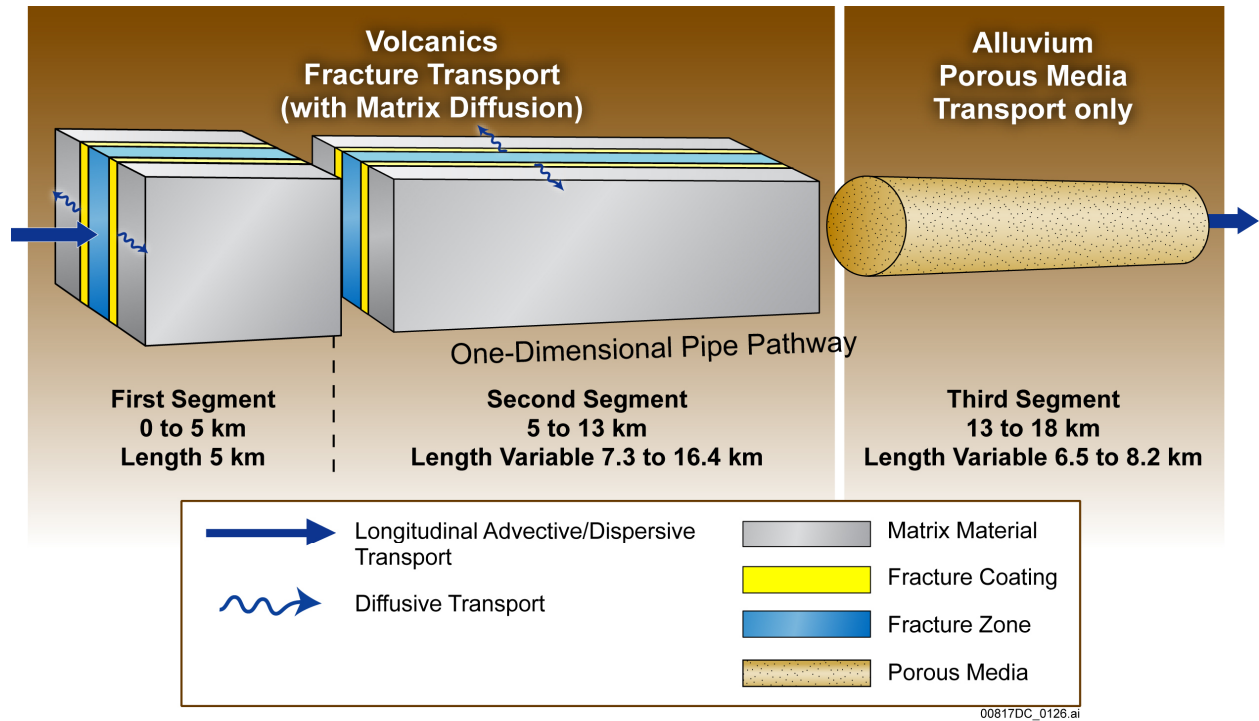
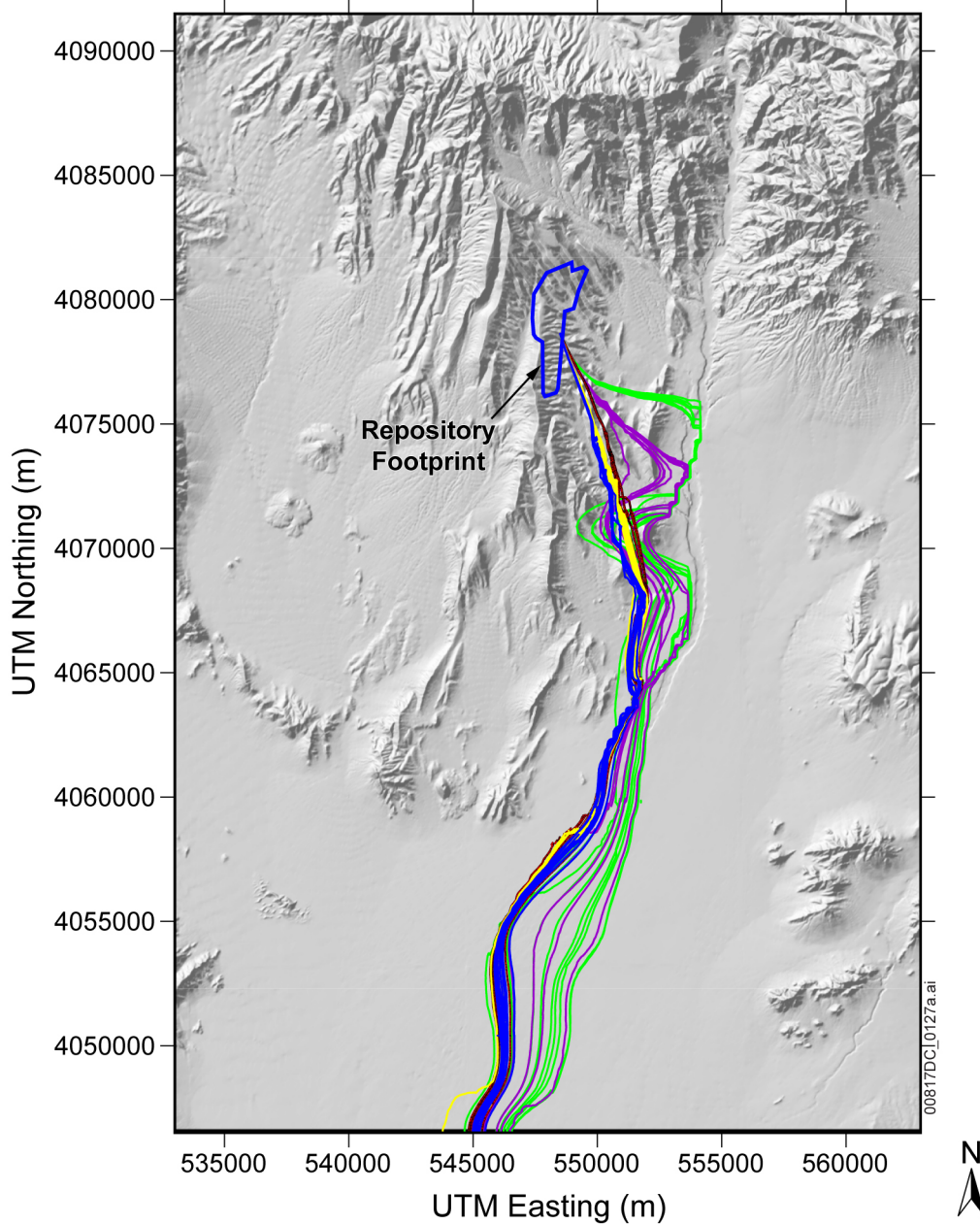


Figure 6.3.10-9. Conceptualization of the 1-D Saturated Zone Flow and Transport Abstraction



Source: Modified from SNL 2008 [DIRS 183750], Figure 6-1 [a].

NOTE: Green, purple, blue, yellow, and red lines show simulated particle paths for particles released from Source Region 1 for horizontal anisotropy values of 0.05, 0.20, 1.0, 5.0, and 20.0, respectively.

Figure 6.3.10-10. Simulated Particle Paths for Different Values of Horizontal Anisotropy in Permeability

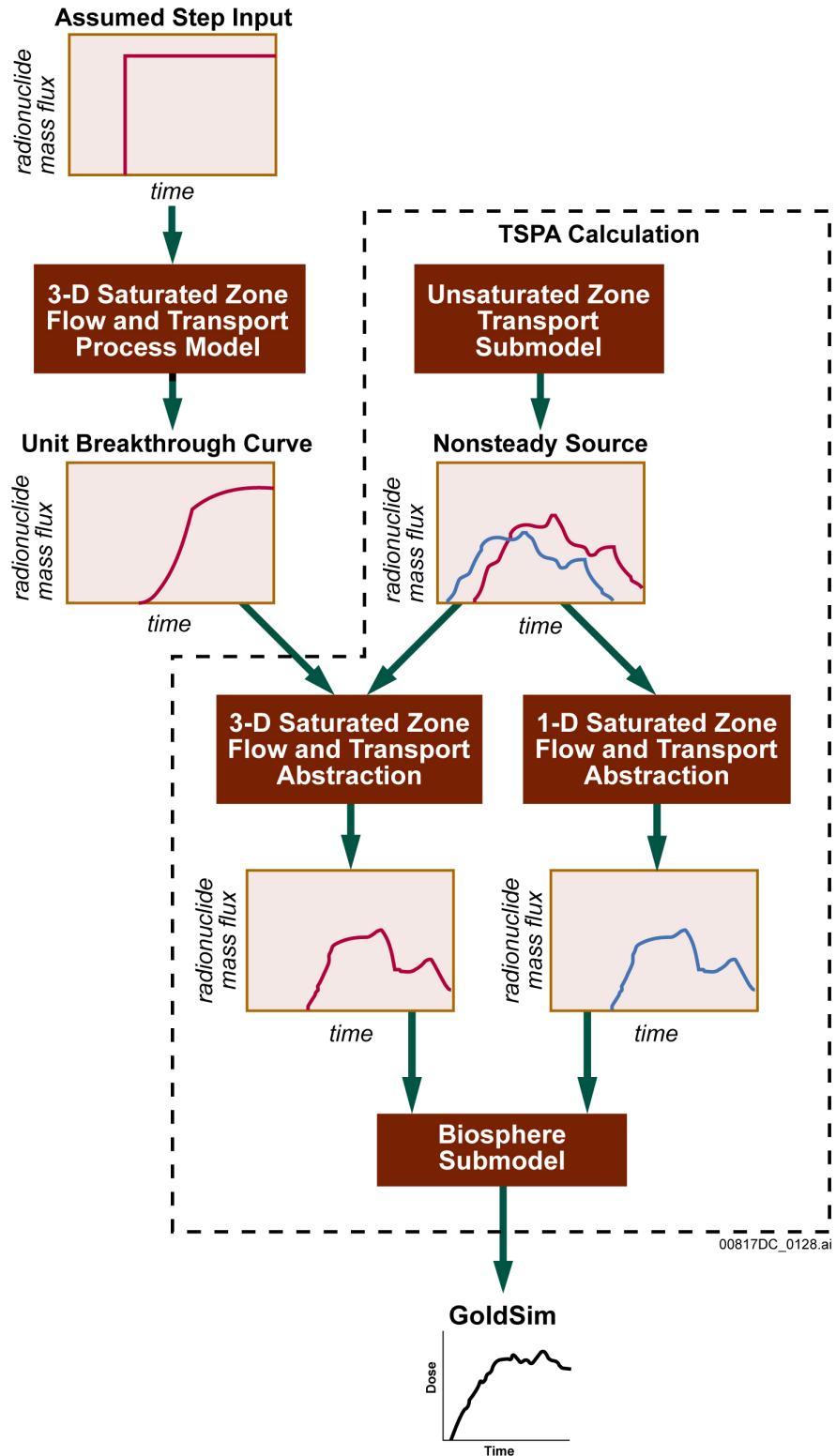


Figure 6.3.10-11. Flowchart of the Implementation of the Saturated Zone Flow and Transport Submodel in the TSPA-LA Model

INTENTIONALLY LEFT BLANK

### 6.3.11 Biosphere

The Biosphere Model Component of the TSPA-LA Model estimates the annual radiation dose to the RMEI that is expected to result if radionuclides are released to the accessible environment from the repository after closure. For the set of scenario classes considered in the TSPA-LA Model, there are two possible radionuclide release pathways from the repository to the accessible environment: one through groundwater and one through the atmosphere with volcanic ejections (tephra). These two radionuclide release pathways result in the two exposure scenarios developed in the biosphere. To eliminate possible confusion with the TSPA scenario classes, these two exposure scenarios, which are developed in the biosphere documents, are called the exposure cases in this TSPA-LA document. The groundwater exposure case applies to those TSPA-LA Model modeling cases that consider the groundwater transport of radionuclides from the repository at Yucca Mountain to the accessible environment. These modeling cases are included in the Nominal Scenario Class, the Early Failure Scenario Class, the Seismic Scenario Class, the Igneous Intrusion Modeling Case of the Igneous Scenario Class, and the Human Intrusion Scenario. The volcanic ash exposure case applies to the Volcanic Eruption Modeling Case of the Igneous Scenario Class, which considers a volcanic release of radionuclides from the repository at Yucca Mountain.

The Biosphere Process Model documented in *Biosphere Model Report* (SNL 2007 [DIRS 177399]) is implemented external to the TSPA-LA Model and is used to develop the capabilities for calculating annual radiation dose to the RMEI using the TSPA-LA Model. The analyses and abstractions of the two exposure cases in the Biosphere Process Model and reported in *Biosphere Model Report* (SNL 2007 [DIRS 177399]) resulted in the following two data sets giving biosphere dose conversion factors (BDCFs) for the groundwater and volcanic exposure cases as inputs to the TSPA-LA Model:

- Groundwater Biosphere Dose Conversion Factors (DTN: MO0702PAGBDCFS.001\_R0 [DIRS 179327])
- Volcanic Biosphere Dose Conversion Factors (DTN: MO0702PAVBPDF.000\_R0 [DIRS 179330]).

An additional set of data was provided in *Inhalation Dose Factors* DTN: MO0702PAINHALA.001\_R0 [DIRS 179329] to estimate the inhalation dose to the RMEI accrued during a tephra deposition.

These BDCFs are used in the Biosphere Model Component of the TSPA-LA Model to calculate the annual dose to the RMEI, which is required to assess compliance with the postclosure individual protection standard in 10 CFR 63.311 [DIRS 178394] and 10 CFR 63.321 for the individual protection standard for human intrusion [DIRS 178394]. In addition to the BDCFs, the data used in TSPA to demonstrate compliance with the groundwater protection standards in 10 CFR 63.331 [DIRS 180319] are titled *Groundwater Protection Standards Conversion Factors* (DTN: MO0702PAGWPROS.001\_R0 [DIRS 179328]) and are included in two calculations: the estimation of annual dose (whole body and individual organs) from beta and photon emitting radionuclides from consuming two liters of well water daily, and the contribution to the gross

alpha activity concentration in groundwater, as defined in 10 CFR 63.331 ([DIRS 180319], Table 1) from radionuclides released from the repository.

Figure 6.3.11-1 uses the example of the groundwater exposure case to show the relationships between the Biosphere Model Component, the SZ Flow and Transport Model Component, and the calculation of annual dose for evaluation of compliance with the individual protection standard and with the groundwater protection standards. Figure 6.3.11-2 summarizes the TSPA-LA Biosphere Model Component, its inputs and outputs, and the technical basis for confidence in the Biosphere Model Component. The inputs for the Biosphere Model Component from the first two and last DTN cited above (the two BDCF sets for the groundwater and volcanic cases and the groundwater protection standards data set) are used in TSPA-LA GoldSim. The other DTN (inhalation dose factors for the period during the volcanic eruption) is used outside the TSPA-LA Model and this use is documented in Section 6.5.2.4.

### 6.3.11.1 Conceptual Models

The two exposure cases considered in the TSPA-LA Model are illustrated on Figures 6.3.11-3 and 6.3.11-4. For the groundwater exposure case, radionuclides enter the biosphere from one or more wells that extract contaminated groundwater from an aquifer. Human exposure arises from using the contaminated water for domestic and agricultural purposes. Groundwater BDCFs apply to all modeling cases except the Volcanic Eruption Modeling Case of the Igneous Scenario Class. In the volcanic ash exposure case, human exposure arises from contaminated tephra deposited on surface soil and the subsequent radionuclide transport from surface soil to other environmental media (e.g., air and plants). Volcanic ash BDCFs apply only to the Volcanic Eruption Modeling Case of the Igneous Scenario Class.

The radionuclides of interest for the Biosphere Process Model, also referred to as the primary radionuclides as tracked in the TSPA-LA Model, depend on the exposure case and are developed in *Radionuclide Screening* (SNL 2007 [DIRS 177424]) and defined in DTN: MO0701RLTSCRNA.000\_R0 [DIRS 179334]. The treatment of radionuclide transport in the Biosphere Process Model is the same for most radionuclides in both exposure cases. However, two radionuclides,  $^{14}\text{C}$  and  $^{222}\text{Rn}$  (a short-lived decay product of  $^{226}\text{Ra}$ ), are modeled differently because of the large amount of stable carbon ( $^{12}\text{C}$ ) in the environment and the gaseous release from soils of  $^{222}\text{Rn}$  and  $^{14}\text{CO}_2$ .

To facilitate modeling for dose calculations, the reference biosphere is developed in the *Biosphere Model Report* (SNL 2007 [DIRS 177399], Section 6.1.1). The reference biosphere has to represent the environment inhabited by the RMEI along with associated human exposure pathways and parameters (10 CFR 63.102(i) [DIRS 180319]). Required characteristics of the reference biosphere are the following:

- Features, events, and processes that describe the reference biosphere must be consistent with present knowledge of the conditions in the region surrounding the Yucca Mountain site (10 CFR 63.305(a) [DIRS 180319]).
- DOE should not project changes in society, the biosphere (other than climate), human biology, or increases or decreases of human knowledge or technology. In all analyses

done to demonstrate compliance with this part, DOE must assume that all of those factors remain constant as they are at the time of submission of the license application (10 CFR 63.305(b) [DIRS 180319]).

- DOE must vary factors related to the geology, hydrology, and climate based upon cautious but reasonable assumptions consistent with present knowledge of factors that could affect the Yucca Mountain Repository system during the period of geologic stability (10 CFR 63.302 [DIRS 178394]) and consistent with the requirements for performance assessments specified in 10 CFR 63.342 [DIRS 178394] (10 CFR 63.305(c), [DIRS 178394]).
- Biosphere pathways must be consistent with arid or semi-arid conditions (10 CFR 63.305(d) [DIRS 180319]).

The RMEI is a hypothetical person who meets the following criteria (10 CFR 63.312 [DIRS 180319]):

- a. Lives in the accessible environment above the highest concentration of radionuclides in the plume of contamination.
- b. Has a diet and living style representative of the people who now reside in the Town of the Amargosa Valley, Nevada, based on surveys that determine current diets and living styles, and for whom the mean values of these factors are used in the assessments conducted for the Individual Protection Standard in 10 CFR 63.311 [DIRS 178394] and the Individual Protection Standard for Human Intrusion in 10 CFR 63.321 [DIRS 178394].
- c. Uses well water with average concentrations of radionuclides based on annual water demand of 3,000 acre-feet.
- d. Drinks two liters of water per day from wells drilled into the groundwater from a point above the highest concentration of radionuclides in the plume of contamination.
- e. Is an adult with metabolic and physiological considerations consistent with present knowledge of adults.

To meet the requirement in 10 CFR 63.312(b) [DIRS 180319], the dietary and living style characteristics of the RMEI were determined based on surveys of people living in the Amargosa Valley, combined with the 2000 census data (Bureau of the Census 2002 [DIRS 159728]) as well as regional and national information on behavioral patterns and food intake (USDA 2000 [DIRS 154158], EPA 1997 [DIRS 116135], and ICRP 1994 [DIRS 153705]). Characteristics of the RMEI were developed, using these data, in a separate analysis (BSC 2005 [DIRS 172827]).

**Groundwater Exposure Case**—In the groundwater exposure case, radionuclides are introduced into the biosphere with groundwater pumped from wells for agricultural and domestic purposes. Once in the biosphere, the radionuclides migrate through various environmental components. During this migration, some of the radionuclides give rise to a dose to the RMEI through one of

three exposure pathways: inhalation, ingestion, or external exposure. Each of the exposure pathways is modeled using the diet, living style, and other characteristics of the RMEI. The biosphere model for the groundwater exposure case considered five environmental components (or submodels): soil, air, plant, animal, and fish. The radionuclides in each of these components can result in exposure to the RMEI. Figure 6.3.11-5 illustrates the relationships among the biosphere submodels indicating the migration of radionuclides in the biosphere between the various biosphere submodels starting with the introduction of contaminated groundwater into the biosphere and resulting in a dose to the RMEI. On Figure 6.3.11-5, arrows point in the direction of radionuclide transfer between biosphere components in the Biosphere Process Model. For example, groundwater is used for human drinking water (to ingestion submodel), animal drinking water (to animal submodel), irrigation water (to soil and plant uptake submodels), fish pond water (to fish submodel), and evaporative cooler water (to air submodel).

The submodels described above are the same for all primary radionuclides with the sole exception of  $^{14}\text{C}$ . Special submodels are used to calculate  $^{14}\text{C}$  concentrations in the surface soil, air, crops, and animal products because the transfer mechanisms for this radionuclide are different from the others in the model by virtue of the presence of the stable carbon ( $^{12}\text{C}$ ) in the biosphere. The transfer of  $^{14}\text{C}$  between submodels follows that for other radionuclides as shown on Figure 6.3.11-5.

The following environmental transport processes are explicitly included in the Biosphere Process Model (SNL 2007 [DIRS 177399], Section 6.3.1.3)

- Radionuclide accumulation in surface soil layers as a result of continuous long-term cultivation using contaminated water
- Resuspension of contaminated soil
- Radionuclide deposition on crop surfaces by dry processes (resuspension of contaminated soil and subsequent adhesion of soil particles onto vegetation surfaces)
- Radionuclide deposition on crop surfaces by interception of contaminated irrigation water
- Removal of surface contamination by weathering processes
- Translocation and retention of contaminants from the deposition site to the edible tissues of vegetation
- Radionuclide uptake from soil by plants through the roots
- Release of radionuclides in gaseous phases,  $^{222}\text{Rn}$  and  $^{14}\text{CO}_2$ , from the soil into the air with subsequent inhalation
- Photosynthesis by crops of  $^{14}\text{CO}_2$  from the atmosphere

- Radionuclide intake by animals through consumption of contaminated feed, water, and soil, followed by transfer to animal products
- Radionuclide transfer from water to air through use of evaporative coolers
- Radionuclide transfer from water to fish.

Exposure to radionuclides in the environment arises when the RMEI's diet and living style give rise to intake of, and external exposure to, radionuclides in environmental media. The Biosphere Process Model then calculates the annual dose from ingestion, inhalation, and external exposure pathways resulting from those intakes and exposures. Table 6.3.11-1 provides a summary of human-exposure pathways for the groundwater exposure case considered in the Biosphere Process Model, including the contributing submodels of the environmental media and the examples of typical activities that may potentially lead to radiation exposure (SNL 2007 [DIRS 177399], Section 6.3.1.1).

The TSPA-LA only considers the release and transport of the primary radionuclides. To avoid underestimating annual dose to the RMEI, the Biosphere Process Model accounts for the decay products of the primary radionuclides after they are introduced into the biosphere. The short-lived decay products with half-lives of less than 180 days are considered to be in secular equilibrium with the parent radionuclide, and their radiation dose contributions are included in the BDCF for the primary radionuclide or a long-lived decay product of the primary radionuclide (SNL 2007 [DIRS 177399] Sections 6.3.1.4 and 6.3.5). The Biosphere Process Model also accounts for the build-up of the primary radionuclides in soil as well as the decay and ingrowth of long-lived decay products in the soil as a result of long-term irrigation (from 25 years up to one thousand years) (SNL 2007 [DIRS 177399] Sections 6.4.1.1 and 6.4.1.2). In this case, the BDCF contributions of the long-lived decay products created in the soil are added to that of the parent primary radionuclides (SNL 2007 [DIRS 177399], Section 6.4.1.2 and Table 6.4-3). The output of the Biosphere Process Model for the groundwater exposure case is the *Groundwater Biosphere Dose Conversion Factors* (DTN: MO0702PAGBDCFS.001\_R0 [DIRS 179327]). This DTN provides the groundwater case BDCFs for all primary radionuclides and the following combination of radionuclides where the effects of longer term decay products are included with the BDCF of the initial primary radionuclide ( $^{226}\text{Ra}$  and  $^{210}\text{Pb}$ ;  $^{232}\text{Th}$ ,  $^{228}\text{Ra}$ , and  $^{228}\text{Th}$ ; and  $^{232}\text{U}$  and  $^{228}\text{Th}$ ). This summation approach allows a realistic assessment of dose to be made if TSPA does not directly consider (i.e., track) all radionuclides.

To support climate change modeling for the TSPA-LA Model, BDCFs for the groundwater exposure case were initially developed for the three climate states (SNL 2007 [DIRS 177399], Sections 6.1.1.2 and 6.11.1.2.2) but were further analyzed for consistency with the regulatory requirements. Future climate forecasts (BSC 2004 [DIRS 170002], Section 6.1) indicate that the climate at Yucca Mountain is reasonably expected to evolve to the cooler, wetter conditions of a glacial transition climate within the first 10,000 years after disposal. Monsoon and glacial-transition (intermediate) climate states are predicted to last until 38,000 years A.P. (after present) (Sharpe 2003 [DIRS 161591], p. 57). Over the period of geologic stability, it is expected that there will be more than one climate cycle. 10 CFR 63.305(c) [DIRS 178394] requires that the DOE vary factors related to climate based on cautious, but reasonable assumptions. At the same time, changes in society, the biosphere (other than climate), human

biology, or increases or decreases of human knowledge or technology should not be projected (10 CFR 63.305(b) [DIRS 180319]). The climate change in the Biosphere Process Model was thus evaluated and addressed from the perspective of natural processes and from the perspective of the factors that are related to human activity.

In the Biosphere Process Model (SNL 2007 [DIRS 177399], Section 6.11.1.2), the effect of climate change on the BDCFs for the groundwater exposure scenario was evaluated from the perspective of the factors that are related to the human society, which 10 CFR 63.305(b) [DIRS 180319] directs DOE not to vary in its performance assessments, and those factors that are independent of human activities, which 10 CFR 63.305(c) [DIRS 178394] directs DOE to vary over the period of geologic stability. The climate-related factors that have the largest effect on the BDCFs depend on human activities and the BDCFs are relatively insensitive to the effects of climate changes in the other factors. Furthermore, the BDCFs for the future climate, which is predicted to be cooler and wetter than the present-day climate, are lower than the corresponding present-day climate BDCFs and would result in lower doses to the RMEI. Therefore, using the present-day climate BDCFs represents a conservative choice, meets the requirements in 10 CFR 63.305(a) and (b) [DIRS 180319], and is appropriate for the assessment of doses to the RMEI for the entire period of the geologic stability (SNL 2007 [DIRS 177399], Sections 6.11.1.2). Thus, for all TSPA-LA dose calculations, the BDCFs for the present day climate are used.

**Volcanic Ash Exposure Case**—The biosphere conceptual model for the volcanic ash exposure case uses a similar reference biosphere and human receptor as the groundwater exposure case. The major difference between the exposure cases is that in this case the radionuclide source consists of contaminated tephra deposited on the ground surface and mixed with soil, rather than the multiple uses of contaminated groundwater. Figure 6.3.11-6 illustrates the relationships among the biosphere submodels indicating the migration of radionuclides in the reference biosphere between the various biosphere submodels starting with the introduction of contaminated tephra into the reference biosphere and resulting in a dose to the RMEI. On Figure 6.3.11-6, arrows point in the direction of radionuclide transfer between components in the Biosphere Process Model.

The following environmental transport processes are explicitly included in the Biosphere Process Model for the ash exposure case (SNL 2007 [DIRS 177399], Sections 6.3.2.1 and 6.3.2.6):

- Resuspension of contaminated soil and tephra from soils both undisturbed and from activities that disturb the soil surface
- Dry deposition of radionuclides on crop surfaces, including resuspension of contaminated soil and subsequent adhesion of soil particles on crop surfaces
- Removal of surface contamination by weathering processes
- Translocation and retention of contaminants from the site of deposition to the edible portions of crops
- Radionuclide uptake by crops through the roots

- Radionuclide intake by animals through consuming contaminated feed and soil, and subsequent transfer to animal products
- Release of radon ( $^{222}\text{Rn}$ ) from the soil.

Because the groundwater is contamination free in the volcanic ash exposure case, fewer exposure pathways are considered, as shown in Table 6.3.11-2, than for the groundwater exposure case. As described in *Biosphere Model Report* (SNL 2007 [DIRS 177399], Section 6.3.2.1), the volcanic ash exposure case does not include a contribution to annual dose from ingestion of drinking water, ingestion of locally produced fish, and inhalation of indoor aerosols generated by evaporative coolers. In addition, the dose contribution from  $^{14}\text{C}$  in solid or gaseous forms is not considered because  $^{14}\text{C}$  was assessed to be a negligible contributor to dose in the volcanic ash exposure case in *Radionuclide Screening* (SNL 2007 [DIRS 177424], Tables 6-7 and 6-8). The consideration of short-lived non-primary radionuclide decay products in the volcanic ash exposure case is the same as discussed above for the groundwater exposure case (i.e., their contributions to dose are included in the BDCFs of the parent radionuclide).

The analysis of BDCFs for the volcanic ash exposure case (SNL 2007 [DIRS 177399], Section 6.12.1.2) indicates that the results of the Biosphere Process Model for the volcanic ash exposure case are relatively insensitive to climate change (BDCF changes over climate are less than 1 percent). Therefore, one set of BDCFs, applies to all climate states considered in the TSPA-LA Model.

### **6.3.11.2 TSPA-LA Model Abstraction**

The objectives of the Biosphere Process Model and analyses are to develop the capabilities and associated data sets to allow TSPA to evaluate compliance with the postclosure individual protection standard in 10 CFR 63.311 [DIRS 178394], the groundwater protection standards in 10 CFR 63.331 [DIRS 180319], and the individual protection standard for human intrusion in 10 CFR 63.321 [DIRS 178394]. In the case of the individual protection standard, this information is identified in *Biosphere Model Report* (SNL 2007 [DIRS 177399], Section 8.1.1). The mathematical abstraction and the required BDCFs for the two exposure cases needed to calculate annual dose to the RMEI from radionuclide concentrations in groundwater or soil at the accessible environment are presented in *Groundwater Biosphere Dose Conversion Factors* (DTN: MO0702PAGBDCFS.001\_R0 [DIRS 179327]) and *Volcanic Biosphere Dose Conversion Factors* (DTN: MO0702PAVBPDCF.000\_R0 [DIRS 179330]). In addition, dose factors to calculate inhalation exposure during the volcanic eruption from predictions of atmospheric concentrations of radionuclides are provided in *Inhalation Dose Factors* (DTN: MO0702PAINHALA.001\_R0 [DIRS 179329]). The dose factors are used outside of the TSPA model to calculate inhalation dose during a volcanic eruption (Section 6.5.2.4).

The information required to demonstrate compliance with the groundwater protection standards is given in *Biosphere Model Report* (SNL 2007 [DIRS 177399], Section 8.1.1), which presents the equations and data that allows the TSPA to use radionuclide concentrations in groundwater to evaluate the whole body and individual organ doses from consumption of two liters of water per day and to calculate alpha particle activity in groundwater as per 10 CFR 63.331 [DIRS 180319].

These data are provided in *Groundwater Protection Standards Conversion Factors* DTN: MO0702PAGWPROS.001\_R0 [DIRS 179328].

To incorporate uncertainty into the TSPA-LA model input, BDCFs were calculated in a manner to propagate the uncertainties of the biosphere input parameters. This was accomplished by conducting a series of 1,000 stochastic model realizations. Uncertain input parameters to the Biosphere Process Model were sampled using Latin hypercube sampling for consistency with the sampling technique used for the TSPA-LA Model as discussed in this report. The resulting set of BDCFs incorporates the uncertainty from those input parameters. The sampling was structured such that for a given iteration the sampled value for each non-radionuclide specific parameter was the same for every radionuclide. This approach ensured that the correlation between BDCFs arising from the commonality of receptor and environmental characteristics was retained. The full set of BDCFs consists of a BDCF for each primary radionuclide for each Biosphere Process Model realization. As listed in Table 6.3.7-2, there are 29 radionuclides for the groundwater exposure case and 22 radionuclides for the volcanic ash exposure case. Table 6.3.11-3 lists the TSPA-LA parameters used to represent groundwater BDCF uncertainty in the TSPA-LA Model. In addition to the BDCFs for the primary radionuclides, the BDCF data set also contains composite values for a few cases where a radionuclide that is individually tracked in the Biosphere Process Model is combined with the BDCF for the much longer-lived parent radionuclide (e.g.,  $^{226}\text{Ra} + ^{210}\text{Pb}$  and  $^{232}\text{Th} + ^{228}\text{Ra} + ^{228}\text{Th}$ ). This approach allows the TSPA the option to only track the parent without systematic underestimation of dose.

Summaries of the parameters and their distributions used to develop BDCFs for the groundwater and volcanic eruption cases are provided in *Biosphere Model Report* (SNL 2007 [DIRS 177399], Tables 6.6-2 and 6.6-3).

**Calculation of Annual Dose to the RMEI for the Groundwater Exposure Case**—The TSPA-LA Model calculates the total annual dose to the RMEI at a given time using the set of BDCFs and radionuclide concentrations in the groundwater used by the RMEI. The total annual dose is the sum of the annual doses from all radionuclides tracked in the TSPA-LA Model as is given in *Biosphere Model Report* (SNL 2007 [DIRS 177399], Sections 6.4.10.4 and 6.11.3):

$$D_{total}(t) = \sum_i BDCF_i \times Cw_i(t) \quad (\text{Eq. 6.3.11-1})$$

where

$D_{total}(t)$  = time-dependent total annual dose from groundwater to the RMEI resulting from the release of radionuclides from the repository. This includes contributions from all radionuclides considered in the TSPA-LA Model (Sv/yr).

$BDCF_i$  = groundwater biosphere dose conversion factor for radionuclide  $i$  (Sv/yr per Bq/m<sup>3</sup>).

$Cw_i(t)$  = time-dependent activity concentration of radionuclide  $i$  in groundwater at the RMEI location (Bq/m<sup>3</sup>).

**Calculation of Alpha Activity Concentration in Groundwater**—The methods and the conversion factor values described in *Biosphere Model Report* (SNL 2007 [DIRS 177399], Section 6.15.1.1) are used to calculate the gross alpha activity concentration in groundwater for evaluation of compliance with the groundwater protection standards in 10 CFR 63.331 [DIRS 180319]. Natural background activity concentrations (DTN: SN0702PASZFTMA.002\_R1 [DIRS 183471]) are added to calculated values for comparison with the limit for combined  $^{226}\text{Ra}$  and  $^{228}\text{Ra}$  activity concentration in groundwater and with the limit for gross alpha activity concentration. The alpha particle activity concentration in the groundwater is calculated in the TSPA-LA Model using the number of alpha particles per decay of each primary radionuclide (DTN: MO0702PAGWPROS.001\_R0 [DIRS 179328]) and using the following equation (SNL 2007 [DIRS 177399], Equation 6.15-1 and Table 6.15-3):

$$C_{\alpha}(t) = \sum_i Cw_i(t) N\alpha_i \quad (\text{Eq. 6.3.11-2})$$

where  $Cw_i(t)$  ( $\text{Bq}/\text{m}^3$  or  $\text{pCi}/\text{L}$ ) is defined above and

$C_{\alpha}(t)$  = the time-dependent total alpha particle activity concentration in groundwater ( $\text{Bq}/\text{m}^3$  or  $\text{pCi}/\text{L}$ )

$N\alpha_i$  = number of alpha particles emitted per one decay of a primary radionuclide  $i$ .

Contributions from radon and uranium are excluded when calculating  $N\alpha_i$ , as directed in 10 CFR 63.331 [DIRS 180319].

**Calculation of Beta-Photon Dose from Drinking Two Liters of Water per Day**—The beta-photon doses to the whole body and individual organs are calculated using conversion factors from *Biosphere Model Report* (SNL 2007 [DIRS 177399], Table 6.15-6); DTN: MO0702PAGWPROS.001\_R0 [DIRS 179328]) and the following equation (SNL 2007 [DIRS 177399], Equation 6.15-4):

$$D(t) = \sum_i Cw_i(t) CF_i \quad (\text{Eq. 6.3.11-3})$$

where  $Cw_i(t)$  ( $\text{Bq}/\text{m}^3$ ) is defined above and

$D(t)$  = time-dependent total annual dose for an individual organ or for the whole body from beta-gamma emitters in the groundwater from daily consumption of 2 liters of water ( $\text{Sv}/\text{yr}$ )

$CF_i$  = conversion factor for calculating beta-photon annual dose for an individual organ or for the whole body from radionuclide  $i$  from daily consumption of 2 liters of water ( $\text{Sv}/\text{yr}$  per  $\text{Bq}/\text{m}^3$ ).

The conversion factors are provided for the following organs (23) and for the whole body:

Adrenals	Muscle
Bone Surface	Ovaries
Brain	Pancreas
Breast	Red Bone Marrow
Stomach Wall	Skin
Small Intestine Wall	Spleen
Upper Large Intestine Wall	Testes
Lower Large Intestine Wall	Thymus
Kidneys	Thyroid
Liver	Uterus
Extrathoracic Airways	Urinary Bladder Wall
Lung	Whole Body

**Calculation of Annual Dose to the RMEI for the Volcanic Ash Exposure Case**—The TSPA-LA Model calculates the total annual dose for the volcanic ash exposure case using the following equations (SNL 2007 [DIRS 177399], Section 6.12.3 and Equation 6.12-1):

$$D_{total}(t, T) = \sum_i D_{all\ pathway,i}(t, T)$$

and

$$D_{all\ pathway,i}(t, T) = BDCF_{ext,ing,Rn,i} Cs_i(t) + (BDCF_{inh,v,i} f(t-T) + BDCF_{inh,p,i}) Cs_{mc,i}(t) \quad (\text{Eq. 6.3.11-4})$$

where

$D_{total}(t, T)$	= total annual dose from all radionuclides at time $t-T$ after a volcanic release of radionuclides from the repository at time $t$ after repository closure (Sv/yr)
$D_{all\ pathway,i}(t, T)$	= all-pathway annual dose for primary radionuclide $i$ at time $t-T$ after a volcanic release of radionuclides from the repository at time $t$ after repository closure (Sv/yr)
$BDCF_{ext,ing,Rn,i}$	= BDCF component for external exposure, ingestion, and inhalation of radon decay products for primary radionuclide $i$ (Sv/yr per Bq/m <sup>2</sup> )
$Cs_i(t)$	= areal radionuclide concentration in a specified depth of surface soil at time $t$ (year) after the repository closure (Bq/m <sup>2</sup> ) calculated in TSPA-LA model
$BDCF_{inh,v,i}$	= BDCF component representing average early-time increase in inhalation exposure in the first year after a volcanic eruption; used in

	calculation of short-term inhalation exposure at post-eruption level of mass loading in excess of nominal mass loading for primary radionuclide $i$ (Sv/yr per Bq/kg)
$BDCF_{inh,p,i}$	= BDCF component for long-term inhalation at nominal level of mass loading for primary radionuclide $i$ (Sv/yr per Bq/kg)
$f(t-T)$	= decay function describing reduction of the annual average mass loading with time at time $t-T$ following a volcanic
$CS_{mc,i}(t)$	= activity concentration of radionuclide $i$ per unit mass of soil in the resuspendable layer of surface soil (critical thickness) at time $t$ (year) after the repository closure (Bq/kg).

The time function,  $f(t)$ , accounts for the reduction of mass loading in the years immediately following a volcanic eruption. The mass loading decreases exponentially with time as (SNL 2007 [DIRS 177399], Equation 6.12-3):

$$f(t - T) = e^{-\lambda(t-T)} \quad (\text{Eq. 6.3.11-5})$$

where

- $\lambda$  = fractional mass loading decrease rate constant (1/yr)
- $t-T$  = time after a volcanic eruption at  $T$  (years);  $t-T = 0$  is the first year after a volcanic eruption.

The mass loading decrease rate is provided by the Biosphere Process Model as an input parameter implemented in the TSPA-LA Model.

Both source terms used in the calculation of doses (Equation 6.3.11-4) (i.e., the areal radionuclide concentration in surface soil,  $CS_i(t)$ , and the mass radionuclide concentration in the resuspendable soil layer,  $CS_{mc,i}(t)$ ), are calculated in the TSPA by weighting the appropriate radionuclide concentrations by the respective expected areas of the distributary channels and the interchannel divides at the location of the RMEI. The radioactive waste mass concentrations in the resuspendable layer of soil,  $CS_{mc,i}(t)$ , and in the surface soil,  $CS_i(t)$ , are determined from the results of the ASHPLUME and FAR models as discussed in Section 6.5.2.2.

These models produce the results in terms of waste volumetric concentration. The waste volumetric concentration can be converted to waste mass concentration in the soil by dividing it by the density of the resuspendable layer,  $\rho_c$ . In the interchannel divides, the density of the resuspendable layer,  $\rho_c$ , can be calculated from the known tephra thickness,  $d_a$ , and density,  $\rho_a$ , and surface soil density,  $\rho_s$ , (SNL 2007 [DIRS 177399], Equation 6.12-2) as:

$$\rho_c = \frac{d_a \rho_a + (d_c - d_a) \rho_s}{d_c} \quad \text{when } d_a < d_c \text{ and}$$

$$\rho_c = \rho_a \quad \text{when } d_a \geq d_c \quad (\text{Eq. 6.3.11-6})$$

where

- $\rho_c$  = bulk density of resuspendable layer of surface soil, including tephra ( $\text{kg/m}^3$ )
- $d_c$  = thickness of resuspendable soil layer (i.e., the critical thickness (m))
- $d_a$  = thickness of initial tephra layer (m)
- $\rho_a$  = bulk density of tephra ( $\text{kg/m}^3$ )
- $\rho_s$  = bulk density of the original surface soil (i.e., without tephra) ( $\text{kg/m}^3$ ).

The TSPA model keeps track of the radionuclide activity concentration per unit mass of waste and apportions the correct activity of each radionuclide to the known waste concentration in the surface soil.

The sampling results of bulk density and tillage depth of the surface soil for individual biosphere model realizations are included in DTN: MO0702PAVBPDF.000\_R0 [DIRS 179330]. In the channels, where the tephra is mixed with soil and diluted, the density of resuspendable layer,  $\rho_c$ , can be approximated by the density of soil,  $\rho_s$  (SNL 2007 [DIRS 177399], Section 6.12.3).

**Calculation of Inhalation Dose Accrued During the Volcanic Eruption**—To calculate the inhalation dose to the RMEI during the eruption phase of a volcanic event (usually lasting less than a year), dose factors for the inhalation exposure pathway are used instead of the all pathway BDCFs. The daily dose from inhaling a specific radionuclide during the tephra fall from a volcanic eruption was calculated external to the TSPA-LA Model. The total daily inhalation dose,  $D_{inh}$ , from concentrations of primary radionuclides in the air was calculated as (SNL 2007 [DIRS 177399], Section 6.15.2.2, Equation 6.15-9):

$$\begin{aligned} D_{inh} &= \sum_i D_{inh,i} \\ &= \sum_i DF_i \times Ca_{i,outdoor} \end{aligned} \quad (\text{Eq. 6.3.11-7})$$

where

- $D_{inh,i}$  = daily inhalation dose (i.e., committed dose from one day's inhalation intake) for a primary radionuclide  $i$  (Sv/d)
- $DF_i$  = inhalation dose factor for a primary radionuclide  $i$  (Sv/d per  $\text{Bq/m}^3$ )
- $Ca_{i,outdoor}$  = one day average activity concentration of a primary radionuclide  $i$  in outdoor air ( $\text{Bq/m}^3$ ).

The inhalation of airborne radionuclides in tephra once they are deposited on the ground and subsequently resuspended is included in the BDCFs. The calculation results show that the expected annual dose (i.e., the probability-weighted annual dose) from inhalation of airborne radionuclides in tephra during the deposition phase is lower by several orders of magnitude than the expected annual dose (as presented in Section 6.1.2) caused by tephra deposited on the ground. Therefore, the contribution of an eruptive phase dose is neglected in the TSPA-LA

Model. See Section 6.5.2.4 for details of this calculation and comparison with the TSPA-LA Model results.

### **6.3.11.3 TSPA-LA Model Implementation**

The Biosphere Process Model provides stochastic BDCFs for the calculation of the annual dose to the RMEI. In addition, deterministic conversion factors for beta and photon dose from drinking two liters of water per day, and the number of alpha particles emitted per decay of primary radionuclides, are provided as inputs to the TSPA-LA Model. The BDCFs are transferred into the TSPA-LA Model in the form of one-dimensional tables, one for each radionuclide, that consist of 1,000 rows, which represent individual model realizations. The conversion factors used to calculate beta-photon dose are in a two-dimensional look-up table consisting of 19 columns representing each of the relevant (i.e., beta-photon emitting), primary radionuclides and three additional columns for the combination of long- and short-lived radionuclide combinations. The table has 24 rows that correspond to individual organs and the whole body. In the case of alpha activity calculations, a look-up table is provided that gives the total number of alpha particles attributable to one radioactive decay of each of the (16) primary radionuclides that include alpha emitters in their short-lived decay chains.

The annual dose to the RMEI is calculated in the TSPA-LA Biosphere Model Component using the BDCFs that convert radionuclide concentrations in groundwater or soil-tephra mixture to an annual all-pathway dose (based on Equations 6.3.11-1 and 6.3.11-4). A discrete distribution, *Bio\_Index* is sampled in TSPA to represent the epistemic model uncertainty from the Biosphere Model. *Bio\_Index*, an equally probable integer from 1 to 1,000 inclusive, is used to randomly select a particular sequence of realizations from the BDCF tables. For the groundwater exposure case, one set of BDCFs, the set corresponding to the present-day climate, is used throughout the modeling time period of the TSPA-LA Model (Section 6.3.11.1). The selected BDCFs are then multiplied by the radionuclide concentrations provided by the SZ Flow and Transport Model Component (or by concentrations in tephra as calculated by the FAR Model [Section 6.5.2.1.3]) to compute the annual dose (Equations 6.3.11-1 and 6.3.11-4). Probability weighting of dose is calculated in the Biosphere Model Component for the Nominal Early Failure (Section 6.4) and Igneous Intrusion Modeling Cases (Section 6.5.1) and the Seismic Scenario Class (Section 6.6). The probability weighting for the Volcanic Eruption Modeling Case is handled in the source term calculation (Section 6.5.2).

The calculations for the groundwater protection standards are based on the activity concentration of each primary radionuclide in groundwater, as calculated from radionuclide concentrations provided by the SZ Flow and Transport Model Component. The alpha particle activity concentration in water and the beta-photon dose from drinking two liters of water per day are then calculated using Equations 6.3.11-2 and 6.3.11-3, respectively. Equations 6.3.11-5 and 6.3.11-6 are implemented in the Volcanic Ash Exposure Submodel under the Volcanic Eruption Modeling Case (Section 6.5.2.2). As noted previously, the inhalation dose during a volcanic eruption period (Equation 6.3.11-7) was not implemented in the TSPA-LA Model because, as a result of external evaluation, it was determined that the contribution from this pathway to the probability-weighted annual dose was insignificant.

#### **6.3.11.4 Model Component Consistency and Conservatism in Assumptions and Parameters**

To enhance understanding of the complex interactions within the TSPA-LA Model, a discussion of consistency among model components and submodels and identification of conservative assumptions in abstractions, process models, and parameter sets supporting the biosphere are discussed as follows.

##### **6.3.11.4.1 Consistency of Assumptions**

It is important to ensure that the parameters and assumptions in each model component or submodel of the TSPA-LA Model are consistent. The first discussion concerns tephra particle sizes during eruptive atmospheric transport and when they are used for the inhalation dose calculation. The second applies to the groundwater release case and concerns the elemental partition coefficients used for transport calculations in the UZ and SZ and those employed in the soil submodel of the Biosphere Process Model.

**Volcanic Tephra Particle Size**—In the Biosphere Process Model, the reference biosphere describes the environment around the location of the RMEI (10 CFR 63.312 [DIRS 180319]), which is located about 18 km south of the repository, (66 FR 55732 [DIRS 156671] III Public Comments and Responses 3.2, p. 55750), as specified in the definition of the *Controlled Area* found in 10 CFR 63.302 [DIRS 180319]. The size of resuspended particles used to calculate the inhalation component of the dose to the RMEI is smaller than the particle size in the ASHPLUME code used to predict atmospheric transport (advection and diffusion) and surface deposition (gravitational settling) of the tephra from a volcanic eruption. After the eruption, fluvial processes redistribute the tephra from the immediate vicinity of the eruption down Fortymile Wash to the location of the RMEI. This Tephra Redistribution Submodel (Section 6.5.2.1.3) does not explicitly consider mechanical processes that generate smaller tephra particles nor is any account taken of subsequent weathering processes. However, the redistribution model does account for the diffusion of radionuclides into the adjacent soil or soil-tephra mixture. This diffusion process is calibrated from measured <sup>137</sup>Cs profiles on channels and inter-channel divides of the upper Fortymile Wash alluvial fan and models the migration of the contaminants in the tephra to the local soil, thereby providing a source of resuspendable contaminated particles. The inhalation dose is calculated in the Biosphere Process Model by using inhalation dose coefficients for 1- $\mu$ m particles, while the ASHPLUME code predictions concern particles greater than 15 to 30  $\mu$ m. This is because of ASHPLUME's inability to accurately represent the transport of tephra particles of mean diameter less than approximately 15  $\mu$ m (Jarzemba et al. 1997 [DIRS 100987], Section 2.1; and SNL 2007 [DIRS 177431], Section 1.3.1). Because the typical mean diameter of tephra particles after an eruption is generally much larger than 15  $\mu$ m, the model is applicable for calculating the distribution of the majority of the mass of potential tephra and radionuclide releases from a possible future eruption at Yucca Mountain (SNL 2007 [DIRS 177431], Section 1.3.1). However, it does not address well the particles in the respirable (less than 4  $\mu$ m) and thoracic (less than 10  $\mu$ m) size range, which are more important for the evaluation of inhalation doses (BSC 2005 [DIRS 172827], Section 6.5.5.1). This apparent difference in the particle size distribution of tephra deposited at the location of the RMEI and the particle size distribution used to calculate inhalation dose to the RMEI becomes less significant with time as tephra particles

weather and radionuclides diffuse and attach to small soil particles. The processes that cause redistribution of the contaminated tephra after the volcanic eruption, as well as other natural processes and human activities at the location of the RMEI, may change the initial particle size distribution of deposited tephra.

**Effect of Volcanic Tephra Particle Size on TSPA**—A study was completed in *Characteristics of the Receptor for the Biosphere Model* (BSC 2005 [DIRS 172827], Section 6.5.5.2) regarding the effect of differences in particle size on predicted inhalation dose. It was concluded that “...the application of dose coefficients for particles with activity median aerodynamic diameter of 1  $\mu\text{m}$  will not underestimate the doses from inhalation of resuspended material and that these dose coefficients are adequate for use in the biosphere model.”

#### **6.3.11.4.2 Identification of Conservatisms in Submodels and Abstractions**

**Dose Coefficients for Internal Exposure**—The dose coefficients for internal exposure (inhalation and ingestion) used to calculate the BDCFs are the most conservative of the values provided in the source reference (EPA 2002 [DIRS 175544]) for a given radionuclide. Different dose coefficient choices correspond to different gastrointestinal absorption fractions for ingestion and, in the case of inhalation, differing transfer fractions from the lung to blood stream for different chemical compounds of a given radionuclide. The conservative values were used because of uncertainty in the final chemical/physical form of the radionuclides supplied to the biosphere from groundwater and the uncertainty in the subsequent evolution of the chemical/physical form in the biosphere (SNL 2007 [DIRS 177399], Sections 6.4.8.5 and 6.4.9.6). This conservatism results in either a realistic estimate of dose or an overestimation of dose.

**Dose Coefficients for External Exposure to Contaminated Soil**—For calculating the external dose from exposure to contaminated soil for the groundwater case, the dose coefficients for an infinite depth of contamination were used. This approach allowed the time evolution of soil build-up to be considered only in the tillage depth while accounting for the external exposure to radionuclides that could have been leached from the surface soil into the deep soil. Use of these dose coefficients is reasonable yet conservative as dose coefficients for an infinite depth and those for a 15-cm depth (note that tillage depths extend up to 30 cm) differ by less than 10 percent for most primary radionuclides (EPA 2002 [DIRS 175544]). Only for radionuclides with strong gamma emissions, such as  $^{226}\text{Ra}$  and  $^{137}\text{Cs}$ , do dose coefficients exhibit a larger difference for these two depths. The use of dose coefficients for an infinite depth cannot underestimate dose.

**Roots in Surface Soil**—All crop roots are considered to be in the surface soil layer (i.e., the soil layer extending down to the tilling depth). For many crops, the root systems can extend to below the tillage depth. This approach effectively assumes (conservatively) that all roots, the source of radionuclide uptake for plants, are exposed to a radionuclide concentration as calculated for the tillage region.

**Resuspended Volcanic Ash**—Radionuclide concentrations in the air were calculated separately for cultivated and uncultivated lands. The concentration of radionuclides in cultivated (i.e., tilled) soil was used to calculate concentrations of radionuclides in crops and animal

products. The concentration of radionuclides in uncultivated soil was used to calculate inhalation and external exposure to the RMEI. This was done because for most of the land area the soil in the reference biosphere would not be cultivated. Using radionuclide mass concentrations of uncultivated soil to calculate inhalation and external exposure is a conservative approach because the concentrations in uncultivated soil would be higher than in cultivated soil where tilling causes additional dilution. Because uncultivated lands would not be disturbed by agricultural activities, tephra would not mix quickly with surface soil and tephra would remain on or near the soil surface where it is available for resuspension (SNL 2007 [DIRS 177399], Section 6.3.2.6). This conservatism results in the overestimation of dose.

**External Exposure from Tephra on the Ground Surface**—Unlike the groundwater exposure scenario, where soil contamination could be deep, tephra and associated radionuclides could be distributed on or near the soil surface and the source for external exposure could be a thin layer of uncultivated soil on the ground surface. Thus, external exposure was evaluated using the dose coefficients for exposure to contaminated ground surface (EPA 2002 [DIRS 175544]) rather than volumetric concentrations. This modeling approximation was reasonable because there is considerably more uncultivated land than cultivated land in Amargosa Valley (BSC 2004 [DIRS 177101], Section 6.2), and the mixing of tephra on uncultivated lands would be limited. The effects of radiation attenuation in the soil and tephra were conservatively minimized (SNL 2007 [DIRS 177399], Section 6.3.2.4). This conservative assumption results in the overestimation of dose in cases where radionuclides are distributed throughout the soil where their radiations are attenuated by the soil layer between the point of emission and the RMEI. For radionuclides with a significant dose contribution from external exposure, such as  $^{137}\text{Cs}$  and  $^{126}\text{Sn}$  this conservatism could overestimate annual dose predictions.

### 6.3.11.5 Alternative Conceptual Model(s) for Biosphere

Section 6.2 outlines the general consideration and treatment of ACMs used to support the TSPA-LA Model. Brief descriptions of the biosphere ACMs as discussed in *Biosphere Model Report* (SNL 2007 [DIRS 177399], Section 6.3.3) and summarized in Table 6.3.11-4 are presented below.

**ACM for Radon Release from Soil**—The conceptual model for radon used in the Biosphere Process Model is based on a radon release factor from radium-contaminated soil. The ACM relies on modeling radon transport in the soil and the atmosphere (Yu et al. 2001 [DIRS 159465], Appendix C). A numerical comparison between the selected model and the ACM shows that the resulting  $^{222}\text{Rn}$  concentrations in air are comparable (SNL 2007 [DIRS 177399], Section 7.4.3.1). The method used in the Biosphere Process Model was selected because it required fewer parameters. The more complex ACM did not produce results different enough to warrant its implementation (SNL 2007 [DIRS 177399], Section 7.3.2.2).

**ACM for Evaporative Cooler**—The conceptual model for evaporative coolers used in the Biosphere Process Model was based on the mechanical operation of evaporative coolers and considered the generation of aerosols as air is forced through a wet, porous surface. An ACM would be to calculate radionuclide concentrations based on differences in absolute humidity between indoor and outdoor air caused by the operation of evaporative coolers. An evaluation of

these two methods showed that they produced results of air activity concentrations that were deemed to be acceptably equivalent (SNL 2007 [DIRS 177399], Section 7.4.3.2).

**ACM for Direct Deposition of Irrigation Water on Plant Surfaces**—The Biosphere Process Model considers a fraction of radionuclides in irrigation water to be directly translocated into edible plant parts with accumulation and weathering occurring during the growing period. An ACM developed in BIOMASS ERB2A (BIOMASS 2003 [DIRS 168563]) considers this process in two sequential steps: (1) movement of deposited radionuclides from external plant surfaces into the plant tissues, and (2) movement of radionuclides from plant tissues into edible parts of the crop. This ACM applies weathering to contaminants that remain on external plant surfaces and also considers food-processing losses (BIOMASS 2003 [DIRS 168563], Section C3). The two models were evaluated using the same input values or using default data from BIOMASS ERB2A (BIOMASS 2003 [DIRS 168563]). The ACM and the selected model produced comparable results with reasonable input values (SNL 2007 [DIRS 177399], Section 7.4.4.1). The ACM was not chosen because it requires parameters that are not commonly used in environmental transport modeling and are, thus, difficult to quantify. In addition, the ACM was developed for a temperate climate and implies infrequent irrigation episodes, which may be inappropriate for the arid or semiarid conditions at Yucca Mountain (SNL 2007 [DIRS 177399], Section 7.3.3.2).

**ACM for Direct Deposition of Airborne Particulates on Plant Surfaces**—In the Biosphere Process Model, resuspended soil deposited on crop leaves is treated in the same manner as intercepted irrigation water. The ACM takes a different approach based on a contamination factor for the external contamination of crops, which is similar to a soil-to-plant transfer factor. Differences between the selected model and the ACM were evaluated using the same input values when the parameters are comparable or by using default data from the published ACM. The evaluation showed that the approach used in the Biosphere Process Model and that used in the ACM produce comparable results for reasonable input values (SNL 2007 [DIRS 177399], Section 7.4.4.3).

**ACM for Animal Product Contamination**—The Biosphere Process Model considers animal contamination resulting from the ingestion of contaminated water, soil, and feed. The GENII Model (Napier et al. 1988 [DIRS 157927]; Leigh et al. 1993 [DIRS 100464]) only includes the consumption of water and feed; however, GENII Version 2 (Napier et al. 2006 [DIRS 177331]) includes soil ingestion, and the BIOMASS ERB2A model (BIOMASS 2003 [DIRS 168563]) includes an additional pathway: inhalation of contaminated air by animals. These animal transport pathways are compared to determine their relative importance (SNL 2007 [DIRS 177399], Section 7.4.5). For this comparison, meat (i.e., beef, pork, and game) was used as an example animal product with  $^{239}\text{Pu}$  as the test radionuclide. Soil ingestion is an important contributor to the total activity concentration in meat and, therefore, is included in the Biosphere Process Model. The inhalation of contaminated dust contributes little to concentrations in meat and, therefore, is not included.

**ACM for  $^{14}\text{C}$  Special Submodel**—The methods used in the Biosphere Process Model to calculate  $^{14}\text{C}$  concentrations in environmental media were different from those used for the other primary radionuclides. Concentrations of  $^{14}\text{C}$  in crops were based on experimental results of the release of  $^{14}\text{CO}_2$  gas from soil (Sheppard et al. 1991 [DIRS 159545]; Yu et al. 2001

[DIRS 159465], Section L.3). The Biosphere Process Model included two transport pathways of  $^{14}\text{C}$  to plants: direct root uptake and intake of  $^{14}\text{CO}_2$  gas by plants during photosynthesis. Six RMEI exposure pathways were considered: external exposure to and ingestion of  $^{14}\text{C}$  in soil, inhalation of  $^{14}\text{CO}_2$  gas and airborne particulate matter containing  $^{14}\text{C}$ , and ingestion of  $^{14}\text{C}$  in crops and animal products. An ACM (Napier et al. 1988 [DIRS 157927], p. 4.89) used different methods to calculate  $^{14}\text{C}$  concentrations. That model considered uptake into plants only from roots and used a very low removal rate of carbon from soil because the model did not account for gaseous release of  $^{14}\text{CO}_2$ . The method used by the biosphere model was chosen because it more realistically considered uptake of  $^{14}\text{CO}_2$  gas into plants, resulting in higher plant concentrations (SNL 2007 [DIRS 177399], Sections 6.3.3, 7.3.6, and 7.4.7). An additional alternative model for calculating concentrations of  $^{14}\text{C}$  in plant and animal products has also been proposed (BIOMASS 2000 [DIRS 154522], Appendix A) but was not considered because the default parameter values necessary to run the model have not been developed by the authors of the model (SNL 2007 [DIRS 177399], Section 7.3.6 and Table 7.3-21).

**ACM for Environment-Specific Inhalation Submodel**—In the Biosphere Process Model, inhalation exposure was treated as a function of environment and human activity because many of the input parameters (mass loading, breathing rate, exposure time, and enhancement factors) would be influenced by human activities. Similar models, called microenvironmental models, were used to assess exposure to particulate matter and other contaminants (Duan 1982 [DIRS 162466]; Mage 1985 [DIRS 162465]; and Klepeis 1999 [DIRS 160094]). An alternative but simpler method that is commonly used in risk assessments is to use one or two environments that are representative of the entire range of people, conditions, and times being modeled. These methods produce the same results if average values used in the biosphere model for each environment are used for the alternative method. The method used in the Biosphere Process Model better incorporates variation and uncertainty in each of the input parameters and provides more transparency for the expected RMEI exposure changes between the groundwater (localized contamination) and volcanic release cases (widespread contamination) (SNL 2007 [DIRS 177399], Sections 6.3.3, 7.3.7, 7.3.8, and 7.4.9).

All seven ACMs are numerically compared with those selected in the Biosphere Process Model. The results indicate that most of the ACMs are numerically similar to those selected, and some ACMs are not chosen because those selected match better conceptually with site-specific conditions. Therefore, none of the ACMs were used in the calculations of BDCFs that support the TSPA-LA Model.

No ACMs were recommended for inclusion in the TSPA-LA Model.

Table 6.3.11-1. Pathways for the Groundwater Exposure Case

Environmental Medium	Exposure Mode	Exposure Pathways	Examples
Water	Ingestion	Water intake	Drinking water and water-based beverages.
Soil	Ingestion	Inadvertent soil ingestion	Recreational activities, occupational activities, gardening, and consumption of fresh fruits and vegetables with attached soil.
Soil	External	External radiation exposure	Activities on or near contaminated soils.
Air	Inhalation	Breathing resuspended particles, gases ( $^{222}\text{Rn}$ and progeny, plus $^{14}\text{CO}_2$ ), and aerosols from evaporative coolers	Outdoor activities, including soil-disturbing activities related to work and recreation; domestic activities including sleeping.
Plants	Ingestion	Consumption of locally produced crops: vegetables, fruits, and grains	Eating contaminated crops.
Animals	Ingestion	Consumption of locally produced animal products: meat, poultry, milk, and eggs	Eating contaminated animal products.
Fish	Ingestion	Consumption of locally produced freshwater fish	Eating contaminated fish.

Source: Modified from Table 6.3-1 in *Biosphere Model Report* (SNL 2007 [DIRS 177399])

Table 6.3.11-2. Pathways for the Volcanic Ash Exposure Case

Environmental Medium	Exposure Mode	Exposure Pathways	Examples
Soil	Ingestion	Inadvertent soil ingestion	Recreational activities, occupational activities, gardening, and consumption of fresh fruit and vegetables with attached soil.
Soil	External	External radiation exposure	Activities on or near contaminated soils.
Air	Inhalation	Breathing resuspended particles; $^{222}\text{Rn}$ and progeny	Outdoor activities, including soil-disturbing activities related to work and recreation; domestic activities, including sleeping.
Plants	Ingestion	Consumption of locally produced crops: vegetables, fruits, and grains	Eating contaminated crops.
Animals	Ingestion	Consumption of locally produced animal products: meat, poultry, milk, and eggs	Eating contaminated animal products.

Source: Modified from Table 6.3-3 in *Biosphere Model Report* (SNL 2007 [DIRS 177399])

Table 6.3.11-3. Groundwater BDCF Uncertainty Representation in the TSPA-LA Model, GoldSim Model File for the Present-Day Climate

TSPA-LA Parameter Name <sup>a,b</sup>	Description
Bio_Index	Uniform random integer (1, 1000) generated in TSPA to select a BDCF vector from the data provided
GW_BDCF_MIC_Ac227	<sup>227</sup> Ac - Modern Interglacial Climate BDCF
GW_BDCF_MIC_Am241	<sup>241</sup> Am - Modern Interglacial Climate BDCF
GW_BDCF_MIC_Am243	<sup>243</sup> Am - Modern Interglacial Climate BDCF
GW_BDCF_MIC_C14	<sup>14</sup> C - Modern Interglacial Climate BDCF
GW_BDCF_MIC_Cl36	<sup>36</sup> Cl - Modern Interglacial Climate BDCF
GW_BDCF_MIC_Cs135	<sup>135</sup> Cs - Modern Interglacial Climate BDCF
GW_BDCF_MIC_Cs137	<sup>137</sup> Cs - Modern Interglacial Climate BDCF
GW_BDCF_MIC_I129	<sup>129</sup> I - Modern Interglacial Climate BDCF
GW_BDCF_MIC_Np237	<sup>237</sup> Np - Modern Interglacial Climate BDCF
GW_BDCF_MIC_Pa231	<sup>231</sup> Pa - Modern Interglacial Climate BDCF
GW_BDCF_MIC_Pb210	<sup>210</sup> Pb - Modern Interglacial Climate BDCF
GW_BDCF_MIC_Pu238	<sup>238</sup> Pu - Modern Interglacial Climate BDCF
GW_BDCF_MIC_Pu239	<sup>239</sup> Pu - Modern Interglacial Climate BDCF
GW_BDCF_MIC_Pu240	<sup>240</sup> Pu - Modern Interglacial Climate BDCF
GW_BDCF_MIC_Pu242	<sup>242</sup> Pu - Modern Interglacial Climate BDCF
GW_BDCF_MIC_Ra226	<sup>226</sup> Ra - Modern Interglacial Climate BDCF
GW_BDCF_MIC_Ra226_Pb210 <sup>c</sup>	<sup>226</sup> Ra & <sup>210</sup> Pb - Modern Interglacial Climate BDCF
GW_BDCF_MIC_Ra228	<sup>228</sup> Ra - Modern Interglacial Climate BDCF
GW_BDCF_MIC_Se79	<sup>79</sup> Se - Modern Interglacial Climate BDCF
GW_BDCF_MIC_Sn126	<sup>126</sup> Sn - Modern Interglacial Climate BDCF
GW_BDCF_MIC_Sr90	<sup>90</sup> Sr - Modern Interglacial Climate BDCF
GW_BDCF_MIC_Tc99	<sup>99</sup> Tc - Modern Interglacial Climate BDCF
GW_BDCF_MIC_Th228	<sup>228</sup> Th - Modern Interglacial Climate BDCF
GW_BDCF_MIC_Th229	<sup>229</sup> Th - Modern Interglacial Climate BDCF
GW_BDCF_MIC_Th230	<sup>230</sup> Th - Modern Interglacial Climate BDCF
GW_BDCF_MIC_Th232	<sup>232</sup> Th - Modern Interglacial Climate BDCF
GW_BDCF_MIC_Th232_Ra228_Th_228 <sup>c</sup>	<sup>232</sup> Th & <sup>228</sup> Ra & <sup>228</sup> Th - Modern Interglacial Climate BDCF
GW_BDCF_MIC_U232	<sup>232</sup> U - Modern Interglacial Climate BDCF
GW_BDCF_MIC_U232_Th228	<sup>232</sup> U & <sup>228</sup> Th - Modern Interglacial Climate BDCF
GW_BDCF_MIC_U233	<sup>233</sup> U - Modern Interglacial Climate BDCF
GW_BDCF_MIC_U234	<sup>234</sup> U - Modern Interglacial Climate BDCF

Table 6.3.11-3. Groundwater BDCF Uncertainty Representation in the TSPA-LA Model, GoldSim Model File for the Present-Day Climate (Continued)

TSPA-LA Parameter Name <sup>a,b</sup>	Description
GW_BDCF_MIC_U235	<sup>235</sup> U - Modern Interglacial Climate BDCF
GW_BDCF_MIC_U236	<sup>236</sup> U - Modern Interglacial Climate BDCF
GW_BDCF_MIC_U238	<sup>238</sup> U - Modern Interglacial Climate BDCF

Source: DTN: MO0705GOLDSIMB.000\_R0 [DIRS 181281] for BDCF data

<sup>a</sup> There are three one-dimensional tables, one for each of the three climate states (MIC = modern interglacial climate, MC = monsoonal climate, and GTC = glacial-transitional climate) modeled for each radionuclide; only the MIC is shown here. Using <sup>227</sup>Ac as an example, the TSPA-LA Model contains the following one-dimensional BDCF tables for the groundwater exposure scenarios: GW\_BDCF\_MIC\_Ac227, GW\_BDCF\_MC\_Ac227, and GW\_BDCF\_GTC\_Ac227.

<sup>b</sup> To incorporate uncertainty into the model input, the biosphere model component ran a series of 1,000 model realizations to define a set of BDCFs for each radionuclide modeled. The resulting probability distribution represents uncertainty in the BDCFs. This set of BDCFs is given in a one-dimensional table for each radionuclide.

<sup>c</sup> These composite BDCF data were defined to provide the opportunity to only consider the release and transport of the long-lived parent radionuclide while retaining the dose consequences of the short-lived progeny.

Table 6.3.11-4. Alternative Conceptual Models Considered for the Biosphere

Alternative Conceptual Model	Overview	Screening Assessment and Basis
Radon release from soil (Air Submodel)	This ACM considers radon transport in the soil and the atmosphere, which requires more input data. The ERMYN conceptual model does not include these processes and uses a simple release factor.	This ACM is screened from the Biosphere Model Component based on an analysis showing that the ACM and the ERMYN Model produce comparable results (SNL 2007 [DIRS 177399], Section 7.4.3.1).
Evaporative cooler (Air Submodel)	This ACM considers an inhalation dose from aerosols generated from evaporative coolers and is based on calculating radionuclide concentrations in the air due to an increase in humidity. The ERMYN conceptual model uses a submodel based on the amount of water evaporated rather than an increase in humidity.	This ACM is screened from the Biosphere Model Component based on an analysis showing that this ACM and the ERMYN Model produce equivalent results (SNL 2007 [DIRS 177399], Section 7.4.3.2).
Direct deposition of irrigated water (Plant Submodel)	This ACM considers two processes: one where the deposited radionuclide moves from external plant surfaces into the plant tissues and the other from plant tissues into the edible portion of the crop. Weathering is applied only to contaminants that remain on external plant surfaces. Food processing loss is also considered in the ACM. The ERMYN conceptual model considers the radionuclides in irrigation water to be directly translocated to the edible parts of plants with weathering and accumulation during the growing period, but without food preparation loss.	This ACM is screened from the Biosphere Model Component based on an analysis showing that this ACM and the ERMYN Model produce comparable results (SNL 2007 [DIRS 177399], Section 7.4.4.1).
Direct deposition of airborne particulates on crops (Plant Submodel)	This ACM is based on the crop external contamination. This contamination factor is very similar to a soil-to-plant transfer factor. The ERMYN conceptual model considers the deposited airborne particles on crop leaves acting the same way as the intercepted irrigation water.	This ACM is screened from the Biosphere Model Component based on an analysis showing that this ACM and the ERMYN Model produce comparable results for reasonable input values (SNL 2007 [DIRS 177399], Section 7.4.4.3).
Animal product contamination (Animal Submodel)	This ACM considers animal inhalation of contaminated air. The ERMYN conceptual model excludes the inhalation of contaminated air as a negligible pathway.	This ACM is screened from the Biosphere Model Component based on an analysis showing that inhalation of contaminated air is not an important contributor to the animal product contamination (SNL 2007 [DIRS 177399], Section 7.4.5).
<sup>14</sup> C Special Submodel ( <sup>14</sup> C Special Submodel)	This ACM considers root uptake as the only mechanism of <sup>14</sup> C transfer to crops. ERMYN also includes <sup>14</sup> C uptake from air during photosynthesis. In addition to ingestion, ERMYN also includes other pathways that result in human exposure to <sup>14</sup> C: external exposure, inhalation of <sup>14</sup> C as gas and in soil, as well as soil ingestion.	This ACM is screened from the Biosphere Model Component based on an analysis showing that the selected <sup>14</sup> C special submodel considers more processes of <sup>14</sup> C transfer to plants than this ACM, which results in a higher <sup>14</sup> C concentration in plants (SNL 2007 [DIRS 177399], Section 7.4.7).
Environment-Specific Inhalation Submodel (Inhalation Submodel)	This ACM uses average values of input parameters for inhalation exposure. The ERMYN conceptual model considers inhalation exposure as a function of the environment because many model parameters, such as mass loading, breathing rate, and exposure time, differ among environments and activities.	This ACM is screened from the Biosphere Model Component based on an analysis showing that the ACM and the ERMYN model produce comparable results (SNL 2007 [DIRS 177399], Section 7.4.9). In addition, it is easier to address uncertainty in the input parameters using environment-specific values.

Source: Table 6.3-5 in *Biosphere Model Report* (SNL 2007 [DIRS 177399])

NOTE: ERMYN = Environmental Radiation Model for Yucca Mountain, Nevada.

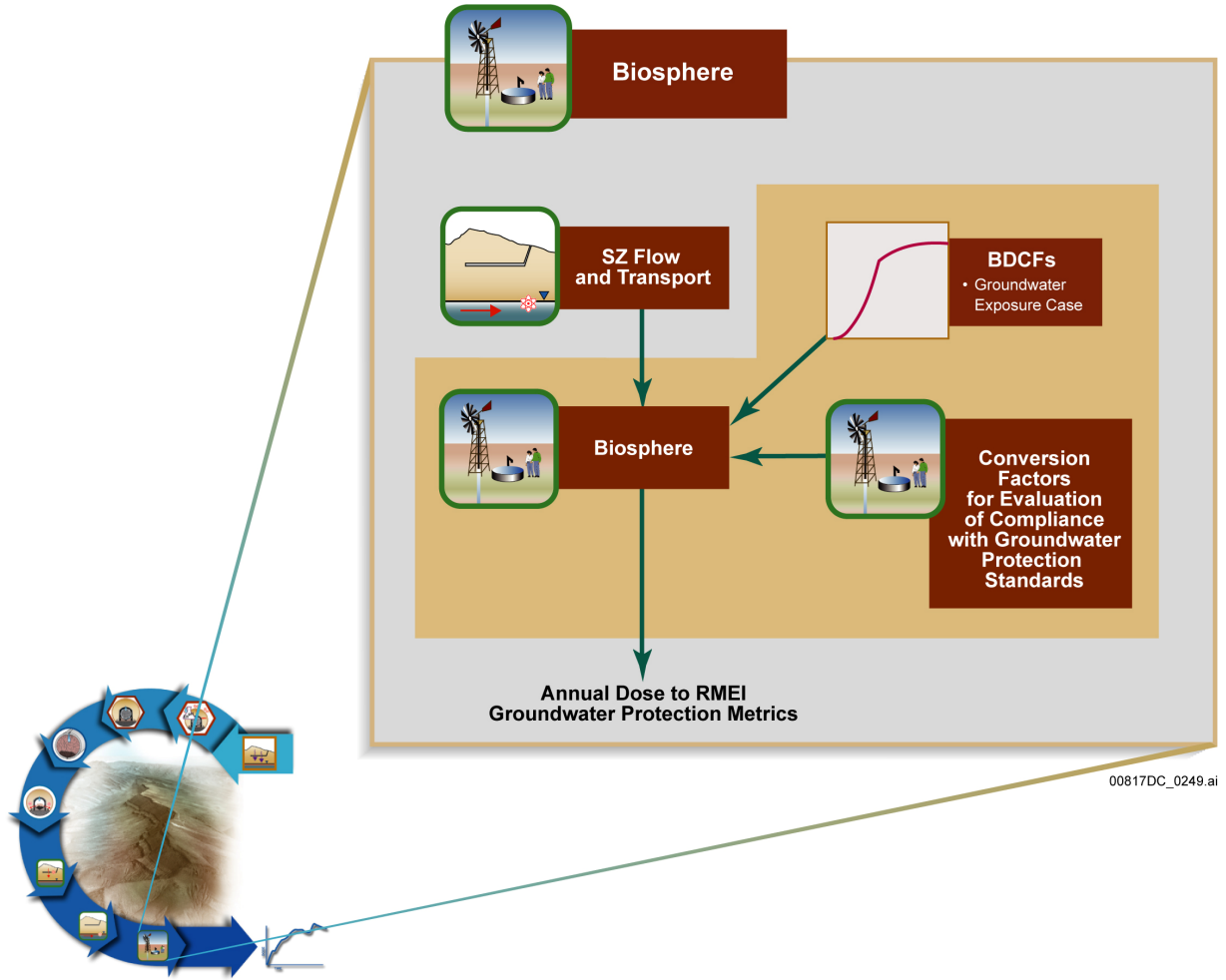
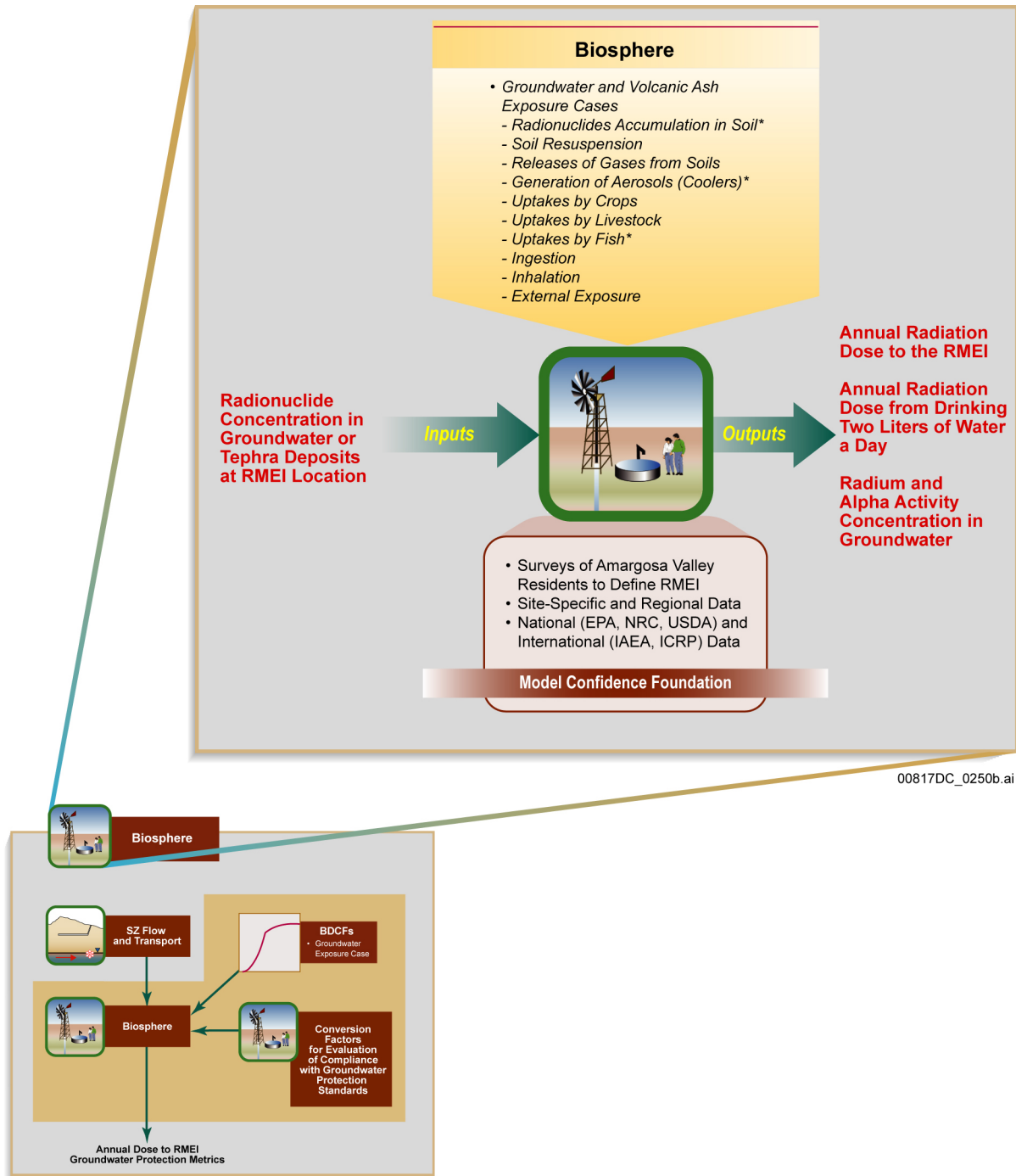


Figure 6.3.11-1. Information Flow Diagram for the Biosphere Model Component of the TSPA-LA Model



NOTE: The flow diagram in the lower part of this figure only depicts the Groundwater Exposure Case. The flow diagram for the Biosphere Volcanic Ash Exposure Case is shown in Figure 6.5-8. The asterisks in the figure identify those environmental transport pathways that are only included in the Groundwater Exposure Case. ICRP = International Commission on Radiological Protection.

Figure 6.3.11-2. Inputs, Outputs, and Basis for Model Confidence for the Biosphere Model Component of the TSPA-LA Model

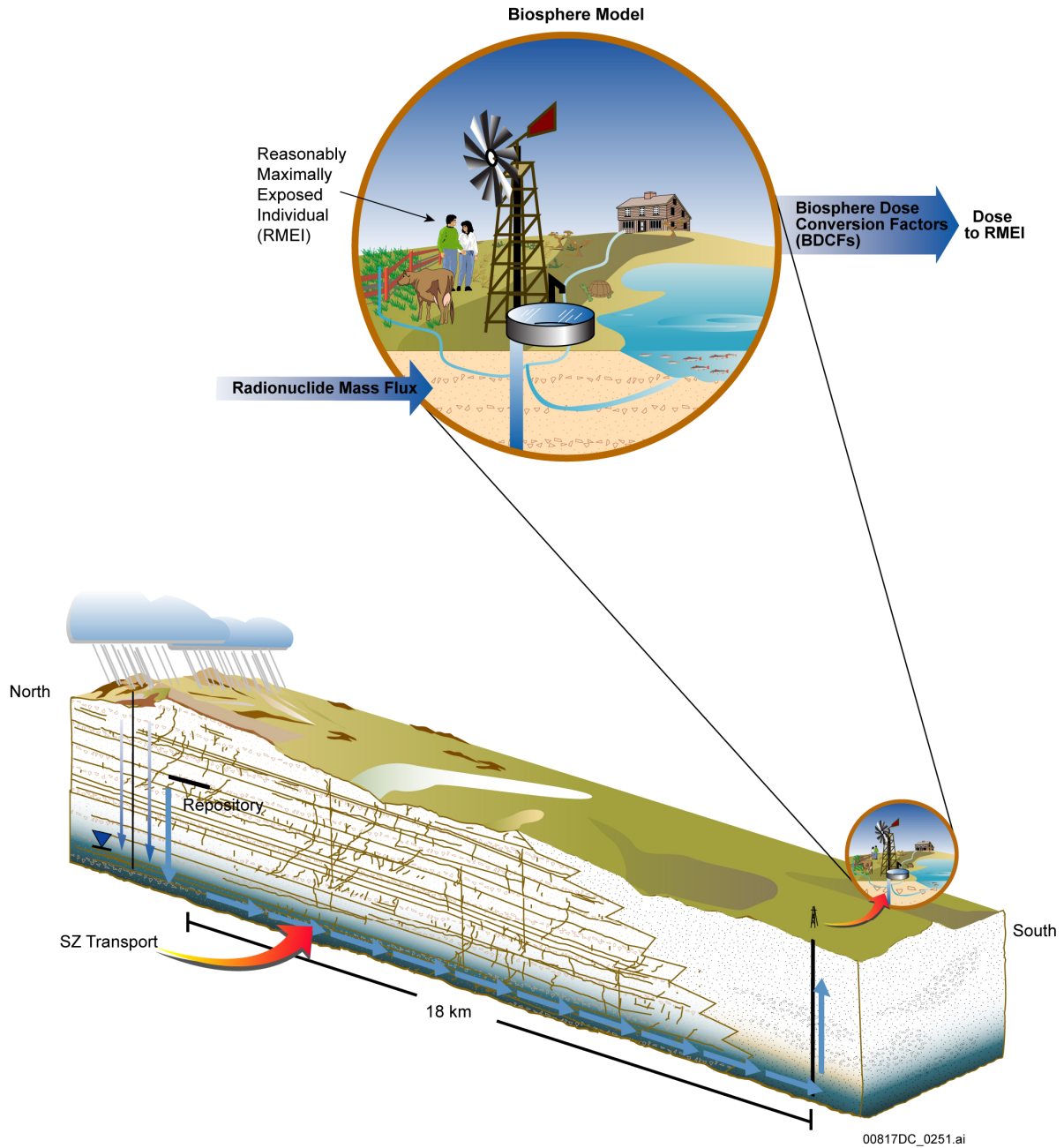


Figure 6.3.11-3. Overview of the Biosphere Groundwater Exposure Case Showing Groundwater Transport of Radionuclides and Exposure to the Reasonably Maximally Exposed Individual

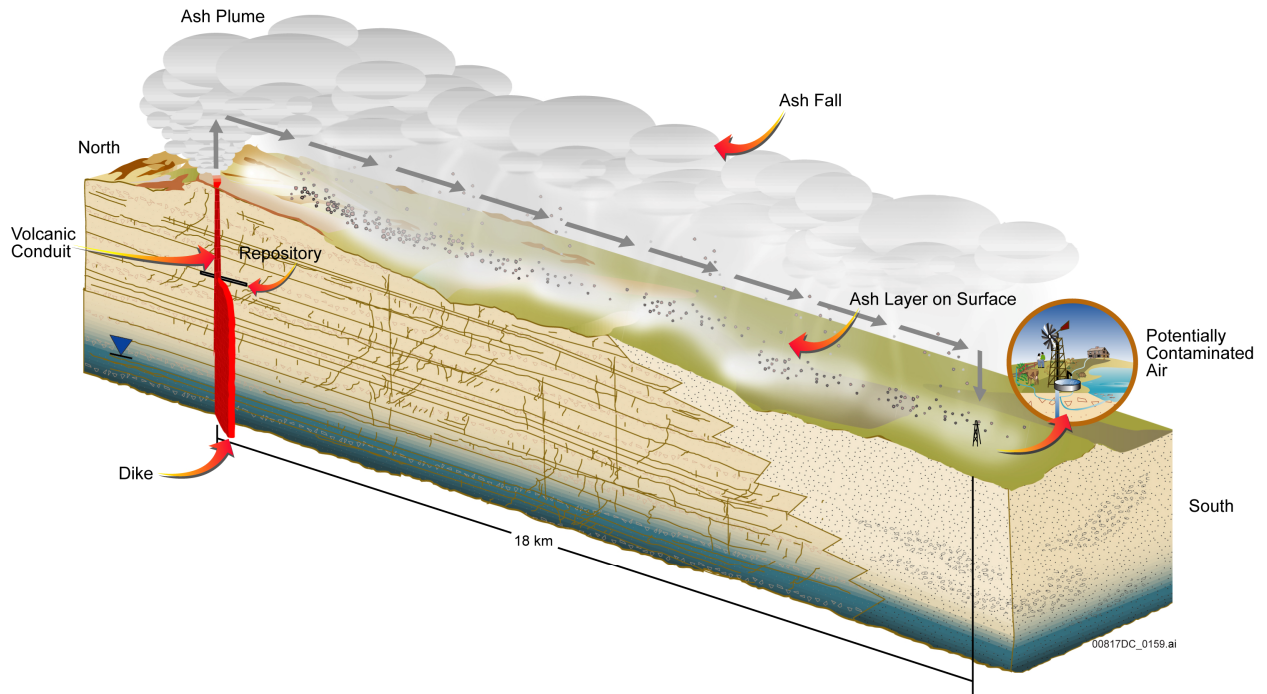
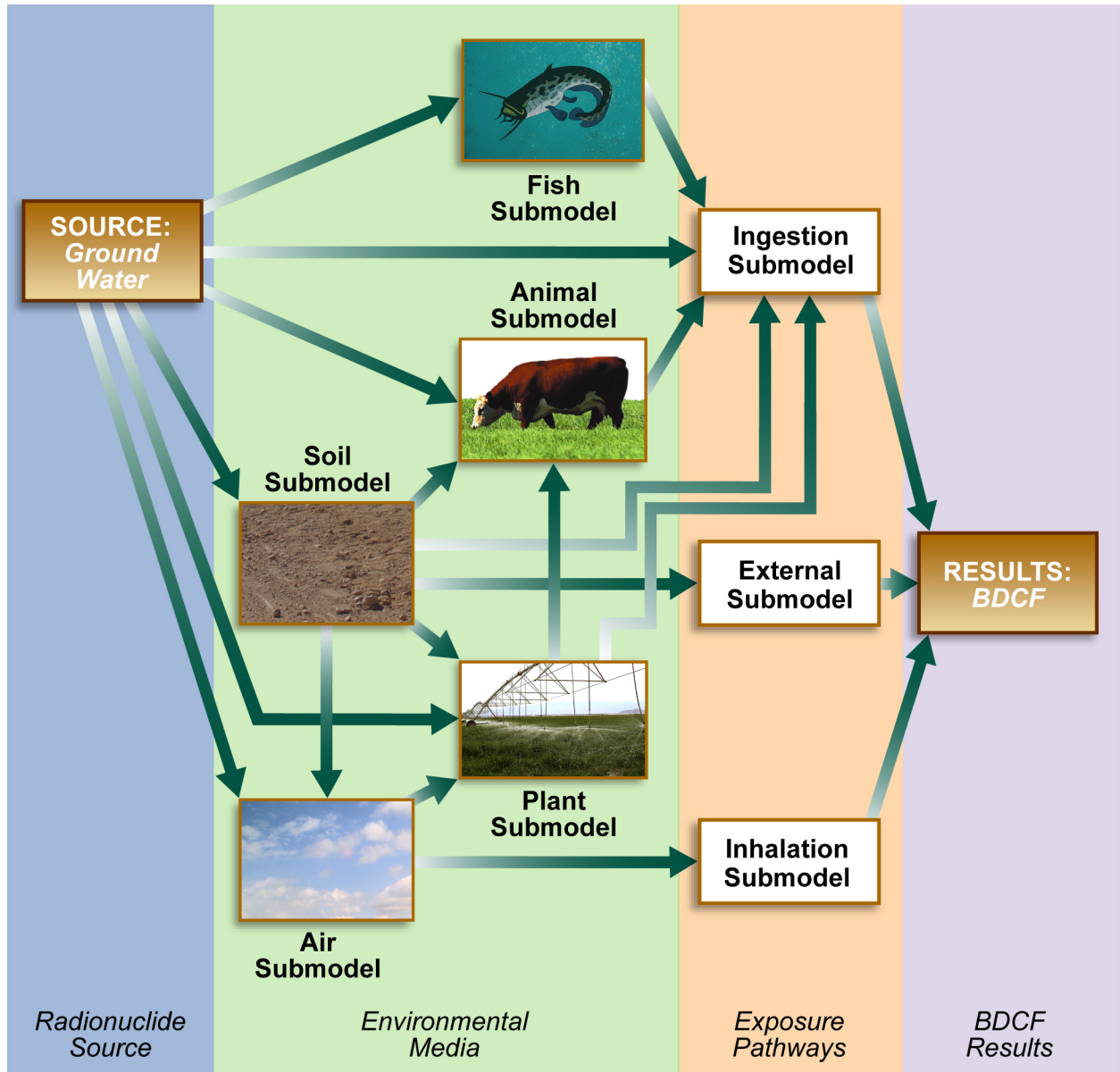


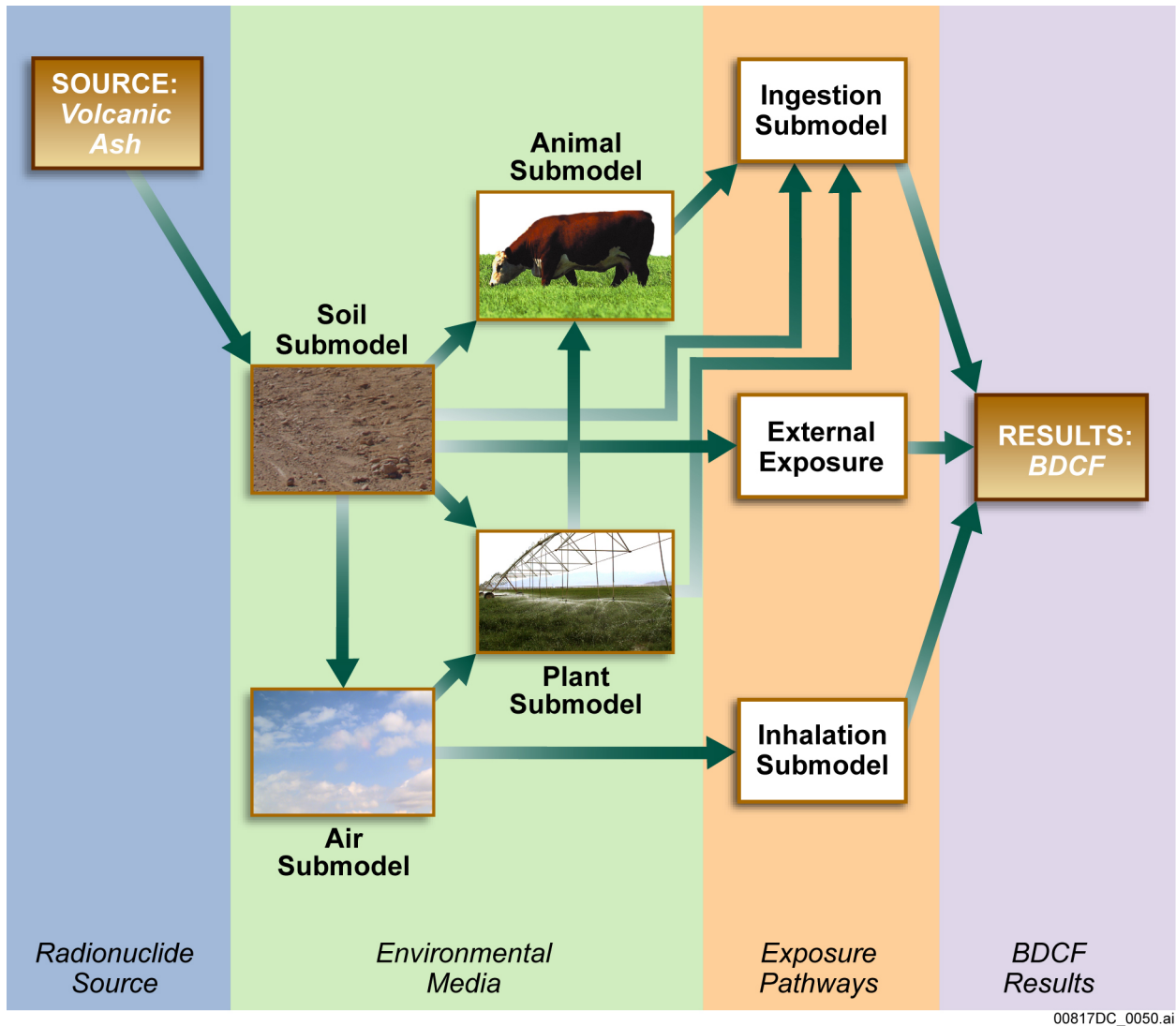
Figure 6.3.11-4. Schematic Representation of the Transport of Radioactive Waste in the Volcanic Ash Exposure Case



00817DC\_0029b.ai

Source: Modified from SNL 2007 [DIRS 177399], Figure 6.3-2.

Figure 6.3.11-5. Relationship among Biosphere Submodels for the Groundwater Exposure Case



Source: SNL 2007 [DIRS 177399], Figure 6.3-4.

Figure 6.3.11-6. Relationship among Biosphere Submodels for the Volcanic Ash Exposure Case

## 6.4 TSPA-LA MODEL FOR THE EARLY FAILURE SCENARIO CLASS

The Early Failure Scenario Class describes future performance of the repository system in the event of early failure of waste packages (WPs) and drip shields (DSs). An early failure is defined as the through wall penetration of a WP or DS due to manufacturing or handling-induced defects at a time earlier than would be predicted by mechanistic degradation models for a defect-free WP or DS. The conceptual models and abstractions for probability of WP and DS early failure are documented in *Analysis of Mechanisms for Early Waste Package/Drip Shield Failure* (SNL 2007 [DIRS 178765], Sections 6.1 through 6.5).

The Early Failure Scenario Class contains two modeling cases: the Drip Shield EF Modeling Case and the Waste Package EF Modeling Case. In the Drip Shield EF Modeling Case, complete failure of the DS is assumed to occur. A WP under an early failed DS is assumed to experience localized corrosion as soon as seepage contacts the WP, since the area of the Alloy 22 WP outer barrier that is contacted by seepage is potentially subject to localized corrosion (Section 6.3.5.2.3). In the Waste Package EF Modeling Case, an early failed WP is considered breached from the beginning of the simulation, and its entire surface area is considered degraded. General corrosion of the DSs due to nominal corrosion processes (Section 6.3.5.1.2) is included in the Waste Package EF Modeling Case.

The two modeling cases in the Early Failure Scenario Class have the same framework as the Nominal Scenario Class Modeling Case. The two modeling cases invoke the same modeling components and submodels as are invoked in the Nominal Scenario Class. That is, the framework includes the TSPA-LA Model components to evaluate the mobilization of radionuclides exposed to seeping water, release from the EBS, transport in the unsaturated zone (UZ) down to the saturated zone (SZ), and transport in the SZ to the location of the reasonably maximally exposed individual (RMEI). In the WP and DS Degradation Model Component, the Nominal Scenario Class WP and DS degradation modes are replaced with the early failure DS and early failure WP degradation modes. The relationships between the TSPA-LA Model components and submodels for the Early Failure Scenario Class are illustrated on Figure 6.4-1. Figure 6.4-2 shows the information flow within the TSPA-LA Model associated with the Early Failure Scenario Class. Figure 6.4-3 indicates the major inputs and outputs of the model components and submodels of the Early Failure Scenario Class, features included in the TSPA-LA Model, and foundation for confidence in the TSPA-LA Model.

The statistical distribution of annual dose is estimated in a Monte Carlo approach in which a set of realizations of repository system characteristics is used to represent the range of uncertainty and variability in the parameters of the TSPA-LA Model components. The mean annual dose is estimated as described in Equation 6.1.2-13 for the Waste Package EF Modeling Case and Equation 6.1.2-14 for the Drip Shield EF Modeling Case.

Section 6.4 can be summarized as follows: Section 6.4.1 describes the conceptual and abstraction models for the Drip Shield EF Modeling Case. Section 6.4.1.1 outlines the DS early failure conceptual model. Section 6.4.1.2 contains the abstraction model corresponding to this conceptual model. Section 6.4.1.3 describes the implementation in the TSPA-LA Model. Section 6.4.2 describes the conceptual and abstraction models for the Waste Package EF Modeling Case. Sections 6.4.2.1, 6.4.2.2, and 6.4.2.3 describe the WP early failure conceptual

model, corresponding abstraction model, and implementation in the TSPA-LA Model. Section 6.4.3 discusses the treatment of uncertainty. Section 6.4.4 discusses consistency of assumptions between TSPA submodels and model components. It also discusses conservatism in model abstractions.

#### **6.4.1 Drip Shield Early Failure Modeling Case**

##### **6.4.1.1 Drip Shield Early Failure Modeling Case Conceptual Model**

Thirteen potential mechanisms that could cause manufacturing defects in welded metallic containers were identified in Section 6.1.6 of *Analysis of Mechanisms for Early Waste Package/Drip Shield Failure* (SNL 2007 [DIRS 178765]). Of these thirteen flaws or processes, four were identified as potentially significant for mechanisms leading to early DS failure. Four processes were retained for further analysis:

- Improper heat treatment
- Base metal selection flaws
- Improper weld filler material
- Emplacement errors.

For the applicable DS defects, the probability of occurrence and consequences for postclosure performance were assessed. The four processes were analyzed using an event tree/fault tree approach (SNL 2007 [DIRS 178765], Section 6.4). The probabilities of occurrence for the four DS early failure mechanisms were combined to yield a probability distribution for the rate of occurrence of undetected defects in DSs. The occurrence of an undetected defect is assumed to result in complete failure of the DS as a barrier to seepage at the time of repository closure (SNL 2007 [DIRS 178765], Section 6.5.2); hence, the probability distribution for the rate of occurrence of undetected defects is equivalent to a probability distribution for the rate of DS early failures. The occurrence of undetected defects is assumed to be independent between DSs; hence, DS early failure is also independent between DSs.

##### **6.4.1.2 Abstraction of Drip Shield Early Failure**

The uncertain rate of DS early failures was abstracted to a log-normal distribution (SNL 2007 [DIRS 178765], Table 7-1). Because DS early failure is independent between DSs, the number of DS early failures can be represented by a Poisson distribution for any particular value of the rate of DS early failures,  $\lambda$ . Appendix B of GoldSim Technology Group 2007 ([DIRS 181727], p. 670) contains a summary of the properties of a Poisson distribution. The Poisson distribution for the number of DS early failures was developed (output DTN: MO0707WPDRIPSD.000 [DIRS 183005], folder: AB-TSPA-DTN-3 (PEF 118)) by integrating the Poisson probability density function for each rate of early failure with the probability density function for the rate of early failure,  $f(\lambda)$ , given by the log-normal distribution. The integral was numerically evaluated over its domain from zero to a truncated upper-bound  $\lambda_m$ , and set at the 0.999999 quantile value for the given log-normal distribution. The log-normal probability density function  $f(\lambda)$  was also adjusted to its truncated upper-bound representation so that the probability density function integrates to one over the specified range. The integral is shown in

Equation 6.4-1, where  $f(\lambda)$  and  $F(\lambda)$  are the probability density function and cumulative distribution function (CDF) of the log-normal distribution,  $N$  is the population of DSs considered,  $n = 0, 1, 2, 3, \dots$  is the count of early failures, and  $p(n)$  is the probability of  $n$  DS early failures.

$$p(n) = \int_0^{\lambda_m} (\lambda N)^n \times \frac{e^{(-\lambda N)}}{n!} \times \frac{f(\lambda)}{F(\lambda_m)} \times d\lambda \quad (\text{Eq. 6.4-1})$$

Table 6.4-1 shows the results of evaluating Equation 6.4-1. The probability of no DS early failures is 0.9834. The probability of only one DS early failure is 0.0155, and the probability of two or more DS early failures is 0.0011. The expected number of DS early failures is given by the sum:

$$\sum_{n=0}^{n_m} p(n) \times n = 0.018 \quad (\text{Eq. 6.4-2})$$

where  $n_m$  is the number of terms in the distribution for the number of DS early failures, chosen so that including more terms in the summation is not significant.

Analyses in *Analysis of Mechanisms for Early Waste Package/Drip Shield Failure* (SNL 2007 [DIRS 178765], Table 7-1) predicted rates for the introduction of defects into DS fabrication but did not predict the impact on repository performance. The report acknowledged that failure of the DS will only occur after degradation processes take place, which may happen hundreds or even thousands of years after emplacement. However, a realistic estimate of the time at which components with defects will fail was considered difficult to develop. Therefore, the report recommended the assumption of complete failure of the DS, with respect to its seepage diversion function, at the time of repository closure for implementation in the TSPA-LA Model (SNL 2007 [DIRS 178765], Section 6.5.2). This assumption will overestimate the potential for radionuclide release early in the life of the repository.

### 6.4.1.3 Implementation of Drip Shield Early Failure in the TSPA-LA Model

The rate of DS early failure is sampled from a log-normal distribution with a median of  $4.30 \times 10^{-7}$  and an error factor of 14 (Table 6.4-2). These inputs need to be adjusted to conform to the input requirements of GoldSim (GoldSim Technology Group 2007 [DIRS 181727], Appendix B, p. 668) for log-normal distributions, which require either the geometric mean and geometric standard deviation (SD) or the true mean and true SD as parameters. First, note that the median is equal to the geometric mean for log-normal distributions (Evans et al. 1993 [DIRS 112115], Chapter 25). Second, the shape parameter,  $\sigma_l$ , is related to the error factor by:

$$\sigma_l = \frac{\ln(\text{errorfactor})}{1.645} = \ln(\text{errorfactor}^{1/1.645}). \quad (\text{Eq. 6.4-3})$$

The shape parameter is the SD of the log transformed variates (Evans et al. 1993 [DIRS 112115], Chapter 25). Therefore, the geometric SD of the log-normal distribution is given by Equation 6.4-4 (GoldSim Technology Group 2007 [DIRS 181727], Appendix B, p. 668):

$$\sigma_g = \exp(\sigma_l) = \text{errorfactor}^{1/1.645} . \quad (\text{Eq. 6.4-4})$$

For the DS early failure implementation, the DSs are associated with the two WP fuel type groups (commercial spent nuclear fuel [CSNF] and co-disposed [CDSP]). The TSPA-LA model makes the simplifying assumption that each DS early failure affects a single WP. The length of a DS is approximately 228 inches (SNL 2007 [DIRS 179354], Table 4-2); the length of a WP varies between 146 and 230 inches (SNL 2007 [DIRS 179567], Table 4-5) and (SNL 2007 [DIRS 179394], Table 4-3)). Thus, the assumption that a DS early failure affects one WP is reasonable.

The TSPA-LA models a DS early failure by removing the DS as a barrier to seepage at the time of repository closure and allowing the full volume of seepage to contact the WP (Section 6.4.1.2).

The TSPA-LA model conservatively assumes that a WP underneath an early failed DS experiences localized corrosion, which completely compromises the outer barrier of the WP at the time of repository closure, allowing both the advective and diffusive transport of radionuclides. Analysis of the Localized Corrosion Initiation Abstraction shows that localized corrosion initiation conditions can be present in the repository for the first few hundred years in a minority of epistemic realizations. Rather than incurring significant computational expense to account for the epistemic uncertainty and the temporal and spatial variation in the initiation of localized corrosion, this simplifying assumption of immediate initiation of localized corrosion is made. Similarly, the TSPA-LA model assumes that localized corrosion rapidly compromises the entire outer barrier of the affected WP, rather than modeling the progression and extent of localized corrosion, to simplify the calculation of expected dose.

DS early failures that occur in locations but that do not experience seepage are assumed to contribute negligibly to the expected dose. In a location without seepage, localized corrosion does not occur because the WP surface is not wetted. Since localized corrosion does not occur, and the Drip Shield EF Modeling Case does not address other events (i.e., seismic events) that could compromise the WP integrity, there are no mechanisms in the Drip Shield EF Modeling Case that would lead to releases from a WP in a location without seepage. Therefore, the assumption of negligible dose impact is justified.

The GoldSim component of the TSPA-LA Model computes the dose resulting from a single DS early failure occurring in each of the 5 percolation subregions (Section 6.3.2.2.1), in a seeping environment, and affecting each type of WP (CSNF or CDSP), for a total of 10 dose histories for each epistemic realization. The GoldSim results are used in Equation 6.1.2-14 with the sampled rate of DS early failure, the distribution of the numbers of WPs of each type, and the seepage fraction for each percolation bin, to calculate the expected dose for each epistemic realization. The mean and median dose is estimated from the ensemble of expected dose results at each point in time.

## 6.4.2 Waste Package Early Failure Modeling Case

### 6.4.2.1 Waste Package Early Failure Modeling Case Conceptual Model

Thirteen potential mechanisms that could result in early failed WPs were identified in Section 6.1.6 of *Analysis of Mechanisms for Early Waste Package/Drip Shield Failure* (SNL 2007 [DIRS 178765]). Of these thirteen flaws or processes, seven were identified as potentially significant for the waste package outer corrosion barrier (OCB). The seven processes retained for further analyses were (SNL 2007 [DIRS 178765], Section 6.3):

- Weld flaws
- Improper heat treatment of OCB
- Improper heat treatment of OCB lid
- Improper stress relief of OCB lid (low plasticity burnishing)
- WP mishandling damage
- Improper base metal selection
- Improper weld filler material.

The processes were assessed for probability of occurrence and consequences for postclosure performance of the WPs.

A more detailed analysis was done for WP weld flaws (SNL 2007 [DIRS 178765], Section 6.3.1) than for the other six processes. This analysis resulted in distributions for the size and number of undetected weld flaws. The characteristics of weld flaws that remain in the WP closure welds can be calculated from these distributions by knowing the per-WP closure weld volume and weld thickness. The TSPA-LA Model utilizes these results, with the critical flaw orientation probability and an applicable depth factor to model where undetected flaws might remain and might result in stress corrosion cracking that could penetrate the WP closure weld. The implementation of the weld flaw analysis requires inputs that are supplied by the TSPA-LA Model file (Section 6.3.5.1.2). Therefore, the implementation of the weld flaw analysis is not part of the Waste Package EF Modeling Case but is part of the Nominal Modeling Case WP and DS degradation analysis (Section 6.3.5.1.2).

The remaining six processes were analyzed using an event tree/fault tree approach (SNL 2007 [DIRS 178765], Section 6.3). Improper base metal selection was rejected as a potential mechanism (SNL 2007 [DIRS 178765], Section 6.3.2), based on the probability of selecting improper base metal material in the fabrication of the OCB of the WP and the probability that the error is not detected.

Results from the event tree analyses of WP event sequences for the remaining five processes were collected into event tree end states and probability distributions for the presence of undetected defects were developed by running 90,000 realizations for these end states (SNL 2007 [DIRS 178765], Section 6.5.1). The occurrence of an undetected defect is assumed to result in early failure of the WP; hence, the probability distribution for the rate of occurrence of undetected defects is equivalent to a probability distribution for the rate of WP early failures. The occurrence of undetected defects is assumed to be independent between WPs; hence, WP

early failure is also independent between WPs. No distinction is made between the different types of WP (i.e., DSNF-Short and DSNF-Long).

#### **6.4.2.2 Abstraction of Waste Package Early Failure**

The uncertain rate of WP early failures was abstracted to a log-normal distribution (SNL 2007 [DIRS 178765], Table 7-1). Because WP early failure is independent between WPs, the number of WP early failures can be represented by a Poisson distribution. The distribution for the number of early failure WPs was developed in an analogous manner to the development described in Section 6.4.1.2 for early failure DSs (output DTN: MO0707WPDRIPSD.000 [DIRS 183005], folder: AB-TSPA-DTN-3 (PEF 118)). Table 6.4-1 shows the results of evaluating Equation 6.4-1 for WP early failures. The probability of no WP early failures is 0.558. The probability of only one WP early failure is 0.224, the probability of exactly two WP early failures is 0.096, and the probability of three or more WP early failures is 0.123. The expected number of early-failed WPs is 1.09, evaluated using Equation 6.4-2, and the probability of WP early failures.

Analyses in *Analysis of Mechanisms for Early Waste Package/Drip Shield Failure* (SNL 2007 [DIRS 178765], Table 7-1) predicted rates for the introduction of defects into WP fabrication but did not predict the impact on the WP performance. The report acknowledged that failure of the WP will only occur after degradation processes take place, which may happen hundreds or even thousands of years after emplacement. However, a realistic estimate of the time at which components with defects will fail was considered difficult to develop. Therefore, the report recommended, for implementation in the TSPA-LA Model, the assumption of complete failure of the WP, with respect to radionuclide containment, at the time of repository closure (SNL 2007 [DIRS 178765], Section 6.5.2). This assumption will overestimate the potential for radionuclide release early in the life of the repository.

#### **6.4.2.3 Implementation of Waste Package Early Failure in the TSPA-LA Model**

The rate of WP early failure is sampled from a log-normal distribution with a median of  $4.14 \times 10^{-5}$  and an error factor of 8.17 (Table 6.4-2). These inputs are adjusted as described in Section 6.4.1.3 to conform to the input requirements of GoldSim.

For WP early failure implementation, the WPs are divided into two fuel type groups denoted by CSNF early failed WPs and CDSP early failed WPs. The GoldSim component of the TSPA-LA Model computes the dose resulting from early failure of a single WP of each type, occurring in each of the five percolation subregions (Section 6.3.2.2.1), with and without seepage in each percolation subregion, for a total of 20 dose histories for each epistemic realization. The GoldSim results are used in Equation 6.1.2-13 with the sampled rate of WP early failure, the distribution of the numbers of WPs of each type, and the seepage fraction for each percolation bin, to calculate the expected dose for each epistemic realization. The mean and median dose is estimated from the ensemble of expected dose results at each point in time.

The WAPDEG V4.07 software (STN: 10000-4.07 [DIRS 181744 and 181064]) is used to cause each early failed WP to fail at the beginning of the simulation (i.e., at the end of the first timestep). A simplified WAPDEG V4.07 input vector is used for this purpose (output

DTN: MO0707WPDRIPSD.000 [DIRS 183005], folder: AB-TSPA-DTN-4 (PEF 88)). The input vector contains a single corrosion-affecting event that uses the power law functional form (BSC 2002 [DIRS 162606], Section 4.2.6.6) to impose an arbitrarily chosen large corrosion rate that causes breach of all WPs in the first time step. In addition, all WPs completely fail at the end of the first timestep. The use of the WAPDEG software allows a relative humidity threshold to be imposed for the initiation of WP failure. General corrosion of DSs over early failed WPs occurs according to the nominal corrosion processes discussed in Section 6.3.5.1.2.

### **6.4.3 Treatment of Uncertainty**

The TSPA-LA Model includes input parameter uncertainty in the Early Failure Scenario Class. See Table 6.4-2 for a list of uncertain parameters specific to the Early Failure Scenario Class. The Early Failure Scenario Class also includes other uncertain parameters associated with the model components and submodels shown on Figure 6.4-1 and described in Section 6.3. The treatment of aleatory uncertainty in the Early Failure Scenario Class is described in Section 6.1.2.4.2.

### **6.4.4 Model Component Consistency and Conservatism in Assumptions and Parameters**

To enhance understanding of the complex interactions within the TSPA-LA Model, a discussion of consistency among model components and submodels and identification of conservative assumptions in abstractions, process models, and parameter sets supporting the DS Early Failure Submodel and the WP Early Failure Submodel are discussed below.

#### **6.4.4.1 Consistency of Assumptions**

The Early Failure Scenario Class does not include potential inconsistencies between model components or submodels since its effect on the TSPA-LA Model is limited to replacing the Nominal Scenario Class conceptual models for DS and WP degradation with the early failure conceptual models. These models are simpler, in the sense that failure mechanisms are not treated in detail and failure is assumed to occur at the beginning of the simulation. No inconsistencies have been identified between the DS and WP Early Failure Submodels and other Submodels of the TSPA-LA Model.

#### **6.4.4.2 Identification of Conservatism in Submodels and Abstractions**

**Consequences of Defects**—Section 6.5.2 of *Analysis of Mechanisms for Early Waste Package/Drip Shield Failure* (SNL 2007 [DIRS 178765]) notes that even if a WP or DS is affected by a type of defect that may lead to its early failure, it does not mean that this WP or DS is due to fail at emplacement in the repository. Failure of the WP will only occur after degradation processes take place, which may happen hundreds or even thousands of years after emplacement. Even if a WP or DS were to fail soon after emplacement because of a defect, its radionuclide inventory might not necessarily be available for transport. This is because most through-wall penetrations, especially cracks from SCC, are usually tight, highly tortuous, and limited in length. A realistic estimate of when components with defects will fail would be difficult to develop and justify given the nature of the problem:

- Physical failure of highly corrosion resistant metallic structures with very small loads under nominal conditions
- The time frames involved—centuries to millennia or longer
- The lack of experience with such engineered systems in standard industrial or engineering practice.

Because of such considerations, an approach to the assumption of complete failure of the components with respect to radionuclide containment or seepage diversion function at the time of repository closure was recommended for implementation in the TSPA-LA Model. This approach will overestimate the potential for radionuclide release early in the life of the repository.

Table 6.4-1. Early Failure Unconditional Probability Values

n (Number of Early Failures)	p(n), Waste Packages	p(n), Drip Shields
0	0.5580	0.9834
1	0.2237	0.0155
2	0.0955	0.0009
≥ 3	0.1228	0.0002

Source: Output DTN: MO0707WPDRIPSD.000 [DIRS 183005], folder: AB-TSPA-DTN-3 (PEF 118)

Table 6.4-2. Uncertain Inputs Used in the Early Failure Scenario Class

TSPA-LA Parameter Name	Description	Units	Distribution	Remarks
UNC_WP_EF	Parameters for probability distribution for undetected defects in WPs. For TSPA purposes, this distribution is the probability that a WP will experience early failure after emplacement.	per WP	Log-normal distribution with a median of $4.14 \times 10^{-5}$ and an error factor of 8.17. (epistemic uncertainty)	DTN: MO0701PASHIELD.000_R2 [DIRS 180508], file: Tables for DTN Readme.doc
UNC_DS_EF	Parameters for probability distribution for undetected defects in DSs. For TSPA purposes, this distribution is the probability that a DS will experience early failure after emplacement.	per WP	Log-normal distribution with a median of $4.30 \times 10^{-7}$ and an error factor of 14. (epistemic uncertainty)	DTN: MO0701PASHIELD.000_R2 [DIRS 180508], file: Tables for DTN Readme.doc

INTENTIONALLY LEFT BLANK

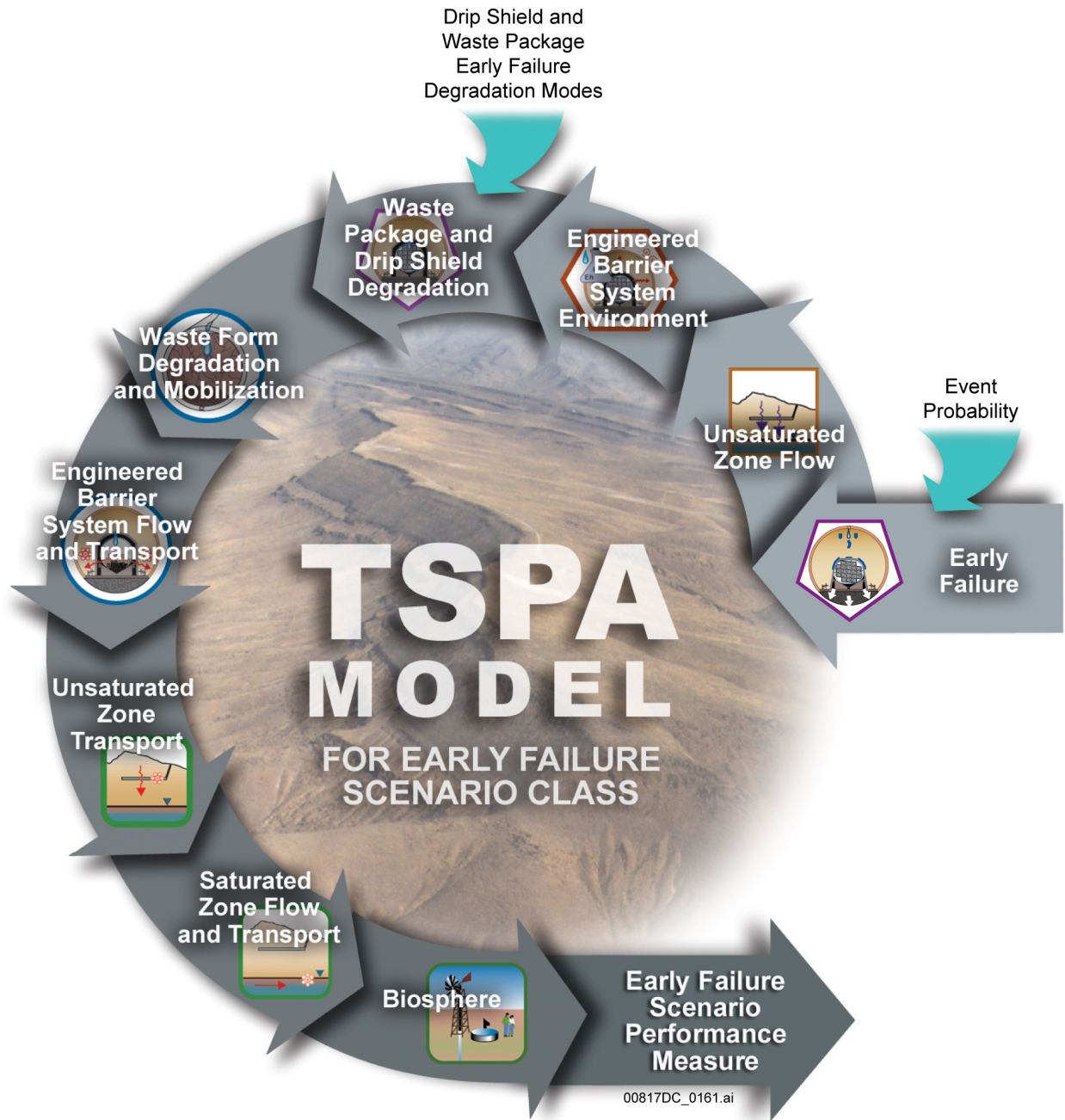


Figure 6.4-1. Schematic Representation of the TSPA-LA Model Components for the Early Failure Scenario Class

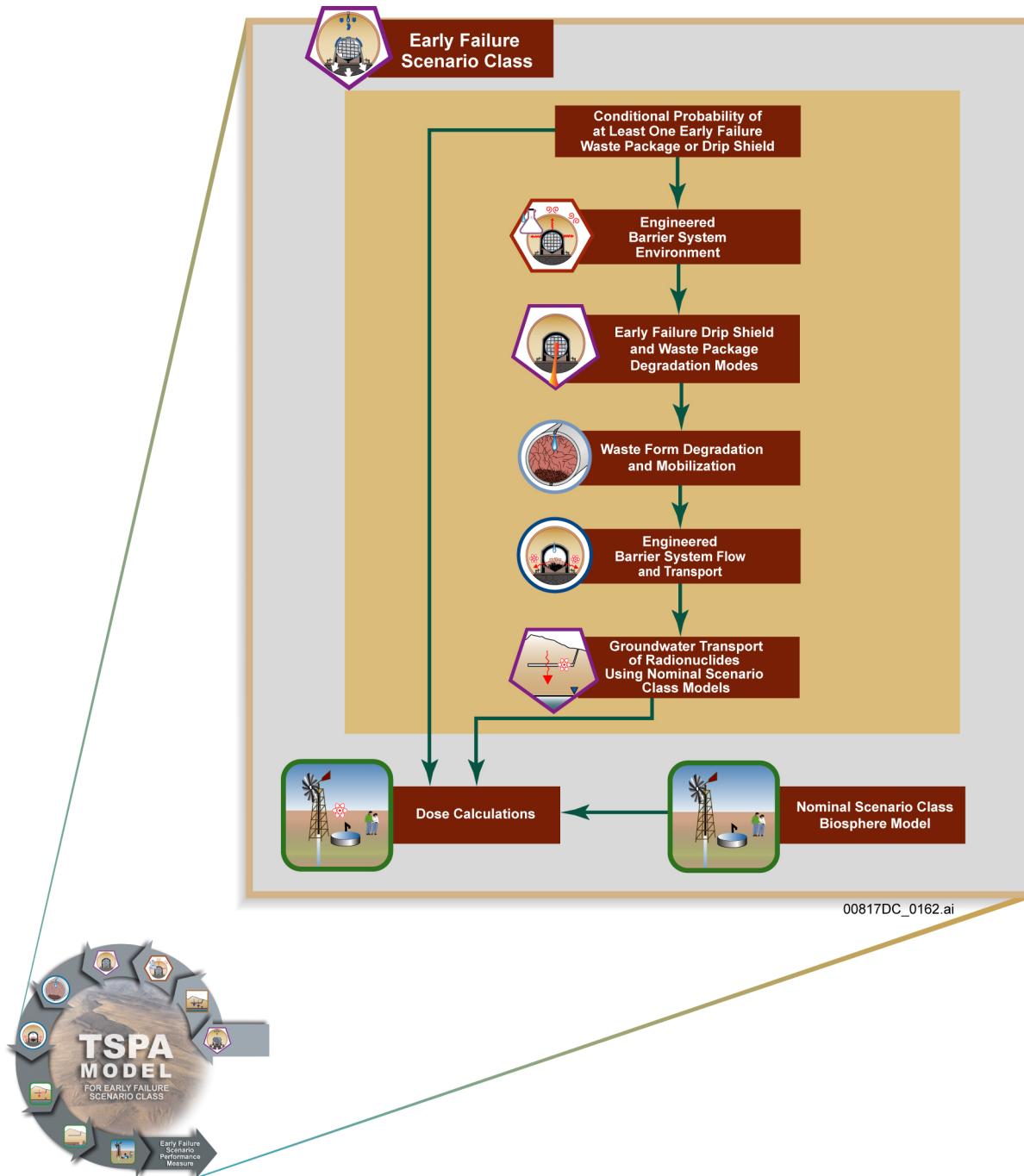


Figure 6.4-2. Information Flow Diagram for the Early Failure Scenario Class in the TSPA-LA Model

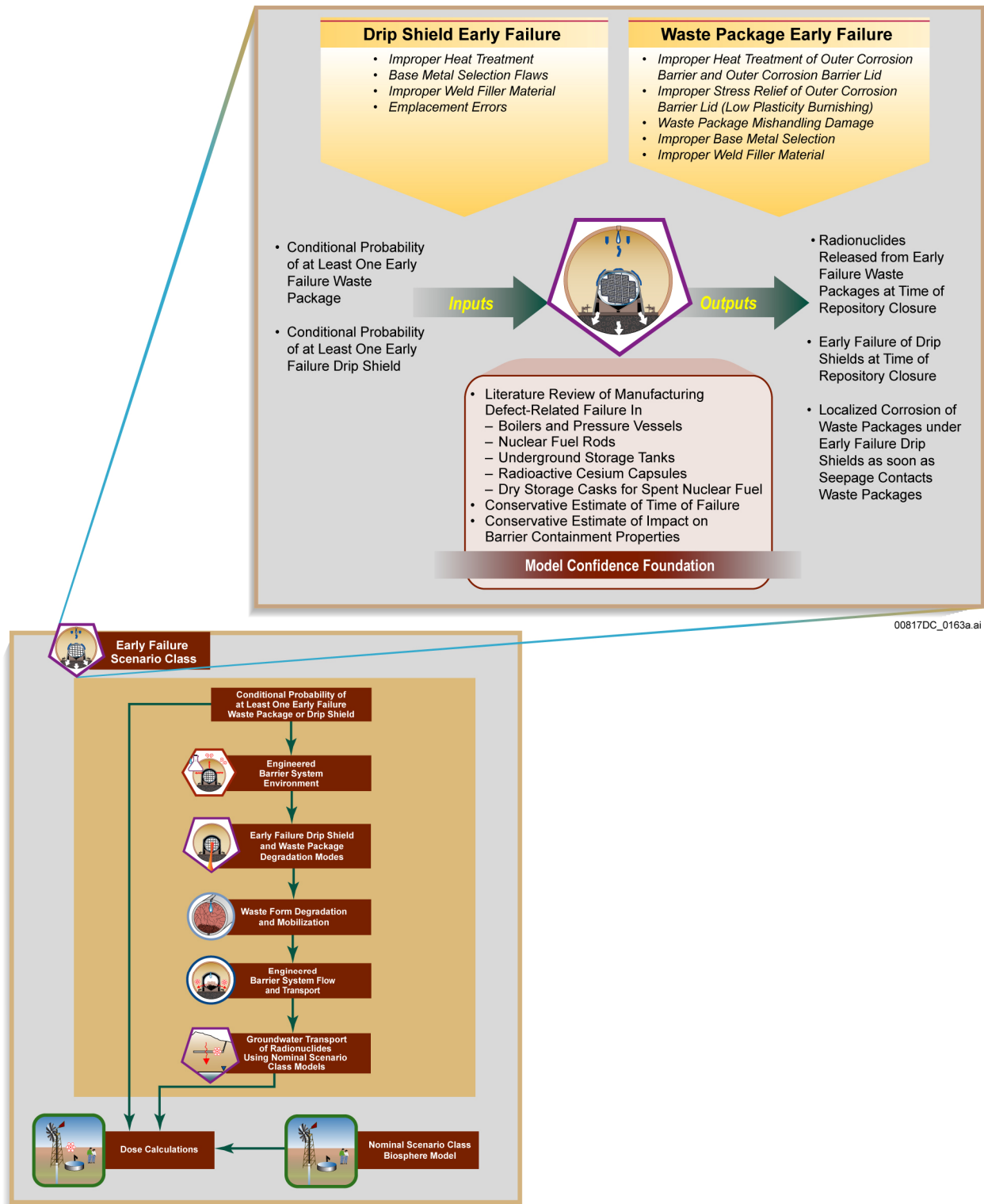


Figure 6.4-3. Inputs, Outputs, and Basis for Model Confidence for the Early Failure Scenario Class

INTENTIONALLY LEFT BLANK